REPORT NO 3, 2D UHRS SURVEY GEOMODEL INTEGRATED WITH CPT AND BH DATA, AREA 1

Danish Offshore Wind 2030 | North Sea 1, Denmark

F217715-REP-003 [02] | 1 November 2024
For Review
Energinet Eltransmission A/S

Document Control

Document Information

Project Title	Danish Offshore Wind 2030
Document Title	REPORT NO 3, 2D UHRS SURVEY GEOMODEL INTEGRATED WITH CPT AND BH DATA, AREA 1
Fugro Project No.	F217715
Fugro Document No.	F217715-REP-003
Issue Number	02
Issue Status	For Review
Fugro Legal Entity	Fugro Netherlands Marine Limited
Issuing Office Address	Fugro House, Hithercroft Road, Wallingford, Oxfordshire OX10 9RB, UK

Client Information

Client	Energinet Eltransmission A/S
Client Address	Tonne Kjærsvej 65, DK-7000 Fredericia, Denmark
Client Contact	Anna Bondo Medhus and Pieter Oudshoorn
Client Document No.	22/02940-12

Document History

Issue	Date	Status	Comments on Content	Prepared By	Checked By	Approved By
01	13 September 2024	For Review	Awaiting client comments	DS/AB/CJS	CJS	LOL
02	01 November 2024	For Review	Updated based on client comments	DS/AB/CJS	CJS	GML

Project Team

Initials	Name	Role
APA	A. Padwalkar	Project Director
ALE	Alistair Leighton	Project Manager
MGN	Malgorzata (Gosia) Nowak	Reporting and Deliverables Project Manager
CJS	Chris Steven	Principal Engineering Geologist
LOL	Lorraine O'Leary	Engineering Geology and Geohazards Team Lead
GML	Grant Lewis	Commercial Manager
DS	Devan Scanlan	Engineering Geologist
AB	Arthur Blouin	Engineering Geologist
SB	Simon Blet	Engineering Geologist

FUGRO
Fugro Netherlands Marine Limited
Prismastraat 4
Nootdorp
2631 RT
The Netherlands

Energinet Eltransmission A/S
Tonne Kjærsvej 65
DK-7000 Fredericia
Denmark

1 November 2024

Dear Sir/Madam,

We have the pleasure of submitting the 'REPORT NO 3, 2D UHRS SURVEY GEOMODEL INTEGRATED WITH CPT AND BH DATA, AREA 1' for the 'Danish Offshore Wind 2030'. This report presents all the results of the geological site survey with geotechnical CPT and BH survey integrated for Sub Area 1. We hope that you find this report to your satisfaction; should you have any queries, please do not hesitate to contact us.

Yours faithfully,

Malgorzata (Gosia) Nowak
Reporting and Deliverables Project Manager

Frontispiece

F217715 - ENERGINET 2030

SUB-AREA 1 BOREHOLE INTEGRATION

0 25 50   100   150   200   250 km

Imagery reproduced from the GEBCO_2022 Grid. GEBCO Compilation Group (2022) GEBCO 2022 Grid; Flanders Marine Institute (2023).
Maritime Boundaries Geodatabase: Maritime Boundaries and Exclusive Economic Zones (200NM), version 12; Esri (2024).
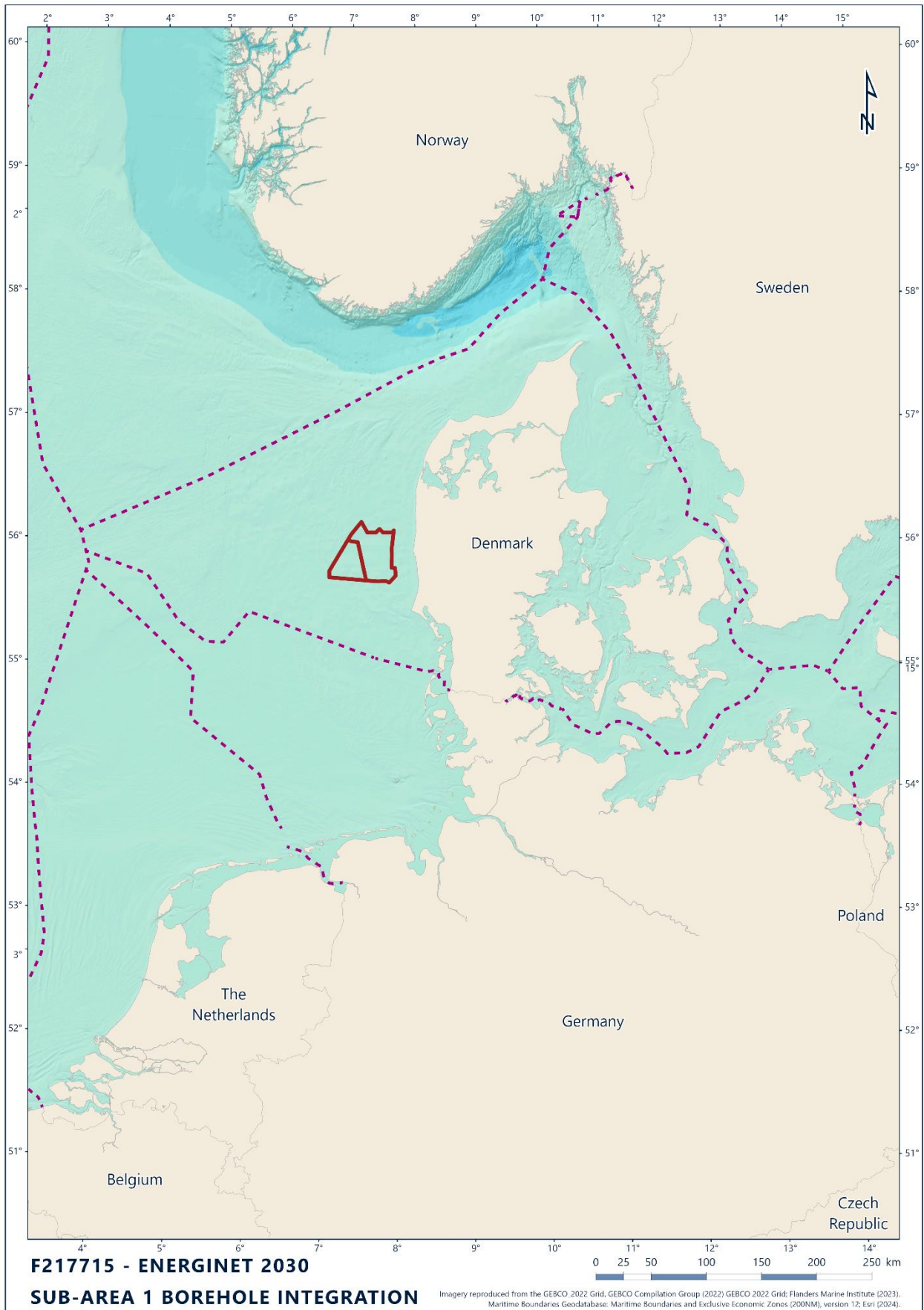
Project Reports Arrangement

1. REPORT NO 1, 2D UHRS BASELINE SURVEY

2. REPORT NO 2, 2D UHRS SURVEY GEOMODEL INTEGRATED WITH CPT DATA, FULL SITE

3. **REPORT NO 3, 2D UHRS SURVEY GEOMODEL INTEGRATED WITH CPT AND BH DATA, AREA 1 (THIS REPORT)**

4. REPORT NO 4, 2D UHRS SURVEY GEOMODEL INTEGRATED WITH CPT AND BH DATA, FULL SITE

Executive Summary

Interpretative Site Investigation	
Survey Dates	10 June to 13 November 2023 (geological) and 27 October 2023 to 16 July 2024 (geotechnical)
Equipment	Multibeam echosounder (MBES), sub-bottom profiler (SBP), 2D ultra high resolution (2D UHR) seismic and cone penetrometers (CPT) and seismic cone penetrometers (sCPT)
Coordinate System	Datum: European Terrestrial Reference System 1989 (ETRS89) Projection: UTM Zone 32N, CM 3°E
Vertical Datum	

Bathymetry
Elevation at the time of the survey ranged from -12.27 m to -33.51 m MSL. A bank with north-north-west to south-south-east orientation is present in the south of the site. Several south-west to north-east and north-west to south-east oriented ridges are to the west of the bank.

Regional Geological History
During the Miocene to Middle Pleistocene, marine, deltaic and fluvial deposits (Base Seismic Until (BSU) and Unit U90) were deposited at the site as a result of the progradation of the Eridanos river system. During the Elsterian glaciation, tunnel valleys and their infill (Unit U70) were formed, and the BSU was glacially deformed. During the Saalian glacial period, tunnel valley infills, glacial deposits (Unit U65) and glaciofluvial sediments (Unit U65 and Unit U60) were deposited. During the Eemian interglacial period marine clays (Unit U50) were deposited. During the Weichselian glacial period, glaciofluvial (U35 and U30) and glaciolacustrine (U30) sediments were deposited. During the last part of the last glacial period, channels were eroded which were filled during the Late Pleistocene (Unit U35) to early Holocene (Unit U20). During the Holocene marine sediments (Unit U10) were deposited.

Geological Features and Geohazards	
Peat and/or organic clay	Peat and/or organic clay is present locally in Unit U10, U20, U30, U50 and U90.
Soft clays	Soft clays are present in Unit U20.
Shallow gas	Evidence for the presence of shallow gas in form of acoustic blanking and/or signal attenuation has been observed on the 2D UHR seismic data in Unit U20 and to a lesser extent in Unit U50.
Gravel, cobbles, and Boulders	Gravel and cobbles may be present in glaciofluvial deposits (Units U30, U35, U60 and U90). Gravel, cobbles and boulders may be present in glacial deposits (Unit U65 and U70).
Buried channels and tunnel valleys	Unit U20, U35, U50 and U60 locally form channel infills. Unit U70 and partially Unit U65 represent the infill of tunnel valleys. Unit U35, U60, U65, U70 and U90 contain internal erosion surfaces and channels.
Glacial deformation	In Unit U65, U70 and the BSU thrust faults were observed which are interpreted to be the result of glaciotectonism.
Faults	In the BSU, normal faults are present in a small area in the south-east of the site.

Spatial Geological Model	
Unit U10	Unit U10 is present throughout most of the site and forms a layer of Holocene marine sand with a maximum thickness of 10 m.
Unit U20	Unit U20 forms infill of spatially variable channels and overbank sand (Unit U20a) and clay (Unit U20b) deposits with a maximum thickness of 28 m.
Unit U30	Unit U30 is a locally present sand unit with a sheet-like geometry with often a clay bed at its base. Its maximum thickness is 13 m.
Unit U35	Unit U35 is a fluvial sand unit with a sheet-like to channelised geometry and a maximum thickness of 24 m.

FUGRO

Unit U36	Unit U36 is a transitional unit between Unit U35 and U50 with internal dipping reflectors comprising silt and sand and reaches a maximum thickness of 20 m.
Unit U50	Unit U50 is a marine clay (Unit U50a) and has a sheet-like to channelised geometry. There is a bed of sand at the base (Unit U50b). It has a maximum thickness of 51 m.
Unit U60	Unit U60 is a fluvial sand unit with a sheet-like to channelised geometry and a maximum thickness of 81 m.
Unit U65	Unit U65 is a glacial unit comprising clay, sand and till with a maximum thickness of more than 150 m.
Unit U69	Unit U69 is a glaciolacustrine unit comprising clay sediments with a thickness of more than 50 m.
Unit U70	Unit U70 is a tunnel valley infill comprising clay, sand and till with a maximum thickness of more than 73 m.
Unit U90	Unit U90 is a fluvial sand unit which is present in the south-west of the site with a maximum thickness of more than 133 m.
BSU (Base Seismic Unit)	The BSU is a stratified Miocene clay and sand which is locally deformed by various types of faults.

Geotechnical Data

A total of 389 locations have been sampled using seabed CPT and SCPT equipment, sampling sediments between 0.4 m and 54.2 m BSF. A further 69 geotechnical locations (which include results from downhole sampling, downhole in situ testing (where applicable), borehole geophysical logging (where applicable), and laboratory testing) between seafloor and 70.8 m BSF were acquired. Geotechnical datasets have been unitised and correlated with geophysical data to create an integrated model for the study area. Geotechnical datasets have been collected in all units. A number of geotechnical sub-units were observed in certain units (U20, U50, U65, U70).

Correlation between geotechnical unit boundaries and geophysical horizons is generally observed to be consistent. Currently correlations use a simple time-to-depth conversion with a velocity of 1730 m/s.

Three groupings of units are observed in geotechnical data, which can be linked to the geological history of the site. Shallow units from U10 to U20 are largely from a post glacial environment. Units U35 to U60 are expected to have been deposited in a glacial environment but are not expected to have been ice loaded. U65 and below may contain ice loaded sediments as well as glacial till deposits.

Geotechnical Zonation

15 geotechnical zones were defined across the study area. These divide the site based on two factors. The first of these is the thickness of U20 sediments, with 4 intervals determined. Thicker areas of Unit U20 may result in deposits of low strength clays that could affect future foundations. The second factor for the zonation of the site is the depth to the top of glacial units U65 and U70. These units represent the shallowest / youngest units associated with a period at the site history where direct glacial action is expected to have affected the geotechnical properties and also result in greater variability in sediment properties. Four conditions subdivide this factor, selected based on there relevance for foundation types. Combined, this results in 16 possible zone scenarios, however for one there was mutually exclusive conditions, resulting in 15 zones.

From the zonation work, the most frequent condition (27%) at the site showed that the thickness of U20 sediments was between 0.1 m and 6 m (typifying overbanking areas with little low strength material) and with a depth of between 10 m to 40 m to the top of glacial (U65/U70 sediments).

_____

Contents

FUGRO

Appendices

Figures in the Main Text

Tables in the Main Text

Abbreviations

2D UHR	Two-dimensional ultra high resolution (As agreed via TQ – 038, throughout the report and charts the name of 2D UHRS has been used, while 2D UUHRS in digital deliverables)
BH	Borehole
BP	Before present
BPD	Below penetration depth
BSF	Below seafloor
BSU	Base Seismic Unit
CM	Central meridian
COG	Centre of gravity
CPT	Cone penetration test
CRP	Common reference point
DOW2030	Danish Offshore Wind 2030
ETRS89	European Terrestrial Reference System 1989
DTS	Desktop study
Fm	Geological Formation
GNSS	Global Navigation Satellite System
ka	1000 years ago
LGM	Last Glacial Maximum
MBES	Multibeam echosounder
MIS	Marine Isotope Stage
MSL	Mean Sea Level
OWF	Offshore wind farm
PEP	Project Execution Plan
REP	Report
RTK	Real-time kinematic positioning
SBP	Sub-bottom profiler
TWTT	Two-way travel time
UTM	Universal Transverse Mercator
VRF	Vessel Reference Frame

FUGRO

1. Introduction

1.1 General

Energinet Eltransmission A/S contracted Fugro to perform the offshore geological site survey for the Danish Offshore Wind 2030 (DOW2030) campaign at the North Sea 1 (NS1) site. DOW2030 programme comprises multiple site investigations. This area of investigation is referred to as North Sea 1, covering an area of ~2200 km^2 of the North Sea west of Jutland with water depths between 10 m and 40 m, roughly between the Horns Rev and Thor offshore windfarm areas.

This report builds on the results from the CPT integrated report (217715-REP-002 2D UHRS Survey Geomodel Integrated with CPT Data, Full Site, Fugro, 2024); integrating the geotechnical borehole survey locations with the mainline survey subsurface data for Sub-Area 1.

The borehole survey for Sub-Area 1 was undertaken between 27 February 2024 to 16 July 2024 performed by the following geotechnical vessels; Excalibur, Gargano and Fugro Voyager. The data were acquired using downhole boreholes and cone penetrometers (CPTs); these locations were based on the borehole and CPT locations chosen from the baseline survey data and mainline survey line plan.

Guidelines on the use of this report have been provided in Appendix A.

Table 1.1 displays the report sequence for the work packages associated with this project, including the geophysical, geotechnical and integration reports.

Table 1.1: Overview of reports, including geophysical, geotechnical and geoconsulting

Type	Deliverable				
Integrated Geoconsulting Reports (See Table 1.2)	217715-REP-002 2D UHRS Survey Geomodel Integrated with CPT Data, Full Site	217715-REP-003 Sub-Area 1 CPT, Borehole & Seismic Integrated Report		217715-REP-004 Full Site CPT, Borehole & Seismic Integrated Report	
Geotechnical Reports	F217703/01 Geotechnics investigation report – Sub-Area 1 Seafloor In Situ Test Locations	F217703/02 Geotechnics investigation report – Sub-Area 2 Seafloor In Situ Test Locations	F217703/03 Geotechnics Investigation report – Seafloor In Situ Test Locations (Jack-up)	F217703/04 Geotechnics Investigation report – Sub-Area 1 Geotechnical Borehole Locations	F217703/05 Geotechnics Investigation report – Sub-Area 2 Geotechnical Borehole Locations
Geophysical Reports	217715-REP-001 Baseline Geophysical	217715-REP-002 Mainline Report			
Notes Reports highlighted in light green constitute input reports for this document. This report is highlighted in dark green. To be completed reports are highlighted in brown					

Table 1.2 explains the purpose of the main four geophysical and integrated reports.

Table 1.2: Overview and purpose of geophysical and geoconsulting integrated reports

Report Number	Report Name	Purpose
217715-REP-001	2D UHRS Baseline Survey	Identify large scale geology and utilising geophysical data to suggest geotechnical locations to investigate relevant units.
217715-REP-002	2D UHRS Survey Geomodel Integrated with CPT Data, Full Site	Provide a more detailed understanding of the site geology from a more in-depth geophysical survey including an integrated 3D geomodel based on seismic and CPT data available at time of submission.
217715-REP-003	2D UHRS Survey Geomodel Integrated with CPT and BH data, Area 1	Integrated 3D geomodel created in the Mainline report, updated with geotechnical information from borehole locations in Sub-Area 1.
217715-REP-004	2D UHRS Survey Geomodel Integrated with CPT and BH data, Full site	Integrated 3D geomodel created in the Mainline report, updated with geotechnical information from borehole locations from entire site.

The project area is located offshore Denmark, approximately 45 nautical miles north-west of Esbjerg in Denmark (Figure 1.1).
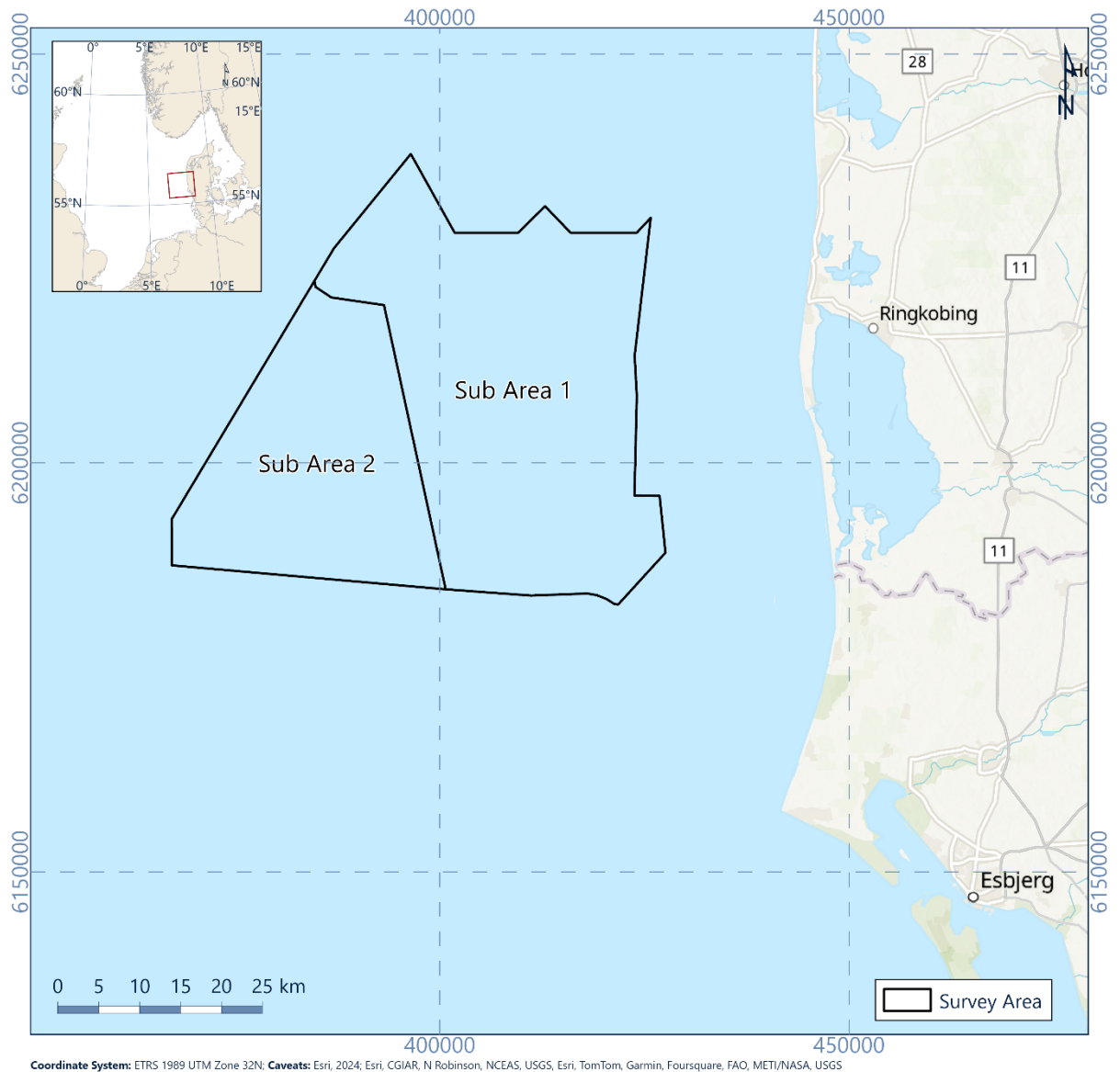
Figure 1.1: Project Location and Sub-Area split

1.2 Scope of Work

Following both the geophysical baseline and mainline surveys, the geotechnical CPT full site campaign and borehole Sub-Area 1 survey; this report will integrate the previous data and build on that with the data collected from the boreholes in Sub-Area 1. This report presents the following scope of work items:

- **Acquisition data review and methodology:** review of all available and recently acquired geological, geophysical and geotechnical data for the site, acquisition vessel information, methodology and data quality;
- **Geological Setting:** a regional geological setting has been developed; providing context to the environment and the geology expected to encounter;

- **Seafloor Conditions:** A description of seafloor conditions in the area using bathymetry, seafloor gradient and seafloor features;
- **Geological Model:** A conceptual model was developed using the seafloor and sub-seafloor conditions, integrated geophysical and geotechnical data from CPTs and borehole locations. Providing predicted soil profiles down to 60 m and associated soil provinces. This section also provides a quantitative geohazard inventory and anthropogenic constraints;
- **Geotechnical Parameters:** Predicted geotechnical parameters were derived to a depth of 60 m per unit with low estimate (LE), best estimate (BE) and high estimate (HE) for each parameter. Where possible, the parameters provided for each soil unit include:
  - Submerged unit weight;
  - Water content;
  - Min/max density values;
  - Atterberg limit test values;
  - Cone resistance;
  - Relative density;
  - Undrained shear strength.

1.3   Geodetic Parameters

The project geodetic and projection parameters are summarised in Table 1.3. Unless stated otherwise, geodetic coordinates presented in this report are as per the datum in Table 1.3.

Table 1.3: Project Geodetic Parameters

Global Navigation Satellite System (GNSS) Geodetic Parameters	
Datum:	ETRS89 (European Terrestrial Reference System 1989)
EPSG Code:	25832
Semi Major Axis:	6 378 137.00 m
Reciprocal Flattening:	298.257222101
Project Projection Parameters	
Grid Projection:	Universal Transverse Mercator
UTM Zone:	32 N
Central Meridian:	009° 00' 00.000" E
Latitude of Origin:	00° 00' 00.000" N
False Easting:	500 000 m
False Northing:	0.000 m
Scale factor on Central Meridian:	0.9996
EPSG Code:	16032
Units:	Metres

1.4   Vertical Datum

The vertical datum was mean sea level (MSL). All water depths were referenced to MSL using post processed GNSS height data collected in real time on board the vessels. GNSS heights were referenced to MSL by means of the WGS84 to DTU21 MSS ellipsoidal to datum separation model.

1.5   Guidelines on Use of Report

Appendix A outlines the limitations of this report in terms of a range of considerations including, but not limited to, its purpose, its scope, the data on which it is based, its use by third parties, possible future changes in design procedures and possible changes in the conditions at the site with time. It represents a clear exposition of the constraints which apply to all reports issued by Fugro. It should be noted that the Guidelines do not in any way supersede the terms and conditions of the contract between Fugro and Energinet Eltransmission A/S.

2. Acquisition Data

2.1 Data Review

2.1.1 Ocean Infinity Geophysical Data

Between 3 April 2023 and 17 September 2023, Ocean Infinity (OI) undertook a geophysical survey of the Energinet 2030 site Sub-area 1. The geophysical survey included collecting bathymetry (MBES), side scan sonar (SSS), sub-bottom profiler (SBP) and magnetometer. The scope of this survey was to provide full coverage of Sub-area 1.

Within this report, Fugro have utilised the MBES data for the seafloor elevation and presented in Section 4 to show seafloor conditions, along with the seafloor sediments and features for a visual representation. No further interpretation or integration of this data has been used.

2.1.2 Fugro Acquired Geophysical Data

Between 14 April and 19 April 2023, a full site baseline survey was acquired using SBP and 2DUUHR data to a depth of 100 m along 10 km spaced lines. The subsequent geophysical mainline survey of 250 m spaced mainline and 1 km spaced crosslines was performed, acquiring further SBP and 2DUUHR data 100 m below seafloor (BSF). The data collected from these surveys has been utilised to understand the sub-seafloor conditions and integrated with the CPT and borehole locations to provide a more confident geological ground model.

Further information on the geophysical data, vessel and equipment used can be found in Section 2.2.1 and in the Baseline Survey Results Report (Fugro, 2023c) and the Full Site Geomodel with CPT data (Fugro, 2024) reports.

2.1.3 Fugro Acquired Geotechnical Data

Two main pahases of geotechnical data acquisition have taken place at the NorthSea I site. Firstly between 27 October 2023 and 6 March 2024 Fugro acquired data from 368 CPT locations that were selected using the results of the Baseline survey and the interim soil provinces. These were used, along with the 2DUUHR data from both the Baseline and Mainlines surveys, for integration purposes to create a more confident geological ground model. Further information on this survey can be found in Section 2.2.2.1 and Full Site Geomodel with CPT data (Fugro, 2024) report.

Following the CPT campaign, between 27 February 2024 and 16 July 2024, Fugro undertook a borehole survey within Sub-area 1. Fugro collected samples and data from 69 borehole locations which include results from downhole sampling, downhole in situ testing (where applicable), borehole geophysical logging (where applicable), and laboratory testing. The data from these locations have been further integrated in this report to build on the initial integration from the CPT campaign.

Further details on the vessel and equipment used for the borehole campaign can be found in Section 2.2.2.2.

2.2 Acquisition Details

This section reviews the vessels used for the data acquisition and the output deliverables available to utilise in the integration reporting.

2.2.1 Geophysical Acquisition

2.2.1.1 Baseline Survey

The Baseline Survey was performed by the MV Arctic between 14 April and 19 April 2023. Figure 2.1 displays the survey track lines for the Baseline Survey. The data were acquired using multibeam echosounder (MBES), sub-bottom profiler (SBP) and 2D ultra high resolution (2D UHR) seismic. Further details can be found in the operations report (Fugro, 2023a).
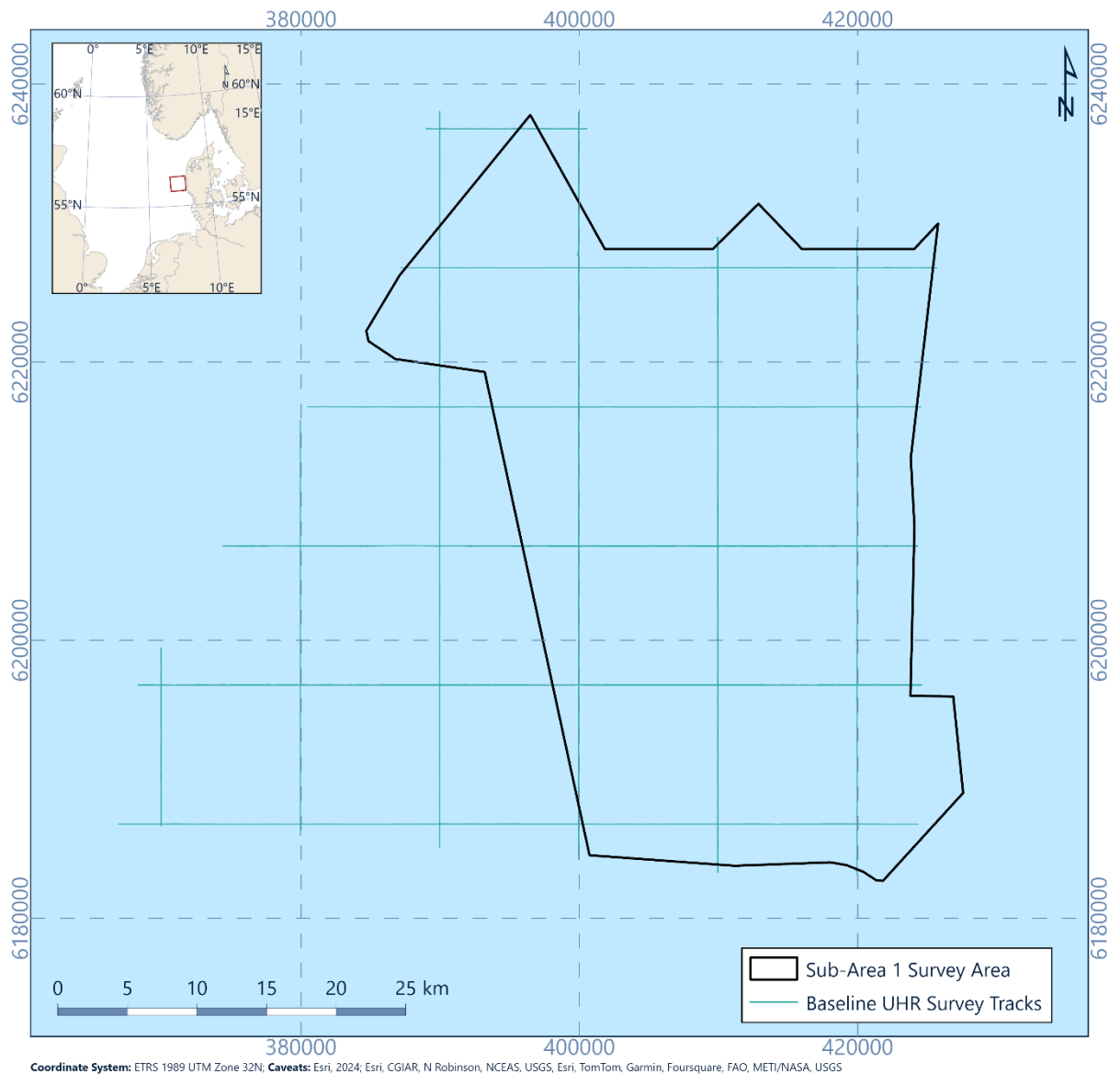
Figure 2.1: Baseline Survey track lines

2.2.1.2 Mainline Survey

The mainline geological survey was undertaken between 10 June and 13 November 2023 performed by vessel MV Fugro Pioneer. The data were acquired using multibeam echosounder (MBES), sub-bottom profiler (SBP) and 2D ultra high resolution (2D UHR) seismic. Further details can be found in the operations report (Fugro 2023b).

The MV Fugro Pioneer scope of work for this project was to survey the main lines and cross lines. The survey grid was covered by main lines with 250 m lines spacing and cross lines with 1 000 m line spacing. This is presented in Figure 2.2.
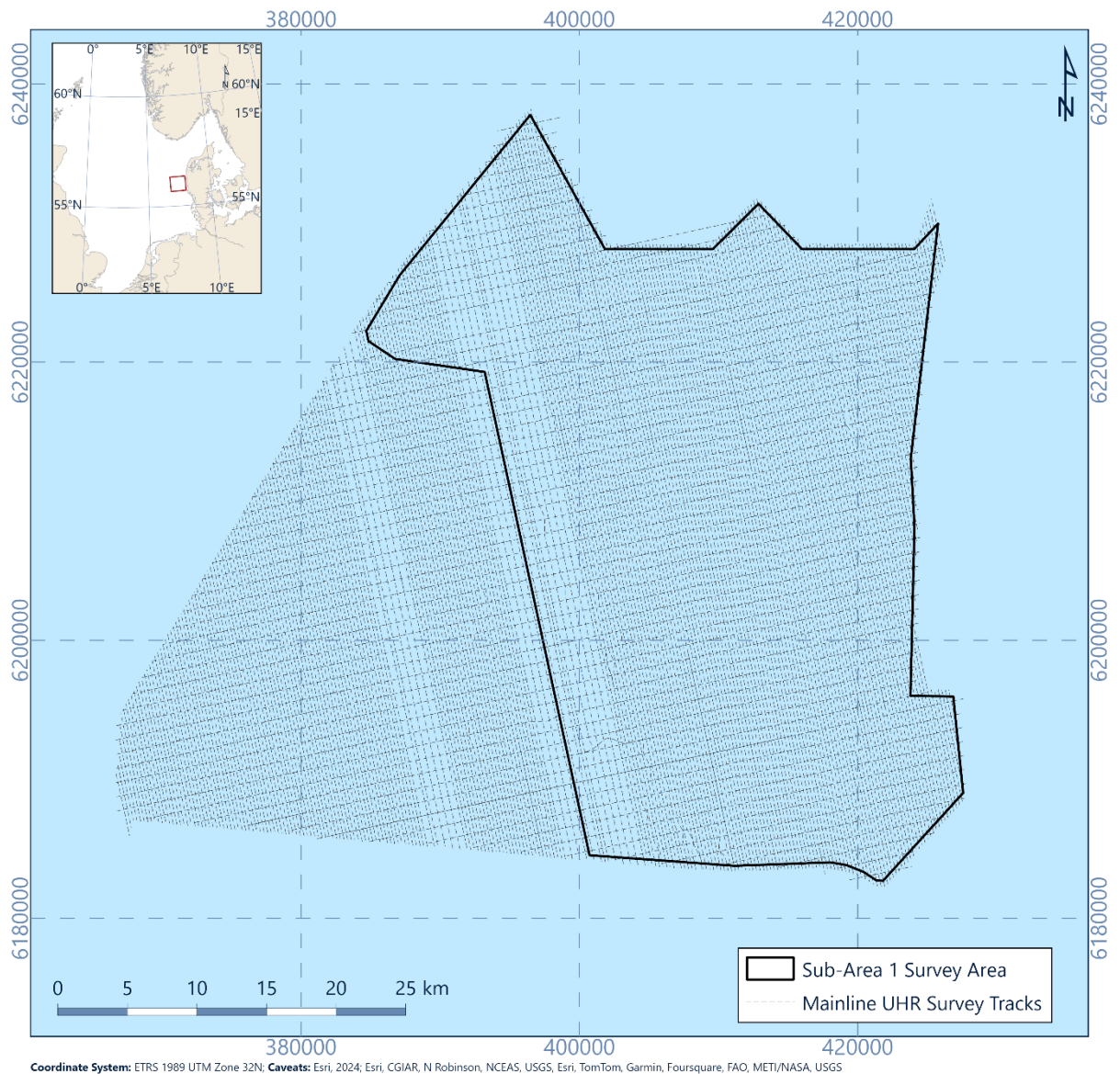
Figure 2.2: Mainline Survey track lines

2.2.2 Geotechnical Acquisition

2.2.2.1 CPT Campaign

The CPT campaign was undertaken between 27 October 2023 and 6 March 2024 by the MV Norman Mermaid.

The MV Normand Mermaid is a Norwegian-built multipurpose survey vessel. The vessel uses dedicated launch and recovery systems and a crane to efficiently deploy various systems through the moonpool and via the stern, such as Fugro's SEACALF® Mk V Deep Drive® unit, high performance corer®, vibrocorer, piston corer, box corer or lighter SEACALF® and SEASCOUT® units.

The MV Norman Mermaid scope of work for this project was to perform seabed CPT geotechnical investigation campaign for both Sub-Area 1 and 2. These included:

- 353 seafloor CPTs (Cone Penetration Tests);
- 15 SCPTs (Seismic CPTs); 12 of which included Seismic Velocity Tests (SVTs).

Figure 2.3 shows the geotechnical locations collected within both Sub-Area 1.
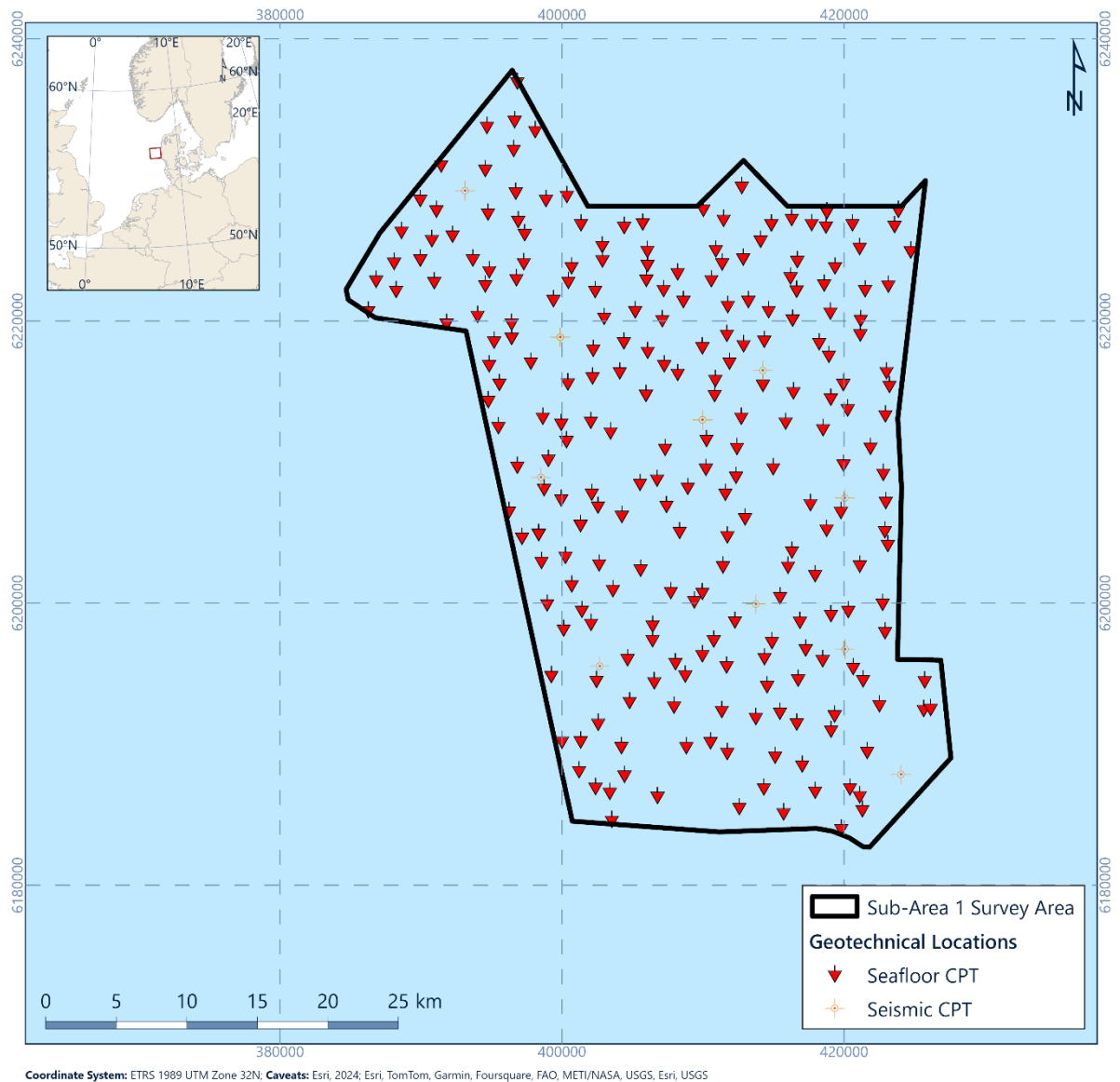
Figure 2.3: CPT and SCPT locations collected

2.2.2.2 Borehole Campaign

The Sub-Area 1 borehole campaign was undertaken between 27 February 2024 and 16 July 2024 utilising the following three vessels; Excalibur, Gargano and Fugro Voyager. Figure 2.4 presents the types of data acquired during the surveys and Figure 2.4 presents the boreholes and downhole CPT locations collected per vessel.
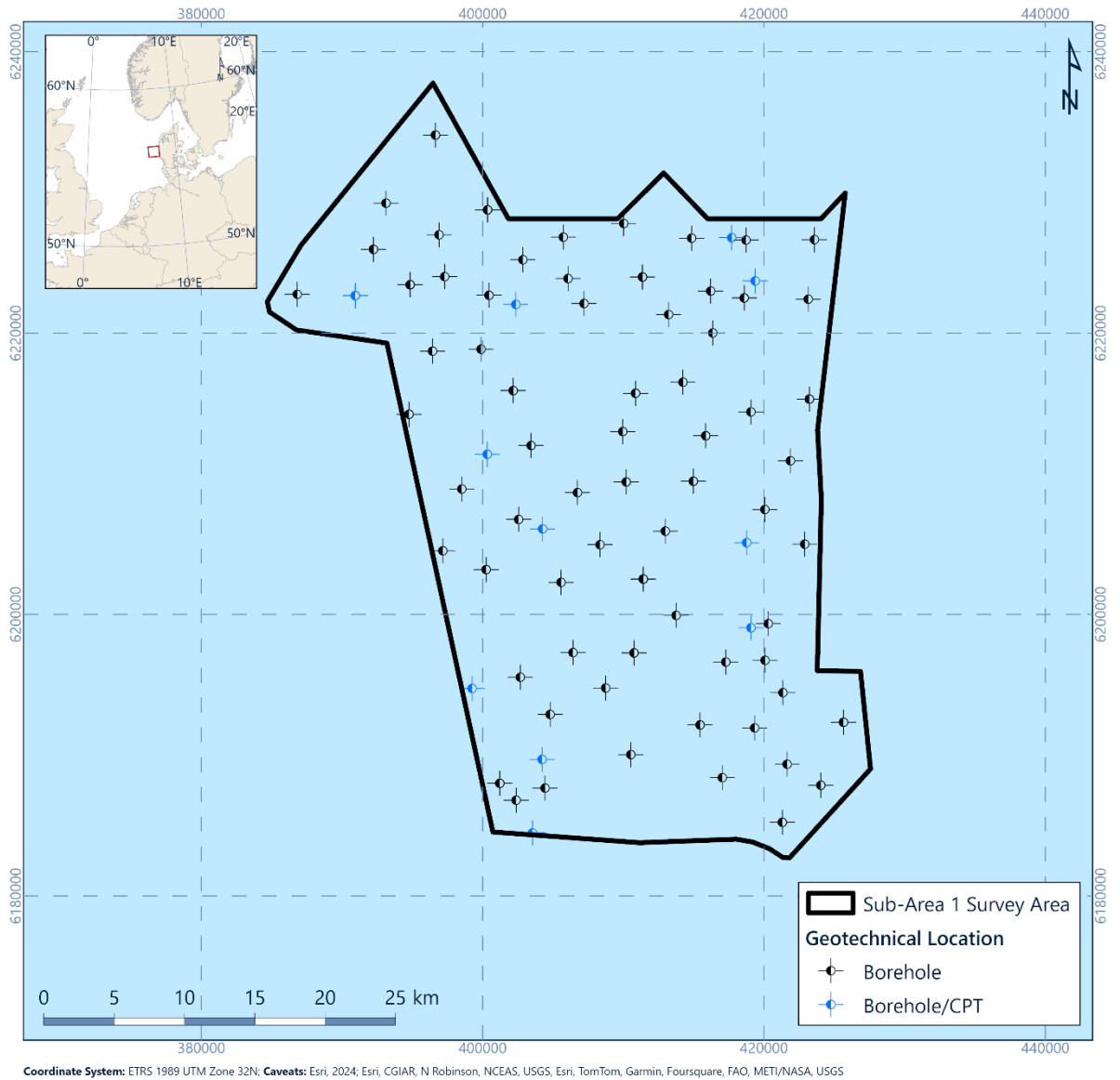
Figure 2.4: Location of borehole locations
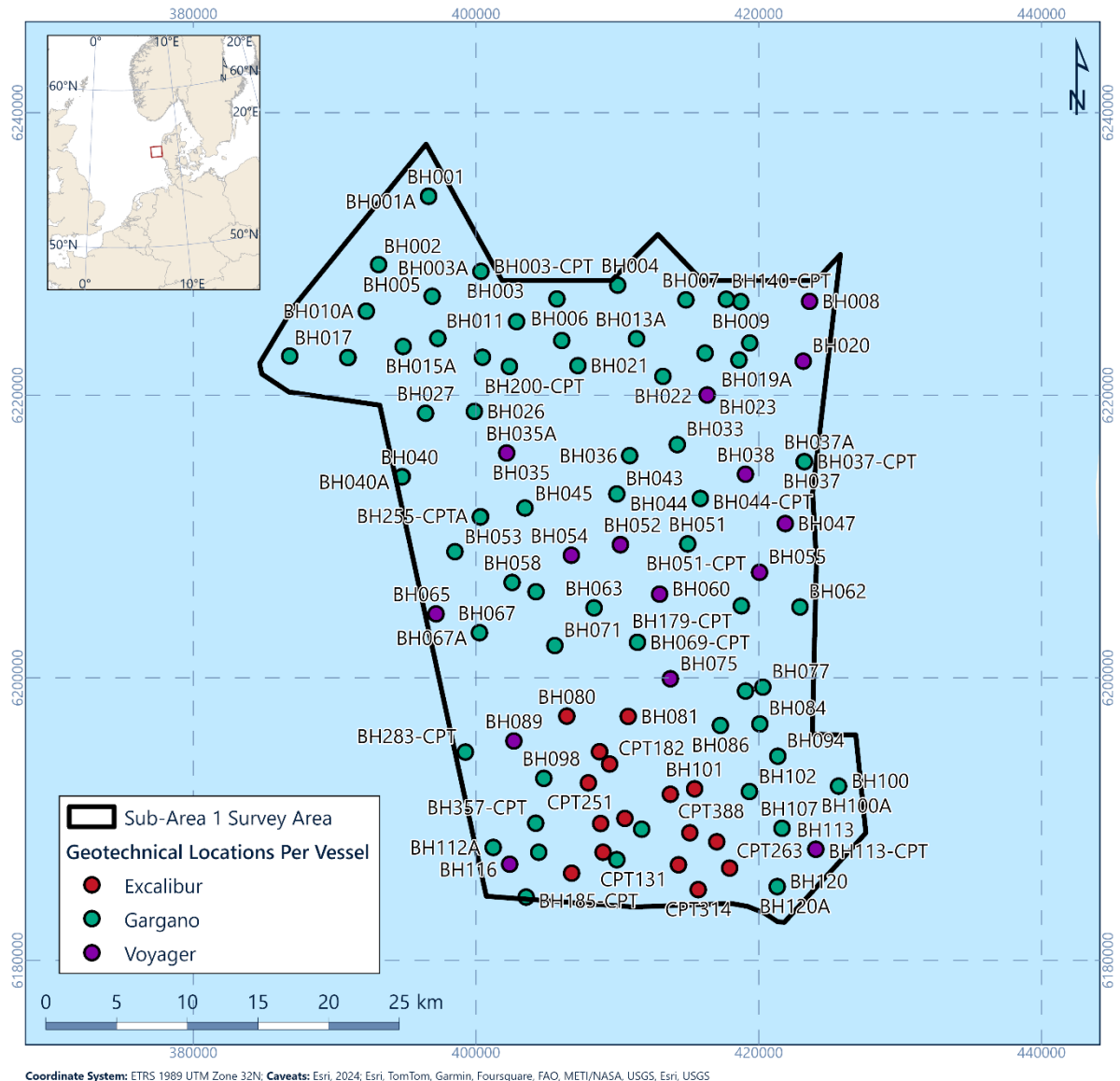
Figure 2.5: Borehole Locations collected per vessel

Excalibur

The Excalibur Barge is a Fugro owned and operated self-elevating platform adapted to specialist geotechnical investigation. The vessel uses a crane to efficiently deploy various systems through the moonpool. The Excalibur operated between 30 April 2024 and 25 June 2024.

The work scope performed by Excalibur in Sub-Area 1 comprises of:

- 16 CPT testing of the seafloor to target depth 55 m BSF;
- 6 geotechnical boreholes to a target depth of 70 m BSF;
- 2 geotechnical boreholes including blind drilling from seafloor to refusal depth of the seafloor CPT and downhole CPT to target depth 55 m BSF.

The Excalibur barge used the following equipment during the campaign; a Fraste CompactRotoSonic (CRS) XL 170 MAX DUO drill rig for drilling and downhole sampling activities. The rig has a pull down force capacity of 50 kN (with sonic mode active) or 55 kN. A single-wall core barrel was used to recover samples using the sonic drilling capability of the drill rig.

A jacking unit comprising a pair of hydraulic rams with a thrust capacity of 20 tonnes is mounted on a removable beam attached to a CR2 marine derrick positioned over the moonpool. CPTs were performed using Fugro Deepcone® piezocone penetrometers with an approximate tip area of 1500 mm^2.

The WISON® Deep Line tool comprises a hydraulic jacking unit with 36 mm OD push rod. The tool is lowered on a hydraulic-electric umbilical via a sheave mounted over the moonpool on a CR2 marine derrick and latches into Geobor S drill pipe. The tool provides a 1.5 m stroke and a thrust capacity of 100 kN which ensures the cone is pushed into the soil at a constant rate of 2 cm/s. CPTs were performed using standard piezocone penetrometers with an approximate tip area of 1000 mm2.

Further information on the equipment used on the Excalibur can be found in operations report for the jack-up (Fugro, 2024d).

Gargano

The MV Gargano is one of Fugro's most experienced DP2 drilling vessels. The vessel is equipped with a R50 heave compensated marine drill rig. The R50 is fitted with an automated tool handler mounted in the compensated working platform. The Gargano is maintaining an exemplary safety record and has a long track record of successfully completed site investigations for various clients in the North Sea, the Mediterranean and West Africa. These operations range up to 300 m below the seafloor in water depths up to 200 m. The Gargano undertook it's work scope activities between 01 March 2024 and 01 July 2024.

The work scope performed by Gargano in Sub-Area 1 comprises of:

■ Twenty-seven (27) borehole sampling (BH) locations;
■ Four (4) combined borehole sampling and down the hole CPT testing locations;
■ Eighteen (18) down the hole CPT testing locations.

During the campaign, the MV Gargano used a Fugro WIPSAMPLER®, which consists of a downhole jacking unit to which 1 m long Shelby tubes are attached and deployed from 'Gargano', for downhole sampling.

A WISON® MkV Cone Penetration (CPT) System deployed from 'Gargano' was used for downhole CPT testing. The WISON® consists of a wireline downhole jacking unit with a 3-metre stroke and a thrust capacity of 90 kN. The system was deployed through the moonpool of the vessel. CPTs were performed using Fugro Deepcone® cone penetrometers

with an approximate tip area of 1000 mm^2. Further details can be found in the ops report (Fugro, 2024e).

Voyager

The MV Fugro Voyager is a fit for purpose designed and constructed geotechnical drilling vessel that provides a stable platform capable of operating independently in remote regions around the world. The design of the Fugro Voyager allows integrated investigation methods to be deployed during one survey program. Fugro Voyager was operational on site between 12 March 2024 to 16 July 2024.

The work scope performed by Fugro Voyager in Sub-Area 1 comprised of:

- 28 geotechnical boreholes with semi-continuous sampling to target depth of 70 m.
  - with 10 boreholes with geophysical logging to target depth of 70 m.
- 2 geotechnical boreholes including blind drilling from seafloor to refusal depth of the seafloor CPT and downhole CPT to target depth 55 m BSF.
- 4 geotechnical boreholes with combined downhole sampling and downhole CPTs to a target depth of 55 m BSF.

Downhole sampling on the MV Fugro Voyager was performed using the Fugro WIPSAMPLER®, which consists of a downhole jacking unit to which 1 m long sample tubes are attached. A range of thin-walled and thick-walled Shelby tubes were supplied.

A WISON® MkV Ecodrive Cone Penetration (CPT) System deployed was used for downhole CPT testing. The WISON® consists of a wireline downhole jacking unit with a 3-metre stroke for CP10 cones (tip area 10 cm^2) cone or 1.5-metre stroke for CP5 cones (tip area 5cm^2). Further details can be found in the ops report (Fugro, 2024f).

Alongside the standard offshore laboratory equipment available on the Fugro Voyager, Fugro mobilised the "Enhanced Offshore Laboratory" (EOL). This allowed for the collection of additional geotechnical text data during the survey. As part of this the following tests were conducted:

- Particle size testing (via dynamic image analysis) – 340 tests;
- Min-max density test – 400 tests;
- Atterberg limits – 200 tests;
- Incremental loading oedometer tests – 140 tests.

EOL testing data has been utilised where applicable, with geotechnical characteristic values in Section 7 utilising this data.

2.3 Data Quality

2.3.1 Quality of Seismic Data

The quality of the SBP and 2D UHR seismic data was monitored throughout the survey and deemed to be good. The technical requirements of the survey with regards to resolution and penetration were met throughout the survey.

A typical penetration depth of 2D UHR seismic data was approximately 150 m BSF. Detailed description of the quality of the 2D UHR seismic data collected during the survey is presented in the seismic processing report attached to the whole site ground model report (Fugro 2024).

Comments on the quality of the SBP data are as follows:

- The penetration depth is closely related to the geology and may vary depending on lateral variation in sub-seafloor conditions. Typical penetration depth was approximately 10 m BSF with a maximum of approximately 20 m BSF;
- In relatively dense units composed predominantly of sand (e.g. Units U10, U35, U60 and U90), penetration was limited;
- In units where the soil conditions are expected to be richer in clay (e.g. Units U20, U30 and U50), penetration was greater;
- The first interpreted horizon below the seafloor (Horizon H10), which forms the base of Unit U10 (see Section 6.2) is always within the penetration depth of the SBP data.

2.3.2 Quality of Geotechnical Data

The quality of the geotechnical data was considered good for the purposes of the current work stage. For Sub-Area 1 geotechnical data includes the seabed CPT and SCPT data from the previous campaign, but also the borehole and selected downhole CPT data from this survey. Therefore, allowing visual unitisation and offshore laboratory testing.

Further details on the geotechnical data and its use are presented in Section 2.5.

2.4 Methodology

2.4.1 Seismic Interpretation

The following strategy was applied for SBP and 2D UHR seismic data interpretation:

- Compiling historical geotechnical, geophysical and geological data from client-provided sources, Fugro database, ongoing Fugro campaign and the public domain (Jensen et al., 2008; COWI, 2021; Fugro, 2023a);
- Loading SEG-Y files (2D UHR seismic and SBP data) in Kingdom Suite version 2022, SQL server express version 2016);
- Loading of seabed CPT data acquired by the M/V Normand Mermaid in Kingdom Suite;
- Loading of borehole data acquired by the M/V Gargano, M/V Fugro Voyager and the self-elevating platform Excalibur in Kingdom Suite;

- Interpretation of seismically distinct horizons, which forms bases of seismic units in the time-domain. The interpreted horizons take into account and were adjusted based on the available seabed CPT data and borehole data, where required;
- Identification and interpretation of key geological features, which can be potential (geo)hazards for offshore infrastructure.

Comments are as follows:

- Horizon H10 was interpreted on the SBP data. All other horizons were interpreted on the 2D UHR seismic data;
- In the areas where horizons are interpreted to be deeper than the maximum depth of penetration of the seismic data (e.g., H65, H70, H90), the horizon were picked at the base of the available seismic section;
- Where clear reflectors are present, the '2D Hunt' and 'Fill' options were used in Kingdom. These options follow the peak or through of each trace, resulting in high accuracy, but the reflector has a serrated appearance. Where these tools were less effective, i.e., where the reflector was less distinct or the boundary between units was in the form of a change in seismic character, horizons were picked manually;
- Time-to-depth conversion of horizons, grids and geological features interpreted on the SBP and 2D UHRS data used a constant velocity of 1730 m/s in the subsurface. This velocity was based on 141 seabed CPT's which were available at the time of determining the velocity model.
- Gridding of horizons was performed within Kingdom Suite 2022 with the following settings: minimum (0) curvature; midway (6) smoothness; cell size 5 m by 5 m; search distance 400 m; gridding extent controlled with polygons, which outline the area where the horizon is interpreted to be present;
- Gridding of seismic anomalies and acoustic blanking was performed within Kingdom Suite 2020 with the following settings: minimum (0) curvature; midway (6) smoothness; cell size 5 m by 5 m; search distance 150 m;
- Isochore grids were calculated by subtracting the grid of the top of the unit from the grid of the base of the unit;
- In the report main text, 'thickness' is used as a synonym to isochore.

2.4.2 Integration

Further integration of geophysical and geotechnical data followed the initial interpretation and integration of geophysical and CPT data to ensure that where available the geophysical interpretation considers the changes and updates in geotechnical properties. Details of the reporting for these work phases is presented in Table 1.2.

Interpretation of the geotechnical (CPT/SCPT and borehole) data was performed based on the previous and newly available geotechnical data (using CPT and borehole correlation and borehole description as presented in Section 6). A single geotechnical interpretation was carried out per geotechnical location, therefore in instances where multiple CPT tests or

boreholes were performed at the same location, a single geotechnical interpretation was performed for the location. The geotechnical interpretation considered changes in derived and measured parameters or changes in geotechnical descriptions that are considered significant and indicative of a change that could be expected to be present across a non-local area.

Final interpretations will be updated based on the collection of additional borehole data in Sub-Area 2, which will be collected during 2025.

Following further geotechnical interpretation, the integration process was followed to define the seismostratigraphic units which combine the geotechnical variations observed in the geotechnical data with seismic character changes.

This was done by importing the CPT and borehole data into the Kingdom project.

CPT log data and offshore laboratory testing included:

- Submerged unit weight (kN/m^3);
- Water content (%);
- Cone resistance (q_c);
- Sleeve friction (F_s);
- Pore pressure (u_2);
- Friction ratio (Rf).

Borehole data solely included formation tops as per geotechnical descriptions and unitization presented in the investigation results report (Fugro, 2024g).

As part of the assessment of the geotechnical data, significant geotechnical or lithological changes were unitised and identified in the data. These were then compared to the initial interpretation of the geophysical data. This process was carried out in near-real time to ensure that the work was updated as the data were collected. A process flow of the integration work is provided in Figure 2.5.
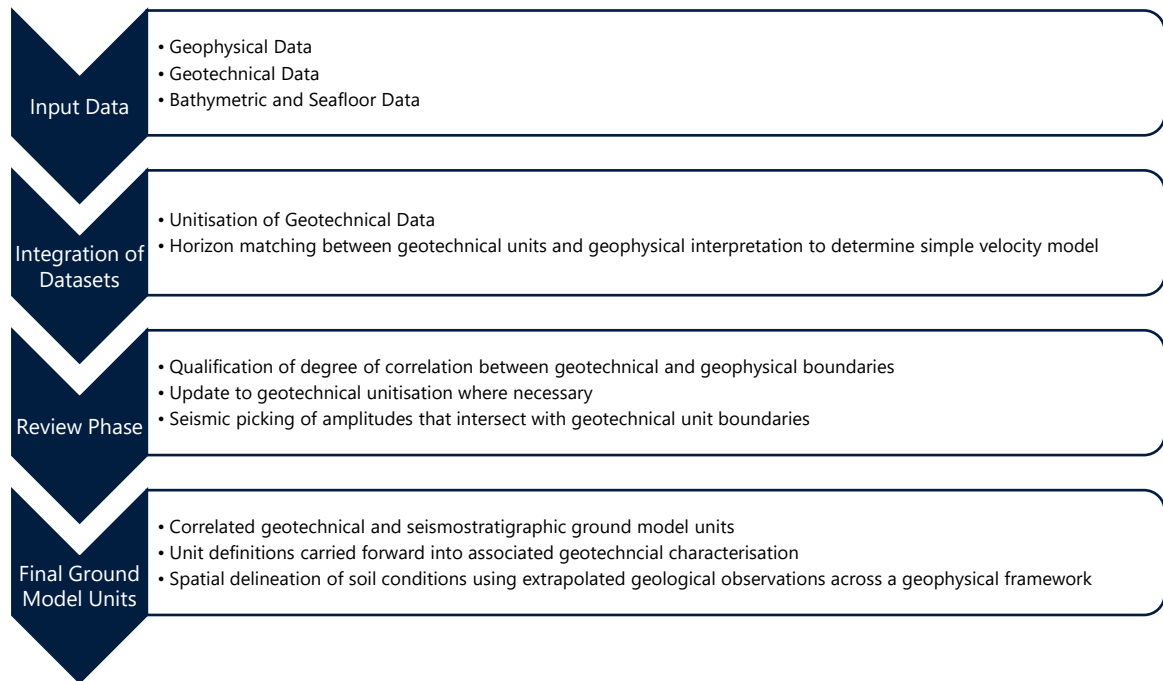
Figure 2.6: Integration of geotechnical and geophysical data workflow

Workshops between the geophysical and geotechnical interpretation teams were carried out with misalignments between the soil units and the interpreted horizons were addressed. Some formation bases were re-evaluated and horizons were partially adjusted. Discrepancy between geotechnical units and geophysical horizons can occur based on several factors. These include:

- Offset between geotechnical locations and geophysical survey data;
- Depth conversion of geophysical data;
- Gradational change between geotechnical properties.

As a result, some inconsistencies between geophysical changes and geotechnical units were observed. These are detailed in Section 6.2.

As part of this process, additional horizons were identified, which were initially not included in the interpretation. This horizon is outlined in Section 6.11.

2.5 Geotechnical Data for Integration

2.5.1 Geotechnical Correlations

From the in-situ Geotechnical data measured data were collected.

From these measured parameter values, derivation parameters are defined. Utilising the derived parameters, classification parameters can also be defined. The approach and methodology for the derivation of CPT and classification parameters is outlined in detail in Appendix B.

The undrained shear strength terms presented in this report are from ISO 14688-2:2018 (ISO,2018b), using the derived CPT parameters and offshore test data. These are presented in Table 2.1. Table 2.2 details the relative density terms for the description of sand units based on relative density ranges (Lambe & Whitman, 1969).

Table 2.1: Consistency terms for undrained shear strength (ISO, 2018a,b)

Strength Term (BS5930: 2010)	Undrained Shear Strength [kPa]
Extremely low	< 10
Very low	10 to 20
Low	20 to 40
Medium	40 to 75
High	75 to 150
Very high	150 to 300
Extremely high	300 to 600
Ultra-high	> 600

Table 2.2: Ranges of relative density for the description of sand units (Lambe & Whitman, 1969)

Relative Density Term	Relative Density [%]
Very Loose	0 to 15
Loose	15 to 35
Medium Dense	35 to 65
Dense	65 to 85
Very Dense	85 to 100
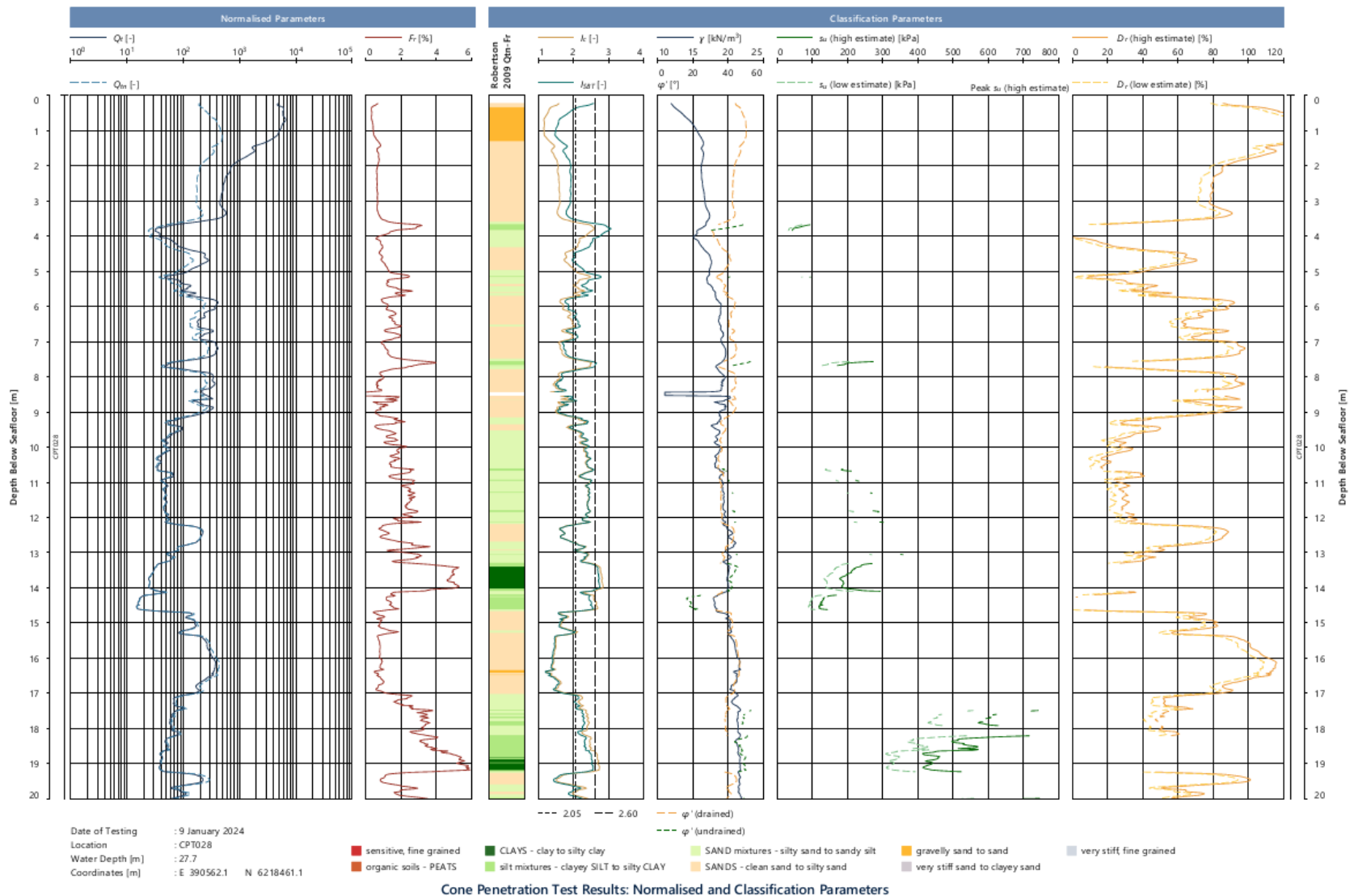
Figure 2.7: Presentation of CPT data including classification parameters

As outlined in Appendix B the methodology for the derivation of CPT and classification parameters based on the CPT data follows standards. Geotechnical properties described per unit in Section 6.

3. Regional Geological History

3.1 General

During the Cenozoic, up to 3 km thick sediment successions were deposited in the North Sea Basin (Knox et al., 2010). Cenozoic and Quaternary deposits increase in thickness from the margins of the North Sea Basin towards its centre (Arfai et al., 2018). The site is located at the margin of the North Sea Basin. Therefore, thinner Quaternary deposits are expected at the site when compared to the centre of the basin. In the North Sea Basin, the Cenozoic comprises three major depositional phases. Firstly, from the Palaeocene to Middle Pleistocene, deposition took place in marine and fluvio-deltaic depositional environments (Section 3.2). Secondly, during the Middle to Late Pleistocene, ice-sheets advanced across the North Sea Basin, resulting in complex glacial and periglacial depositional environments (Section 3.3). Finally, after the last glacial maximum, the North Sea Basin was flooded resulting in marine depositional environments (Section 3.4).

3.2 Palaeocene to Middle Pleistocene

During this period, a fluvial system (names 'Eridanos river') drained the Baltic Sea Basin in the direction of the North Sea Basin (Cohen et al, 2014; Gibbard and Cohen, 2015; Gibbard and Lewin, 2016). Throughout the Palaeocene to Middle Pleistocene, this river system with associated depositional environments prograded into the North Sea Basin. During the Miocene, marine clays were deposited at the site (Figure 3.1; EMODnet, 2023). Eventually, the prograding delta reached the site and marine and fluvial sands were deposited during the Early to Middle Pleistocene (Figure 3.2; Gibbard and Lewin, 2016).
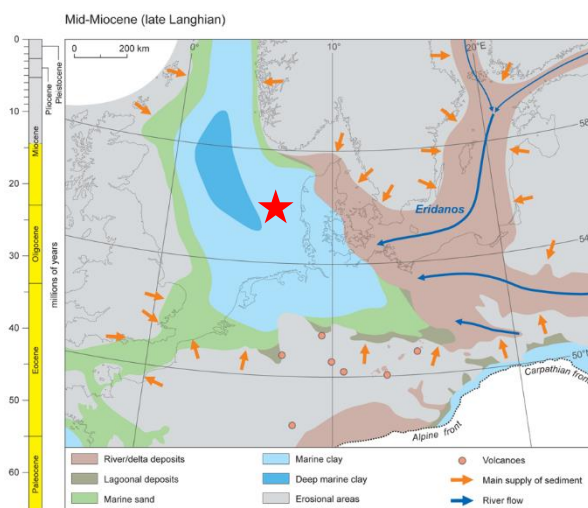
Figure 3.1: Palaeogeography of the North Sea during the Miocene (after Gibbard & Lewin, 2016). The red star indicates the location of the site
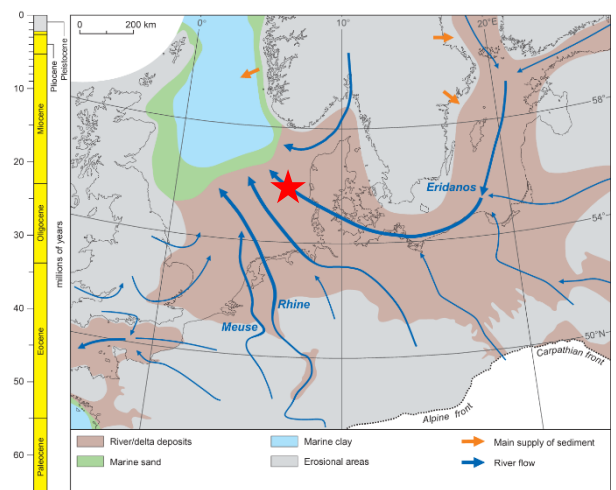
Figure 3.2: Palaeogeography of the North Sea during the Early to Middle Pleistocene (after Gibbard & Lewin, 2016). The red star indicates the location of the site

3.3   Middle to Late Pleistocene

During the Middle to Late Pleistocene ice-sheets advanced into the North Sea Basin during glacial periods, with intervening marine deposition during interglacial periods. Figure 3.3 illustrates the change in stable marine oxygen isotope ratios over time. A high ratio (grey in Figure 3.3) corresponds with glacial periods, a low ratio (white in Figure 3.3) corresponds with interglacial periods (Hughes et al., 2020). The named glacial and interglacial periods at the bottom of Figure 3.3 corresponds with geomorphologic units in north-west Europe and are likely to be recognized as morphologic units in the subsurface.
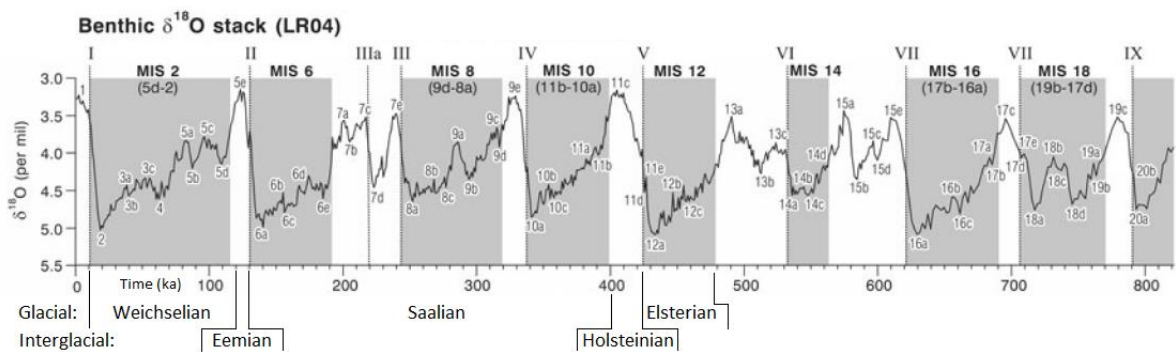
Figure 3.3: Graph illustrating the Marine Isotope Stages used for geological dating (modified after Hughes et al., 2020). The grey areas indicate glacial periods with increased presence of O_{18}, and the white areas indicate interglacial periods with lower O_{18}

3.3.1   Elsterian Glacial Period

The Elsterian glacial period corresponds with the MIS (Marine Isotope Stage) 12 (Figure 3.3); Gibbard and Cohen, 2015). The Elsterian is the first period of significant ice advance into the North Sea Basin. At its peak, the ice sheet covered Scandinavia, Britain, and most of the North Sea Basin, including the site (Figure 3.4). During this period subglacial tunnel valleys eroded into the underlying sediment (Figure 3.5). As the ice sheets began to retreat, the channels were progressively filled with clays, silts and sands which were subsequently overconsolidated by successive glacial stages (Huuse and Lykke-Andersen, 2000b; Kirkham et al., 2021).
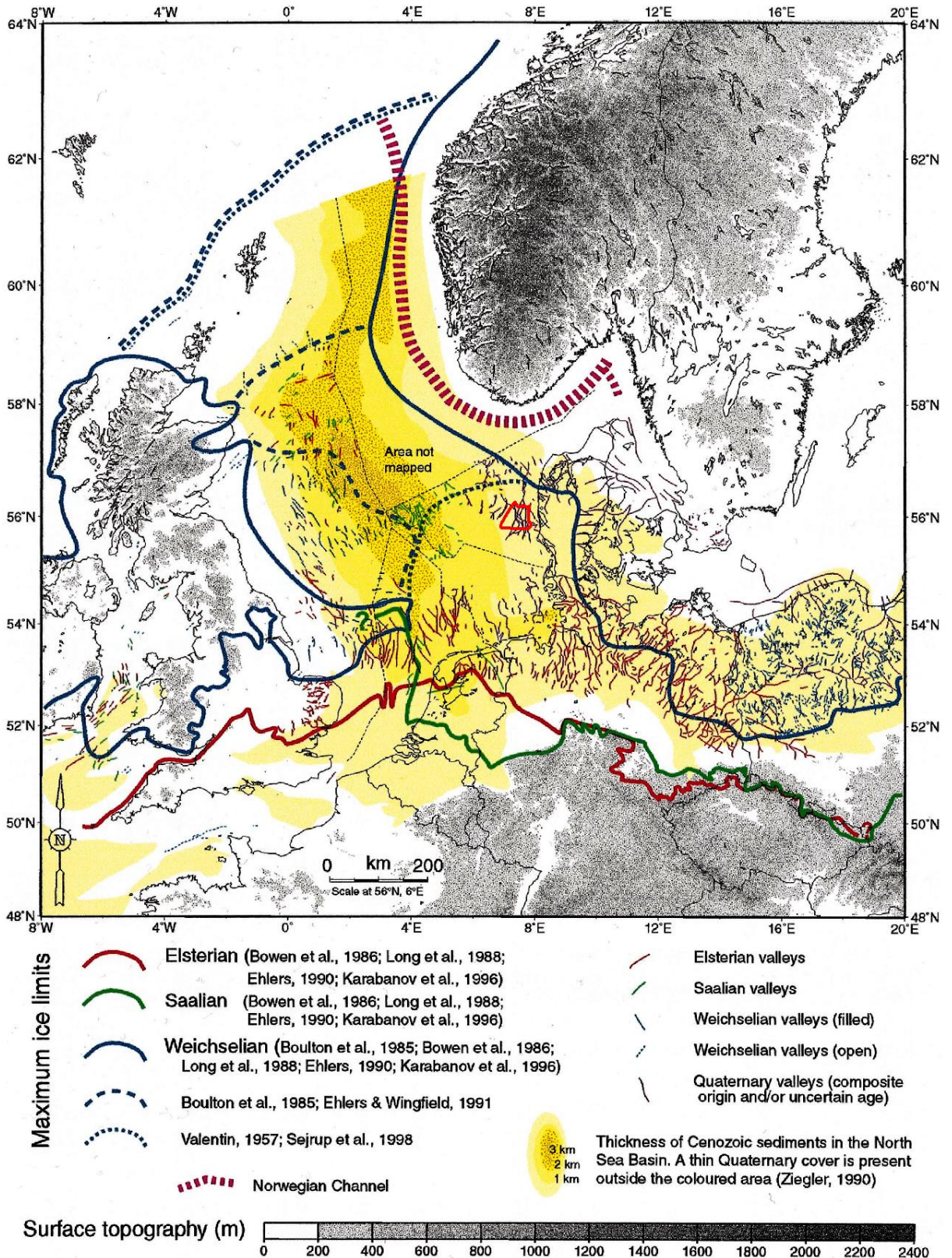
Figure 3.4: Extent of ice sheets and tunnel valleys during the Pleistocene in the North Sea (after Huuse and Lykke-Andersen, 2000b). The location of the site is indicated in red

The Formation of Tunnel Valleys
1. Heavily pressurised water beneath ice sheets incises weaker areas of the underlying sediment
2. As the overlying ice thickens and incisions develop, the hydrostatic pressure increases causing overdeepening of the tunnel valley
3. As the glacial stage weakens, variable subglacial and glacio-proximal sediments are deposited in tunnel valley bottoms

Figure 3.5: Glacial tunnel valley formation

3.3.2 Holsteinian Interglacial Period

The Holsteinian interglacial periods corresponds with the MIS 11 (Figure 3.3; Hughes et al, 2020, Cohen et al, 2014) and it follows the Elsterian glacial period. The Holsteinian represents a period of global rise in temperatures and the retreat of the Elsterian ice sheets. During the marine transgression the area offshore Denmark was most likely characterised by a shallow and later deep marine environments (Gibbard and Lewin, 2016). Deposits of the Holsteinian filled in the tunnel valleys of the Elsterian glacial period. In the Horns Rev area just south of the site, Holsteinian marine clays are reported to be present (Jensen et al., 2008).

3.3.3 Saalian Glacial Period

The Saalian glacial period comprises multiple stadials and interstadials and corresponds with the MIS 6 to MIS 10 (Figure 3.3; Lang et al, 2018; Hughes et al, 2020; Gibson et al, 2022). Specifically, three major stadial are identified: MIS 6, MIS 8, and MIS 10. These stadial are separated by interstadial: MIS 7 and MIS 9.

The coverage of the Saalian ice sheet varied significantly over time. Its' extend during the early and middle Saalian is poorly understood in Europe, because very little evidence has been confidently linked to the period (Batchelor et al, 2019; Hughes et al, 2020). During the late Saalian, the ice sheet reached its maximum extend. The Danish Sector of the North Sea was completely covered by ice at this time (Figure 3.4; Lang et al, 2018; Lang et al, 2019). Several types of deposits are related to the Saalian glacial period. Firstly, sets of tunnel valleys

were formed below the Saalian ice sheet (Huuse & Lykke-Andersen, 2000b; Nielsen et al., 2008). Secondly, sediments were deformed by glaciotectonism during the Saalian (Huuse and Lykke-Andersen, 2000a; Larsen and Andersen, 2005; Høyer et al., 2013; Winsemann et al., 2020; Cartelle et al., 2021). Glaciotectonism is the result of ice sheet advance folding previously deposited sediments. Lastly, several periglacial deposits are related to the Saalian glacial period, such as fluvial outwash plains (Friborg, 1996) and proglacial lakes (Lang et al., 2018). Onshore Denmark, in south-west Jutland, the Saalian landscape has been preserved as several 'hill islands' (bakkeø) comprising glacial till deposits (Figure 3.6; Friborg, 1996).

3.3.4 Eemian Interglacial Period

The Eemian interglacial period corresponds to MIS 5 (Figure 3.3; Cohen et al, 2022; Wohlfarth, 2013) and it followed on the Saalian glacial period. During the Eemian interglacial the global temperature increased, and the ice sheets melted, resulting in eustatic sea level rise (Figure 3.3). After a brief period of fluvial depositional environments at the end of the Saalian glacial period (Friborg, 1996), the Danish Sector of the North Sea was flooded (Figure 3.6). During this period there was a transition from lacustrine environments with peat deposition (Cohen et al, 2022) to open marine environments with clay deposition.
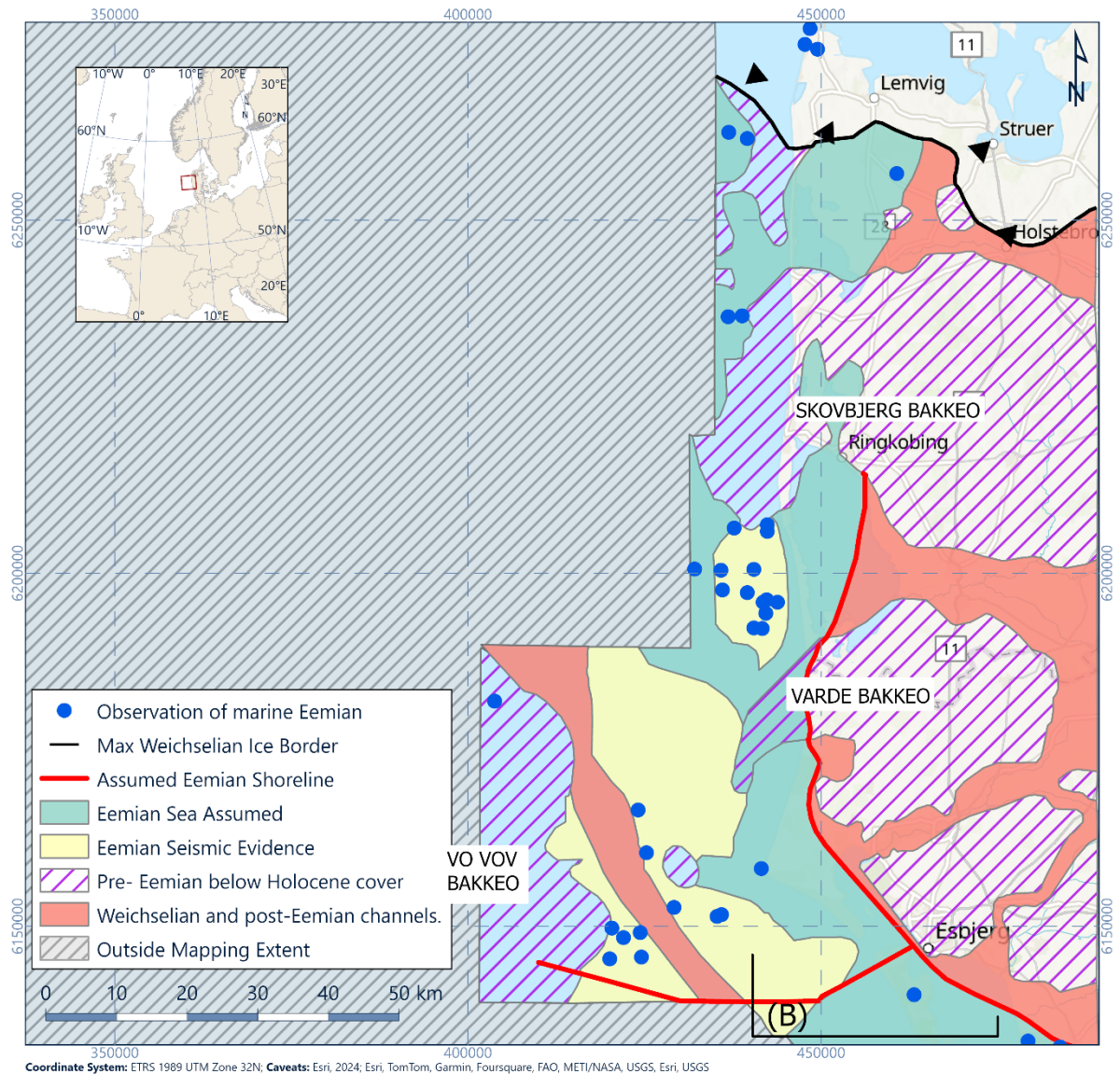
Figure 3.6: Map of south-western Jutland and nearshore area during the Eemian transgression. The location of the site is approximately underneath the legend (Konradi et al, 2005)

3.3.5   Weichselian Glacial Period

The Weichselian glacial period corresponds with MIS 2 and MIS 4 (Hughes et al, 2015) and it followed the Eemian interglacial period (Figure 3.3). During the Weichselian the global temperature and sea level began to decrease. As a result, the Danish Sector of the North Sea was exposed subaerially and fluvial systems developed (Figure 3.7 and Figure 3.8; Houmark-Nielsen, 2011; Möller et al, 2020).

Northern Europe was subjected to multiple major pulses of glacial expansion and retreat during this period (Houmark-Nielsen, 2011). During the Last Glacial Maximum, the ice sheet reached is maximum extend and reached Jutland and the northern part of the Danish Sector of the North Sea, however the site was not covered by the ice sheet (Figure 3.6).
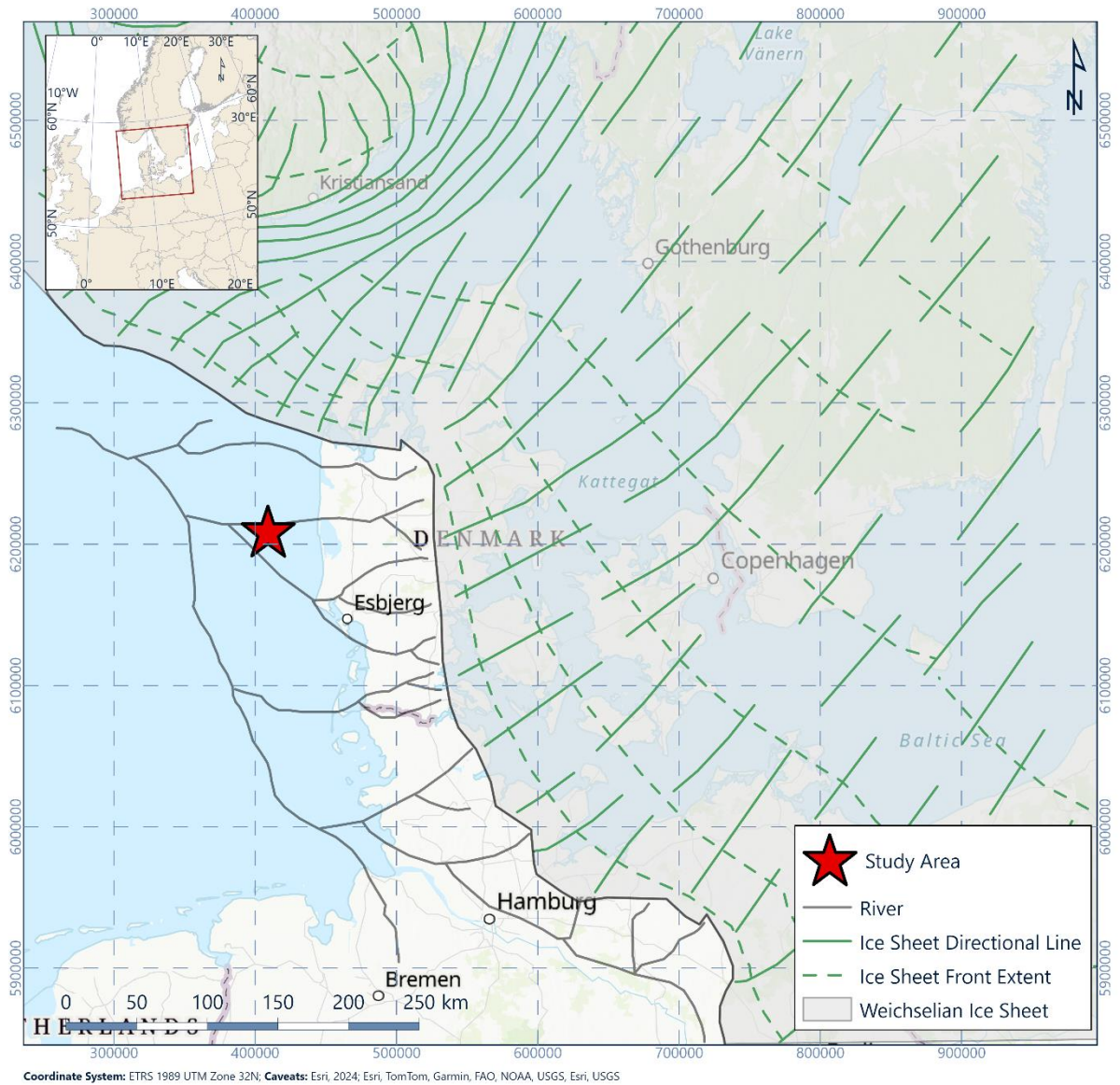
Figure 3.7: Denmark during the Last Glacial Maximum (22 to 20 kaBP), Houmark-Nielsen, 2011.
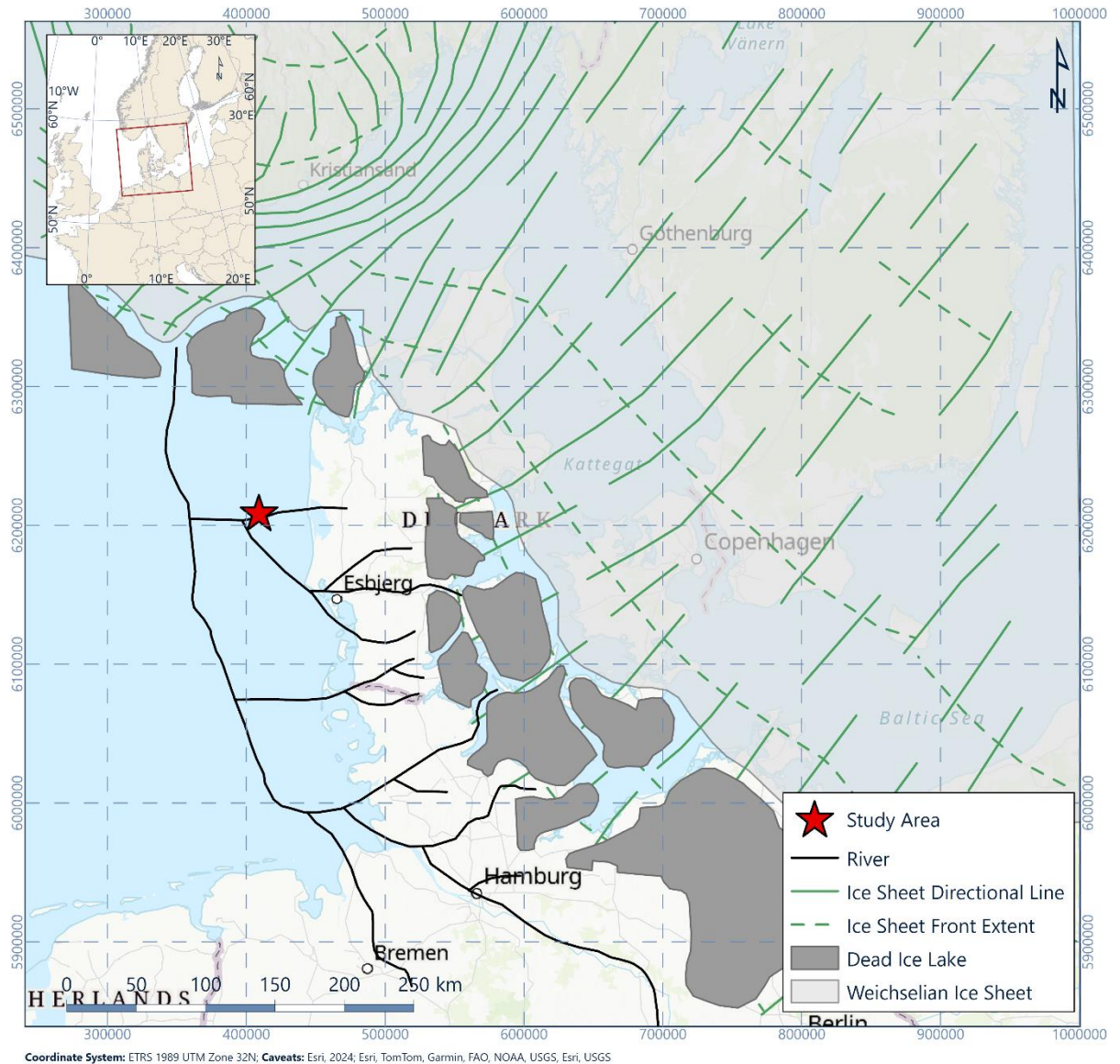
Figure 3.8: Denmark just after the Last Glacial Maximum (20 to 19 kaBP), Houmark-Nielsen, 2011.

3.4   Holocene

During the Holocene, global temperature levels started to increase. The melting of the ice sheets led to a rise in sea levels (Harrison et al, 2018) and the terrestrial environments were gradually flooded (Houmark-Nielsen, 2011; Möller et al, 2020). They gradually transitioned to lacustrine and coastal environments, and they were eventually drowned by the rising sea level at the start of the Holocene.

The coastline reached the site approximately 8000 years BP (Before Present; Figure 3.9; Walker et al, 2020). Approximately 7000 years BP (Walker et al, 2020) the site was completely drowned by the marine transgression and the depositional environment gradually changed to marine (Figure 3.10).

Figure 3.9: Map of the North Sea 8200 cal BP (Walker et al, 2020). The red star indicates the location of the site
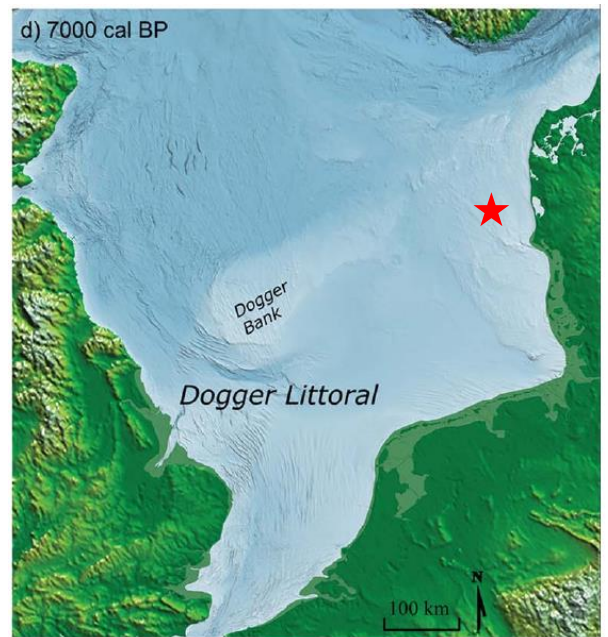
Figure 3.10: Map of the North Sea 7000 cal BP (Walker et al, 2020) . The red star indicates the location of the site

4. Seafloor Conditions

4.1 Bathymetry

From the final Ocean Infinity bathymetry data received, elevation ranges from -12.27 m to -33.51 m MSL present in Figure 4.1. A north-north-west to south-south-east oriented bank is present in the south of the site, with several additional south-west to north-east and north-west to south-east oriented ridges around it.
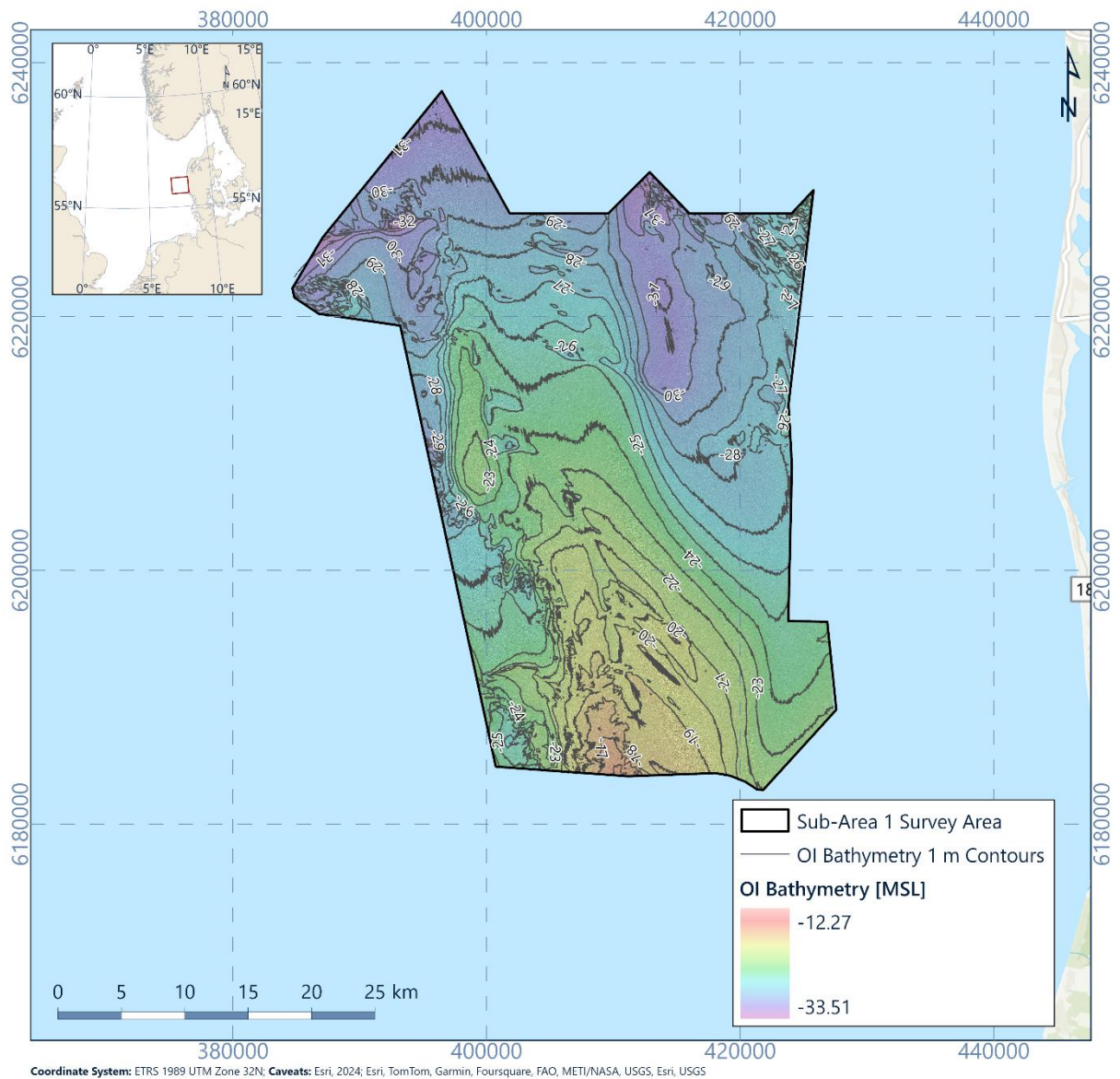
Figure 4.1: Bathymetry [MSL], provided by Ocean Infinity

4.2   Seafloor Gradient

The seafloor gradient, shown in Figure 4.2, was derived from the Ocean Infinity bathymetry. Primarily the site is <1° in gradient, with areas in the south-eastern corner and small sections in the north-east and north-west corners of the site sitting between 1° to 5°. There are very small isolated locations that area highlighted as > 5° in gradient, however these are not visible at this scale.
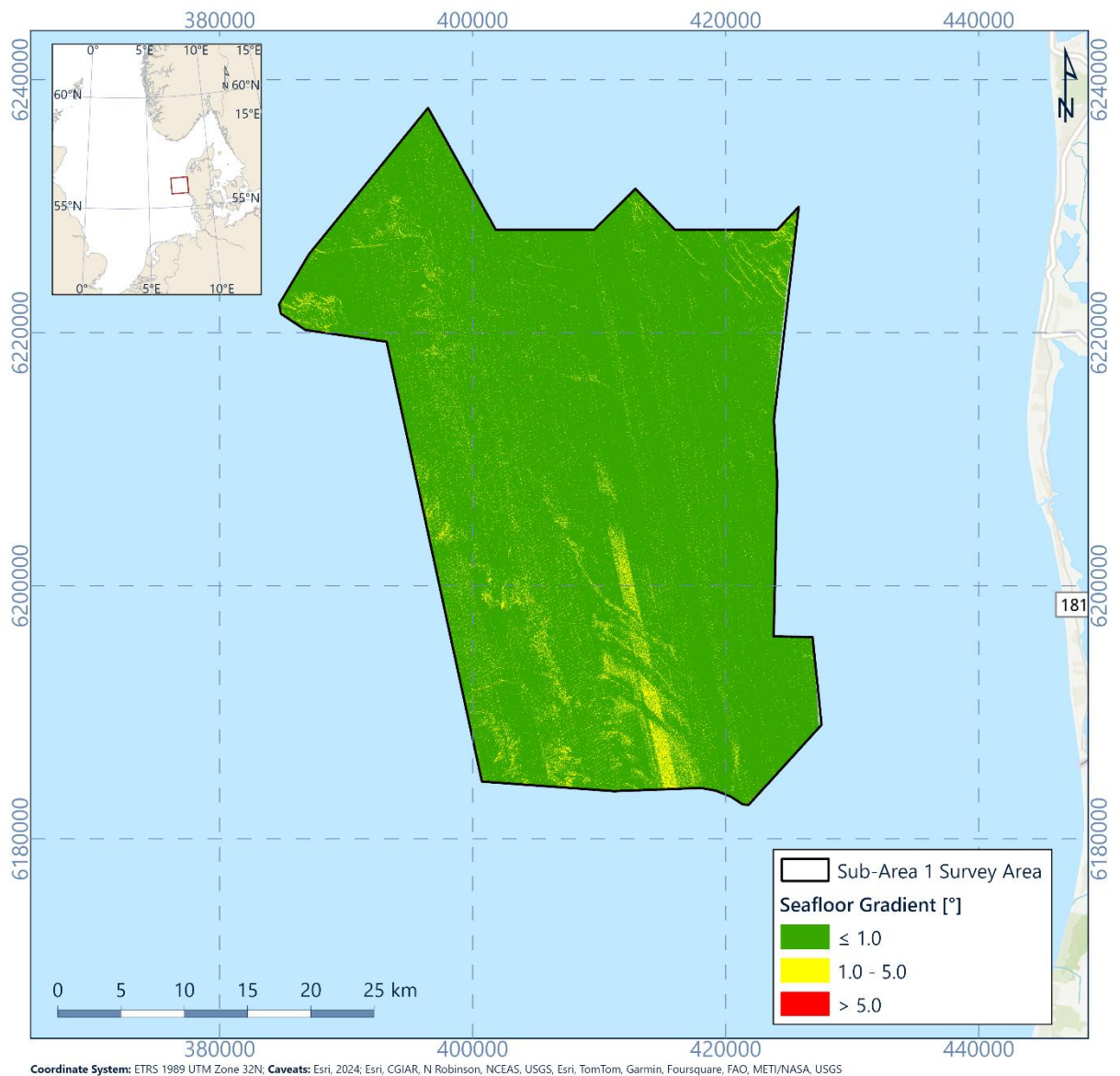
Figure 4.2: Seafloor gradient, derived from Ocean Infinity bathymetry

4.3   Seafloor Features

Figure 4.3 shows the seafloor interpretation produced by Ocean Infinity. Some integration of these seafloor sediments is provided in Section 6.
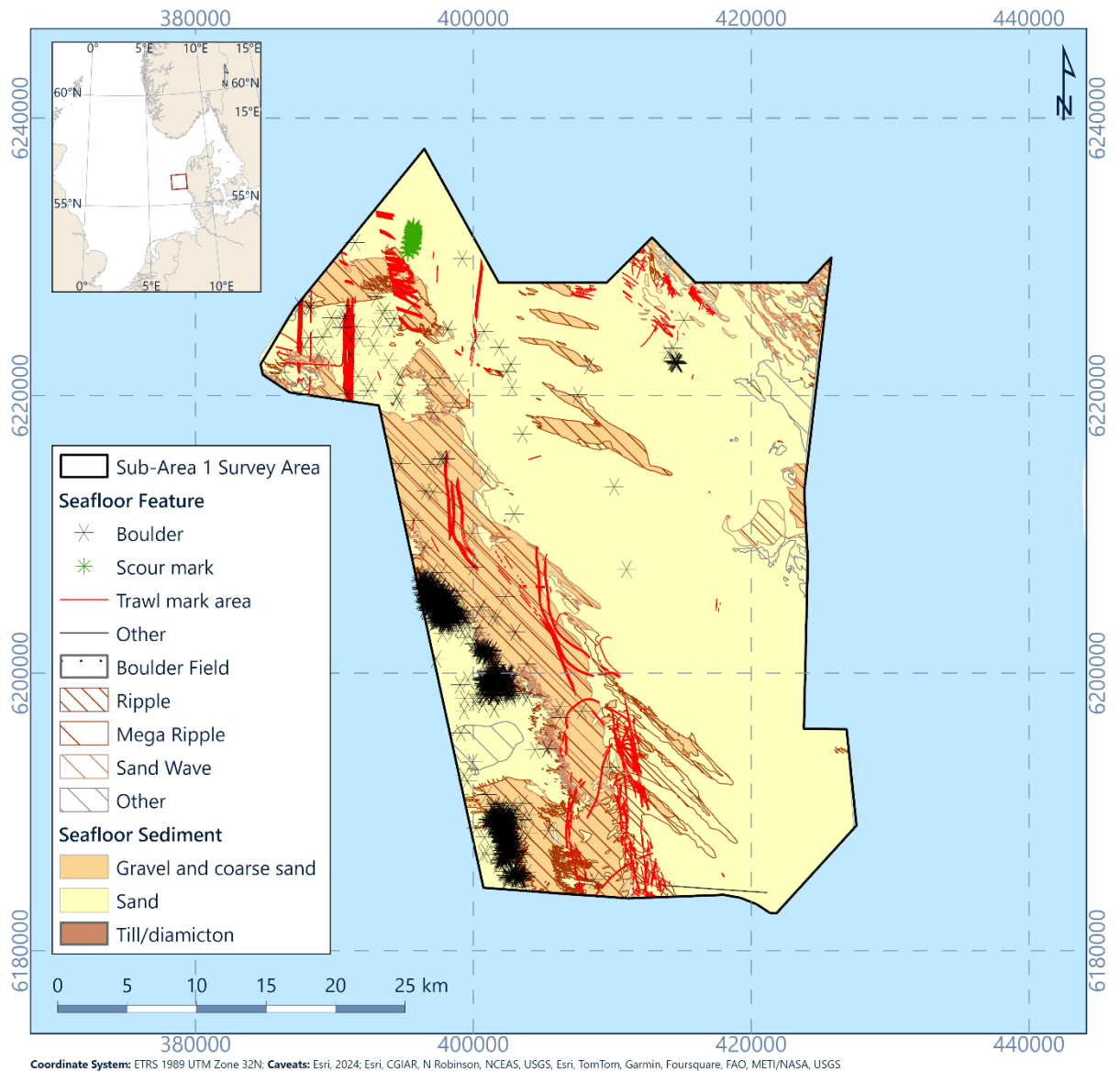
Figure 4.3: Seafloor Features, provided by Ocean Infinity

5. Conceptual Geological Model

The following section outlines how the geological model for the study area has been derived to delineate spatially the integrated geotechnical and geophysical datasets. As outlined in Section 2.4.2, a series of integrated units have been defined across the study area. As interpretation of geophysical data and geotechnical data were performed in conjunction with one another, by an integrated team, there was not initial interpretation of geotechnical data separately and then attempts to bring these separate work packages together.

Figure 5.1 and Table 5.1 provide a conceptual model of the interpreted horizons and associated units.

Eleven horizons were interpreted, which delineate the base of eleven units, with a further unit present below the basal horizon.

Depositional environment and age are interpreted based on the geological setting combined with the geophysical character of the seismic facies, soil type and geotechnical properties.

The following additional considerations should be noted:

- Units U35, U60, part of U65 and U90 are similar regarding environment of deposition and expected soil type. They are interpreted as fluvial deposits. As a result, their architecture is complex and locally difficult to distinguish from each other;
- Units U65 and U70 can both form the infill of tunnel valleys and are locally difficult to be distinguished from each other;
- Horizons are defined by the grids derived for each unit. In instances where geological processes associated with the units are expected to be variable and complex, grids may simplify certain units. This is likely the case for Unit U20;
- The previous two points are especially valid in the west of the site where these units are relatively thin and only locally present.
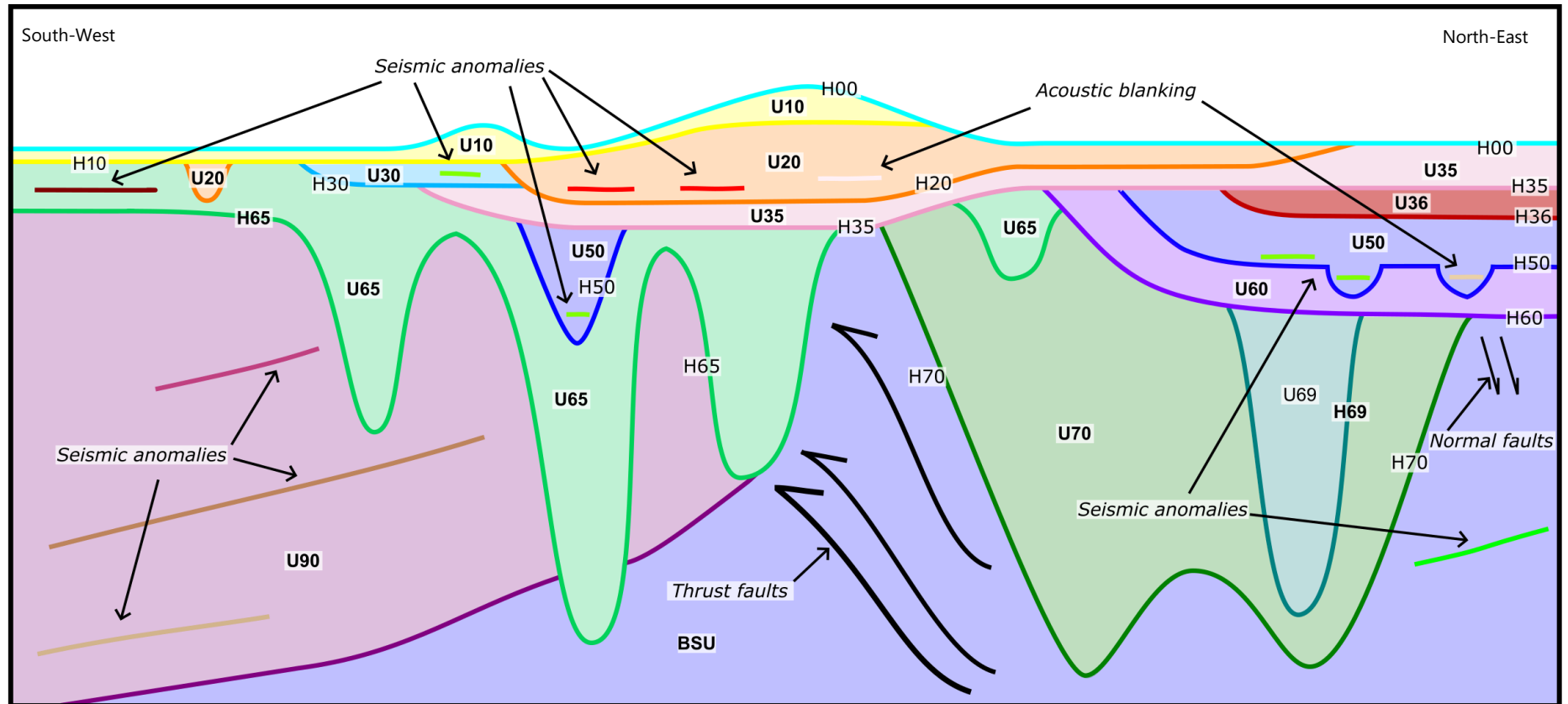
Figure 5.1: Conceptual model of the interpreted horizons and units in the top 200 m

Table 5.1: Overview of the interpreted horizons and soil units

Unit	Horizon [Colour*] / Base	Seismic Character	Soil Type†	Depositional Environment‡	Age‡	Stress History[x]
U10	H10 [LightYellow]	Acoustically transparent with point reflectors	SAND, fine to coarse, poorly sorted to well-sorted, slightly silty to very silty, occasionally slightly gravelly, with frequent fine-grained organic matter, with few to occasionally many shell fragments, occasionally with mica crystals, light olive brown to very dark grey, non-calcareous	Marine	Postglacial	A
U20a	H20 ^ [Orange]	Stratified to acoustically transparent; locally forms channel infill	SAND, fine to medium, sorted, slightly silty to very silty, occasionally clayey, occasionally slightly gravelly, with frequent fine-grained organic matter, with few to occasionally many shell fragments, olive grey to very dark grey, non-calcareous locally calcareous	Freshwater to Marine	Postglacial	A
U20b			SAND, fine to medium, poorly sorted to sorted, slightly clayey to clayey, slightly silty to very silty, occasionally with fine-grained organic matter, with few shell fragments, occasionally with few mica crystals, grey to dark grey, non-calcareous to slightly calcareous transitioning to CLAY, low to high plasticity, silty, slightly sandy to sandy, with few pockets of fine-grained organic matter, with few shells and shell fragments, olive grey to very dark grey, slightly calcareous transitioning to PEAT, slightly decomposed, occasionally decomposed to strongly decomposed, clayey, occasionally sandy to very sandy, dark brown to black			
U30	H30 [DeepSkyeBlue]	Complex – stratified to chaotic, with locally internal erosion surfaces and high amplitude positive polarity internal reflectors	SAND, fine, occasionally fine to medium, poorly sorted to sorted, silty, with few fine-grained organic matter, light olive brown to very dark grey, non-calcareous to slightly calcareous, with a thick to very thick bed of CLAY, low to high plasticity, silty, with pockets of fine-grained organic matter, with mica crystals, dark grey to very dark grey, calcareous	Meltwater / Freshwater	Glacial (Weichselian)	B1
U35	H35 [LightOrchid]	Complex with locally internal erosion surfaces and high amplitude positive polarity internal reflectors; locally forms channel infill	SAND, fine to medium, occasionally coarse, sorted, slightly silty to silty, slightly gravelly to gravelly, with fine-grained organic matter, occasionally with mica crystals, grey to dark grey, non-calcareous to slightly calcareous, with occasional thick beds of CLAY, low to medium plasticity, slightly to very sandy, occasionally silty, grey to dark grey, slightly to highly calcareous	Meltwater	Glacial (Weichselian)	B1

FUGRO

Unit	Horizon [Colour*] / Base	Seismic Character	Soil Type[†]	Depositional Environment[‡]	Age[‡]	Stress History[x]
U36	H36 [Maroon]	Stratified, locally with clinoforms	SAND fine to medium, sorted, slightly silty to very silty, occasionally slightly gravelly, occasionally with pockets of fine-grained organic matter, occasionally with few shells and shell fragments, greenish grey to dark greenish grey, non-calcareous to slightly calcareous with occasional very thick beds of CLAY, low to medium plasticity, slightly to very silty, occasionally sandy, with pockets of fine-grained organic matter, with few shells and shell fragments, greenish grey to dark greenish grey, slightly calcareous to calcareous	Marine	Glacial (Weichselian)	B1
U50a	H50 ^ [Blue]	Acoustically transparent; locally forms stratified channel infill	CLAY, low to high plasticity, slightly to very silty, sandy to very sandy, occasionally slightly gravelly, with pockets of fine-grained organic matter, with few shell fragments, dark to very dark grey, slightly calcareous to calcareous	Marine	Interglacial (Eemian)	B1
U50b			basal thick bed of SAND, fine to medium, poorly to well sorted, silty to very silty, occasionally with shell fragments, grey to dark grey, non-calcareous to calcareous			
U60	H60 [Violet]	Complex – with internal erosion surfaces and high amplitude positive internal reflectors; locally forms channel infill	SAND, fine to medium, occasionally coarse, poorly sorted to sorted, occasionally well sorted, occasionally slightly silty, occasionally slightly gravelly to gravelly, with few pockets of fine-grained organic matter, with rare wood fragments, occasionally with few shell fragments, occasionally with mica crystals, grey to dark grey, non-calcareous to slightly calcareous, with a basal medium bed to thick bed of GRAVEL, fine to coarse, unsorted to poorly sorted, occasionally sandy to very sandy, multi-coloured, non-calcareous	Meltwater	Glacial (late Saalian)	B2
U65	H65 [MediumAquaMarine]	Variable from acoustically transparent, stratified to acoustically complex with internal erosion surfaces and inclined stratification	Thicky to very thickly interbedded CLAY, low to high plasticity, sandy to very sandy, occasionally slightly silty to silty, occasionally slightly gravelly to gravelly, with traces of fine-grained organic matter, with traces of shell fragments, occasionally with mica crystals, sark grey to very dark grey, slightly calcareous to highly calcareous and SAND, fine to medium, occasionally coarse, poorly sorted to sorted, slightly silty to silty, occasionally clayey to very clayey, occasionally with few pockets of fine-grained organic matter, with traces of wood fragments, with rare laminae of peat, occasionally with few shell fragments, grey to dark grey, non-calcareous to slightly calcareous	Marine Freshwater Meltwater Glacier	Glacial (Saalian)	C1
U69	H69 [DarkCyan]	Well stratified. Forms upper part of tunnel valley infill	CLAY, low to high plasticity, occasionally very high plasticity, slightly to very silty, sandy to very sandy, occasionally slightly gravelly, with few pockets of silt or sand, occasionally with few shell fragments, with few mica crystals, dark greenish grey to dark grey, calcareous	Lacustrine?	Interglacial (Holsteinian)	C1

FUGRO

Unit	Horizon [Colour*] / Base	Seismic Character	Soil Type[†]	Depositional Environment[‡]	Age[‡]	Stress History[x]
U70	H70 [DarkGreen]	Acoustically chaotic. Forms lower part of tunnel valley infill	medium to very thickly interbedded CLAY, low to high plasticity, occasionally very high plasticity, sandy to very sandy, occasionally slightly silty to silty, occasionally slightly gravelly, with few pockets of silt or sand, with few pockets of fine-grained organic matter, occasionally with mica crystals, blocky or slickensided, dark grey to very dark grey, slightly calcareous to calcareous and SAND, fine to medium, occasionally coarse, poorly sorted to sorted, slightly silty to very silty, occasionally slightly clayey to clayey, occasionally slightly gravelly to gravelly, with few laminae of fine-grained organic matter, occasionally with layers and laminae of clay, grey to dark grey, non-calcareous to slightly calcareous, occasionally with STONES, occasionally with basal thick to very thick beds of CLAY TILL to SILT TILL, low to high plasticity, occasionally very high plasticity, slightly sandy to sandy, slightly gravelly to gravelly, with few pockets of sand, dark greyish brown to very dark greyish brown, calcareous	Marine Freshwater Meltwater Glacier	Interglacial (Holsteinian) and Glacial (Elsterian)	C2
U90	H90 [DarkMagenta]	Complex – chaotic to stratified (horizontal and inclined reflectors), with internal erosion surfaces	SAND, fine to medium, occasionally coarse, sorted, occasionally slightly silty to silty, occasionally slightly gravelly, with few laminae of fine-grained organic matter, grey to dark greyish brown, non-calcareous	Meltwater to freshwater	Glacial (Pre-Elsterian)	C2
BSU	N/A [Dark Blue]	Well stratified, locally the stratification is less well defined	medium to very thickly interbedded CLAY, medium to high plasticity, slightly silty to silty, occasionally slightly sandy, occasionally slightly gravelly, with few fine-grained organic matter, with few laminae of silt, occasionally with few shell fragments, slickensided, very dark grey to black, non-calcareous and SAND, fine, poorly sorted to well sorted, very silty, occasionally very clayey, occasionally slightly gravelly, with laminae of clay and silt, grey to very dark grey, non-calcareous to slightly calcareous	Marine	Miocene	D

Notes
* - Colour nomenclature follows Kingdom project
† - Soil type based on borehole data collected in sub area 1
‡ - Depositional Environment and Age according to the Danish Standard (Larsen et al., 1995)
x - A: Normally consolidated; B: Possibly overconsolidated as a result of subaerial exposure; C: Overconsolidated as a result of glacial loading; D: Pre-Quaternary, therefore possibly lithified; Number is the number of subaerial exposures or number of periods with ice cover
^ - no single horizon can be mapped to delineate the sub geotechnical units

FUGRO

6. Integrated Geological Model

6.1 Introduction

The following section outlines the spatial geological model associated with the integration of datasets at the North Sea 1 site. Integration plates are provided in addition to other charting deliverables. Each unit is presented in Sections 6.3 to 6.14, with further details presented in charting deliverables. An overview of charts associated with the integrated geological model are presented in Section 9.

6.2 Integration of Datasets Confidence and Uncertainties

The exercise of integration of datasets and the creation of geological units across the study area is outlined in the integration methodology (Section 2.4.2). The following section outlines the uncertainty in the model after this process. Some uncertainty is inherent in the modelling work as a result of the coverage of datasets.

Integration charts are provided as plates at the end of the report to overview the location specific integration.

6.2.1 Gridding of Units

Gridding of integrated geophysical horizons has been performed as part of the spatial ground modelling. Further details on the approach to gridding is outlined in Section 2.4.1, however some uncertainty can be expected based on the density of input datasets.

In limited areas of the Sub-Area1 site, line spacing of inline 2DUHR data was greater than the 250 m plan. In the west of the site this is visible where data collection line spacing was increased to 500 m. In addition, in limited localised areas within the study area, line spacing is greater than 250 m associated with acquisition challenges and limited infill opportunities. This results in greater extrapolation within grid data and may result in greater uncertainty in spatial model units. The line plan is presented in Figure 6.1, and shows areas of missing inlines.
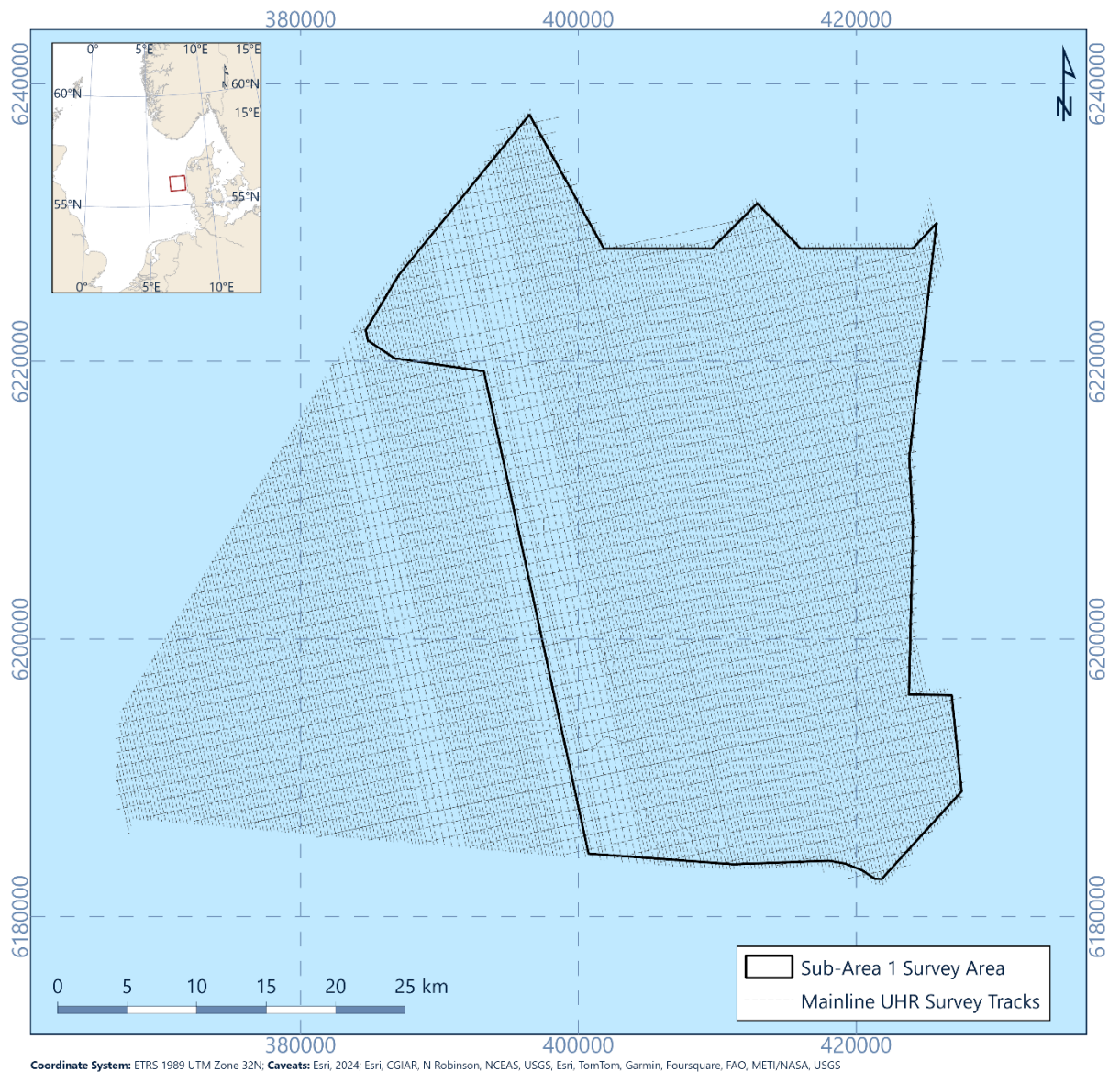
Figure 6.1: Line plan

In addition, units which have a channelised nature are likely to have greater uncertainty in the extrapolated grids. An example of this challenge is presented in Figure 6.2. This is expected to lead to greater horizontal and vertical uncertainty in the model. This is of particular challenge when there are larger depth changes over a short distance and when changes in depth are parallel with inline orientation.
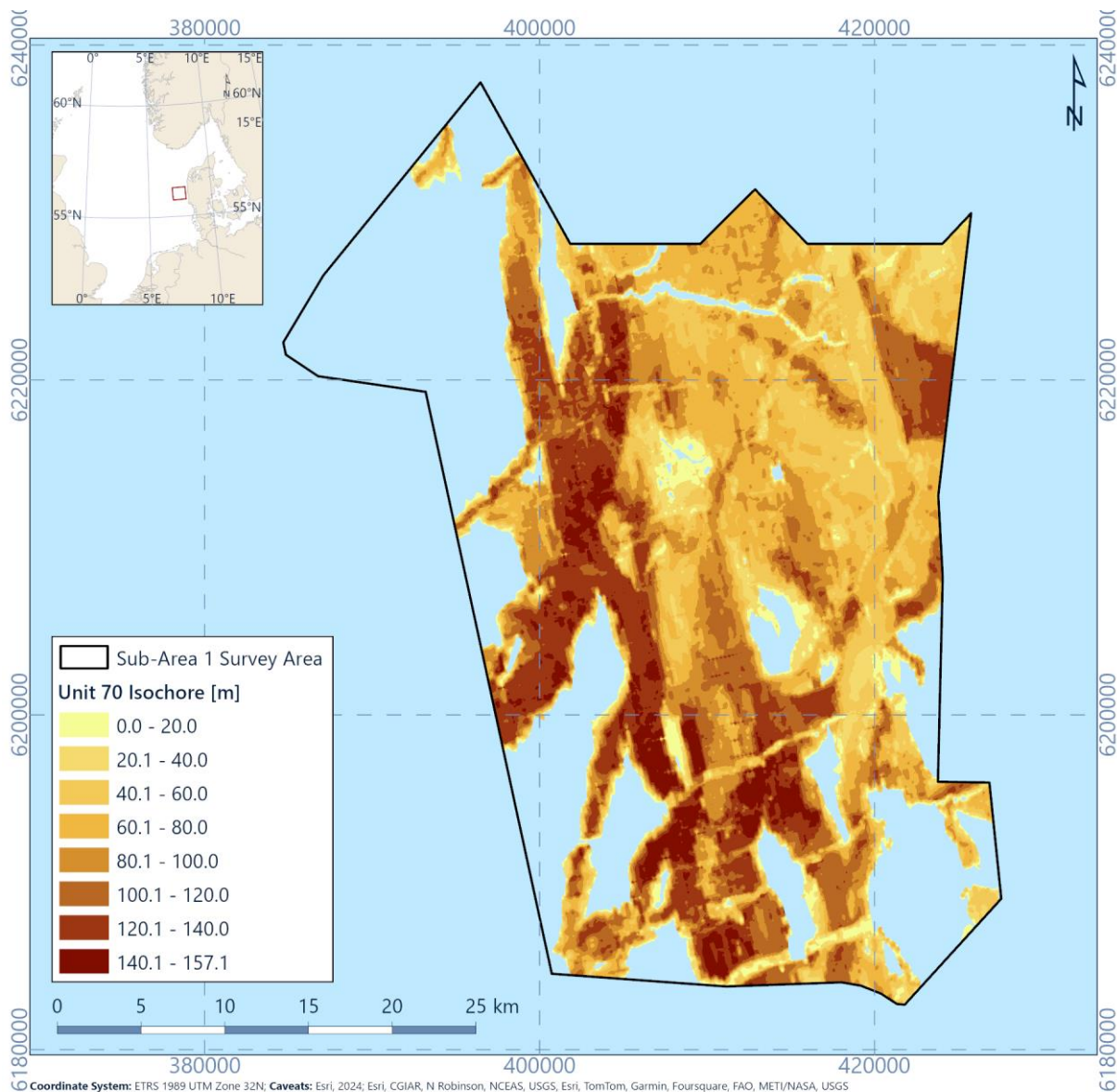
Figure 6.2: Gridding around channelised units

It should also be noted that the base of channelised units often have highly complex geometries when considering the likely depositional processes, therefore it is unlikely that 2D data acquisition will fully capture these complexities.

6.2.2 Time Depth Conversion

Current geophysical data has been depth converted as outlined in Section 2.4.1. This depth conversion has utilised a single seismic velocity of 1730 m/s. This depth conversion value was selected based on correlations between geotechnical and geophysical data for all units. It should be noted however that variability within unit velocities is expected. It is recommended that a future modelling exercise is performed to define a complete velocity model for the study area to further refine vertical uncertainty in the spatial model.

6.2.3   Further Unit Updates

Although further revision to the integration of geophysical horizons with geotechnical datasets has been performed as part of this work, no update in the horizons outside of Sub-Area 1 have been made compared to the work provided in Integrated Report no 2. As a result, there is still uncertainty in the nature of some units in this area due to the relatively complex nature of the channelised areas. An example of this is Unit U50, where the nature of the channelised areas of this unit on the western edge of the Sub-Area 1 site is currently limited by the availability of geotechnical data in these areas to integrate and resolve the complexity of these units. It is expected that further revisions to the interpretation of this area may be presented once 2025 geotechnical data are available.

6.3   Spatial Geological Model - Unit U10

6.3.1   Seismic Character

Unit U10 is present across almost the entire site (Figure 6.3). It is locally absent, most notably in the east and north of the site. Unit U10 has an average thickness of less than 1 m, locally it is thicker, reaching a maximum thickness of 10 m (Figure 6.4), however within Sub-Area 1 the thickness are less (5 m maximum). The areas where Unit U10 is thicker correspond with shallow water depths (Figure 6.5). However, the shallowest water depth in the south of the site is not associated with an increased thickness of Unit U10, but with Unit U20. In the south of the site Unit U10 forms a series of ridges and banks. The largest of these is a north-north-west to south-south-east oriented bank, approximately 10 km wide just to the west of Sub-Area 1. Around this bank there is a series of north-east to south-west oriented ridges up to 3 km wide, and north-west to south-east oriented ridges up to 1.5 km wide.

The basal horizon of Unit U10 is flat to undulating and generally a medium to high amplitude positive reflector. In the north and east of the site, where Unit U10 overlies Unit U20, the basal horizon H10 gradually becomes difficult to distinguish from internal reflectors within Unit U20. In those areas the shallowest laterally continuous reflector was interpreted as horizon H10.

The internal seismic character is acoustically transparent to chaotic on the 2D UHRS data and more variable from acoustically transparent to chaotic with discontinuous to continuous internal reflectors on the SBP data (Figure 6.5).
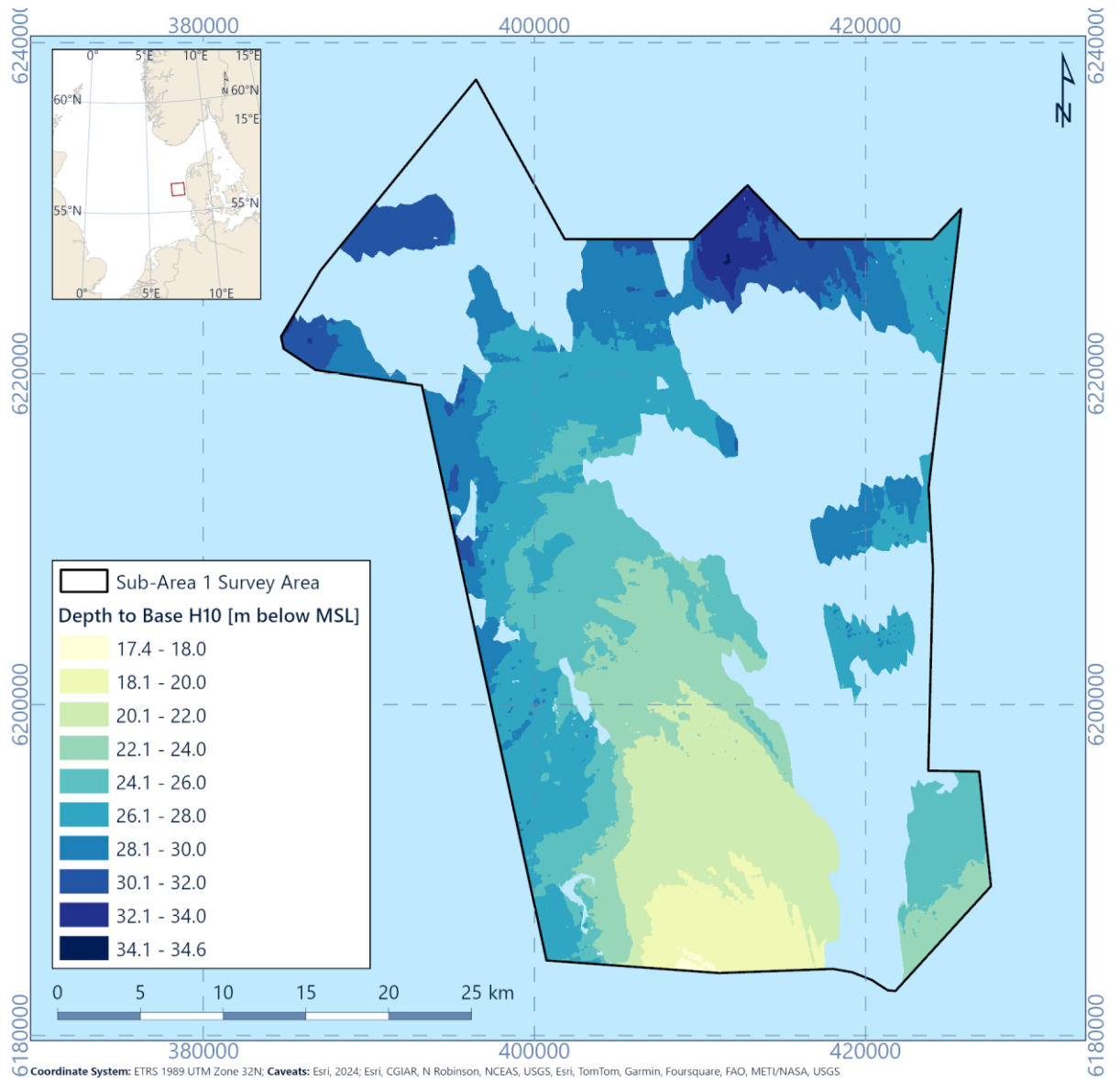
Figure 6.3: Depth of horizon H10 (base of Unit U10) relative to MSL
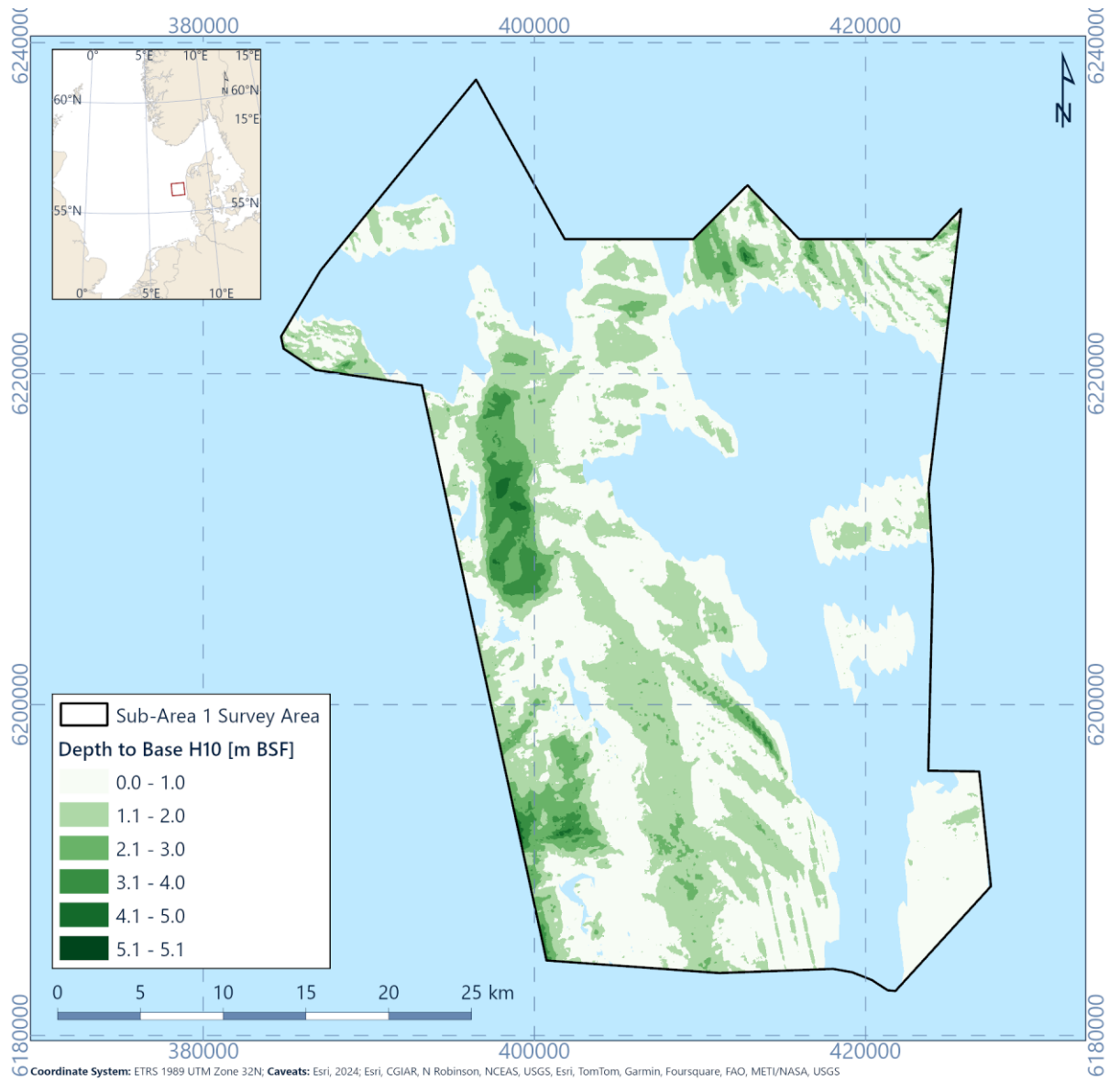
Figure 6.4: Depth of Horizon H10 (base of Unit U10) metres BSF (and isochore map of Unit U10)
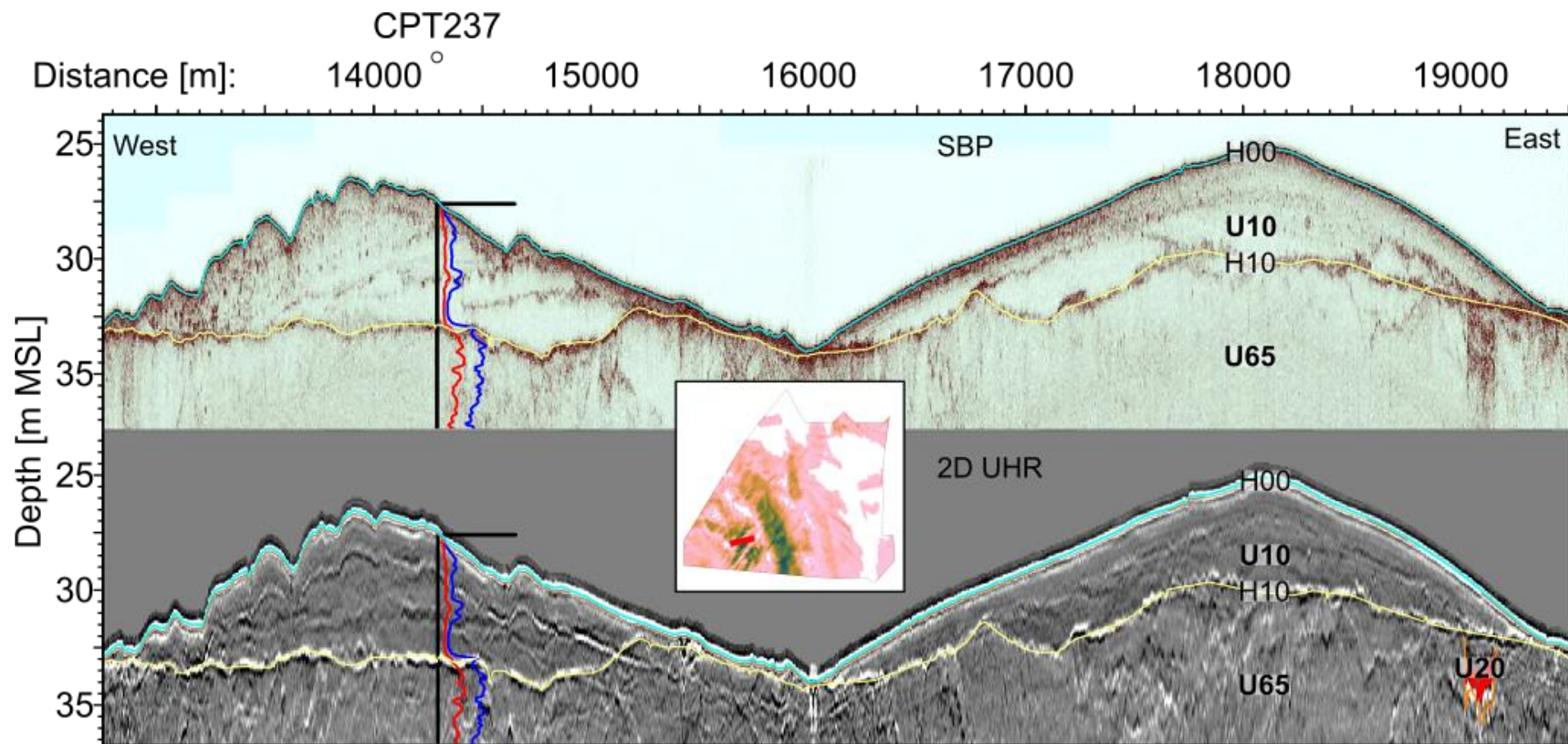
Figure 6.5: SBP and 2D UHR seismic data example of Unit U10. Line EAXC405P1, CPT237. CPT scale: Blue is q_c with a scale from 0 to 80 MPa and red is f_s with a scale of 0 to 2 MPa. Examples are from Sub-Area 2, but show good examples of seismic response and geotechncial data

6.3.2 Integration and interpretation

It is interpreted that Unit U10 represents postglacial (Holocene) marine sands, which were deposited in the early stages of and after the Holocene transgression.

Where Unit U10 gradually overlies Unit U20, it is interpreted that Unit U10 and Unit U20 represent a gradual transition from non-marine to marginally marine to fully marine environments.

The largest thickness of U10 is observed in the centre of the site and is associated with a sand bank and sand ridge features. These are interpreted to be palaeo-coastlines, which formed around the bathymetric highs between 8.2 and 7.0 ka BP (Figure 3.8, Figure 3.9).

A conceptual schematic diagram of the depositional environment associated with Unit U10 is presented in Figure 6.6.
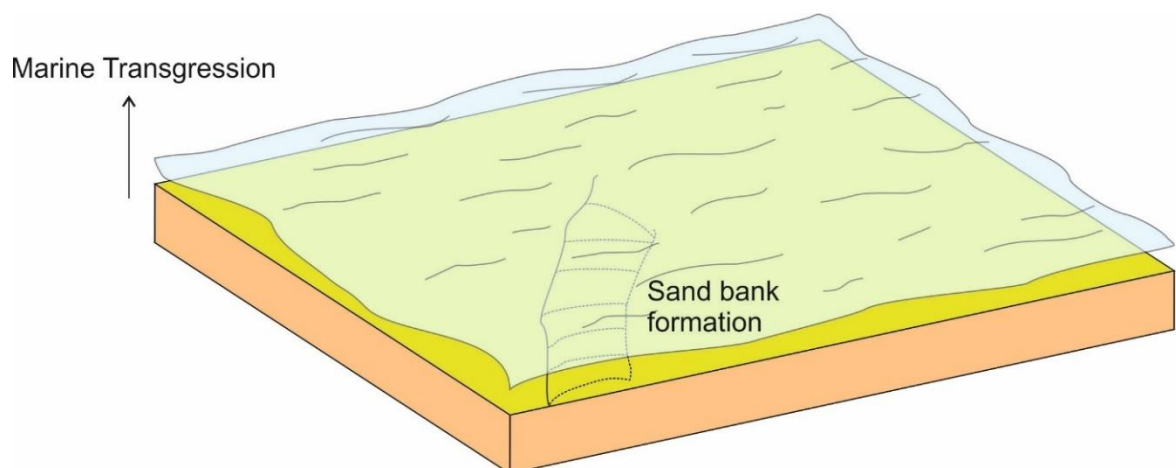
Figure 6.6: Schematic diagram of U10 deposition in the early Holocene marine environment

Correlation between seismic data of U10 and seafloor mapping presented in Section 4.3 suggests that greater thicknesses of U10 correspond with areas of seafloor mapping of gravel and coarse sands. This supports environmental depositional interpretations associated with U10 of higher energy shallow marine environments compared to underlying U20 sediments. Figure 6.7 displays the correlation between the geophysical interpretation and geotechnical locations. Integration between geophysical and geotechnical datasets are generally good, with limited inconsistencies. Where inconsistencies are observed, it is interpreted that these are a result of areas where very thin deposits of U10 are observed in geotechnical data which were not mapped in geophysical data. Correlation coefficient values for the base of U10 (H10) are typically higher than 0.8.

BH002
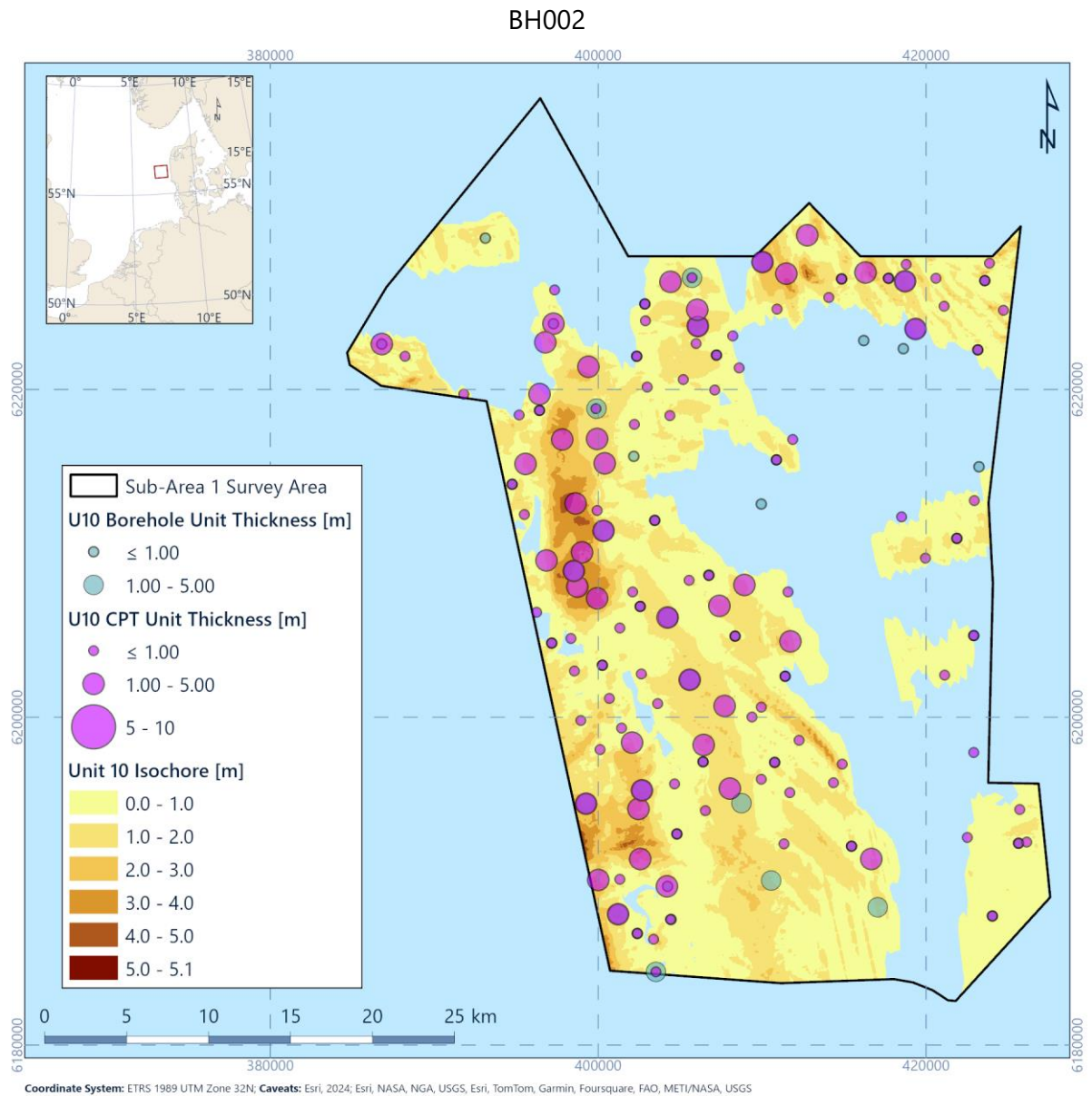
Figure 6.7: Isochore for U10 corelated with geotechnical data recoveries

Unit U10 is almost exclusively observed as a sand sediment, with grain sizes ranging from fine to coarse. Organic matter and shell fragments are both noted in sample data, highlighting the possible reworked nature of the material from underlying, older sand sediments.

6.4 Spatial Geological Model - Unit U20

6.4.1 Seismic Character

Unit U20 forms the infill of spatially variable up to 10 km wide channels and overbank deposits of these channels with a west to east or north-west to south-east orientation forming a tributary network (Figure 6.8, Figure 6.9). The thickness reaches up to approximately 30 m (Figure 6.10, Figure 6.11). The infill of narrow (less than 1 km) tributary

channels is less than 10 m thick (Figure 6.12). Beyond the confinement of the main channels, Unit U20 forms a relatively thin layer of up to approximately 5 m thick.

The base of Unit U20 is marked by horizon H20, which is a low to high amplitude positive reflector. Unit U20 is generally associated with Unit U35, which it directly overlies.

Internally, Unit U20 is acoustically transparent or stratified with low to medium amplitude reflectors dipping towards the east (Figure 6.12). At the base and margins of channels, the seismic character is more variable. Often the base of Unit U20 is formed by a seismic anomaly with a negative polarity (See Section 6.15.1). Where Unit U20 is relatively thick, often a seismic anomaly associated with acoustic blanking is present (see Section 6.15.3). Fugro have reviewed if further horizons within U20 can be picked across the study area, however no consistent horizons are mappable across the area to delineate the geotechnical transitions that are observed within the U20 sediments.

FUGRO
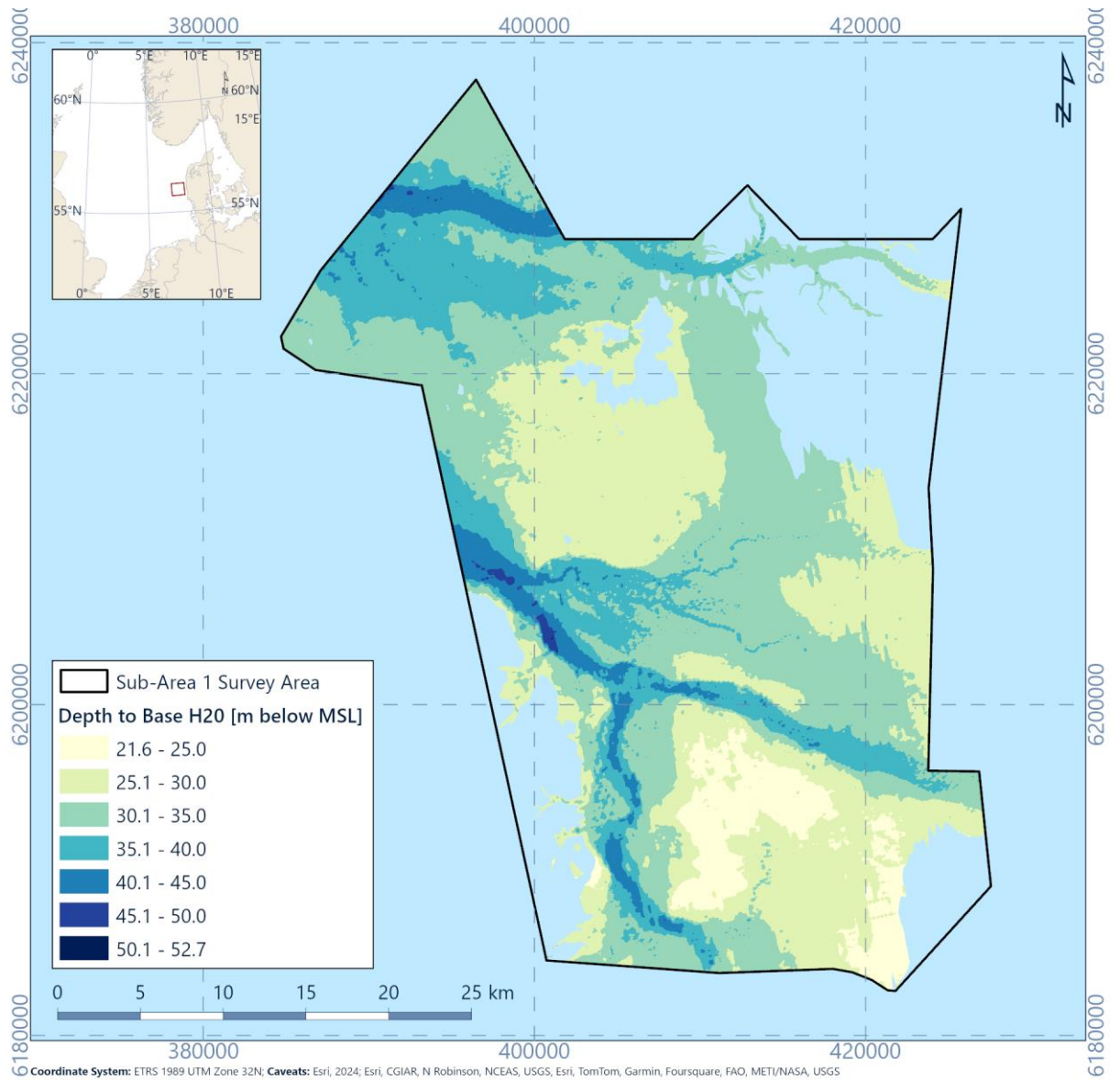
Figure 6.8: Depth to horizon H20 (base of Unit U20) relative to MSL
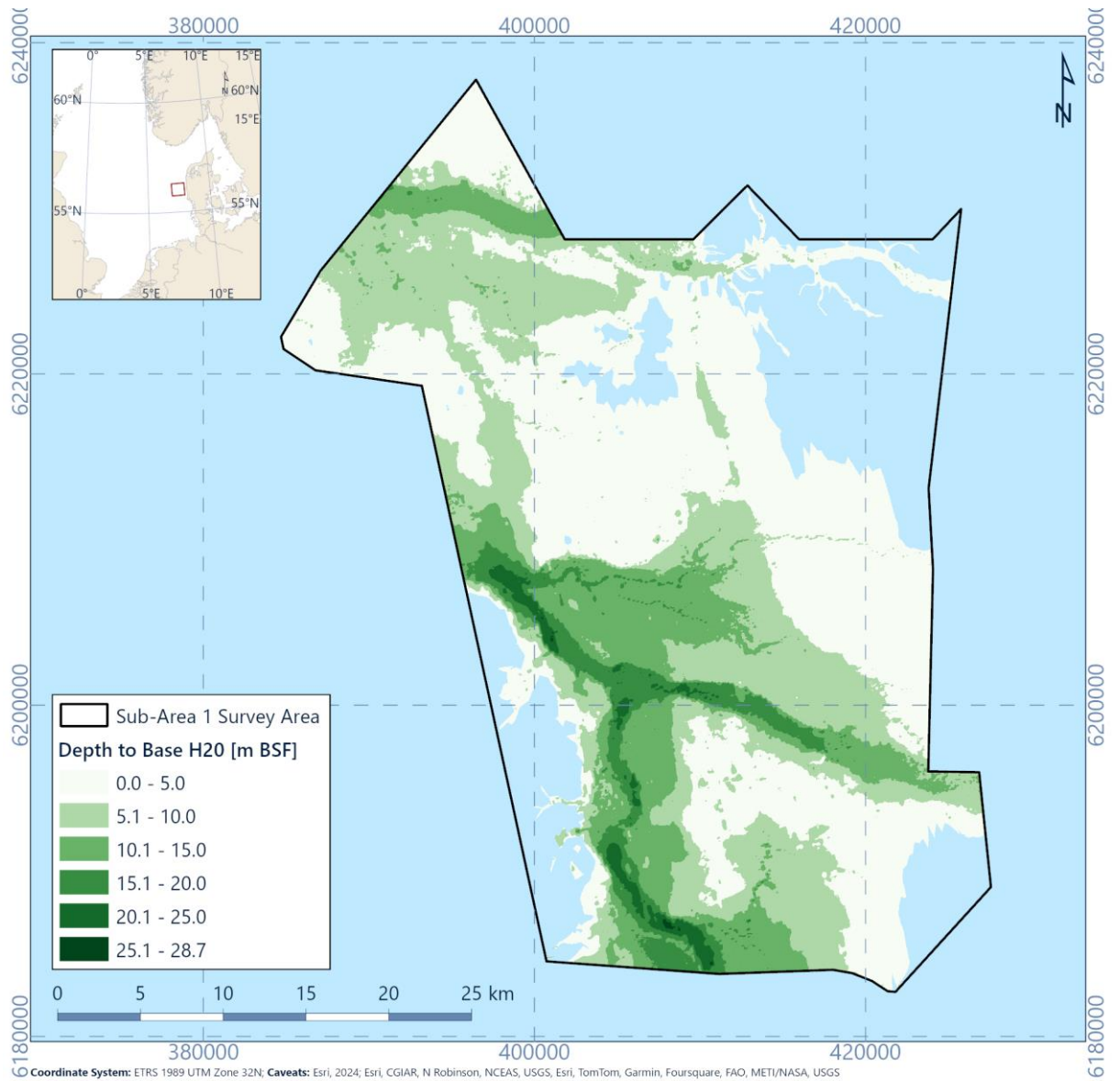
Figure 6.9: Depth (metres BSF) to horizon H20 (base of Unit U20)
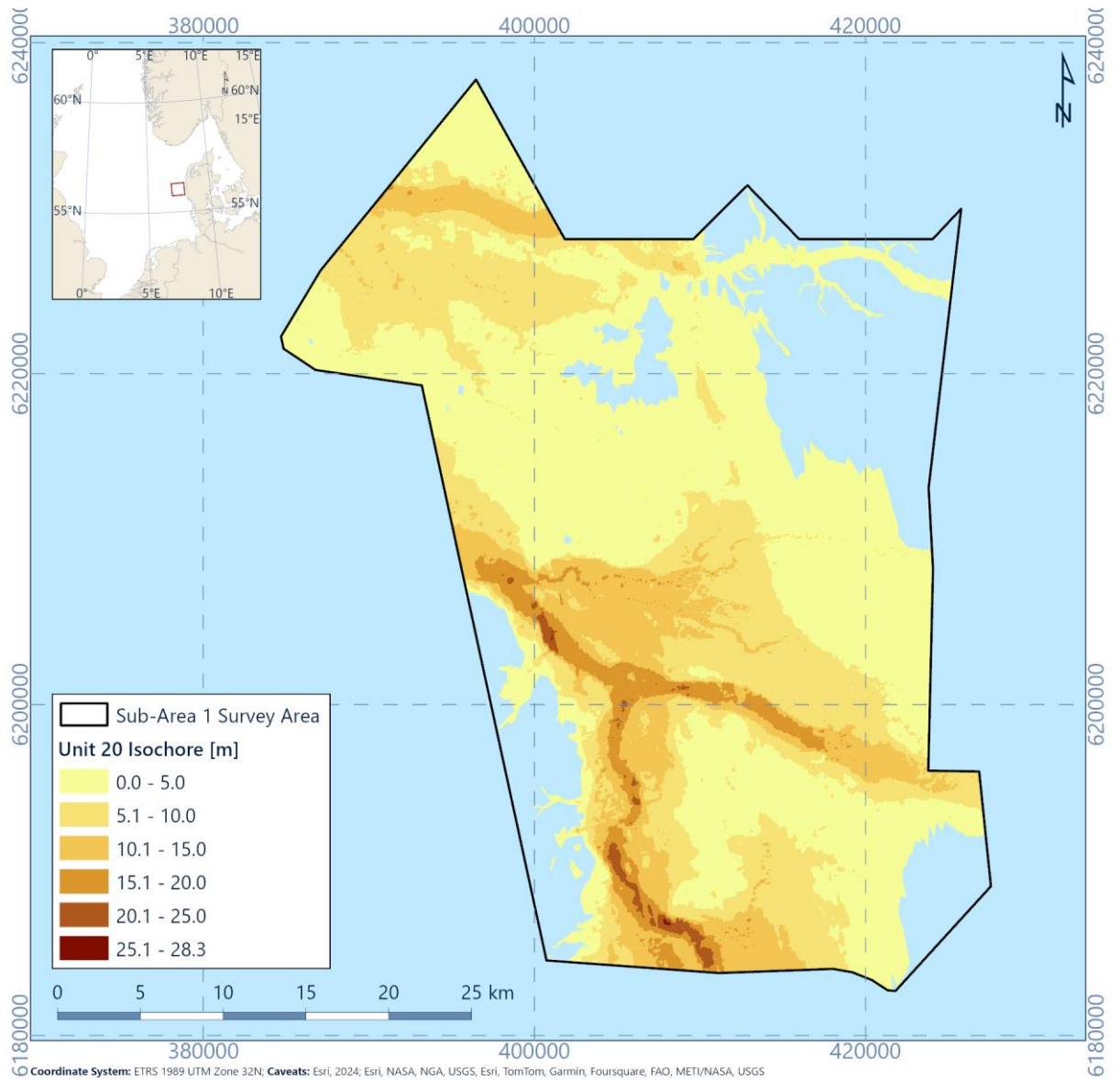
Figure 6.10: Isochore of Unit U20
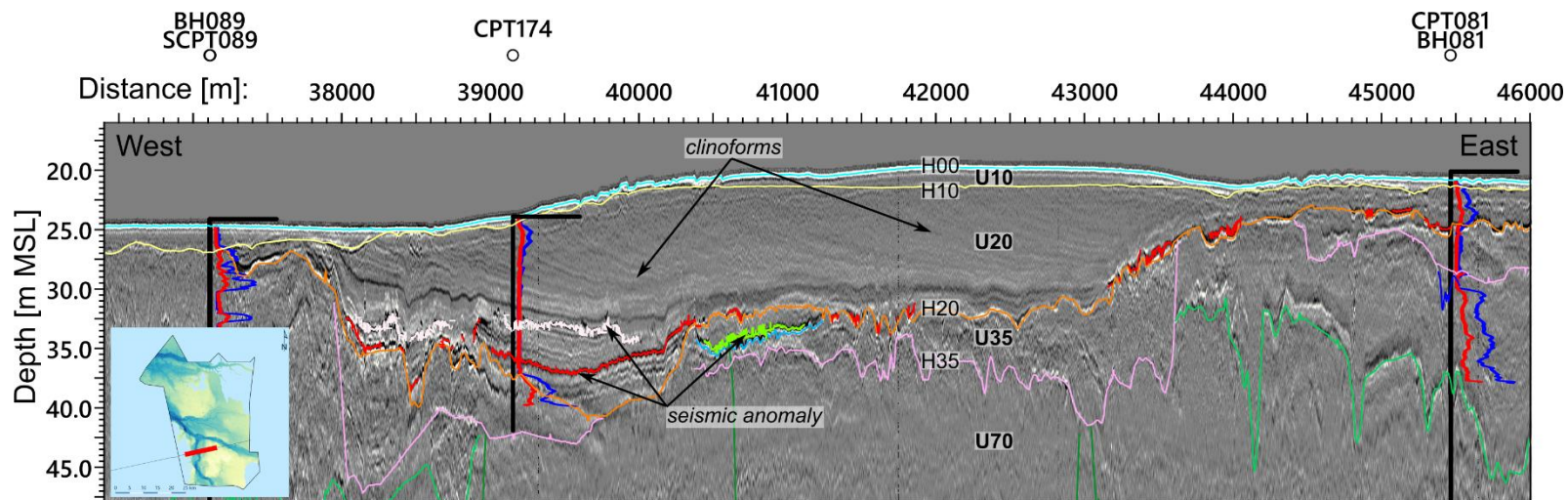
Figure 6.11: 2D UHR seismic data example showing the wide and deep channel of Unit U20. Line EAXD408P1, CPT081, SCPT089 and CPT174. Blue is q_c with a scale from 0 to 80 MPa and red is f_s with a scale of 0 to 2 MPa
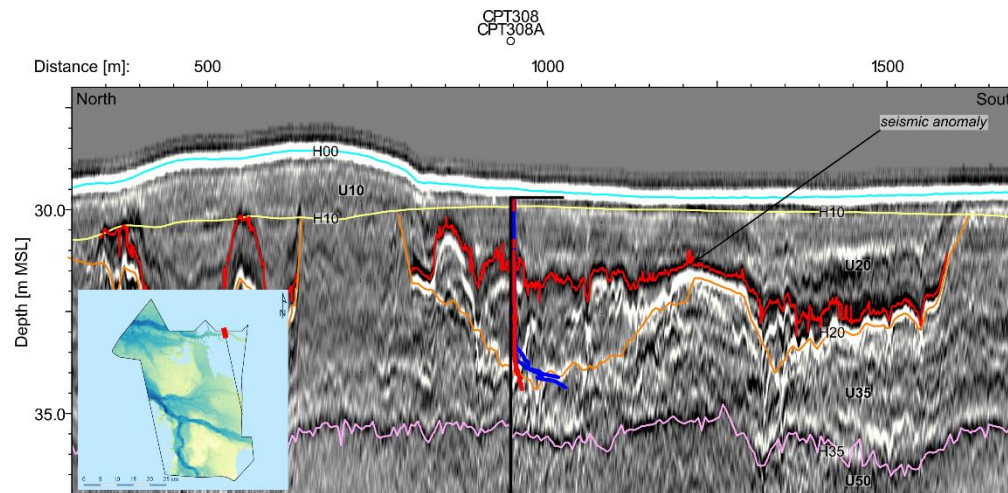
Figure 6.12: 2D UHR seismic data example showing a small channel of Unit U20. Line EABB336P1, CPT308A. CPT scale: Blue is q_c with a scale from 0 to 80 MPa and red is f_s with a scale of 0 to 2 MPa

6.4.2 Integration and interpretation

Unit U20 comprises a network of three main channels and several secondary distributary channels. It is interpreted that Unit U20 was deposited in estuarine and marine depositional environments when the site was flooded during the postglacial transgression that followed the deglaciation after the Last Glacial Maximum (LGM), likely between 8000 and 7000 years BP (Figure 5.7 to Figure 5.9).

Sampling and CPT data within Unit U20 shows that there is a gradational change from coarser sediments in the upper section of the units to finer grained cohesive sediments in the lower sections of the unit, particularly focused within the channelised areas. This is reflected in the geotechnical unitisation that splits them into U20a and U20b. As this was not identifiable in the geophysical data no integration is possible currently for this sub-unit split.

Figure 6.13 and Figure 6.14 show the correlation between the thickness of Unit U20 in the seismic data, with the geotechnical locations for U20a and U20b. As can be seen with the figures, U20b is largely constrained to the channel incision areas, whereas U20a is present across the area. Table 5.1 further describes the differences between U20a and U20b. This difference is also reflected in the thickness of U20a, with greatest thickness of the unit present in the channel areas, but in the more downstream areas. Correlation between the base of U20 in geophysical and geotechnical data shows very good correlation coefficients, suggesting high confidence in extrapolation using geophysical datasets.
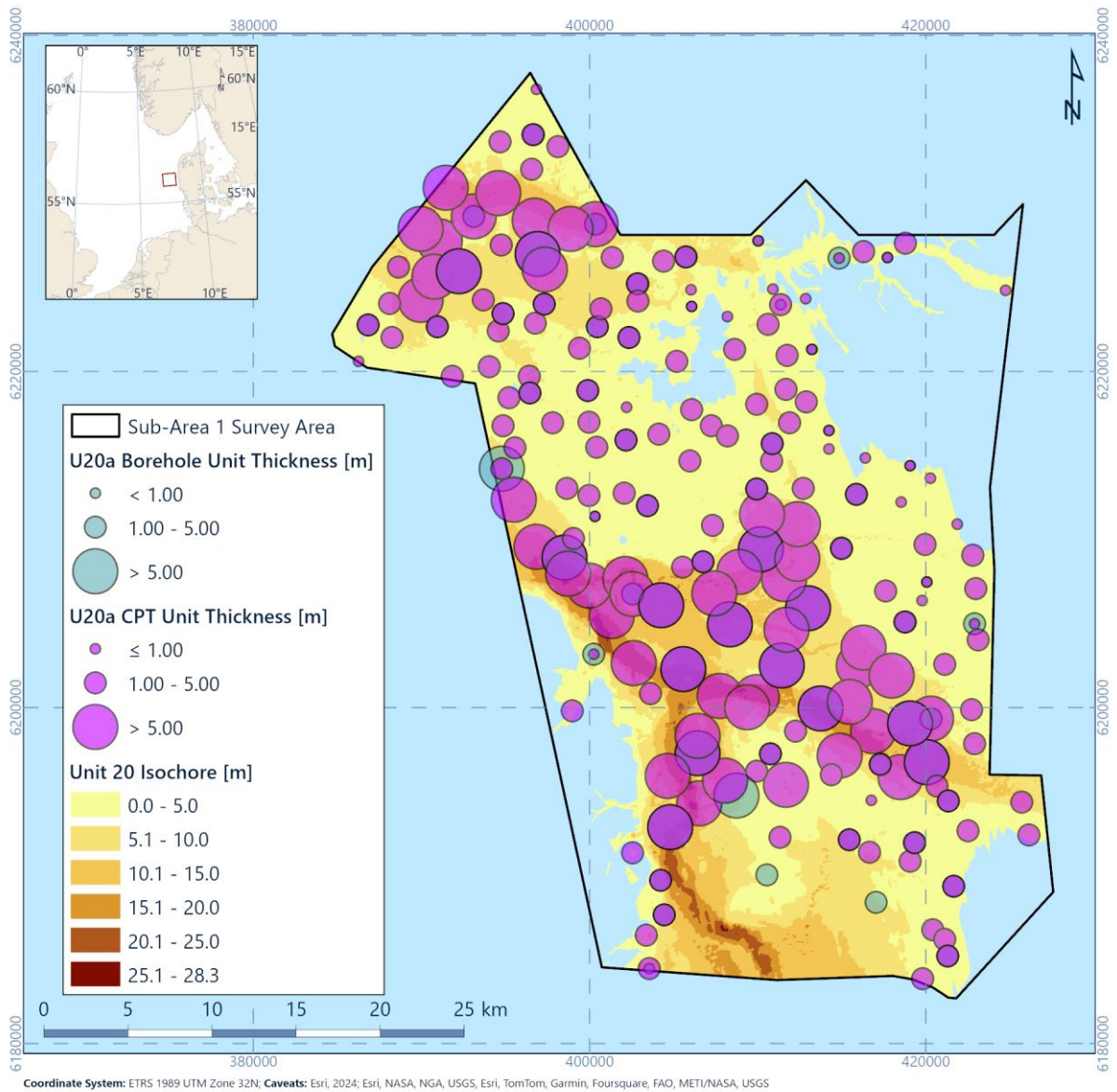
Figure 6.13: Isochore for U20 corelated with geotechnical data recoveries
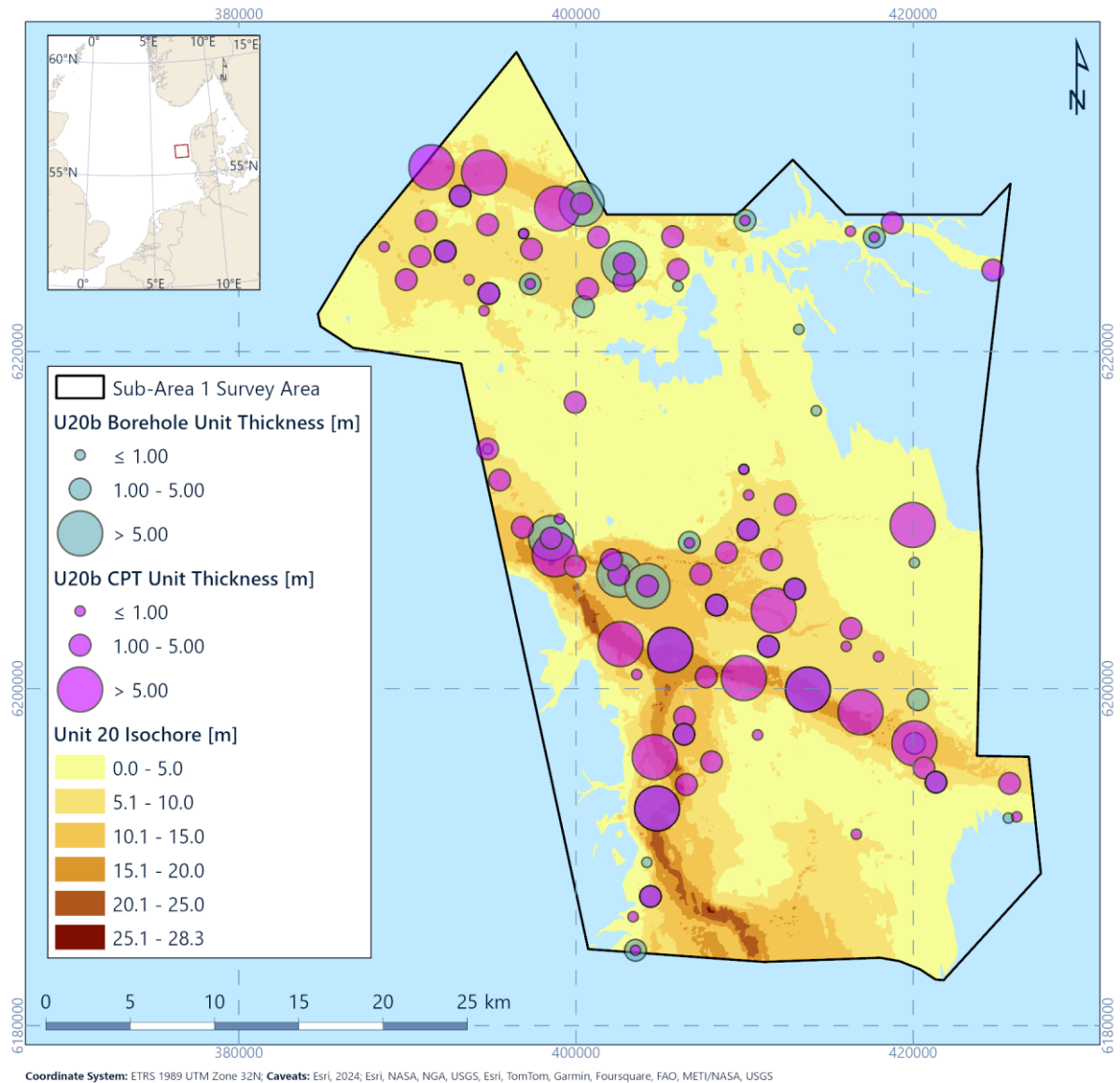
Figure 6.14: Thickness of U20b correlation between geophysics and geotechnical data

The presence of peat or organic-rich clay (Figure 6.11, Figure 6.12) is represented by a seismic anomaly with a negative polarity in the 2D UHR seismic data, observed in geotechnical sample data and decrease in CPT cone resistances and an increase in friction ratio. The peat at the base of Unit U20 is evidence for subaerial deposition following the deposition of Unit U30 and U35 during the Weichselian glacial period (Figure 6.15). It is interpreted that Unit U20 is the Holocene infill of the Weichselian incised valleys (Figure 6.15). The normally consolidated clay (Unit U20b) is evidence for a low energy marine environment. The combination of clinoforms and the coarsening upward successions of clay to the sand of Unit U20a indicates coastline progradation and shallowing of the water depth.

The orientation of the primary and secondary channels indicates that Unit U20 is a buried extension of the modern river systems that drain the western Jutland (western Denmark) to the North Sea (Figure 3.7; Konradi et al, 2005; Friborg, 1996).

FUGRO
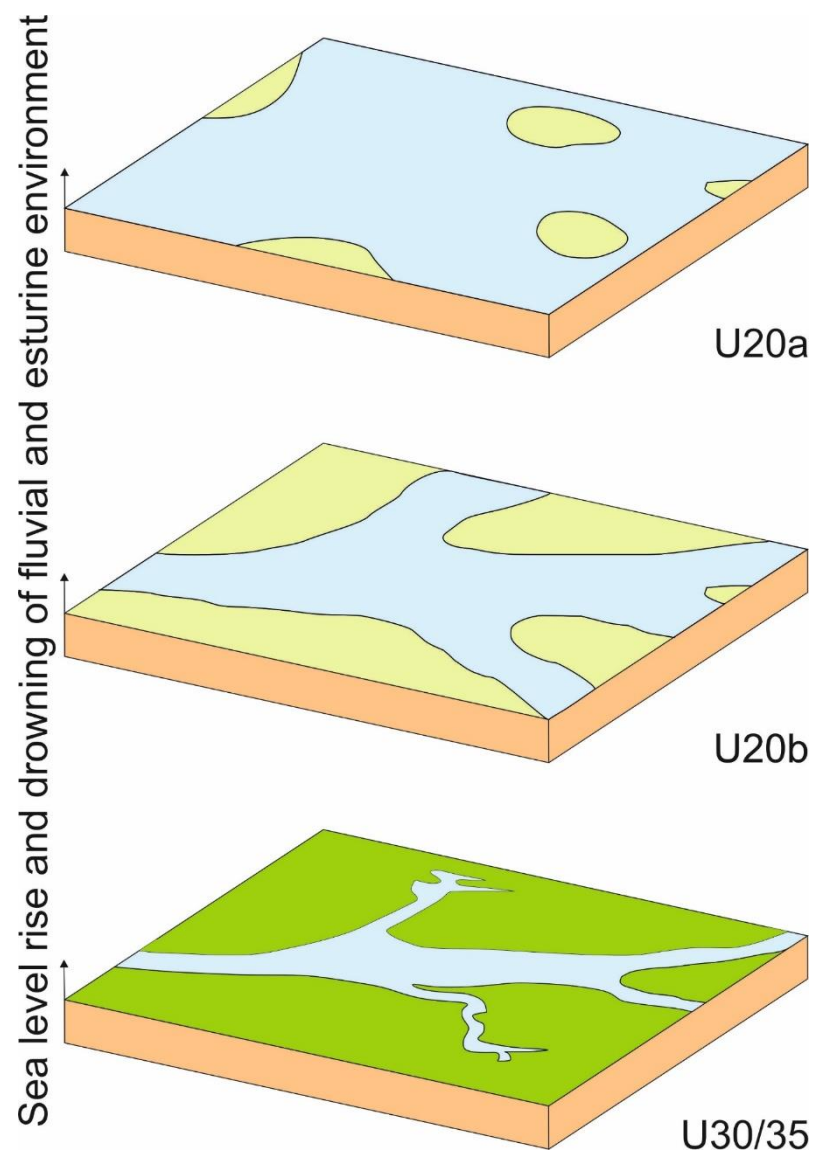
Figure 6.15: Marine transgression at end the Weichselian glacial period and the resulting environment at the site with respective units deposited

At the base of the unit high amplitude areas often correspond to organic deposits as observed in BH data. An example of the peat deposits is presented in Figure 6.16. This shows a deposit associated with a small tributary system in the north of the study area. Due to the localized nature of the channel and amplitude anomalies this area is not currently among the mapped amplitude anomalies presented in Section 6.15.1.
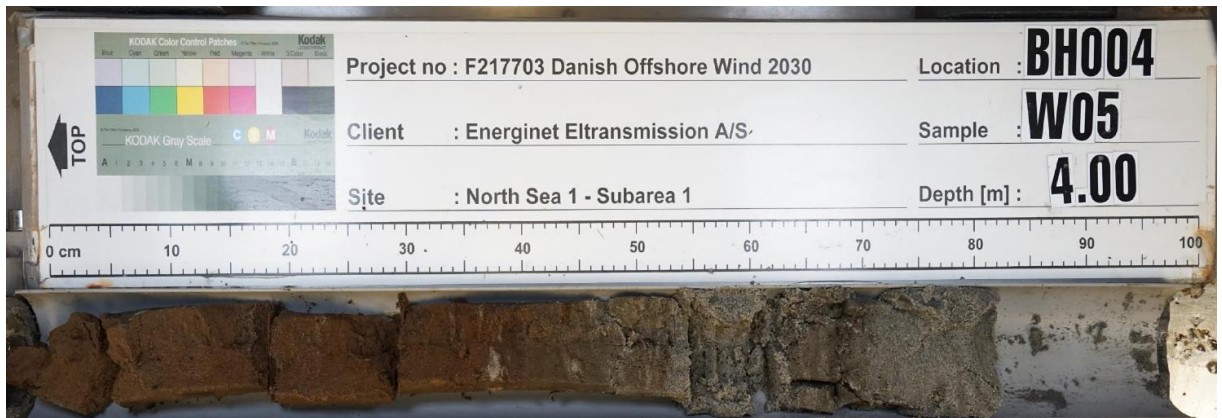
Figure 6.16: Example of peat deposits within U20

Geotechnical unitisation splits U20, however currently it is not possible to consistently map the two subunits in 2DUHR datasets. It should be noted that observed instances of U20b are present in mapped channel thalwegs, including both large channel features and in localised tributary channels observed in the site.

U20a materials are observed to be almost entirely sands in sampling geotechnical datasets with variable secondary component of silt sediments. Organic matter is also frequently observed within the U20a sediments highlighting the likely connectivity to terrestrial sediment source inputs, despite the interpretation of gradual sea level transgression during this period.

U20b sediments are observed to be more variable, with an approximate split between sand and clay sediments in sampling data. This likely highlights the variable depositional environment that U20b sediments were deposited within.

6.5 Spatial Geological Model - Unit U30

6.5.1 Seismic Character

Unit U30 is present locally in small areas, mainly in the north-west and south-west of the site and reaches a maximum thickness of 12 m (Figure 6.17, Figure 6.18, Figure 6.19). It is observed in the overlying and underlying units (U20 and U35).

The unit has a sheet-like geometry with a horizontal to undulating base. The base is marked by horizon H30, a low to medium amplitude positive polarity reflector. Internally, the unit is acoustically complex, or acoustically transparent to locally stratified with medium amplitude parallel reflectors (Figure 6.20).
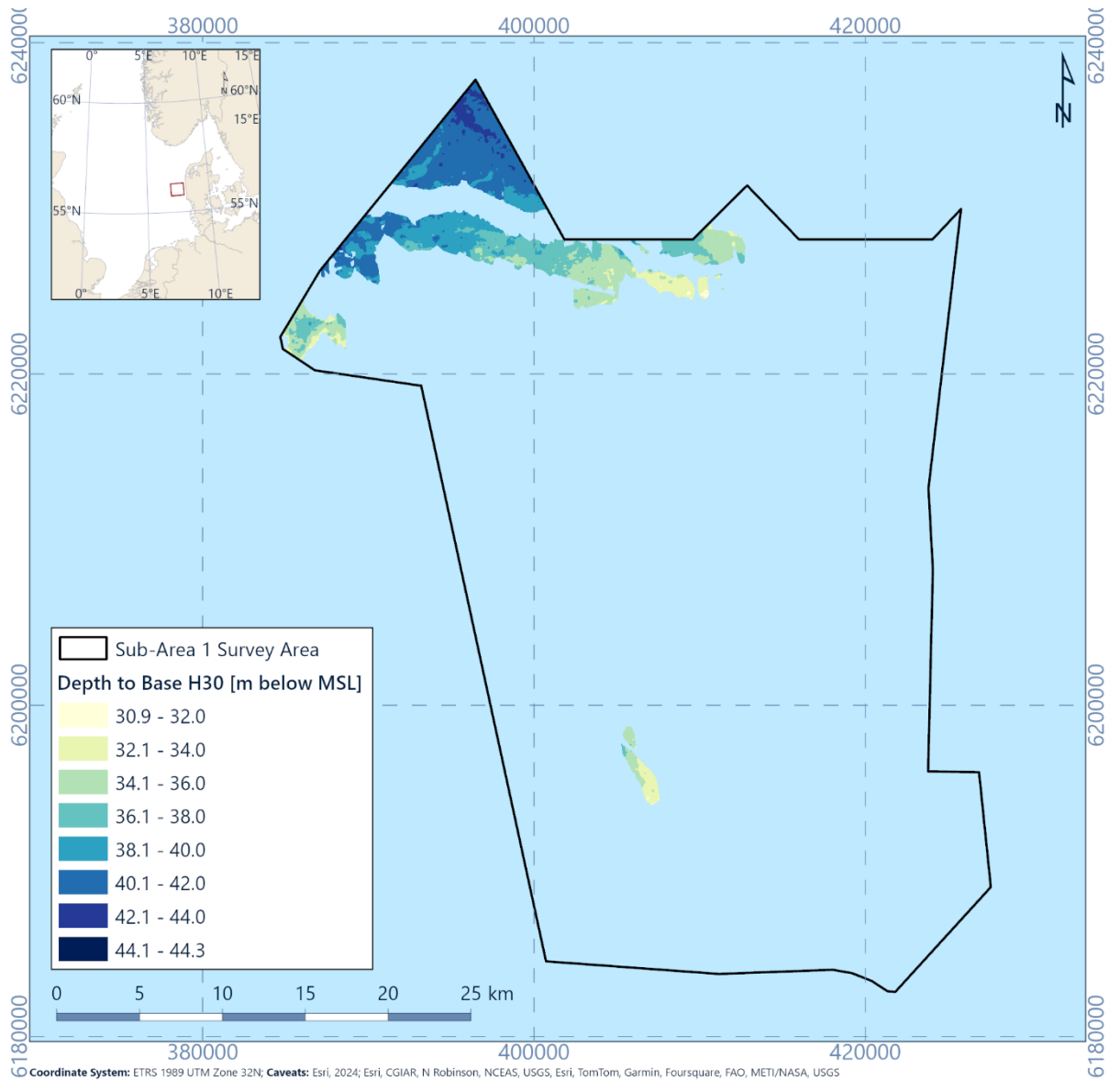
Figure 6.17: Depth to horizon H30 (base of Unit U30) relative to MSL
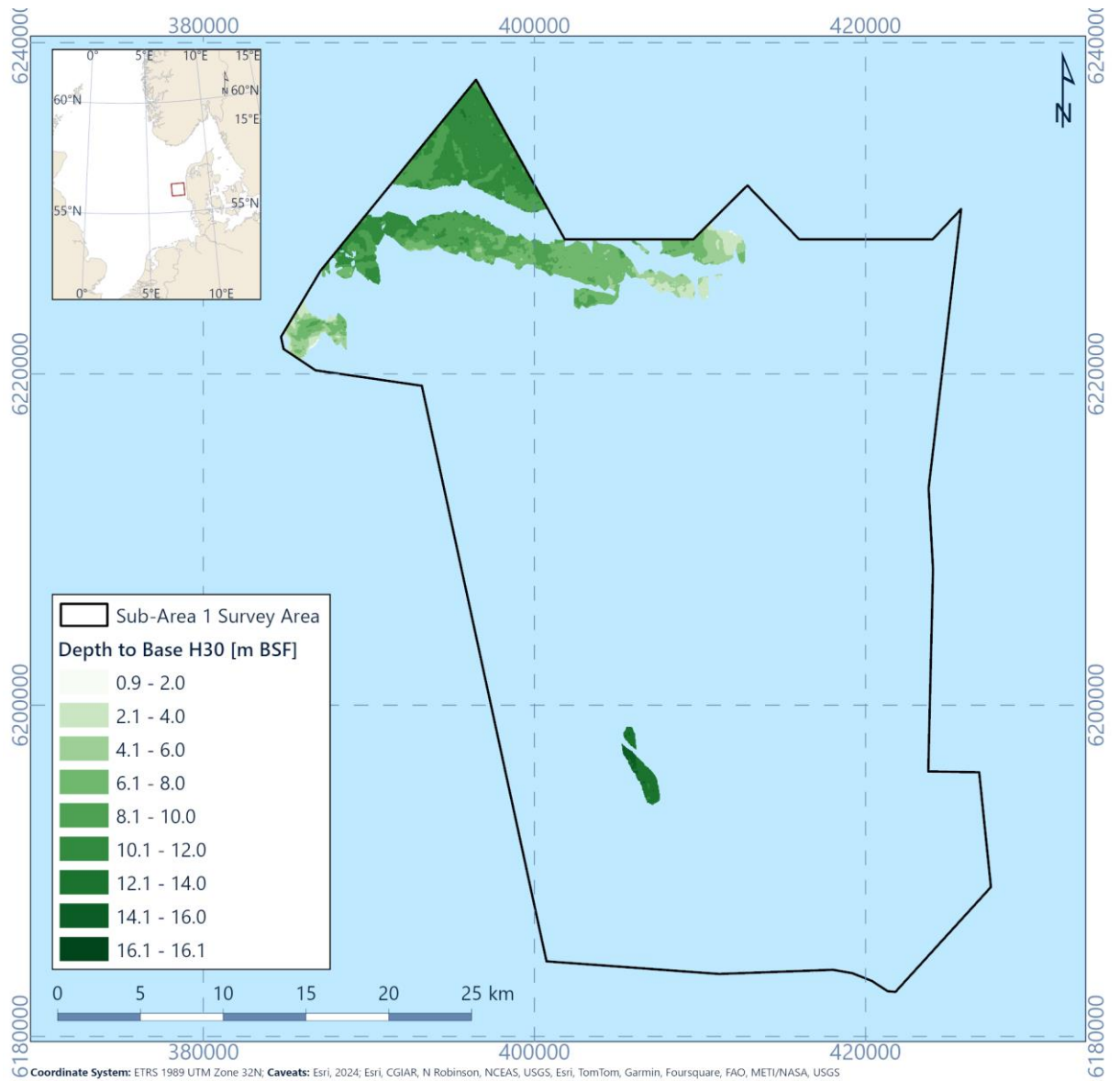
Figure 6.18: Depth to horizon H30 (Base of Unit U30) relative to seabed
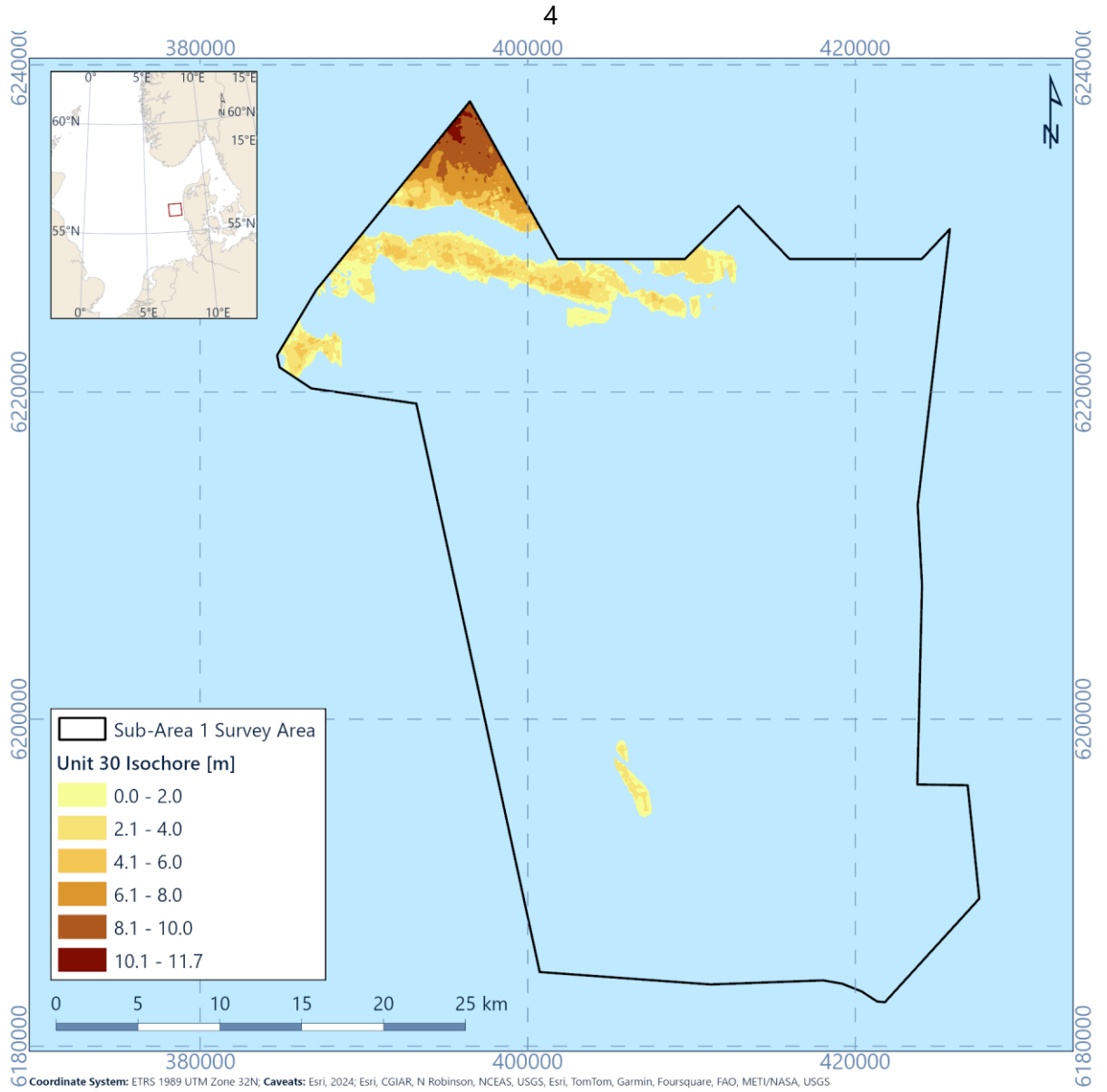
Figure 6.19: Isochore of Unit U30
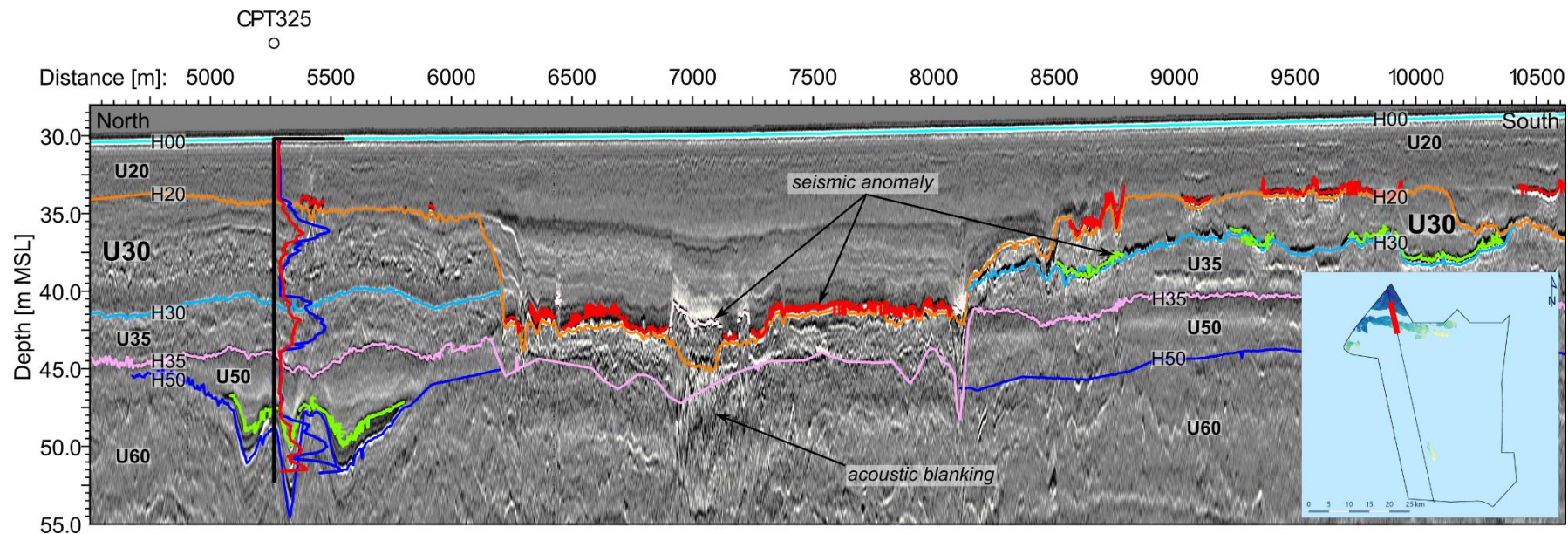
Figure 6.20: 2D UHR seismic data example of Unit U30. Line EAAN253, CPT325. CPT scale: Blue is q_c with a scale from 0 to 80 MPa and red is f_s with a scale of 0 to 2 MPa

6.5.2 Integration and interpretation

It is interpreted that Unit U30 was deposited in a meltwater (glacio-fluvial) environment based on the acoustically complex seismic character and silty and clayey sand dominated soil type. The sand sediments may represent a series of abandoned channels associated with glacio-fluvial output and a continuation of the northern most channel area as observed in underlying U35 sediments. Sands within the unit are observed to be of variable sorting and generally fine. Figure 6.21 displays the correlation between the U30 geophysics and geotechnical locations. Correlation between datasets is generally good. One location is outside mapped horizons, however thickness is less than 2 m and reflects the challenge of differentiating between U30 and underlying U35 in areas.
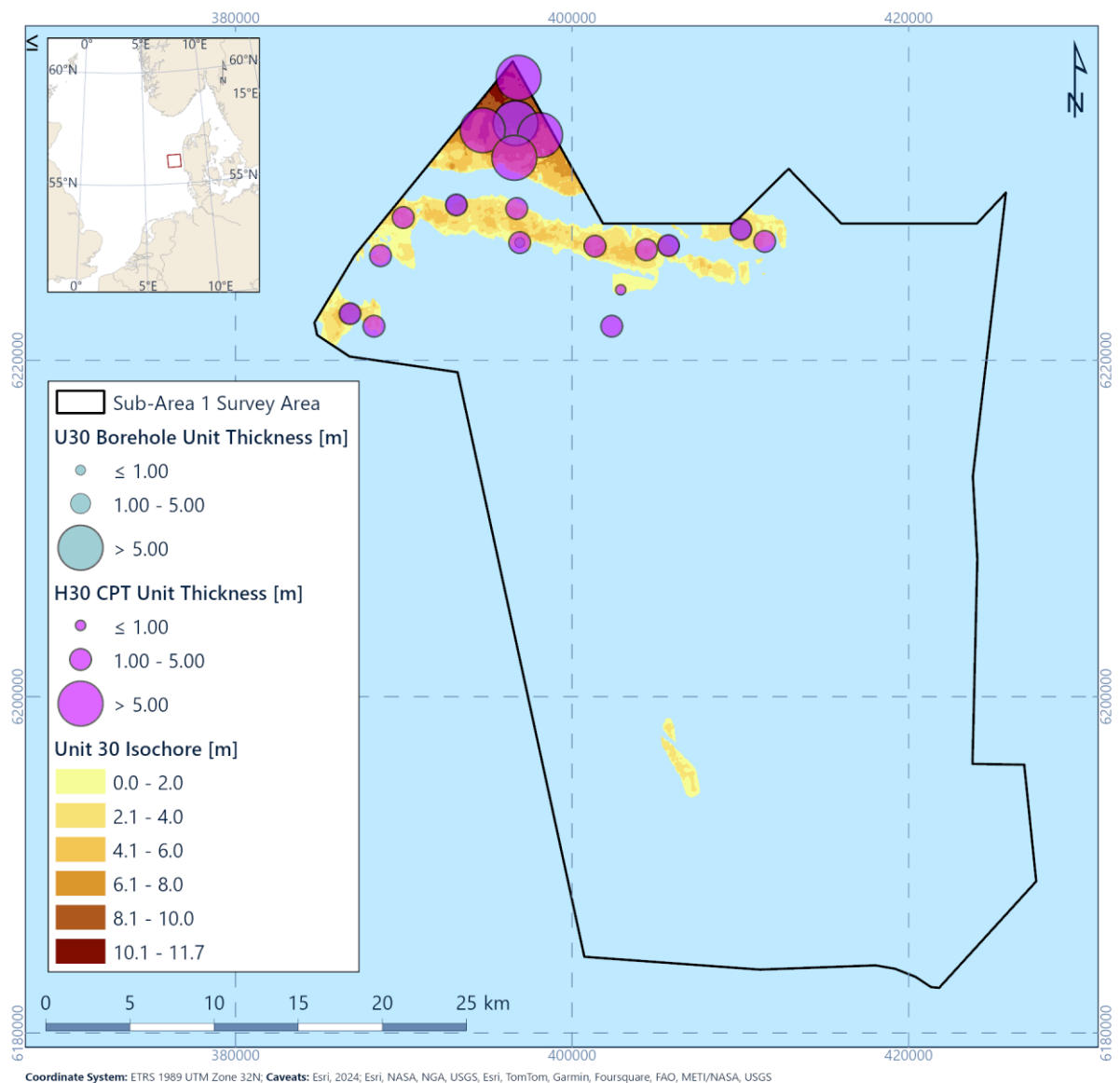
Figure 6.21: Isochore for U30 corelated with geotechnical data recoveries

The clay bed at the base of Unit U30 which correlates over km's to 10's of km's is interpreted to be a freshwater (pro-glacial lacustrine) clay. This is supported by the presence of peats and organic rich clays, interpreted to be deposited in a lacustrine environment. Clays and possible peats are observed on both side of the mapped U30 sediments. The stratigraphic position of this unit between deposits interpreted as Weichselian (Unit U35) and late Weichselian to Holocene (Unit U20) indicates a glacial (Late Weichselian) age. The presence of peat deposits may allow future dating of the unit.

6.6 Spatial Geological Model - Unit U35

6.6.1 Seismic Character

Unit U35 is present in the north, east and south-west of the site. The unit has a sheet-like to channelised geometry (Figure 6.22, Figure 6.23). The average thickness approximately 5 m and locally reaches a maximum thickness of approximately 25 m (Figure 6.24).

In the north and east of the site, Unit U35 usually overlies Units U50 and U60 (Figure 6.25). The basal horizon H35 is flat to undulating and locally forms a channelised base. Where Unit U35 is channelised, it is in general associated with Unit U20 (Figure 6.11), however some geometries of channels visible in H35 are orientated in different directions to the U20 channel areas, suggesting changes in channel orientation over the depositional period associated with U35.

Internally, this unit is characterised by chaotic seismic facies to locally horizontal and inclined stratification and internal erosion surfaces (Figure 6.25). Locally in the lower part of Unit U35, high amplitude positive reflectors are present which may represent gravel beds (see Section 6.13.4).
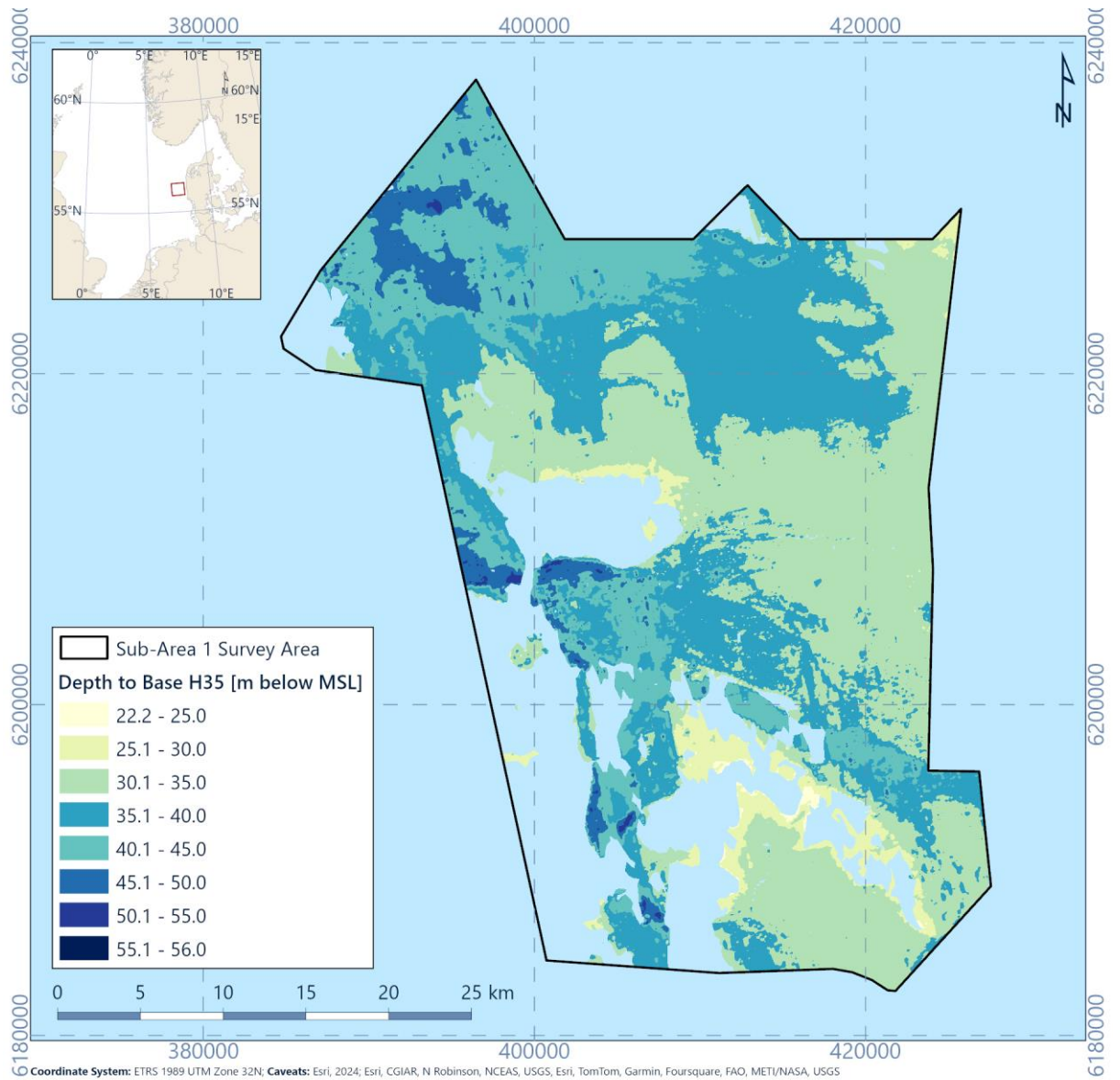
Figure 6.22: Depth to horizon H35 (base of Unit U35) relative to MSL
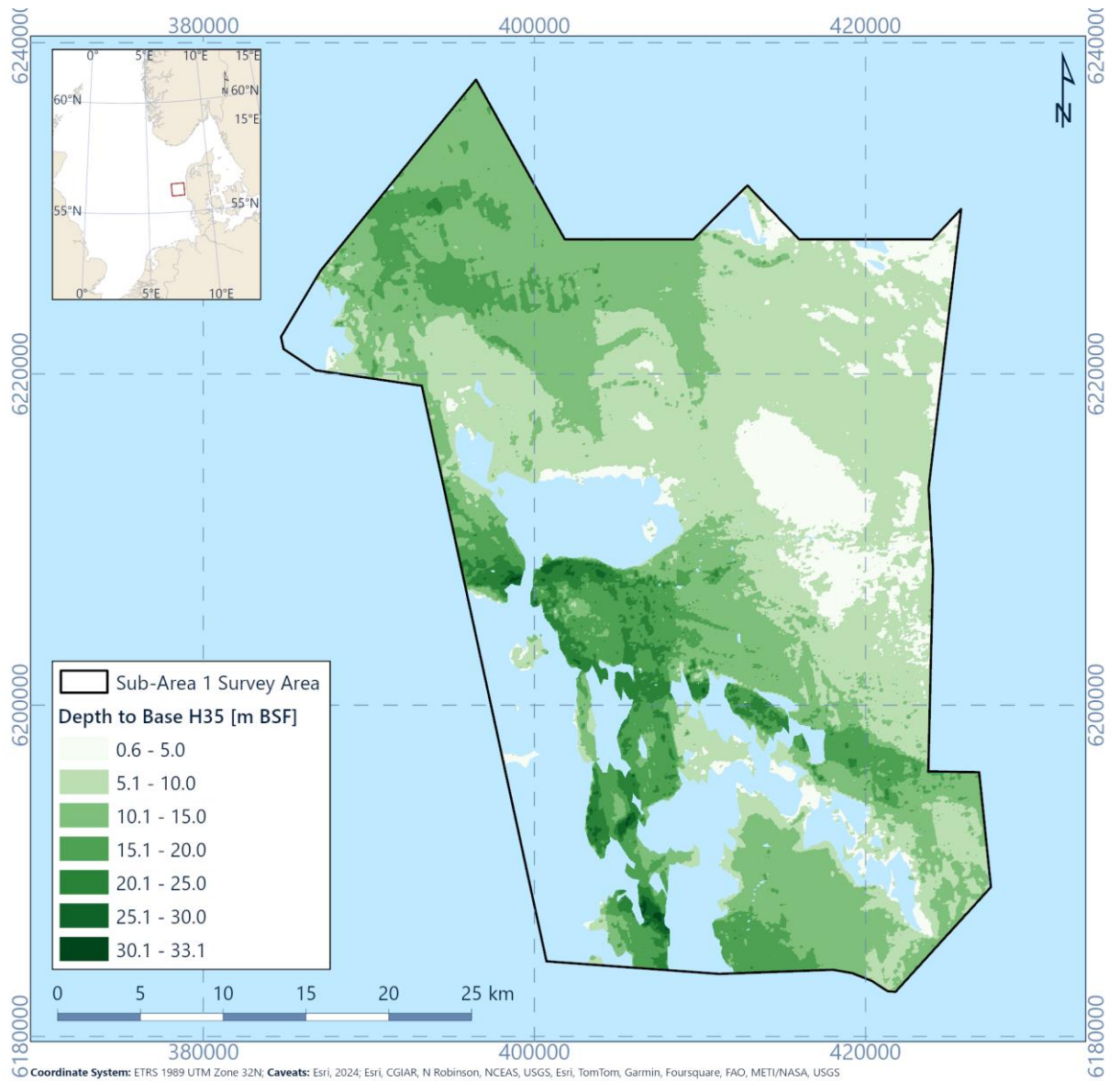
Figure 6.23: Depth to horizon H35 (Base of Unit U35) relative to seabed
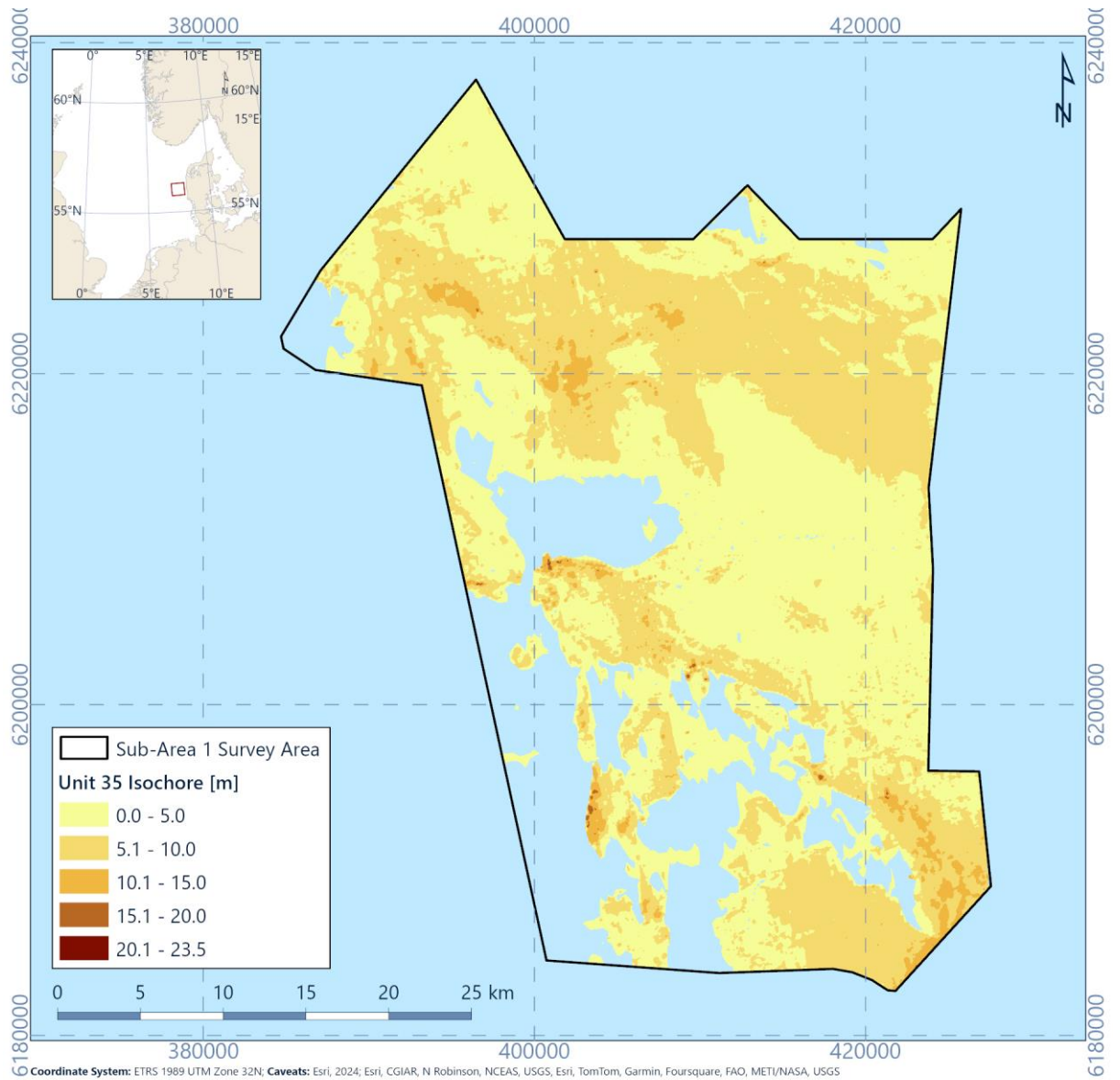
Figure 6.24: Isochore of Unit U35
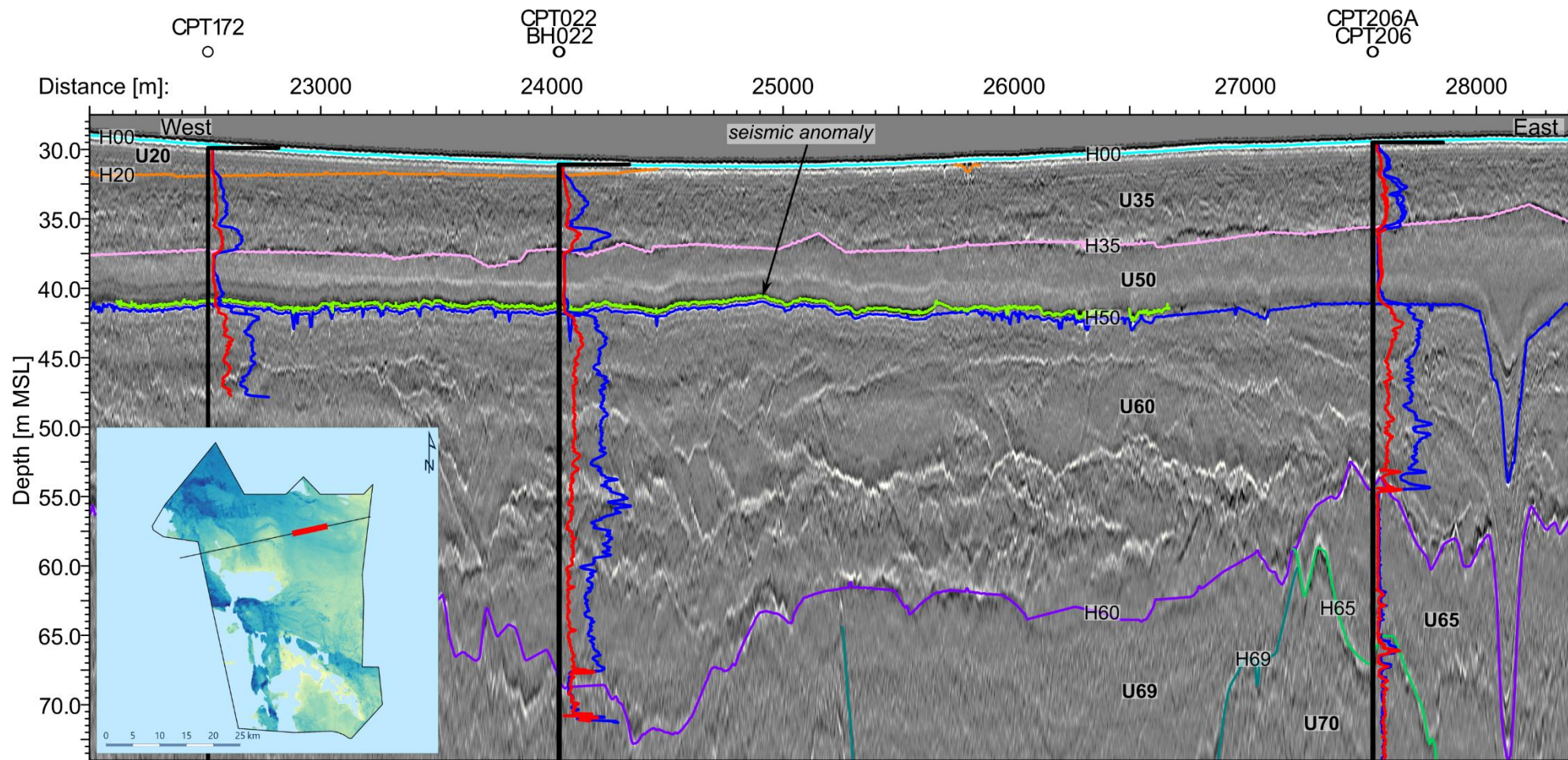
Figure 6.25: 2D UHR seismic data example of Unit U35. Line EAXA385P2, CPT172, CPT022 and CPT206A. CPT scale: Blue is q_c with a scale from 0 to 80 MPa and red is f_s with a scale of 0 to 2 MPa

6.6.2   Integration and interpretation

The erosional base of this unit, internal erosion surfaces, variable internal seismic character, and sand dominated soil type, may indicate that this unit was deposited in a meltwater (braided glacio-fluvial) depositional environment. The local presence of more clay-rich soil in Unit U35 in the north-east of the site can be explained by the proximity of low energy pro-glacial lacustrine depositional environments (Figure 3.7). Unit U35 overlies Unit U50, which is of Eemian age (Konradi et al., 2005; Larsen & Andersen, 2005). This indicates that Unit U35 was deposited during the Weichselian glacial period after the Eemian interglacial period. The interpretation is consistent with the presence of a proglacial outwash plain during the Weichselian (Figure 3.7, Figure 3.8). The relative location of the outwash sources likely changed during the Weichselian period which may reflect some of the variable channel geometries present within the unit.

Figure 6.26 shows the correlation between the thickness of U35 in the geophysical data compared to the geotechnical locations. Thickness of units are consistent with the geophysical data. Channel areas also seen in U20 represent the greatest thickness, highlighting the continuity between this and the overlying units despite the changes in channel orientations. Correlation between geotechnical datasets and geophysical horizons is good with high corelation coefficient values. Greatest discrepancy is seen in areas with incised based of the unit leading to variations over short distances.
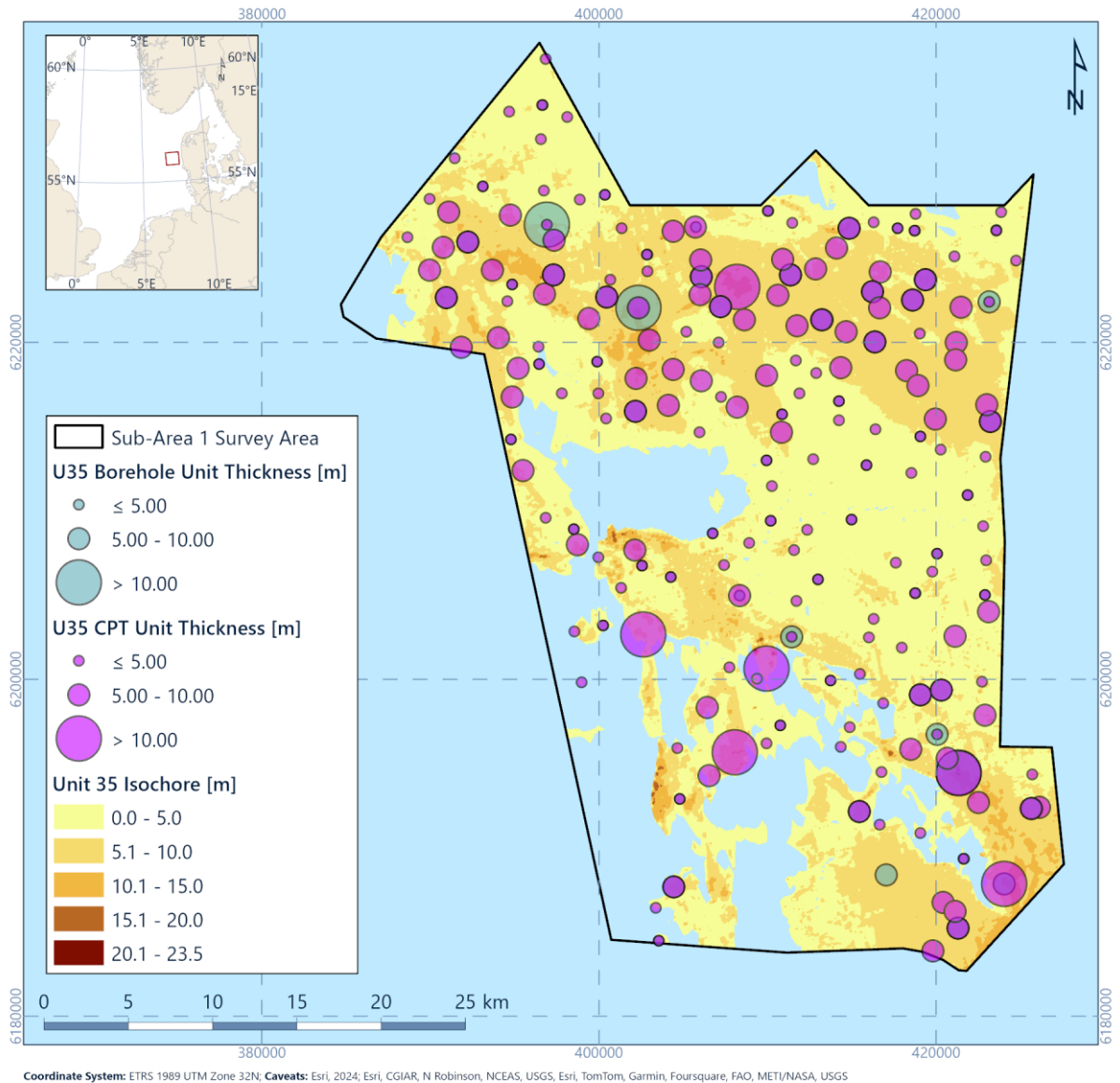
Figure 6.26: Isochore for U35 corelated with geotechnical data recoveries

6.7 Spatial Geological Model - Unit U36

6.7.1 Seismic Character

Unit U36 is present locally in the east of the site (Figure 6.27, Figure 6.28). The average thickness is approximately 5 m and reaches locally a maximum thickness of approximately 24 m (Figure 6.29). Unit U36 gradually overlies Unit U50 and is often overlain by Unit U35.

The unit is characterized by stratified seismic facies, with parallel to sub-parallel, dipping to sub-horizontal reflectors (Figure 6.30). In the north, reflectors are dipping towards the south, while in the south towards the north. Towards the west of the unit, the stratification becomes more horizontal and the amplitude of the stratification decreases (Figure 6.30).
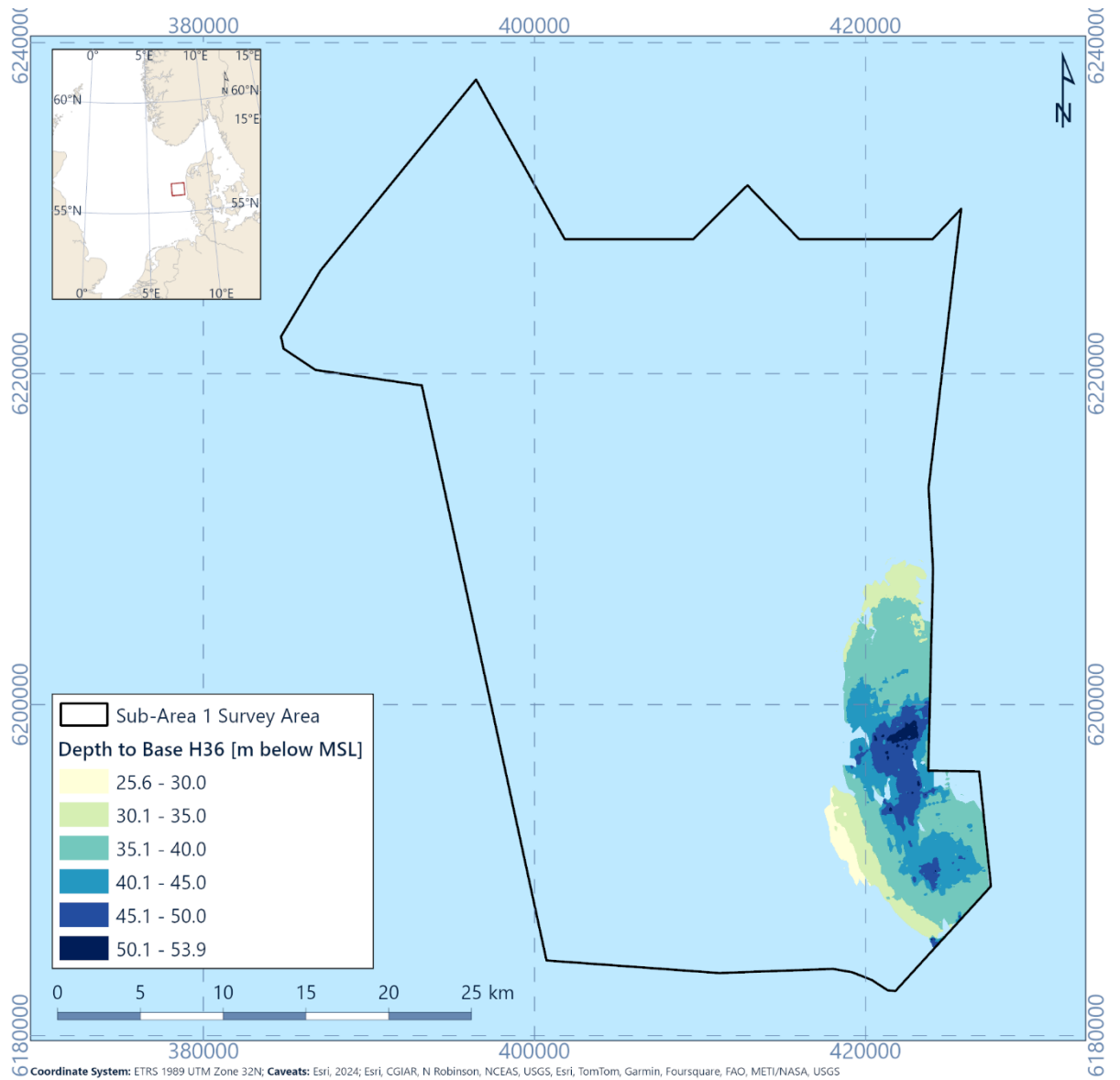
Figure 6.27: Depth to horizon H36 (base of Unit U36) relative to MSL
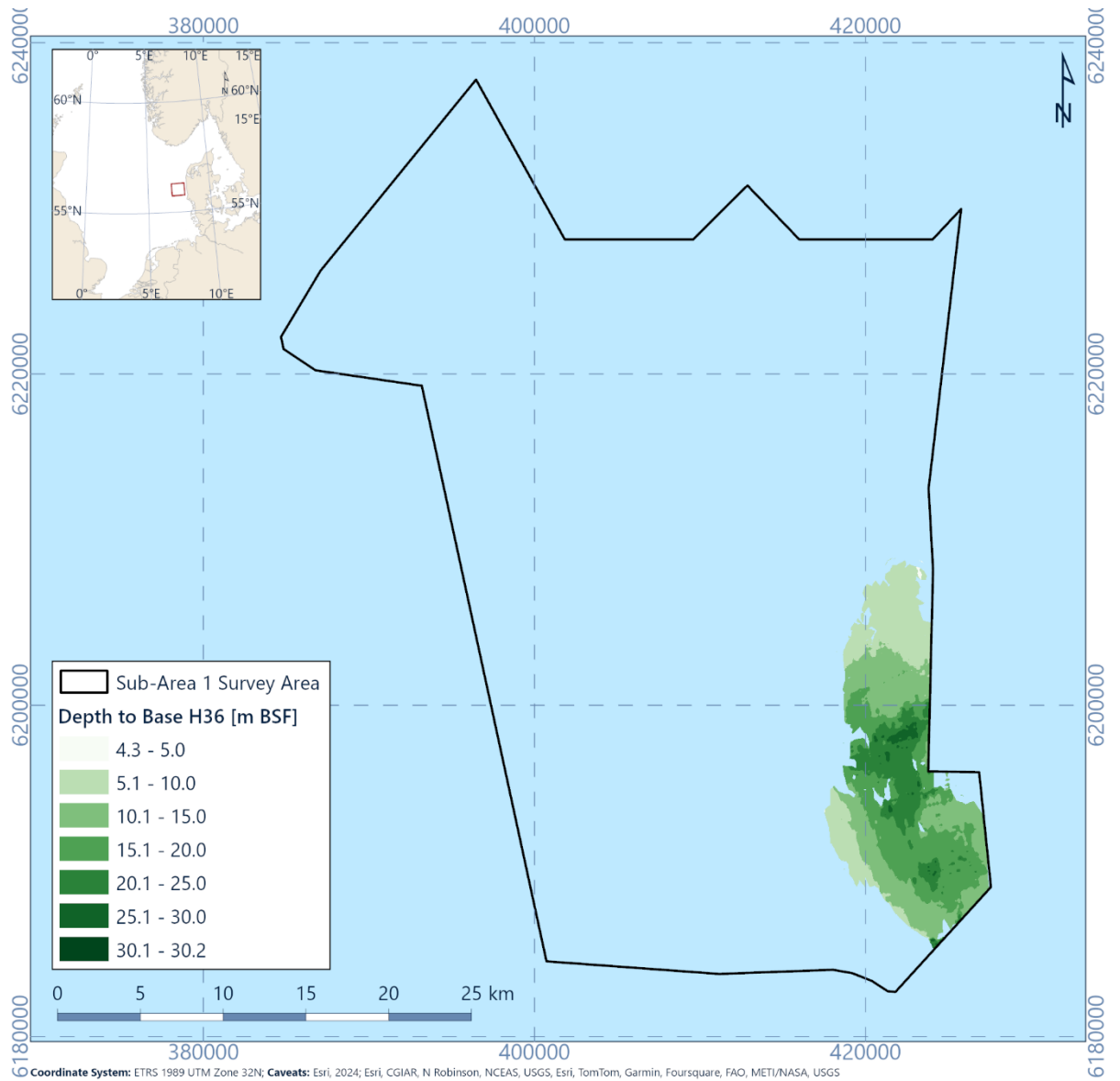
Figure 6.28: Depth to horizon H36 (Base of Unit U36) relative to seabed
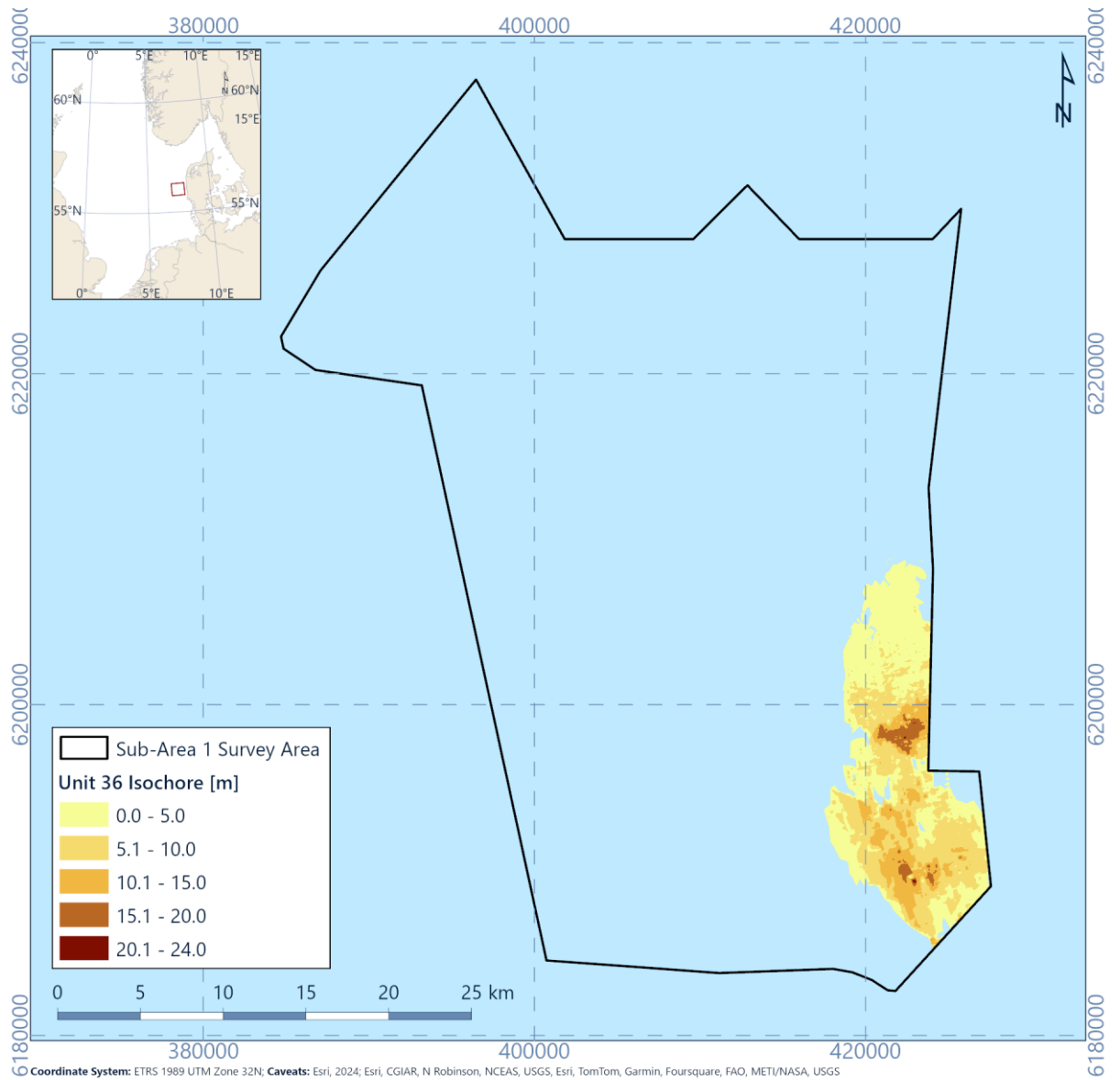
Figure 6.29: Isochore of Unit U36
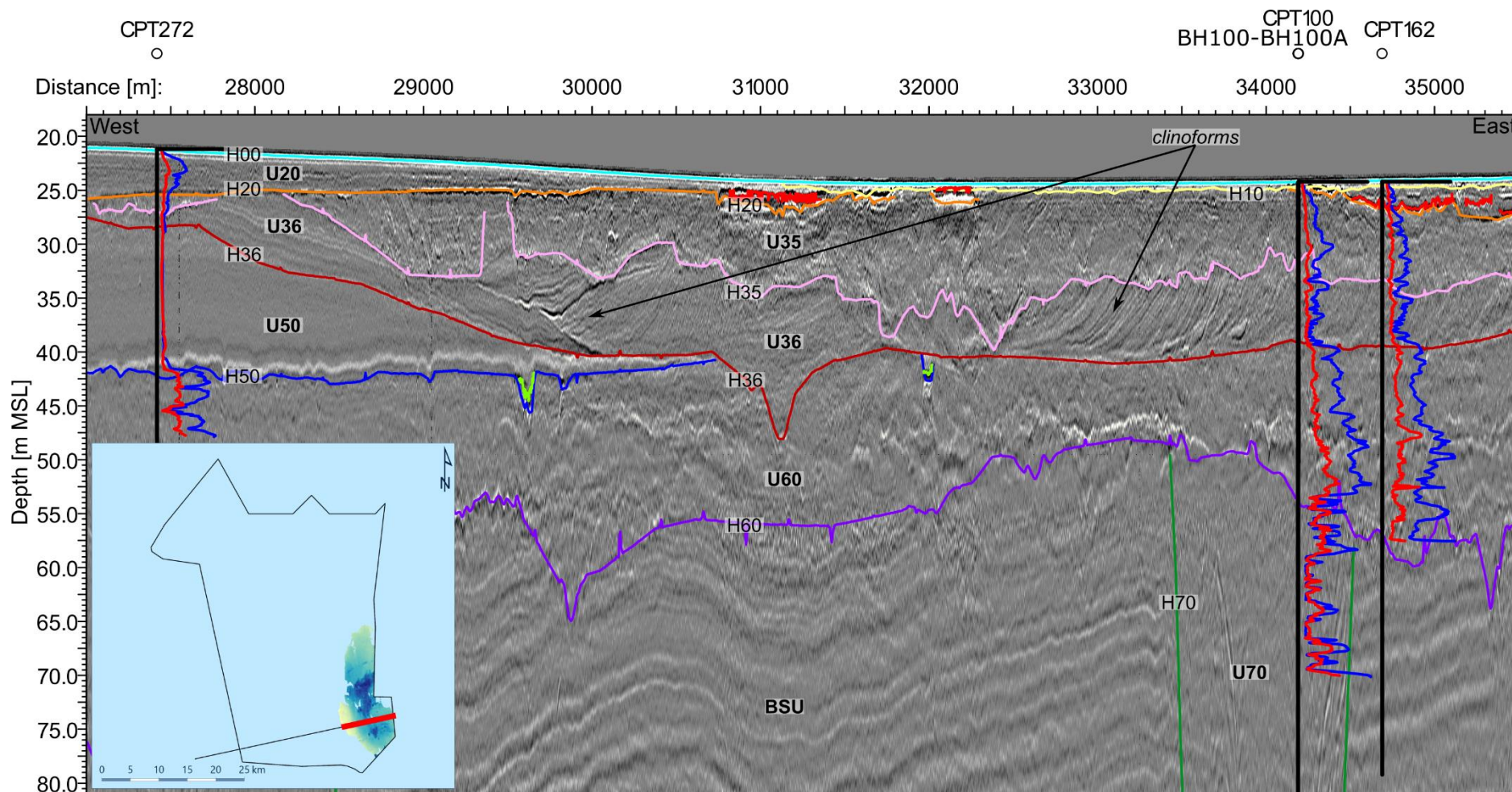
Figure 6.30: 2D UHR seismic data example of Unit U36. Line EAXD416P1, CPT272, CPT100 and CPT162. CPT scale: Blue is q_c with a scale from 0 to 80 MPa and red is f_s with a scale of 0 to 2 MPa

FUGRO

6.7.2 Integration and interpretation

Unit U36 comprising silty sand with beds of clay is a transitional unit between the marine clay of Unit U50 and the meltwater (glacio-fluvial) sand of Unit U35. The presence of clinoforms and the coarsening upward succession of Unit U50, U36 and U35 may indicate that Unit U36 was deposited in a deltaic marine environment. It is interpreted that the river system (represented by Unit U35) supplying sediment to a marine environment (represented by Unit U50) enters the marine area and forms the delta deposits seen in Unit U36. The variable dip direction of the stratification in Unit U36 can be explained by the presence of multiple delta lobes, which prograded in different directions.

Due to the stratigraphic position of Unit U36 between the Eemian marine clay of Unit U50 and the Weichselian glacio-fluvial sand of Unit U35, it is interpreted that this unit is of Late Eemian to Early Weichselian age. Figure 3.6 shows channels from post Eemian periods that may be associated with the delta like deposits of U36.

Figure 6.31 displays the integration between the thickness of U36 in the geophysics and geotechnical locations. Some inconsistencies between geophysical and geotechnical datasets are seen in the north of the unit, due to the gradational change of sediment types from the sands of U36 to the laterally equivalent clays of U50, making integration more challenging in this area. Good correlation in the centre of the unit though is observed.
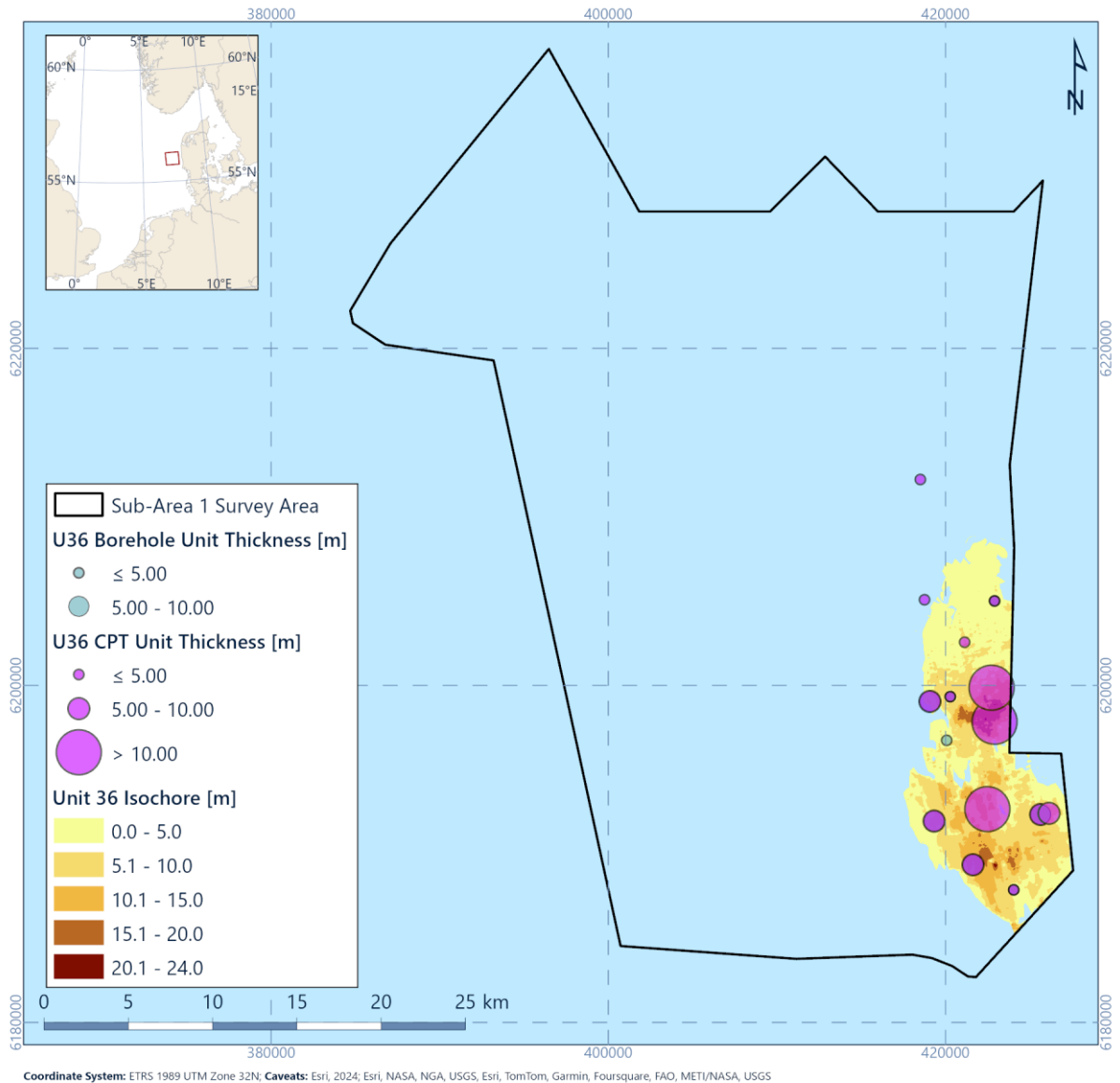
Figure 6.31: Isochore for U36 corelated with geotechnical data recoveries

6.8 Spatial Geological Model - Unit U50

6.8.1 Seismic Character

Unit U50 is mainly present in the eastern half of the site, where it forms a sheet-like geometry unit (Figure 6.32, Figure 6.33, Figure 6.34). Across the rest of the site the unit is present in localised areas where it forms channel infills (Figure 6.35). The average thickness is approximately 8 m and very locally reaches approximately 50 m (Figure 6.34). Where Unit U50 forms a channel infill, it is often associated with tunnel valleys of Unit U65 (Figure 6.35).

Internally, Unit U50 is acoustically transparent to weakly stratified in the east of the site (Figure 6.35). Where Unit U50 forms channel infill, it is well stratified (Figure 6.35). In the east, the basal horizon H50 if often overlain by a flat low amplitude positive reflector (Figure 6.35).

A seismic anomaly with a high amplitude negative polarity is regularly present at the base of Unit U50 (See Section 6.15.1). Locally, acoustic blanking is associated with channels at the base of Unit U50 (See Section 6.15.3).
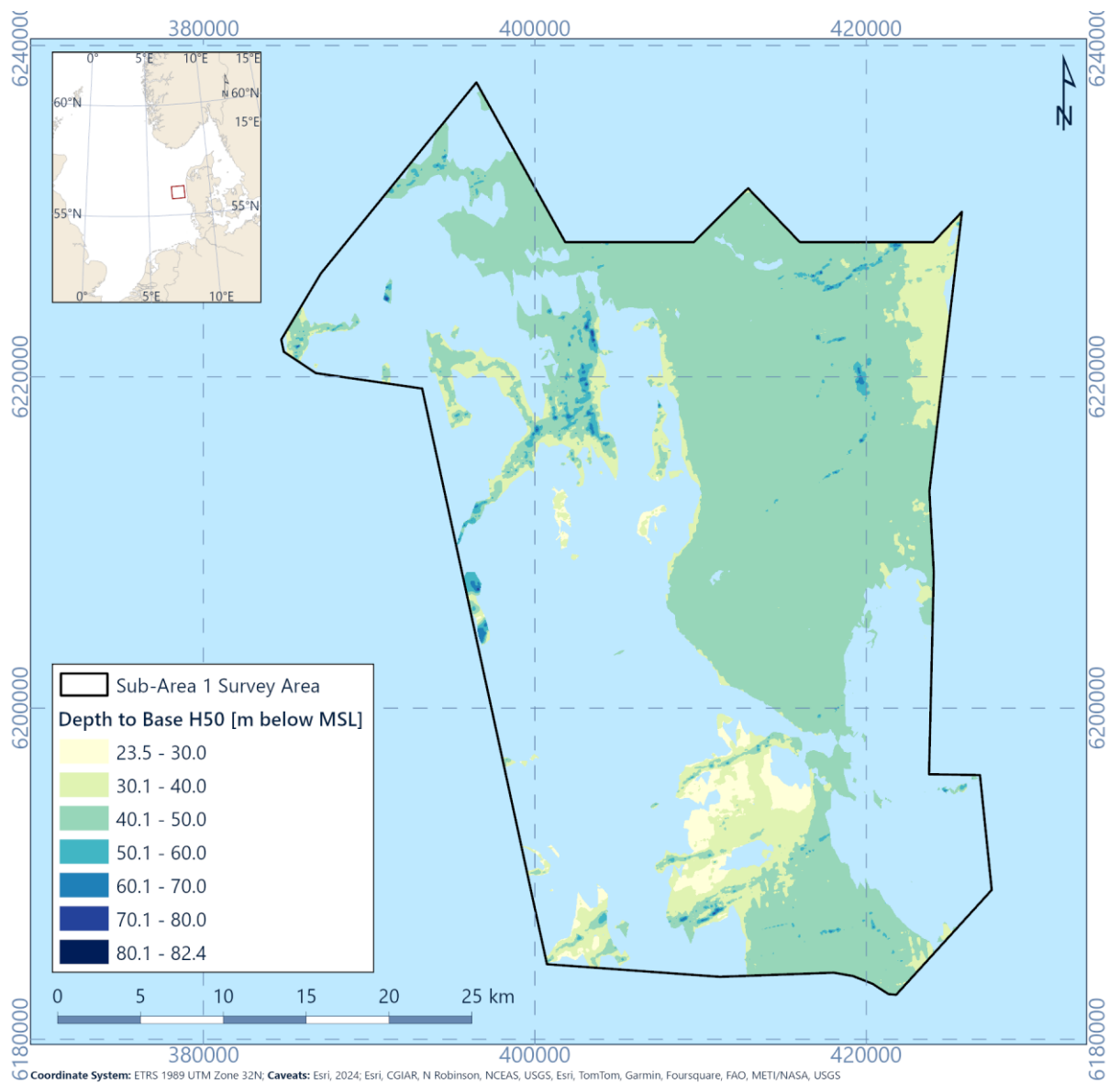
Figure 6.32: Depth to horizon H50 (base of Unit U50) relative to MSL
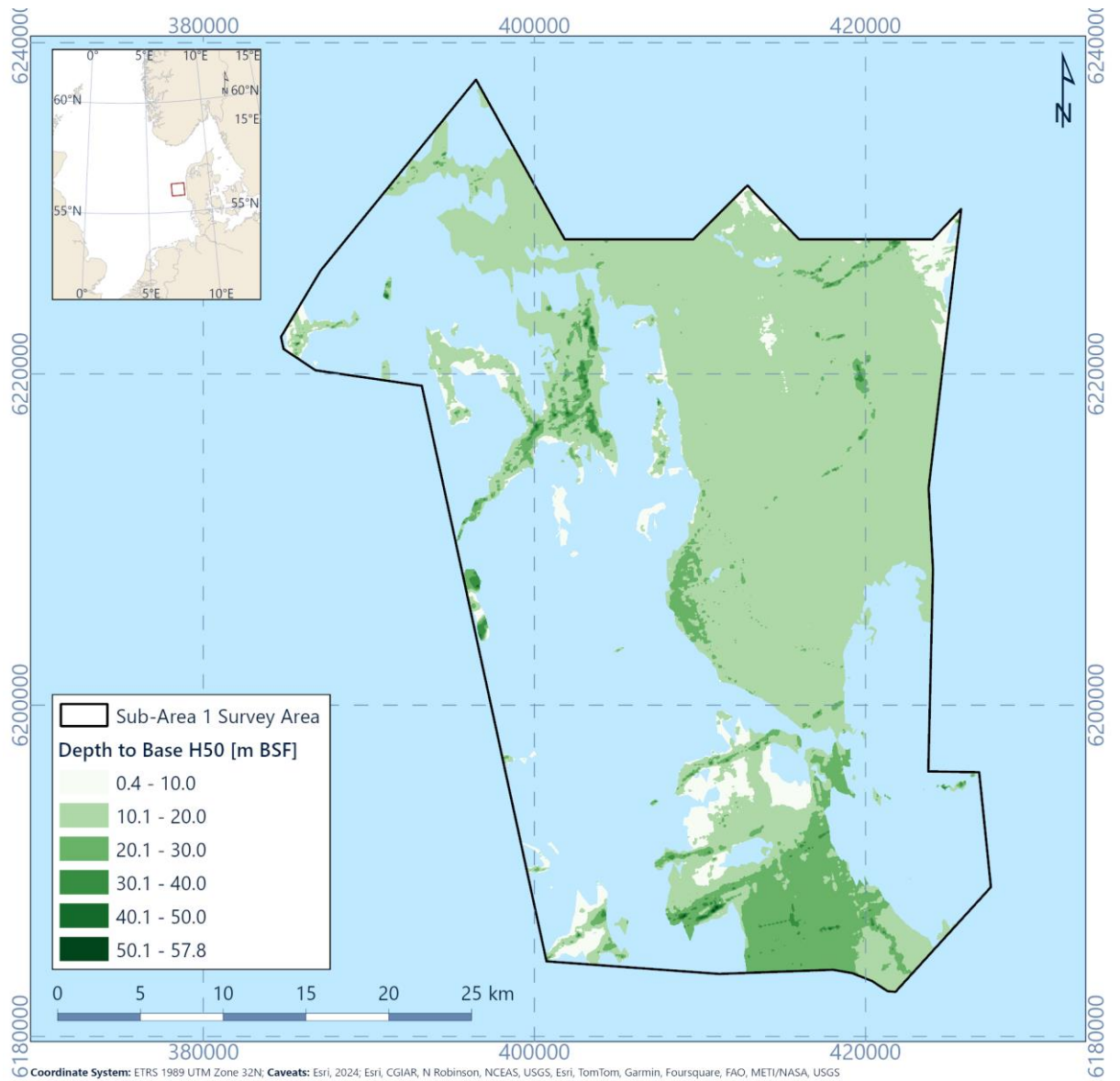
Figure 6.33: Depth to horizon H50 (Base of Unit U50) relative to seabed
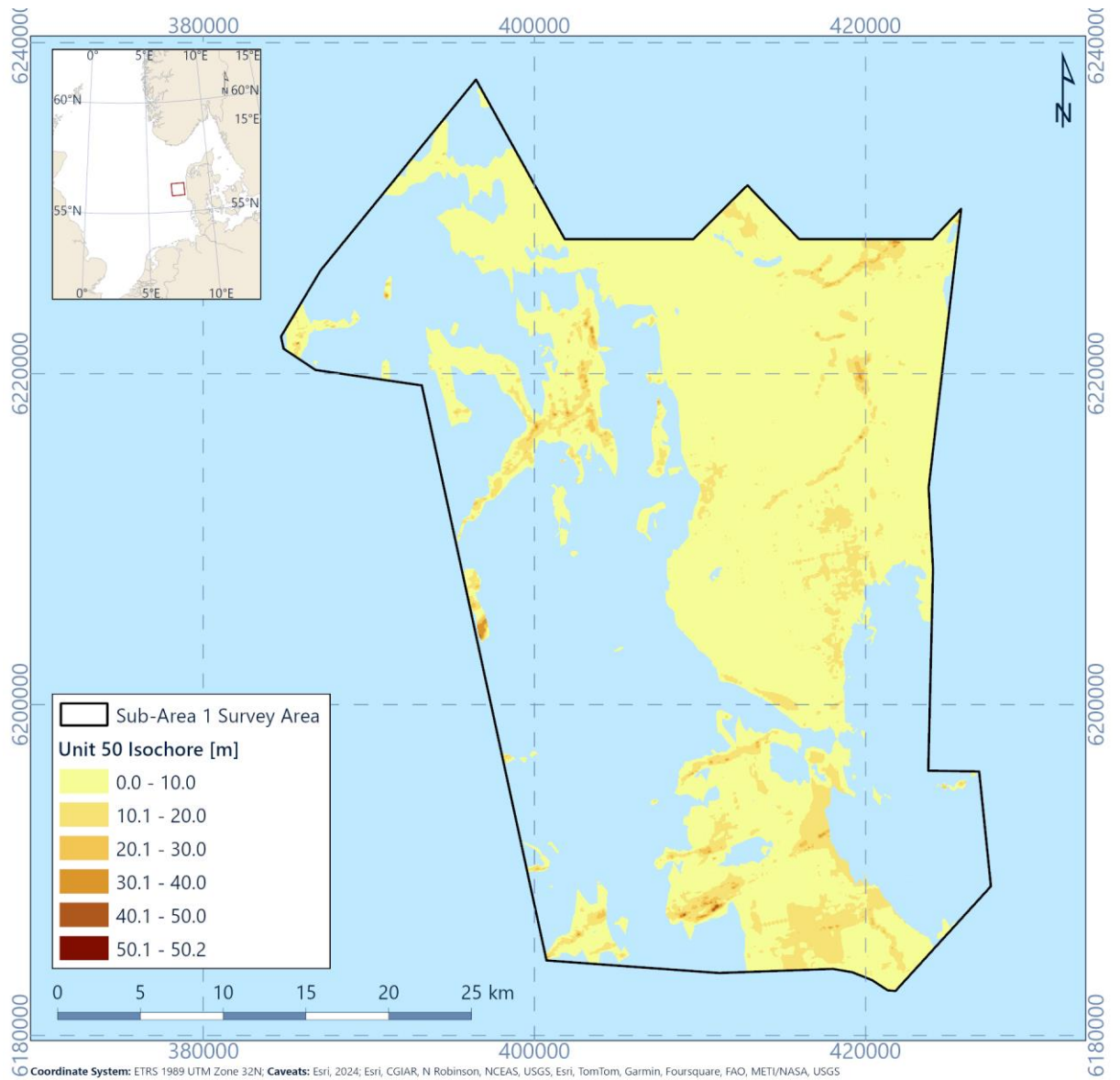
Figure 6.34: Isochore of Unit U50
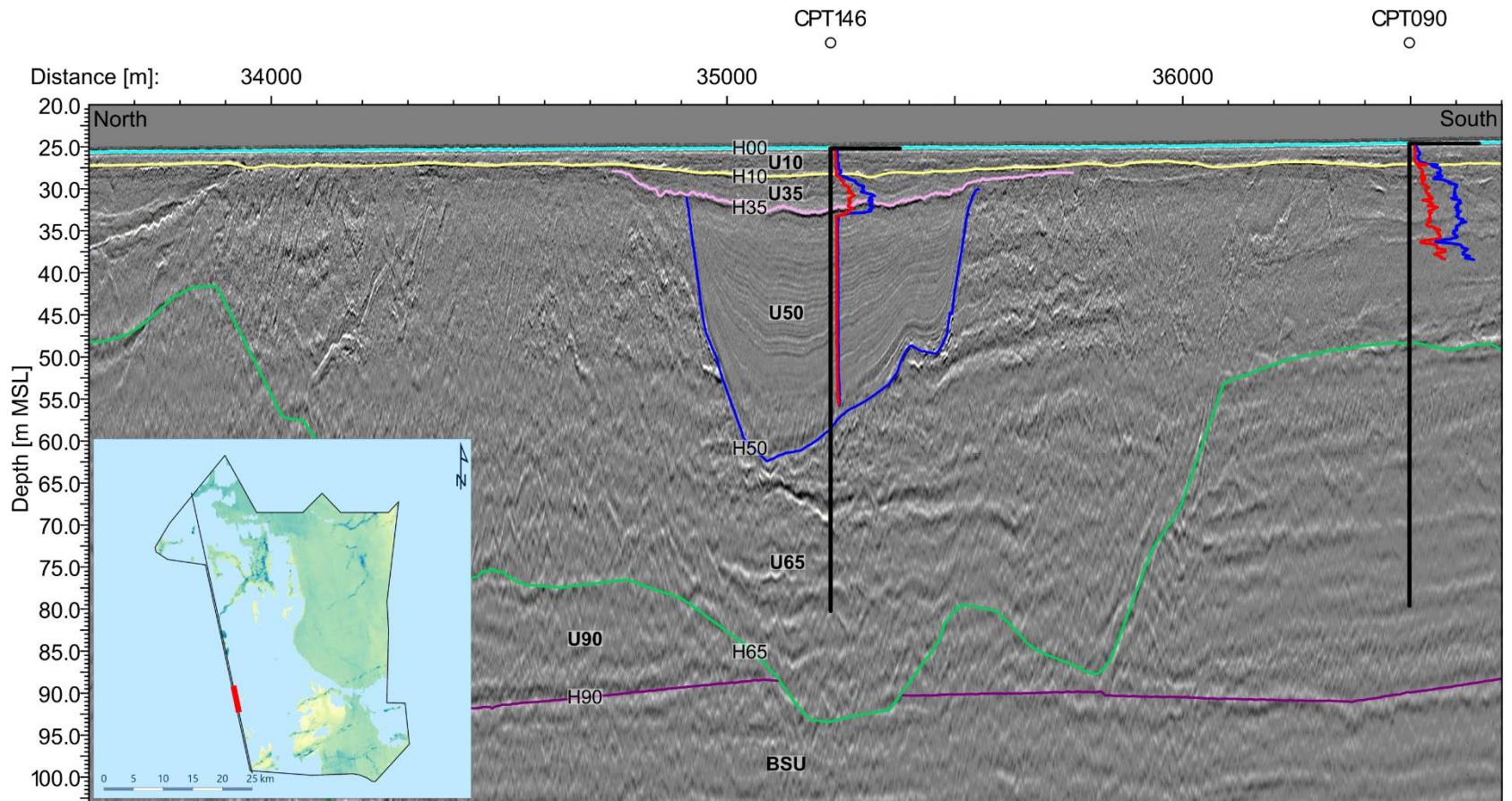
Figure 6.35: 2D UHR seismic data example of Unit U50. Line EAAH228P1, CPT146 and CPT090. CPT scale: Blue is q_c with a scale from 0 to 80 MPa and red is f_s with a scale of 0 to 2 MPa

6.8.2   Integration and interpretation

The acoustically transparent to stratified seismic character and clay soil, may indicate that Unit U50 was deposited in low energy freshwater (lacustrine) and marine environments.

The fluvial channels of pre-existing river systems (Unit U50 and Unit U65) were initially filled as they were gradually drowned by the rising sea level at the beginning of the Eemian interglacial period. Sand that was previously deposited in those channels was reworked and deposited again as a thin layer of sand at the base of Unit U50 (Unit 50b). Afterwards, due to a further rise in sea level, the depositional environment shifted to marine with clay being deposited.

It is interpreted that Unit U50 was deposited during the Eemian interglacial period and correlating to Eemian marine clays to the south-east and east of the site (Figure 3.6, Konradi et al., 2005; Larsen & Andersen et al., 2005).

Within the channelised areas in the west of the site, there may be greater uncertainty in the extents mapped with limited ability to map the complex geometries between seismic inlines. Infill of depressions as observed in the areas of U50 in the west of the site may reflect similar depositional processes as those observed in U69, with a possible time period between the deposition of these sediments compared to the marine deposits observed in the west of the site. Figure 6.36 shows the correlation of the thickness of U50 between the geophysics data and geotechnical locations. Good corelation between datasets is observed across the site.
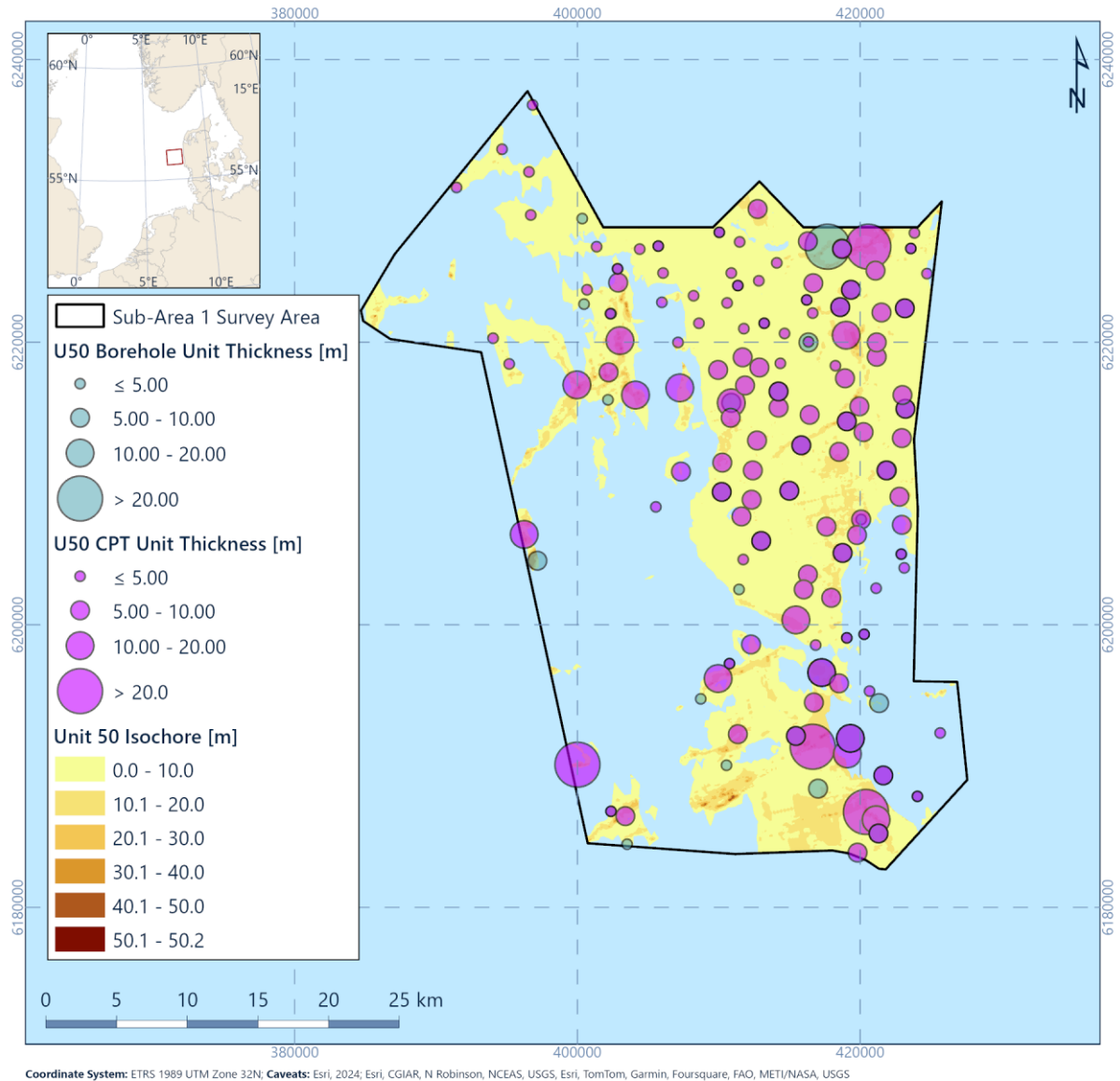
Figure 6.36: Isochore for U50 corelated with geotechnical data recoveries

6.9 Spatial Geological Model - Unit U60

6.9.1 Seismic Character

Unit U60 is present in the north and east of the site (Figure 6.37, Figure 6.38). It is absent in the south-west of the site. Unit U60 forms the sheet-like infill of a wide (approximately 20 km wide) but shallow (approximately 30 m) valley (Figure 6.39). This valley has steep margins, which have a sinus-shape in planform (Figure 6.40). Locally, Unit U60 increases slightly in thickness close to the margins of the valley (Figure 6.39). The basal horizon H60 is flat to undulating (Figure 6.37, Figure 6.38). Locally, where the base of Unit U60 is channelised, it reaches a maximum thickness of approximately 80 m (Figure 6.39).

Internally, Unit U60 has a complex seismic character. This includes chaotic seismic facies to horizontal and inclined stratification and the presence of internal erosion surfaces. Locally

FUGRO

high amplitude positive reflectors are present, which may represent gravel beds (see Section 6.15.4).
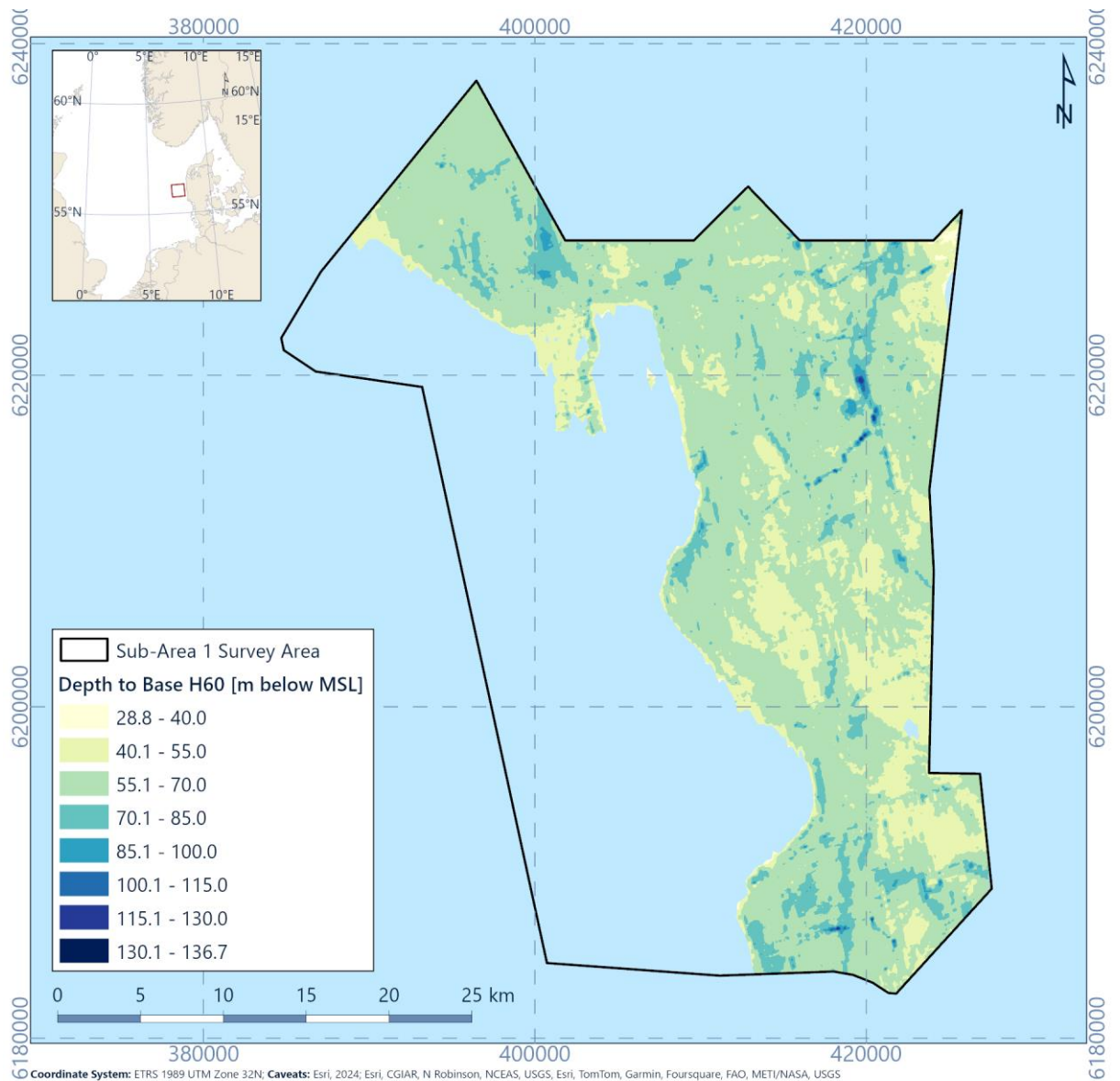
Figure 6.37: Depth to horizon H60 (base of Unit U60) relative to MSL
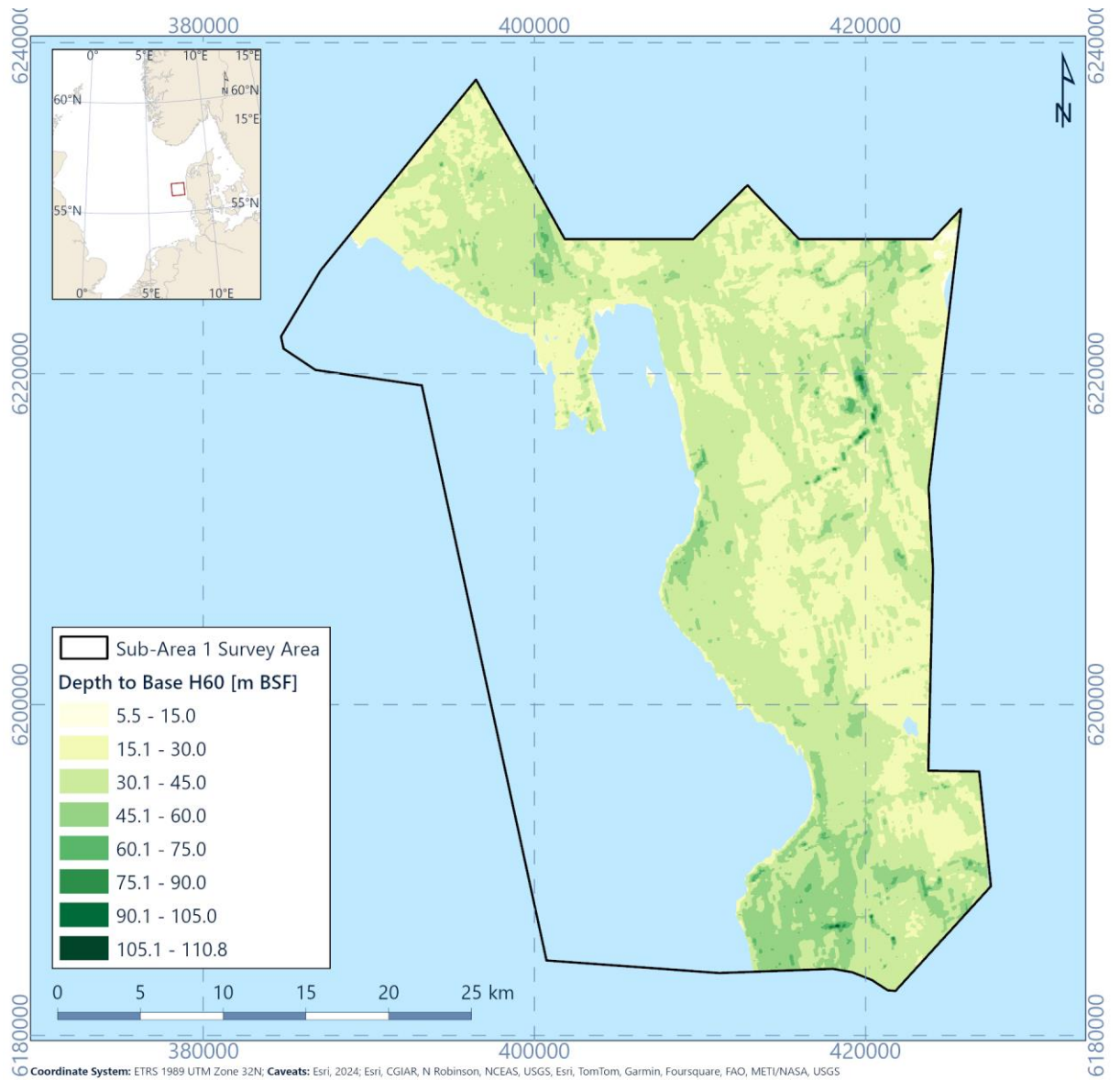
Figure 6.38: Depth to horizon H60 (Base of Unit U60) relative to seabed
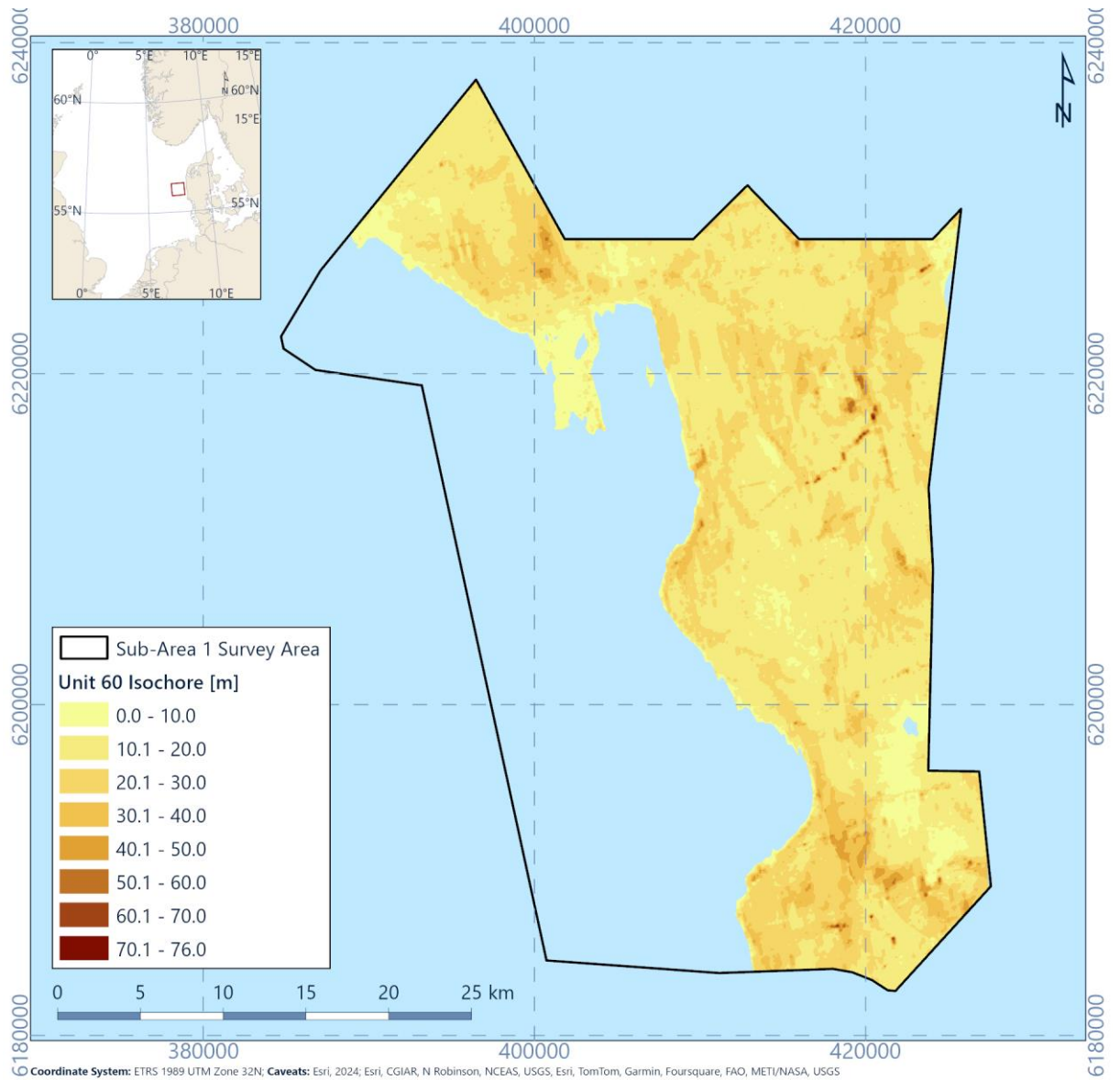
Figure 6.39: Isochore of Unit U60
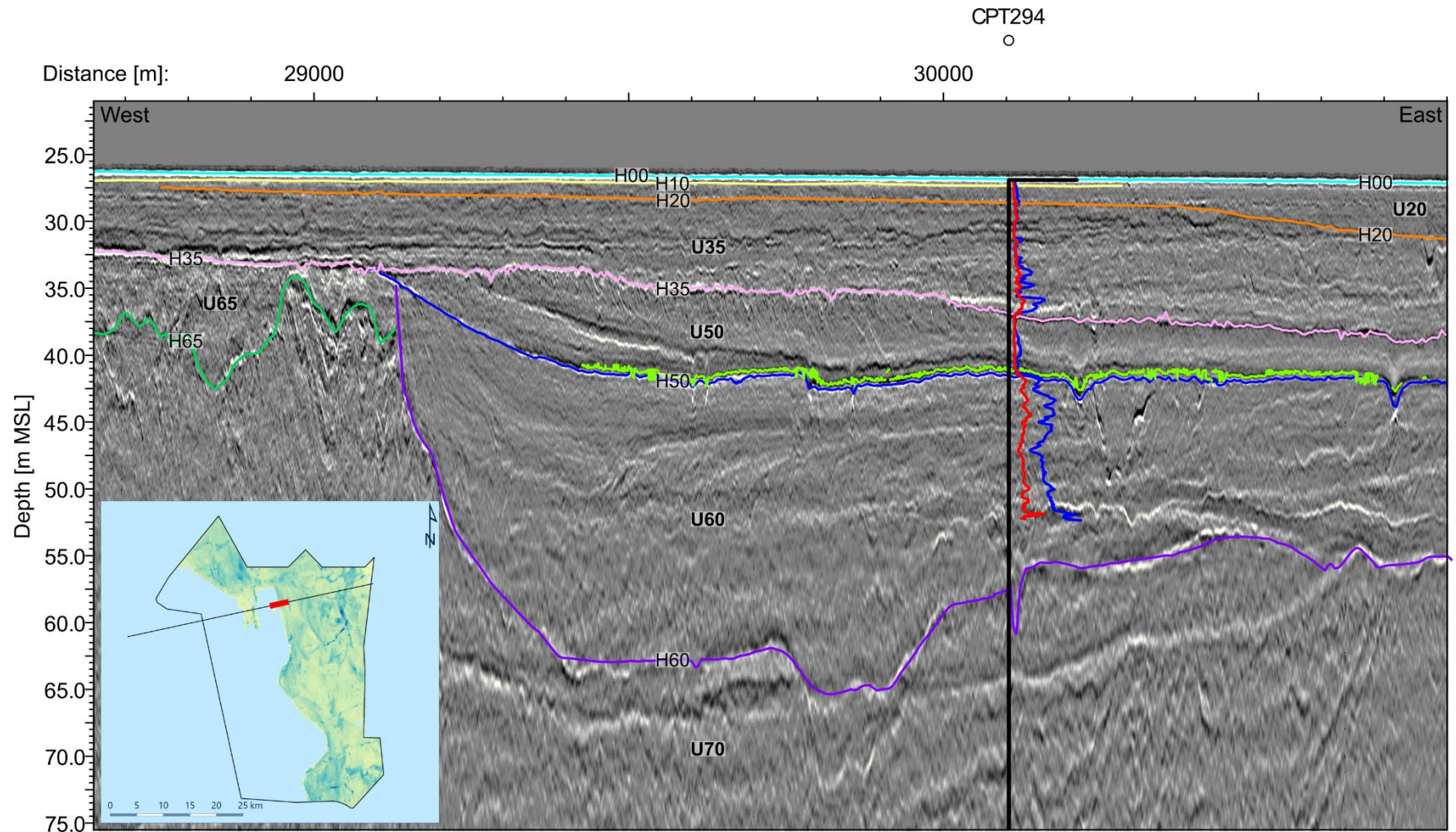
Figure 6.40: 2D UHR seismic data example of the Unit U60. Line EAXA384P1, CPT294. CPT scale: Blue is q_c with a scale from 0 to 80 MPa and red is f_s with a scale of 0 to 2 MPa

6.9.2   Integration and interpretation

The erosional base of Unit U60, the variable internal seismic character with internal erosion surfaces, and sand dominated soil type, may indicate that this unit was deposited in a meltwater (braided glacio-fluvial) depositional environment. The geometry of the basal horizon H60 suggests that the wide valley was eroded by a meandering channel.

Sediments deposited within boreholes in U60 are predominantly sands with some gravels and organic material within, supporting the interpretation of a fluvial environment. There is a basal gravel bed in areas of U60 as well, highlighting the erosive nature of the unit.

Figure 6.41 displays the integration between the thickness of U60 within the geophysics and geotechnical locations.

The stratigraphic position of Unit U60 between Unit U65 (interpreted as Saalian age) and Unit U50 (interpreted as Eemian age), suggests that Unit U60 was deposited in the latest stage of the Saalian glacial period, when the ice sheets already retreated from the site and were replaced by a fluvial outwash plain (Friborg, 1996; Konradi et al. 2005). Correlation between datasets is generally good. Limited outliers are identified however associated with the infilling of depressions in U70 by U60 sediments. In addition the boundary between sands in U60 and sands in U70 can be challenging to identify in geotechnical data BH075 is an example of this challenge.
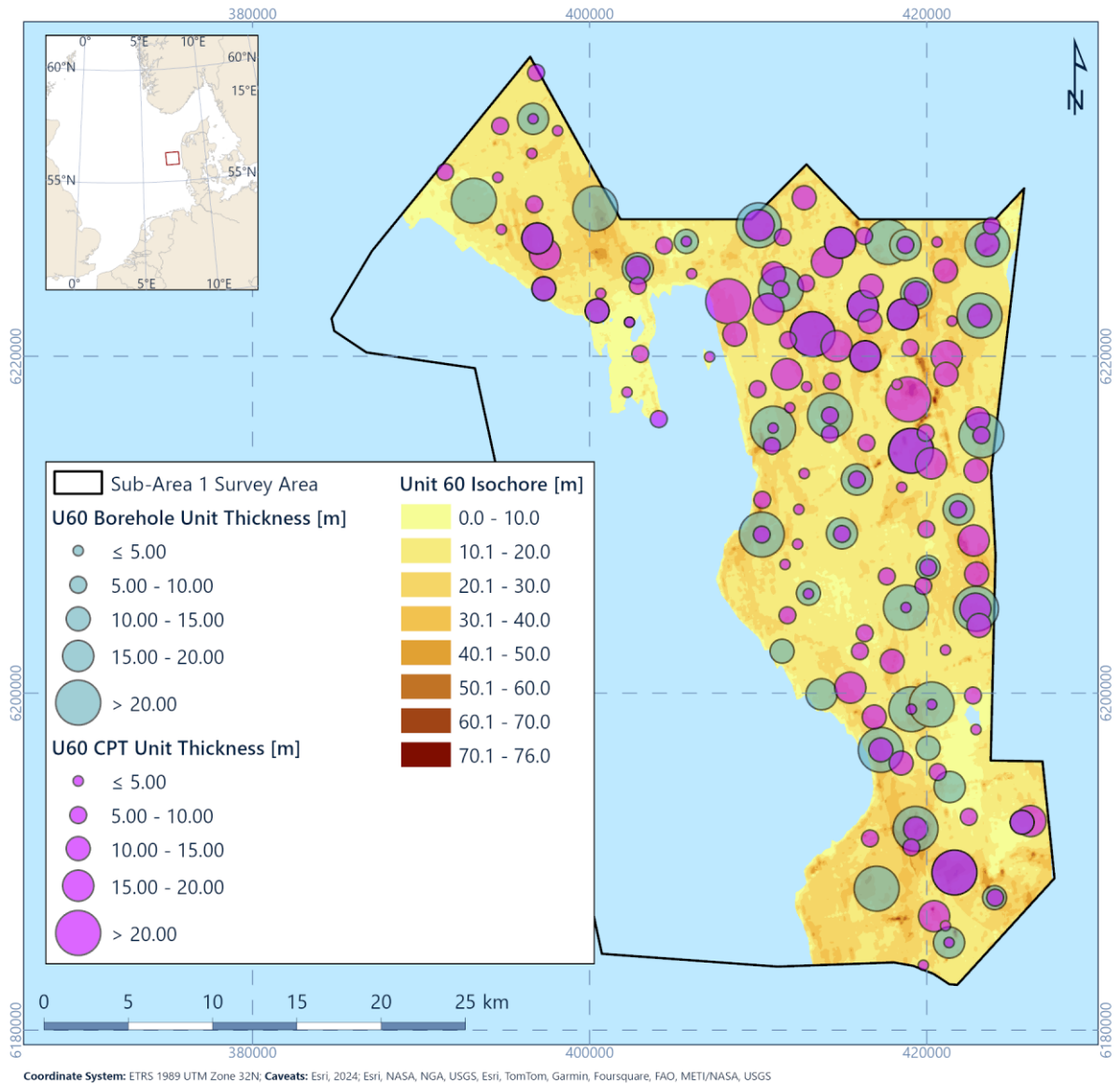
Figure 6.41: Isochore for U60 corelated with geotechnical data recoveries

6.10   Spatial Geological Model - Unit U65

6.10.1   Seismic Character

Unit U65 is present mainly in the south-west of the site, and its presence becomes more intermittent towards the north-east of the site (Figure 6.42, Figure 6.43). The unit forms the infill of tunnel valleys deep incisions as well as a layer with sheet-like geometry. Where Unit U65 has a sheet-like geometry it gradually overlies Unit U90, on the western edge of study area. The boundary between Unit U65 and U90 is picked such that the stratified and lateral continuous seismic character is included in Unit U90, and internal erosion surfaces with a laterally variable seismic character are part of Unit U65. However, due to the gradual transition between Unit U90 and Unit U65, the pick of this boundary is locally uncertain. The thickness is generally up to 35 m in inter valley areas and reaches a maximum thickness of

more than 150 m in tunnel valleys (Figure 6.44). These tunnel valleys are 500 m to 2000 m wide.

Unit U65 has a variable and complex seismic character. This includes chaotic seismic facies, horizontal and inclined stratification, internal erosion surfaces and facies that are acoustically transparent (Figure 6.35, Figure 6.40, Figure 6.45). This variable seismic character is also reflected in the variable sediment characteristics.

Within the study area the tunnel valleys filled with Unit U65 have an overall west-south-west to east-north-east orientation and the orientation (Figure 6.42, Figure 6.45). Their infill has a variable seismic character, exhibiting horizontal and inclined stratification, acoustically transparent to chaotic seismic facies (Figure 6.45).
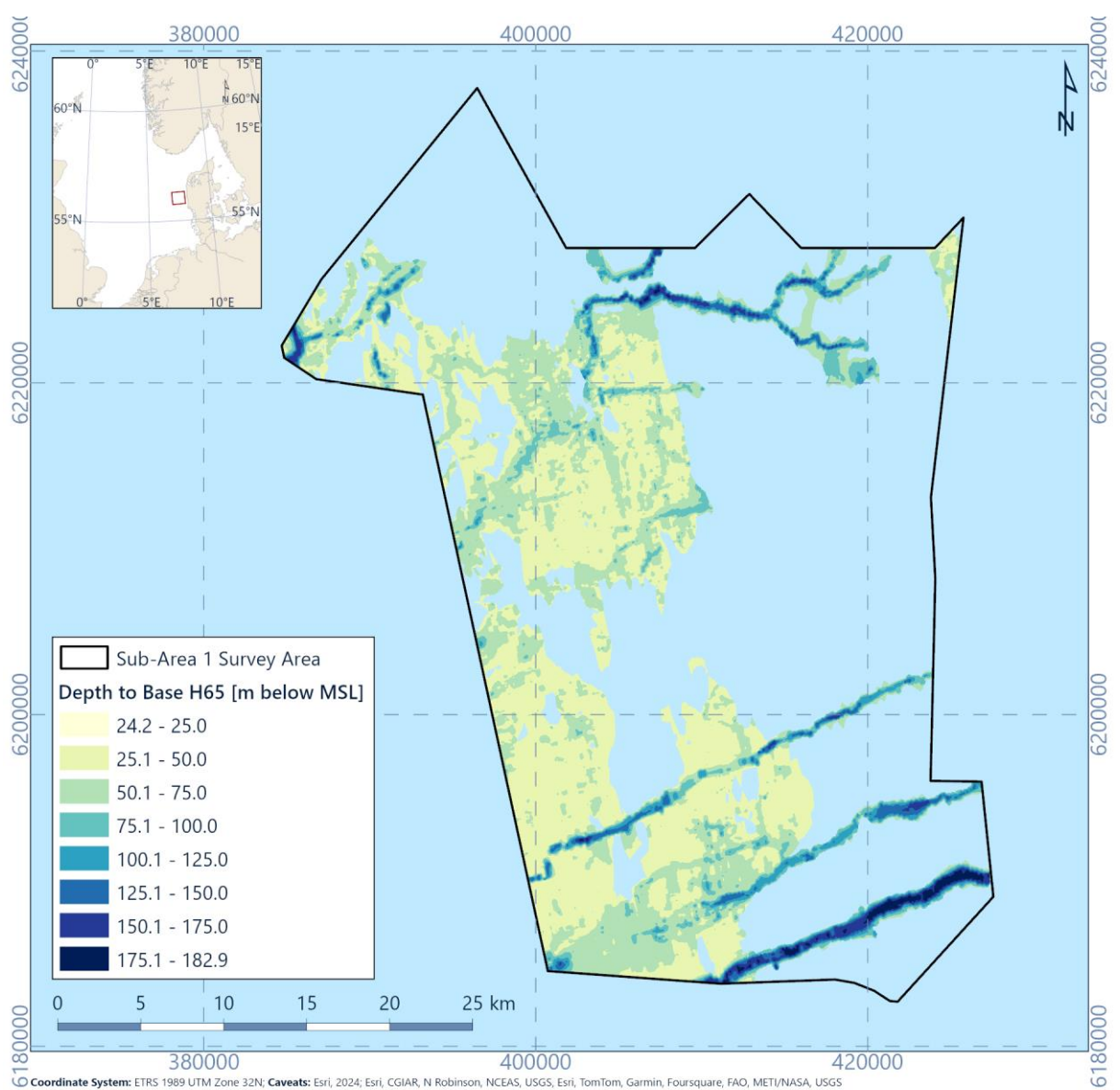
Figure 6.42: Depth to horizon H65 (base of Unit U65) relative to MSL
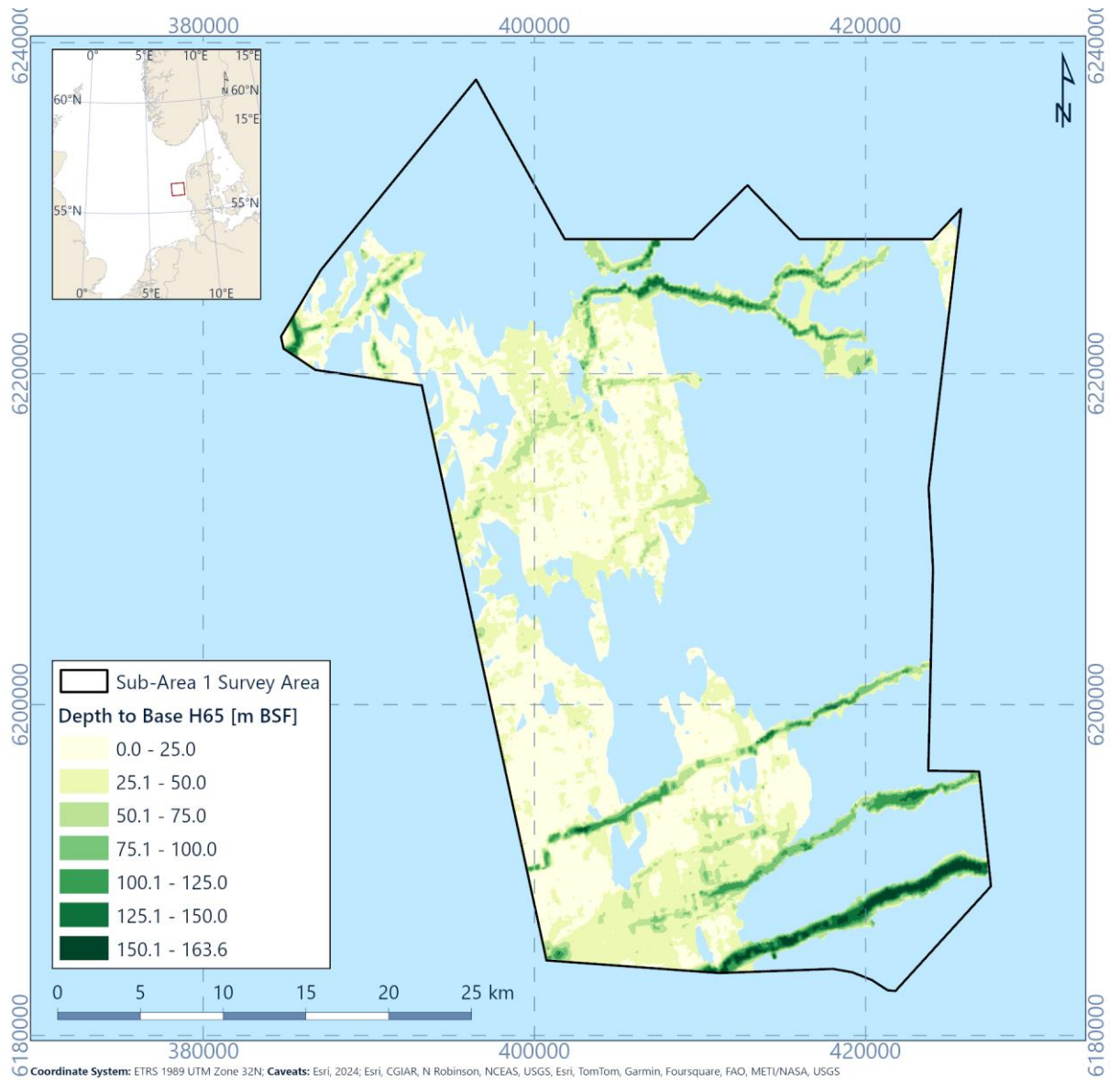
Figure 6.43: Depth to horizon H65 (Base of Unit U65) relative to seabed
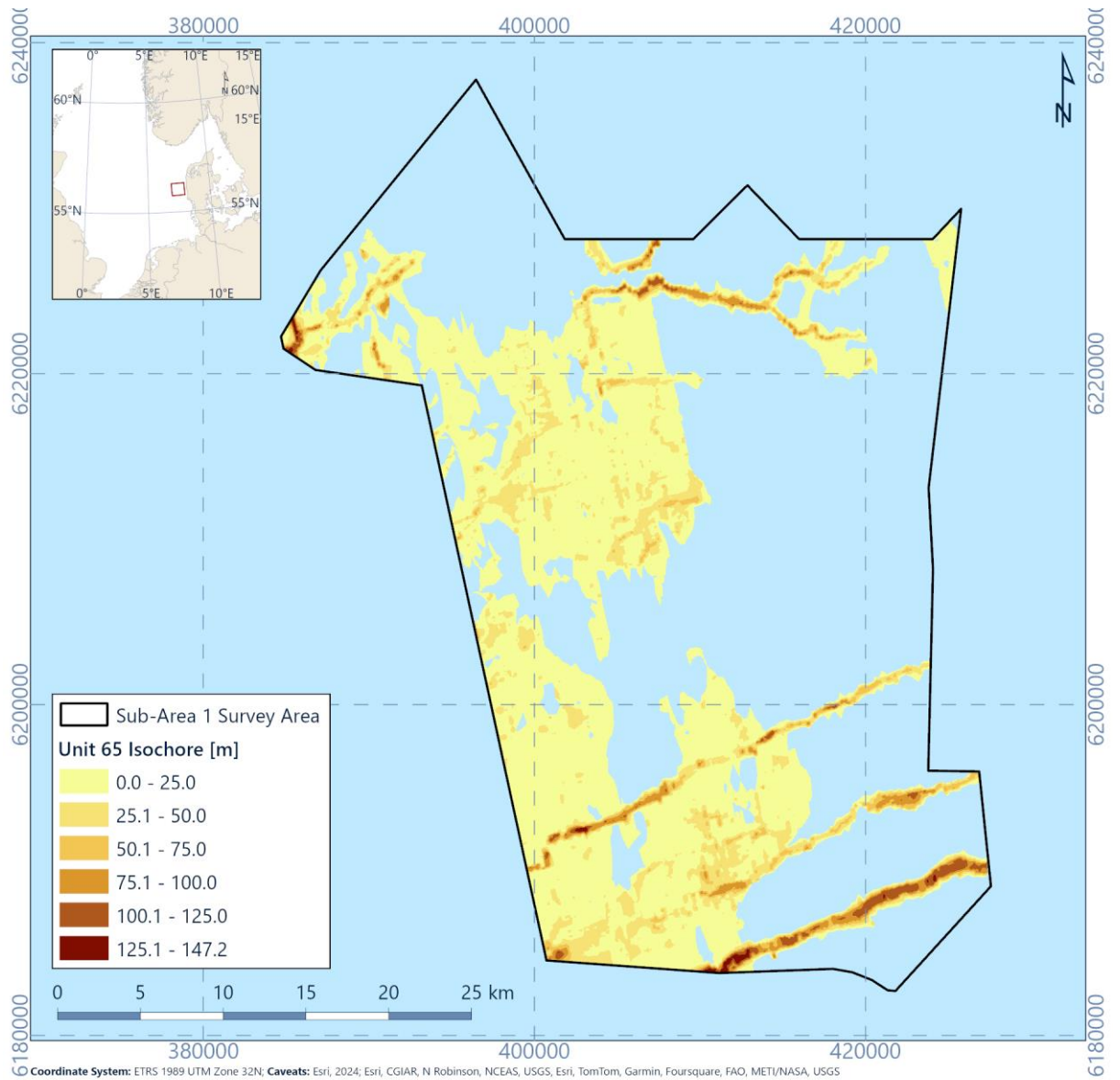
Figure 6.44: Isochore of Unit U65
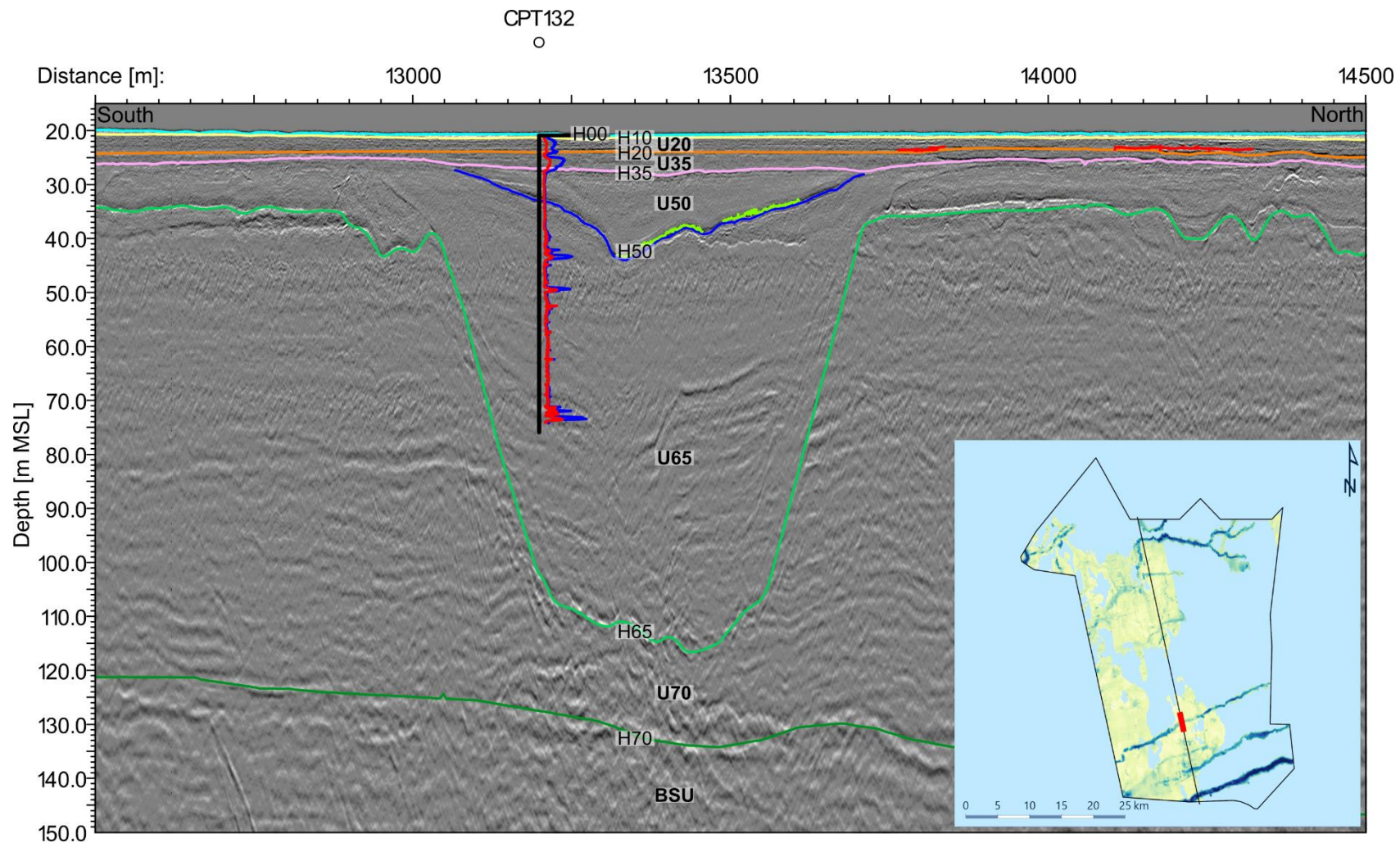
Figure 6.45: 2D UHR seismic data example of Unit U65. Line EAAT275P2, CPT132. CPT scale: Blue is q_c with a scale from 0 to 80 MPa and red is f_s with a scale of 0 to 2 MPa

6.10.2   Integration and interpretation

The wide variety of acoustic characters and soil types, and the presence of tunnel valleys, may indicate that Unit U65 comprises sediments of several glacial and periglacial depositional environments.

Sand dominated soils are interpreted to correspond to meltwater (glacio-fluvial) deposits. The seismic facies show internal erosion surfaces and horizontal to inclined stratification. Seismic anomalies in these deposits are interpreted to be a result of the presence of overbank peat beds (see Section 6.15.1).

Clay deposits are interpreted to represent deposition in a low energy freshwater (glacio-lacustrine) or (glacio-) marine setting. These deposits has an acoustically transparent to well stratified seismic character.

The tunnel valley features are also observed within the U65 package, with a chaotic seismic character. These areas have variable soil types including till and are interpreted to be glacier deposits, however may also have variable infill from proceeding environments. The tunnel valley features are orientated in a northeast-south west orientation suggest ice advance from the east. This may represent late Drenthe or Warthe 1 ice advance phases (Winsemann et all, 2020).

Unit U65 can be correlated to variable glacier deposits in south-west Jutland (onshore Denmark), which are Saalian in age. Onshore Jutland, the Saalian glacier deposits form a Saalian glacial landscapes called 'hill islands' (bakkø; Figure 5.6; Friborg, 1996; Konradi et al. 2005). The Saalian glacial period includes several stadials and interstadials (Figure 3.3). The complexity of Unit U65 can be attributed to this long period with deposition in variable depositional environments.

Geotechnical properties within the U65 sediments reflect the likely variable depositional environment represented by the unit (Figure 6.46). Primary lithologies are evenly split between sand and clay sediments. Often clays and sands have high secondary components of gravels, highlighting possible glacial till sediments. Within valley features more clays may be observed than outside of the valley areas, however in both instances high variability of soil types are observed. Correlation between datasets is generally good, however only limited geotechnical datasets penetrate the unit. In addition some of the western channelised areas are not captured in the geotechnical datasets, leading to greater uncertainty on the infill nature.
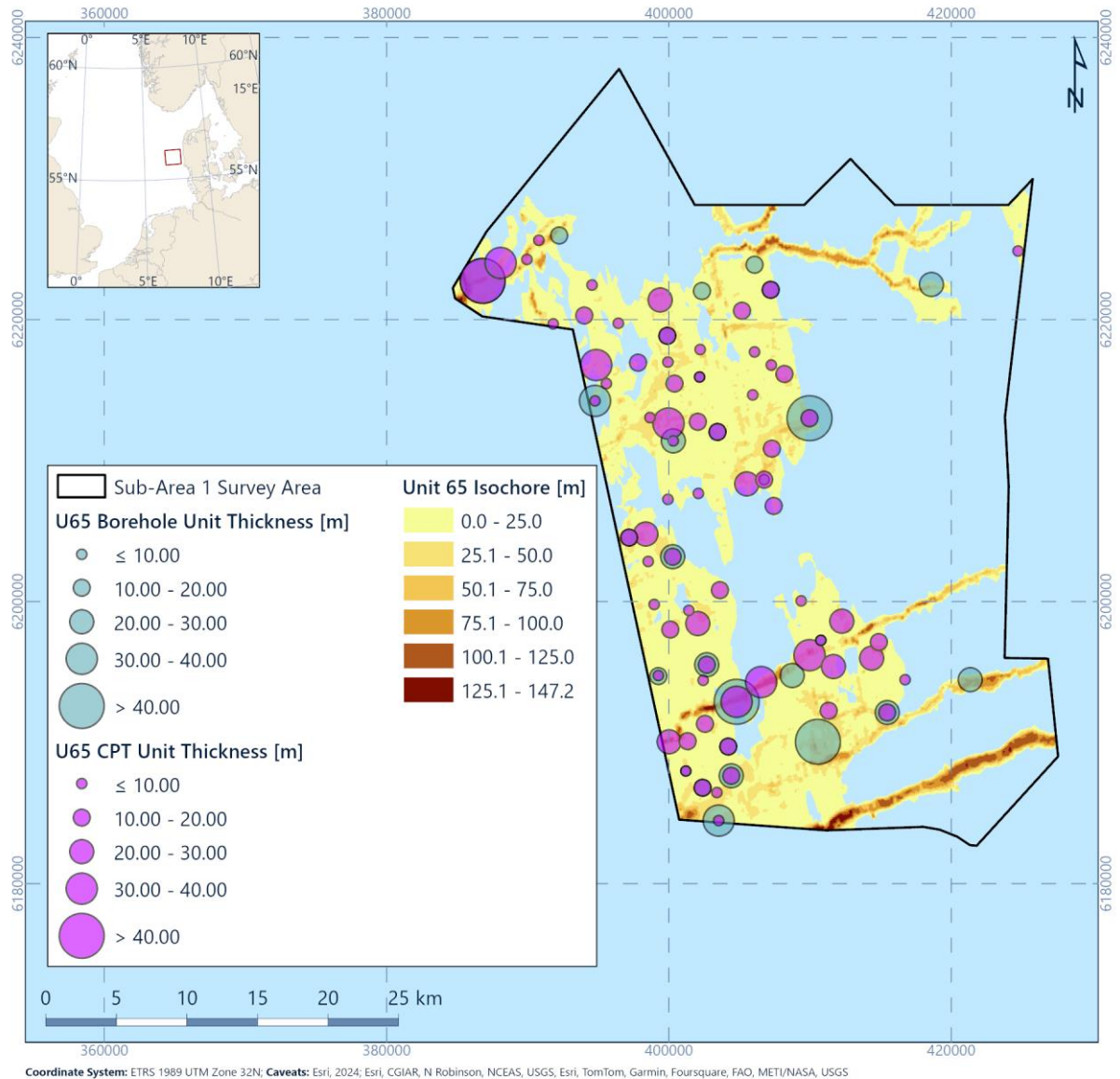
Figure 6.46: Isochore for U65 corelated with geotechnical data recoveries

Based on the overconsolidated nature of the clays it is likely that a period of ice sheet advance during the Saalian with overconsolidation and possible higher strengths near the top of the unit suggesting direct ice loading.

6.11 Spatial Geological Model – Unit U69

6.11.1 Seismic Character

Unit U69 forms the upper part of the infill of deep tunnel valleys with a north to south orientation (Figure 6.47, Figure 6.48). The unit lies within the larger tunnel valley formations that are delinated by Unit 70 (Figure 6.55), and represents the upper portion of these sediments. The base is marked by horizon H69, which is characterized by the onlap of reflectors onto the horizon. The seismic character of unit is defined by stratified or

FUGRO

acoustically transparent seismic data. In some areas it can be up to approximately 105 m thick (Figure 6.49)
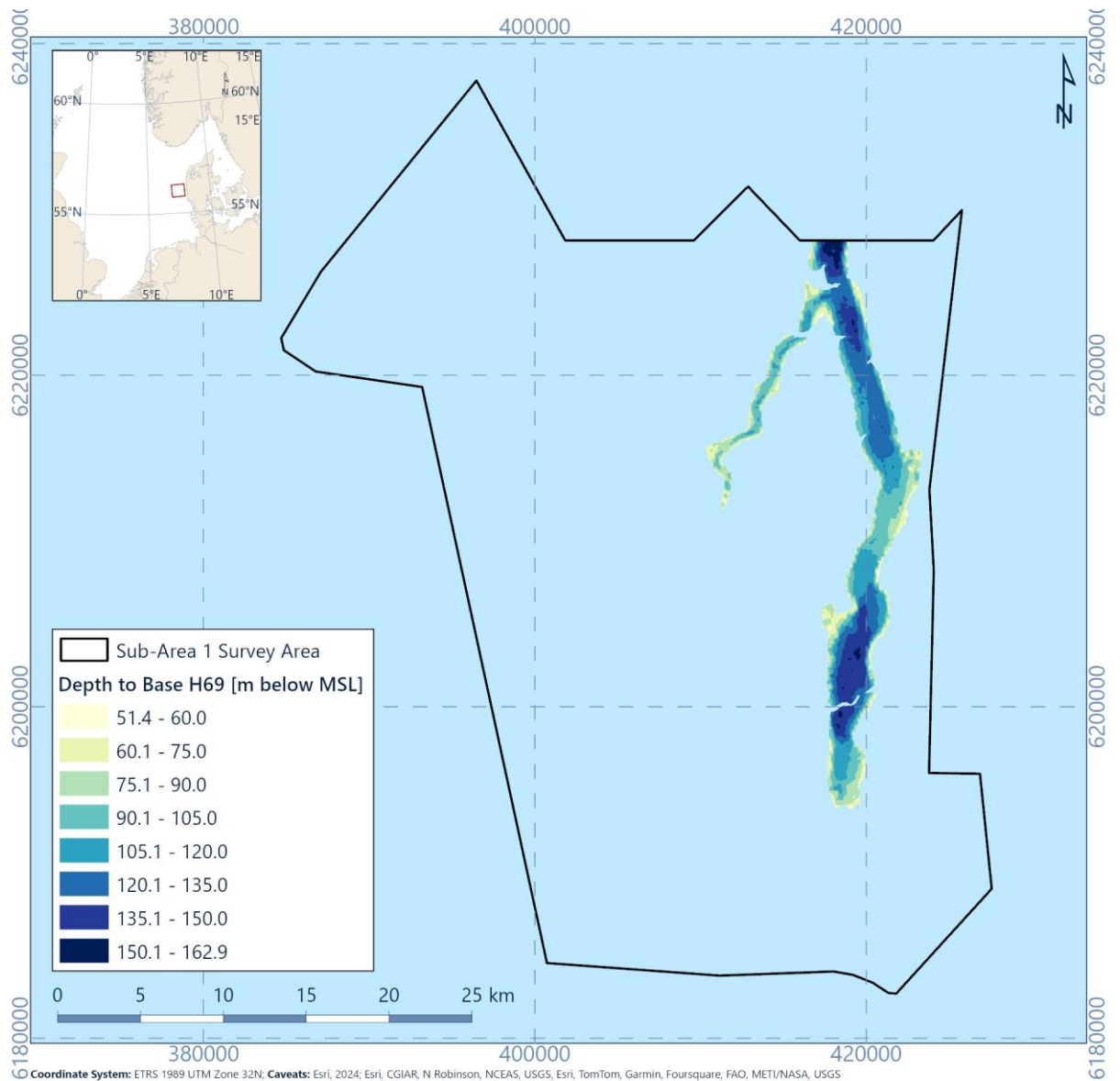
Figure 6.47: Depth to horizon H69 (Base of Unit U69) relative to MSL
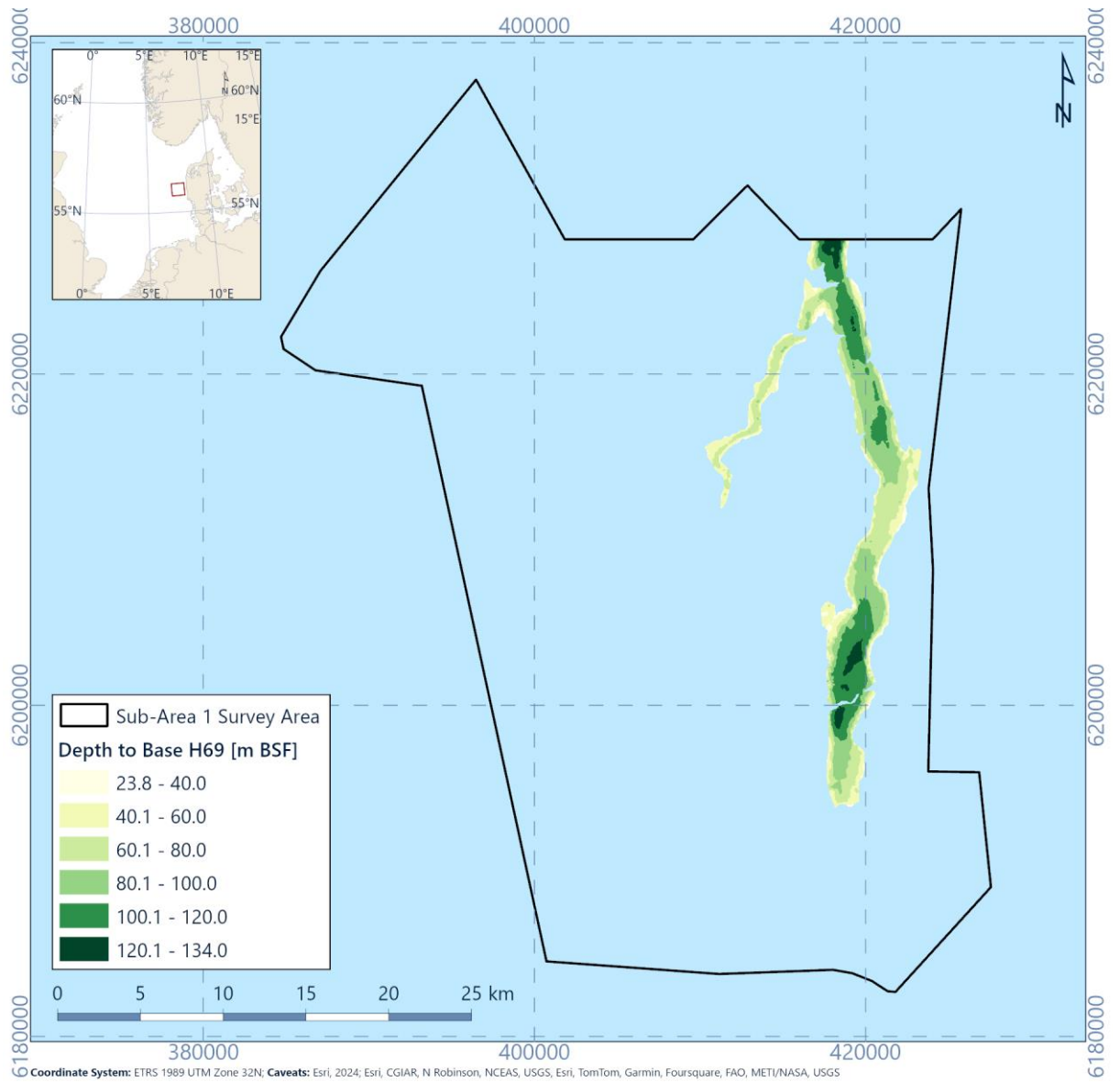
Figure 6.48: Depth to horizon H69 (Base of Unit U69) relative to seabed.
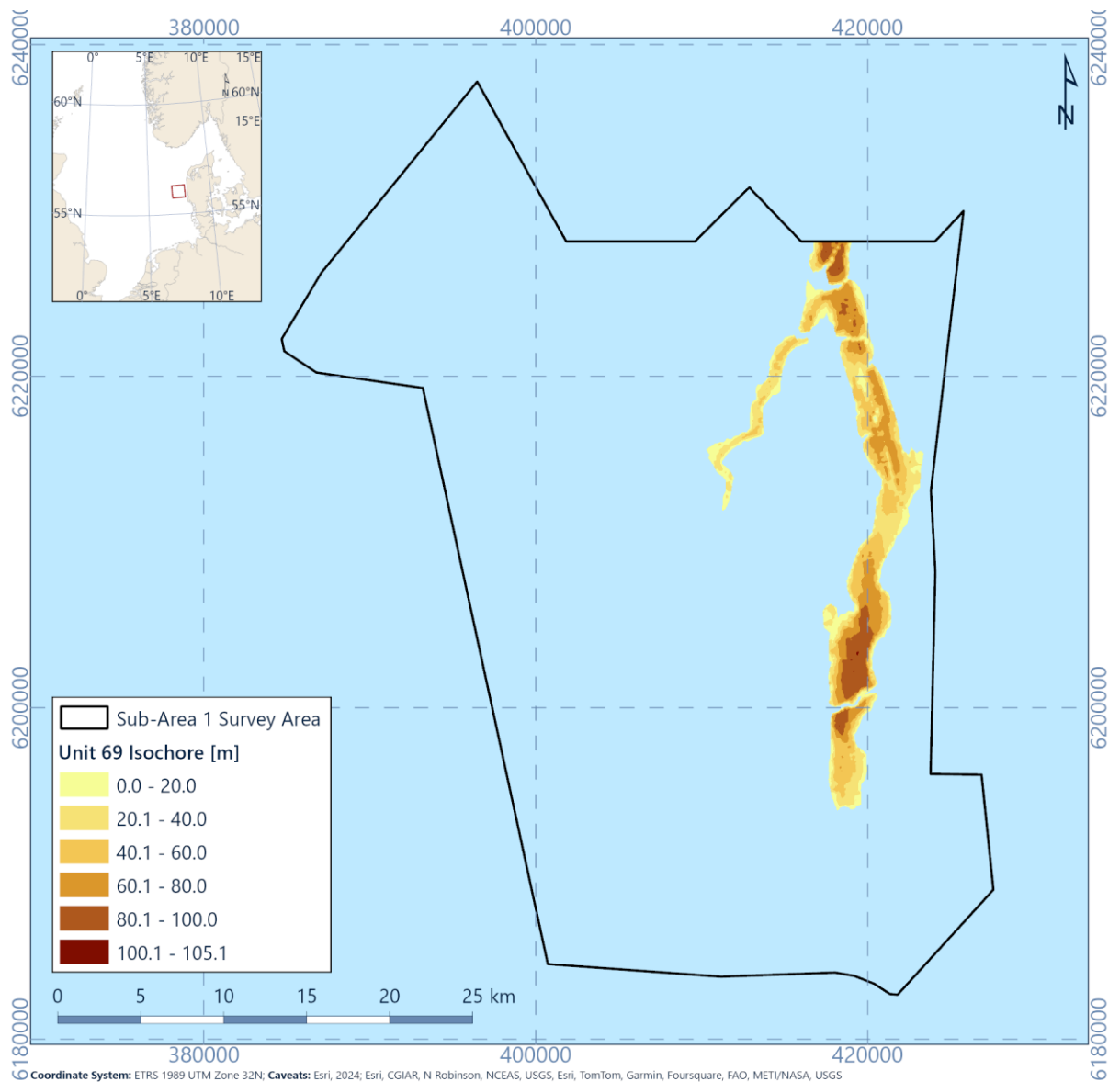
Figure 6.49: Isochore of H69

6.11.2   Integration and Interpretation

Unit U69 is interpreted to represent infill material within tunnel valley features. As these sediments are anticipated to have been deposited post formation of the valley feature itself, and based on the seismic character and consistent geotechnical properties (see section 7.2).

Based on the characteristics of the unit it is anticipated that the sediment likely formed in a glacio-lacustrine or glaciomarine environment, post Elsterian ice sheet retreat. It is likely that these sediments may have been deposited in the Holsteinian interglacial period. Unlike the underlying infill of the tunnel valley; this means that original deposition occurred in a relatively consistent environment. The topographic depressions associated with the tunnel valley features likely formed a focus for sediment accumulation.

Geotechnically the unit is very consistent with clay sediments with variable secondary components. The presence of some shell fragments may suggest that some connectivity to a marine environment may have occurred.
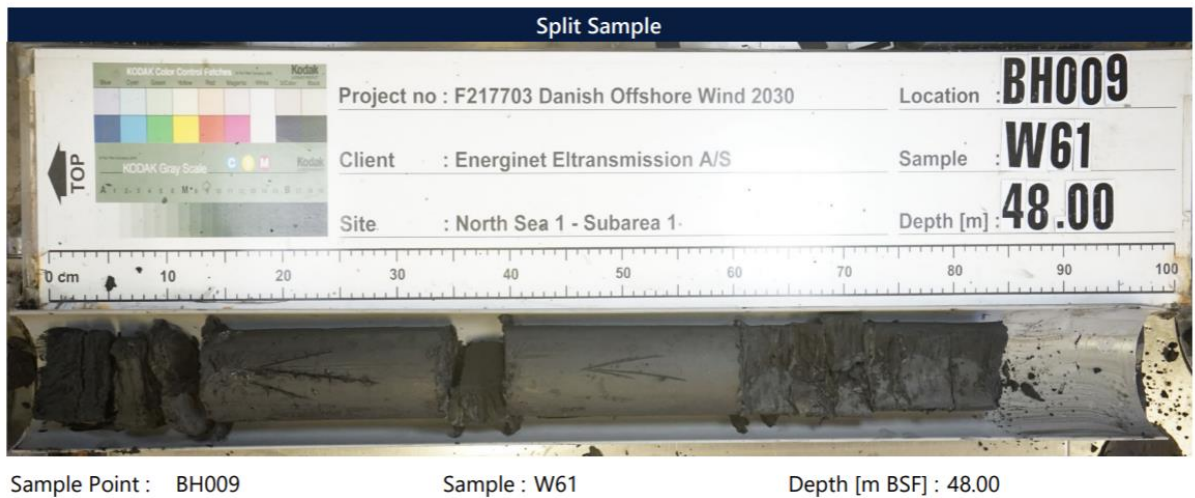
Figure 6.50: Example of U69 clay sediments

Figure 6.51 shows the integration between the thickness of U69 in the geophysics compared to the geotechnical locations. Good corelation between the top of the unit in geotechnical and geophysical datasets is observed. Only very limited locations penetrated the H69 horizon, making it challenging to comment on the quality of integration at the base however where they do, there is agreement between datasets.
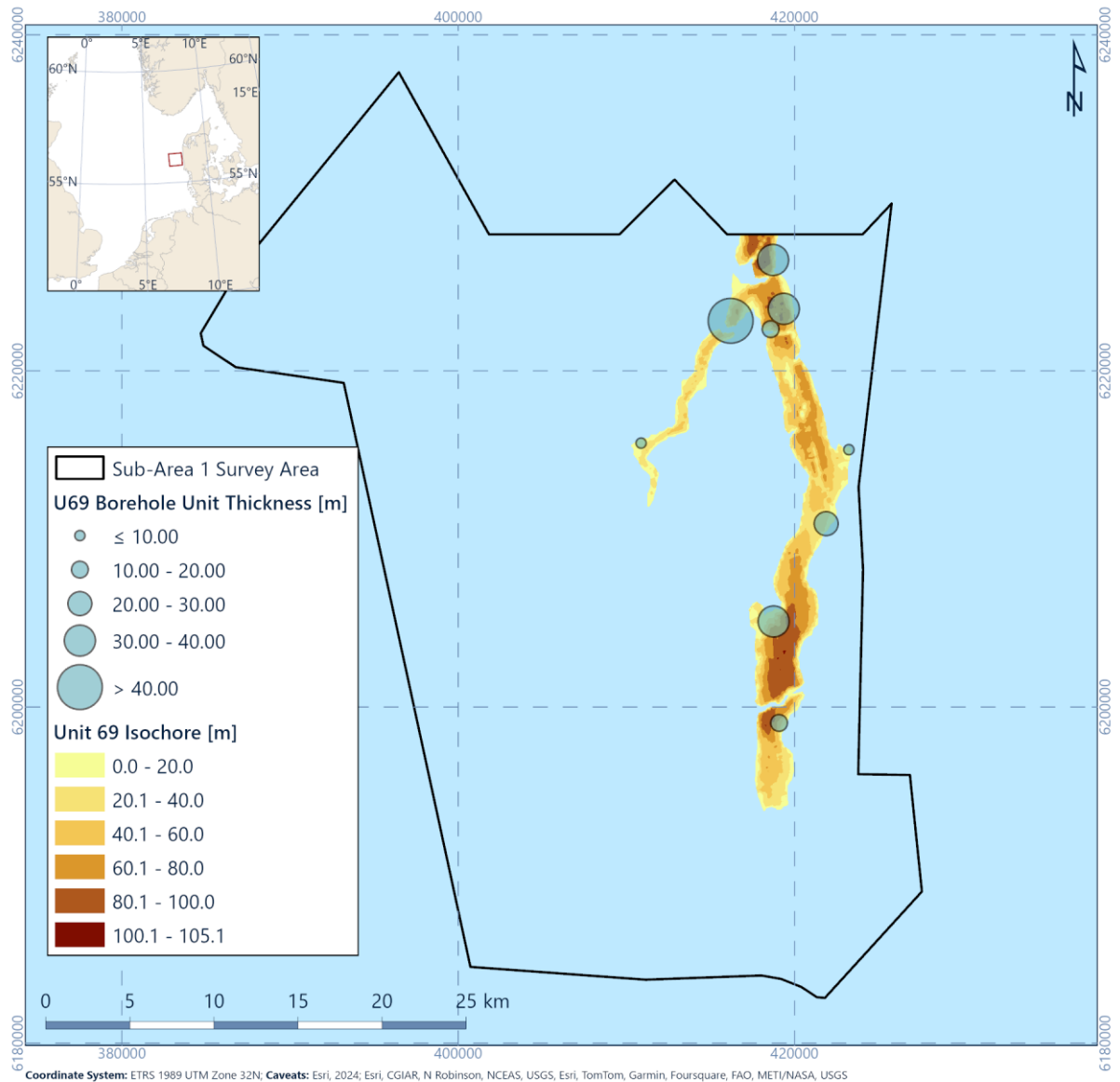
Figure 6.51: Isochore for U69 corelated with geotechnical data recoveries

6.12 Spatial Geological Model - Unit U70

6.12.1 Seismic Character

Unit U70 forms the infill of deep tunnel valleys with generally a north to south orientation (Figure 6.52, Figure 6.53,Figure 6.54). The base is marked by horizon H70, which often lies deeper than the maximum penetration of the 2D UHR seismic data (i.e. approximately 200 m below MSL). The tunnel valleys form a complex spatial network with intersecting tunnel valleys of different generations (Figure 6.52).

Multiple seismic facies are observed in Unit U70 (Figure 6.55) with seismic character varying from semi-transparent to chaotic areas. Often in association with the U69 sediments, are deeper seismic packages with similar characteristics as the overlying units, however based on their depth these have not been delineated in the current model.
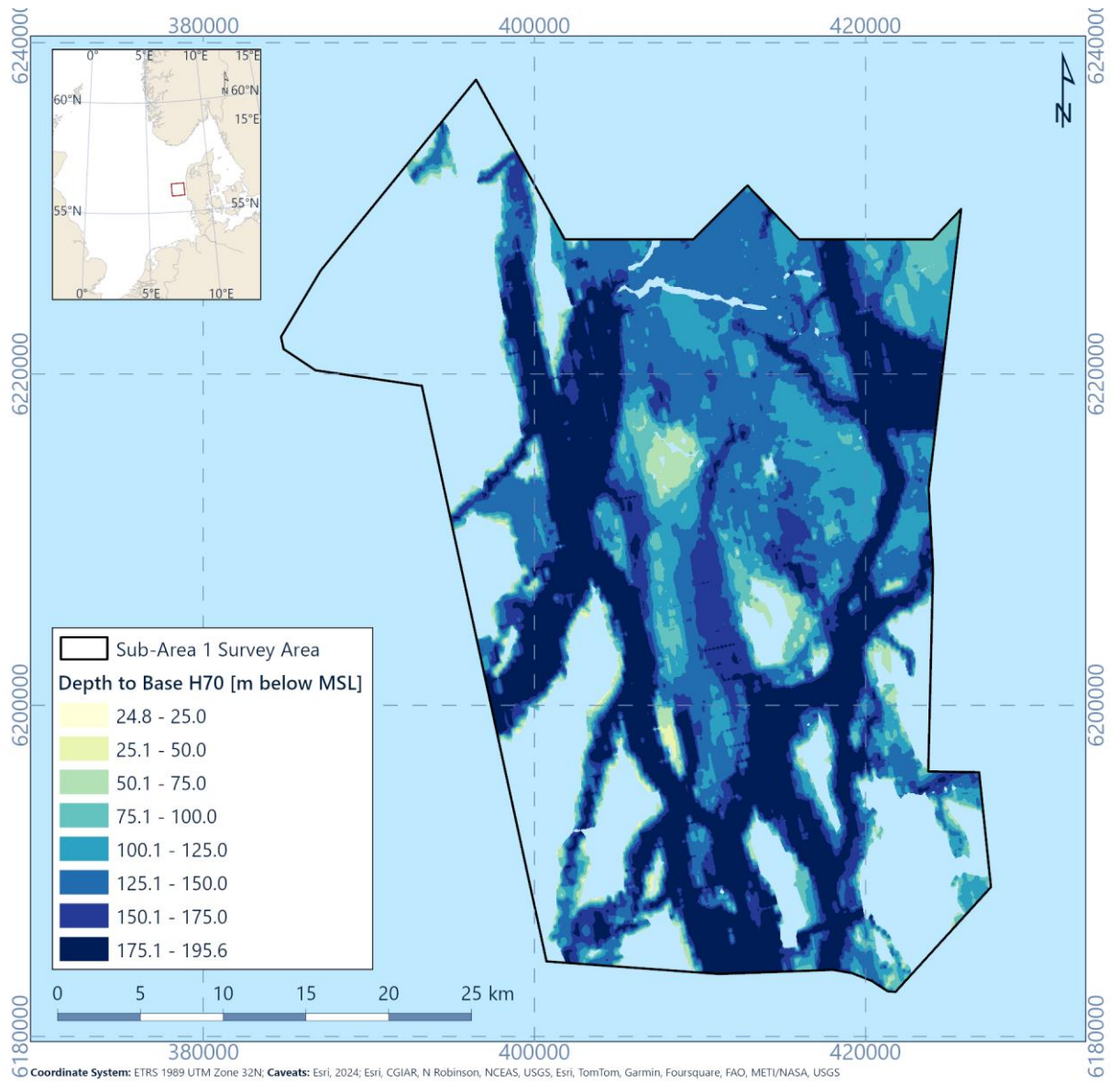
Figure 6.52: Depth to horizon H70 (Base of Unit U70) relative to MSL
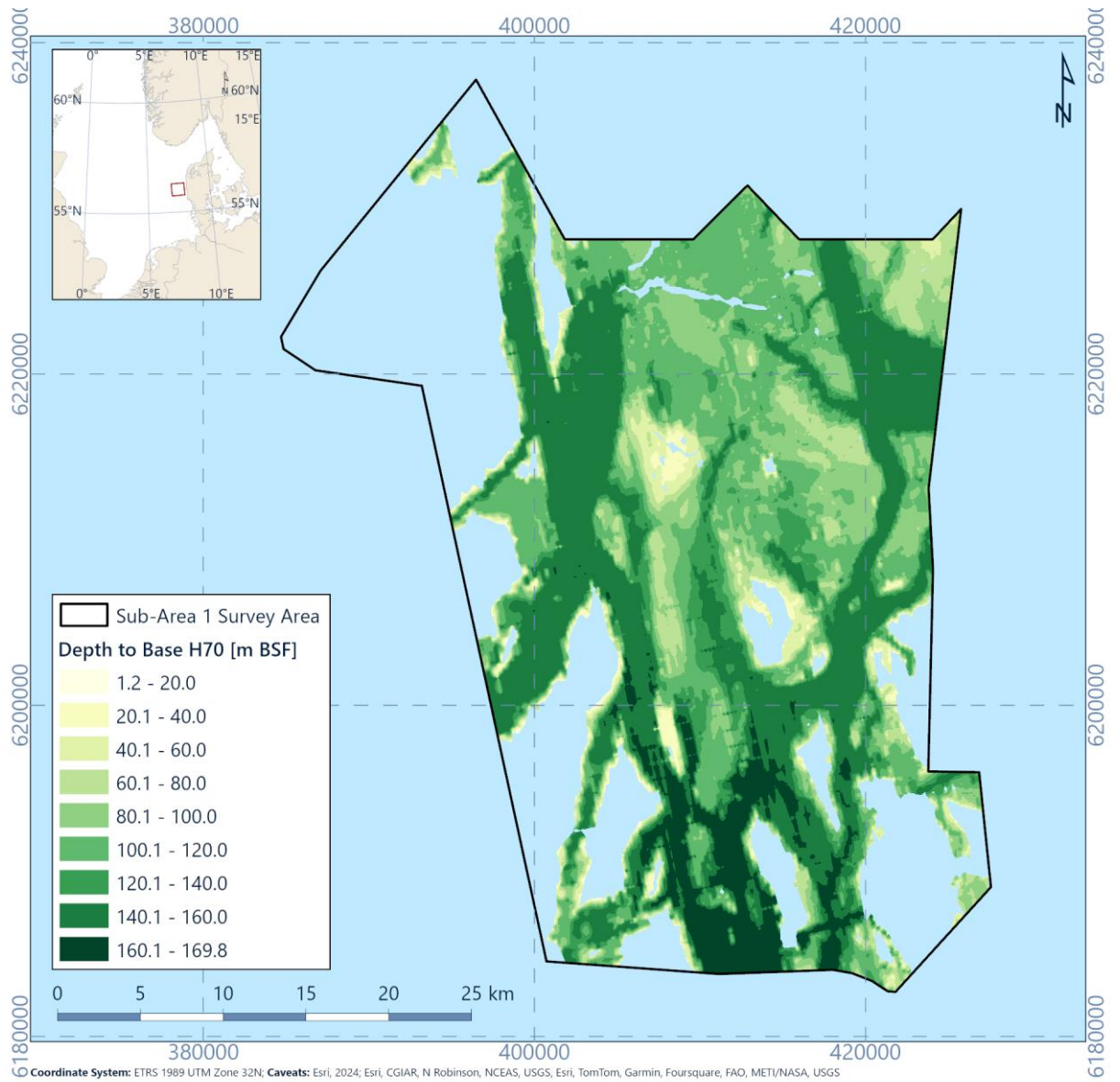
Figure 6.53: Depth to horizon H70 (Base of Unit U70) relative to seabed
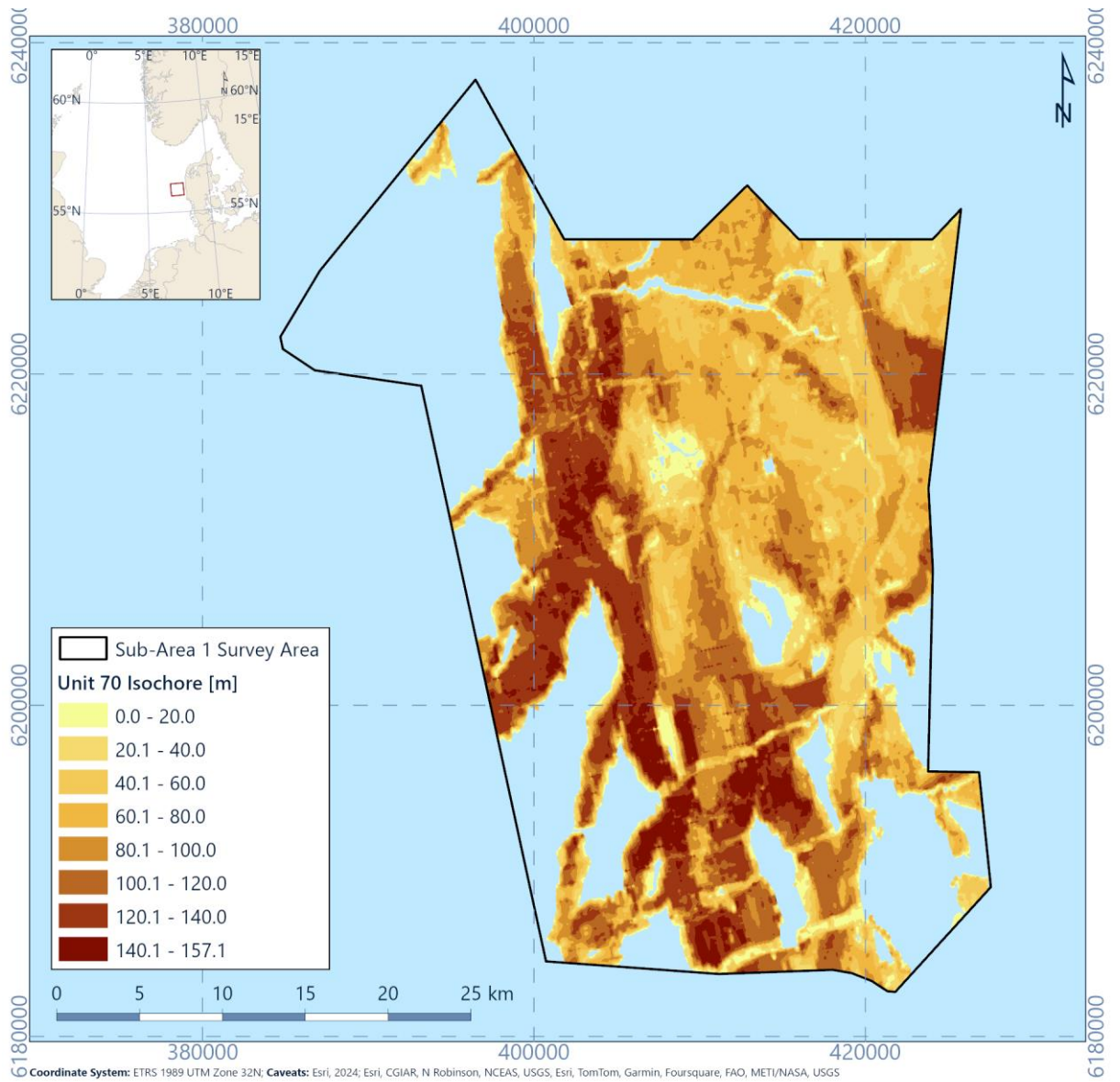
Figure 6.54: Isochore of Unit U70
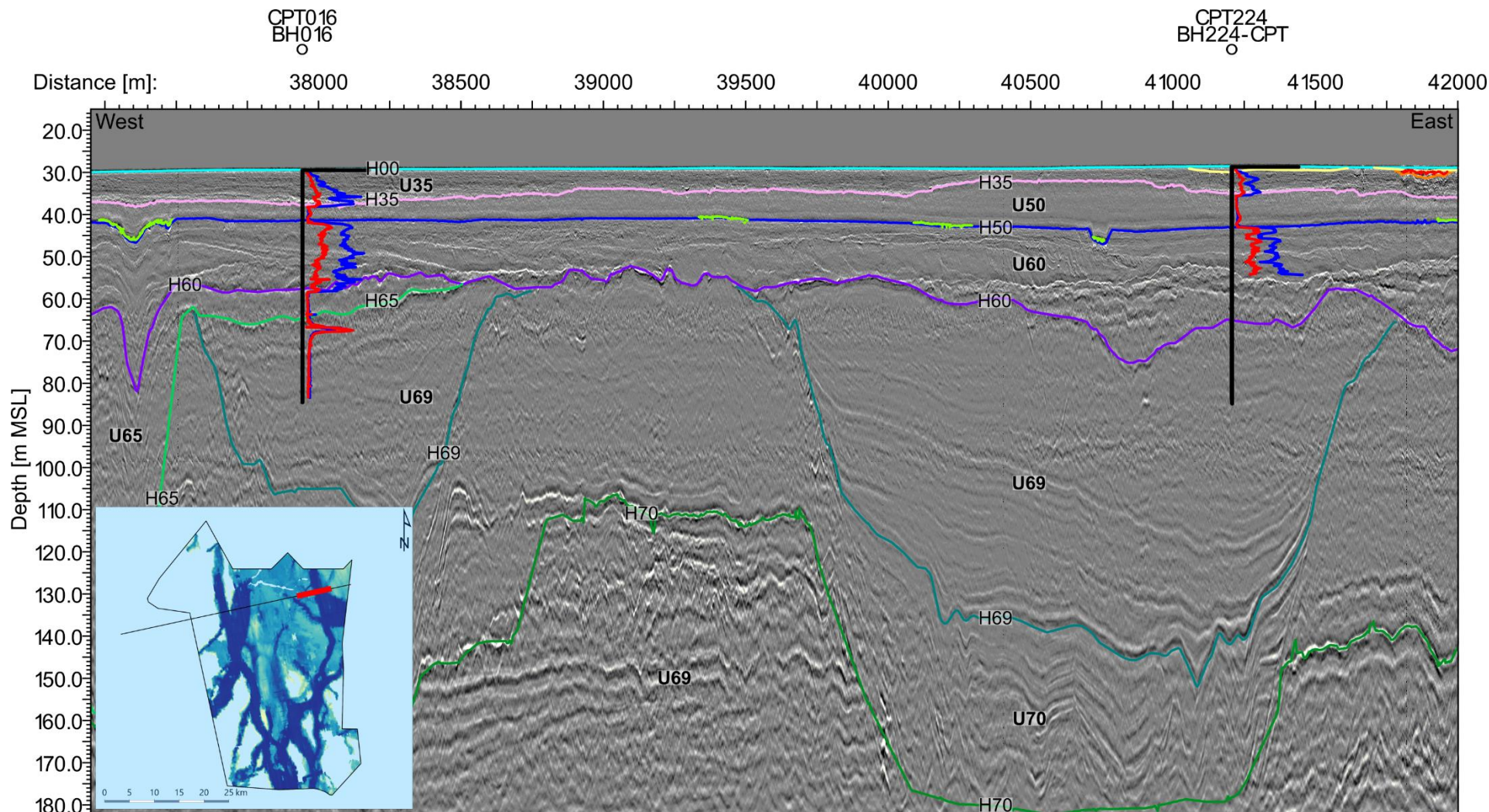
Figure 6.55: 2D UHR seismic data example of Unit U69 and U70. Line EAXA384P1, CPT016, CPT224. CPT scale: Blue is q_c with a scale from 0 to 80 MPa and red is f_s with a scale of 0 to 2 MPa

6.12.2   Integration and interpretation

Unit U70 is interpreted to be the syn- to post-glacial infill of glacial tunnel valleys, which included variable glacial meltwater and glacier deposits and interglacial freshwater and marine depositional environments (Huuse and Lykke-Andersen, 2000b; Kirkham et al., 2021). In this area of the Danish Sector of the North Sea, tunnel valleys are often age-dated as from the Elsterian glacial period (Figure 3.4; Huuse and Lykke-Andersen, 2000b). In addition to the tunnel-valley incisions, areas between incisions in the north-east of the site have variable thickness of U70 sediments (Figure 6.56). These are likely additional glacial deposits from the Elsterian glacial period. Geotechnical data are highly variable reflecting the deposition environment. Further details on this are presented in Section 7. Some inconsistency in the integration of geotechnical data with geophysical horizons are observed in the south-east corner of the site, where U60 sediments overly possible inter valley areas of U70, making seismic picking challenging due to the similar seismic character and geotechnical properties.

fUGRO
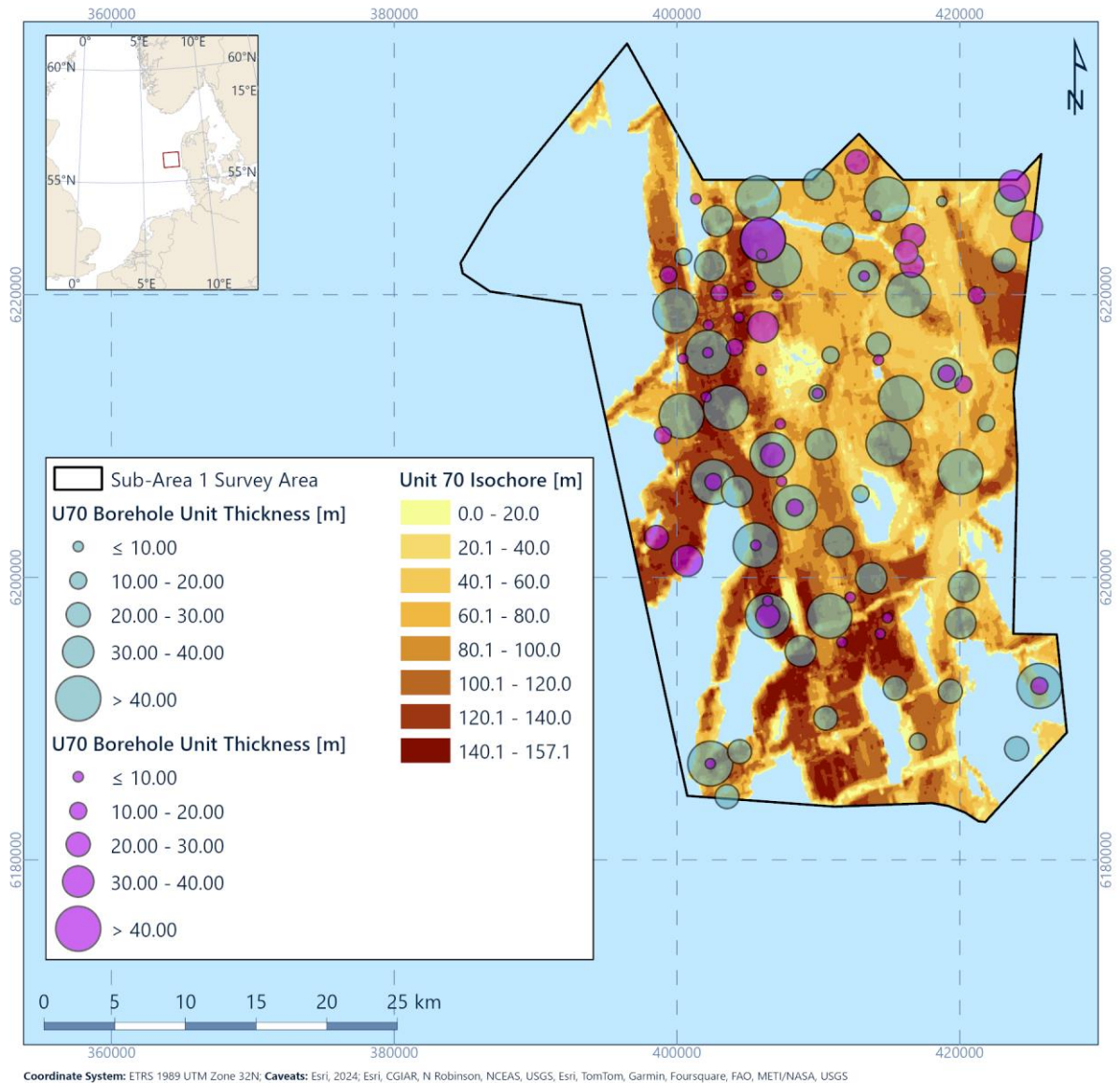
Figure 6.56: Isochore for U70 corelated with geotechnical data recoveries

6.13 Spatial Geological Model - Unit U90

6.13.1 Seismic Character

Unit U90 is present in the south-west of the site (Figure 6.57, Figure 6.58, Figure 6.59). The unit has a sheet-like geometry. The base dips towards the south-west and in the most south-west part of the site the base lies below the maximum penetration of the 2D UHR seismic data (Figure 6.45, Figure 6.55, Figure 6.60).

Internally, this unit has a stratified to complex seismic character. The stratification is formed by discontinuous reflectors with variable amplitudes. Locally internal erosion surfaces and high amplitude seismic anomalies with negative polarity are observed in Unit U90 (see Section 6.15.1).

FUGRO
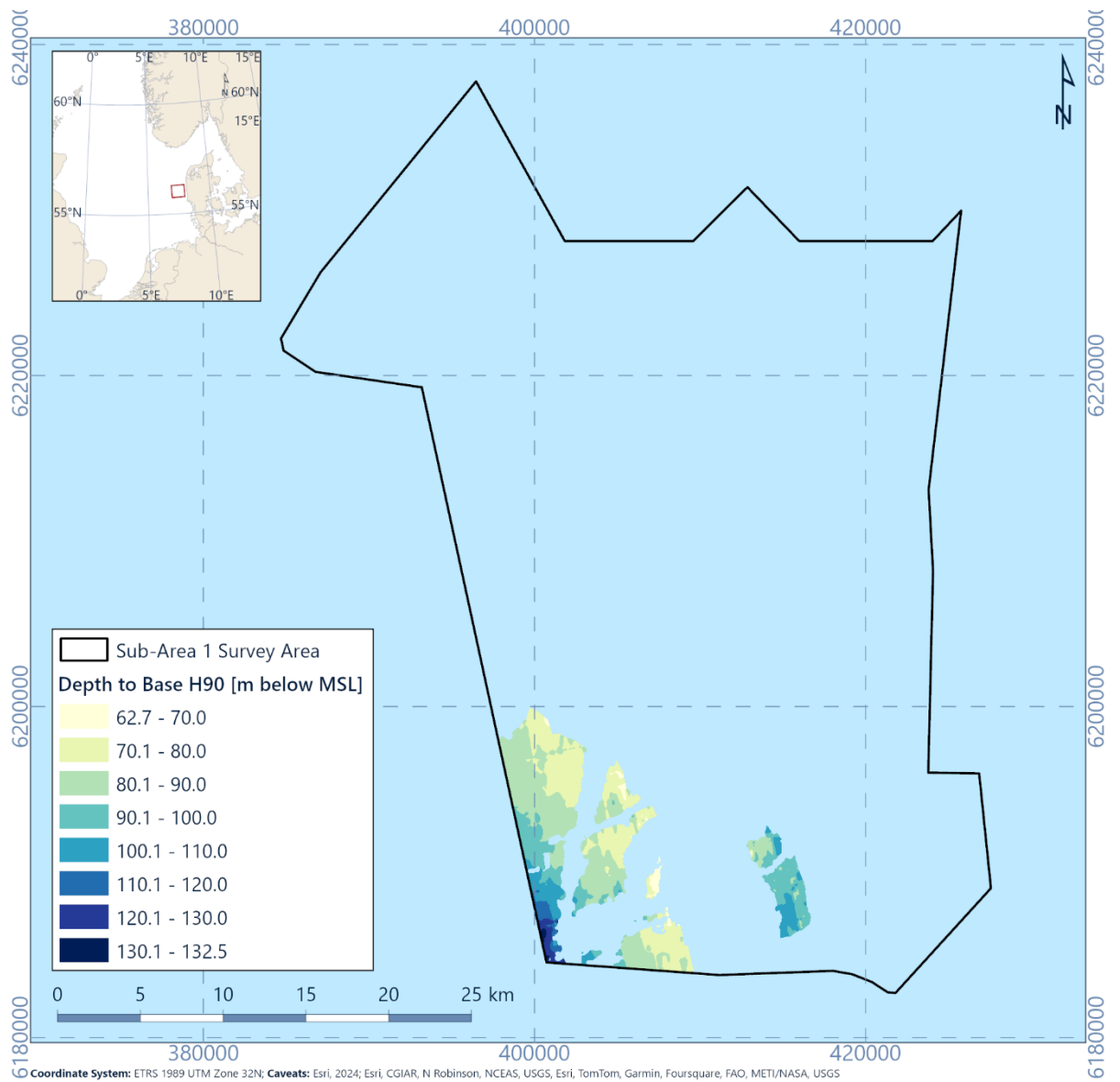
Figure 6.57: Depth to horizon H90 (Base of unit U90) relative to MSL
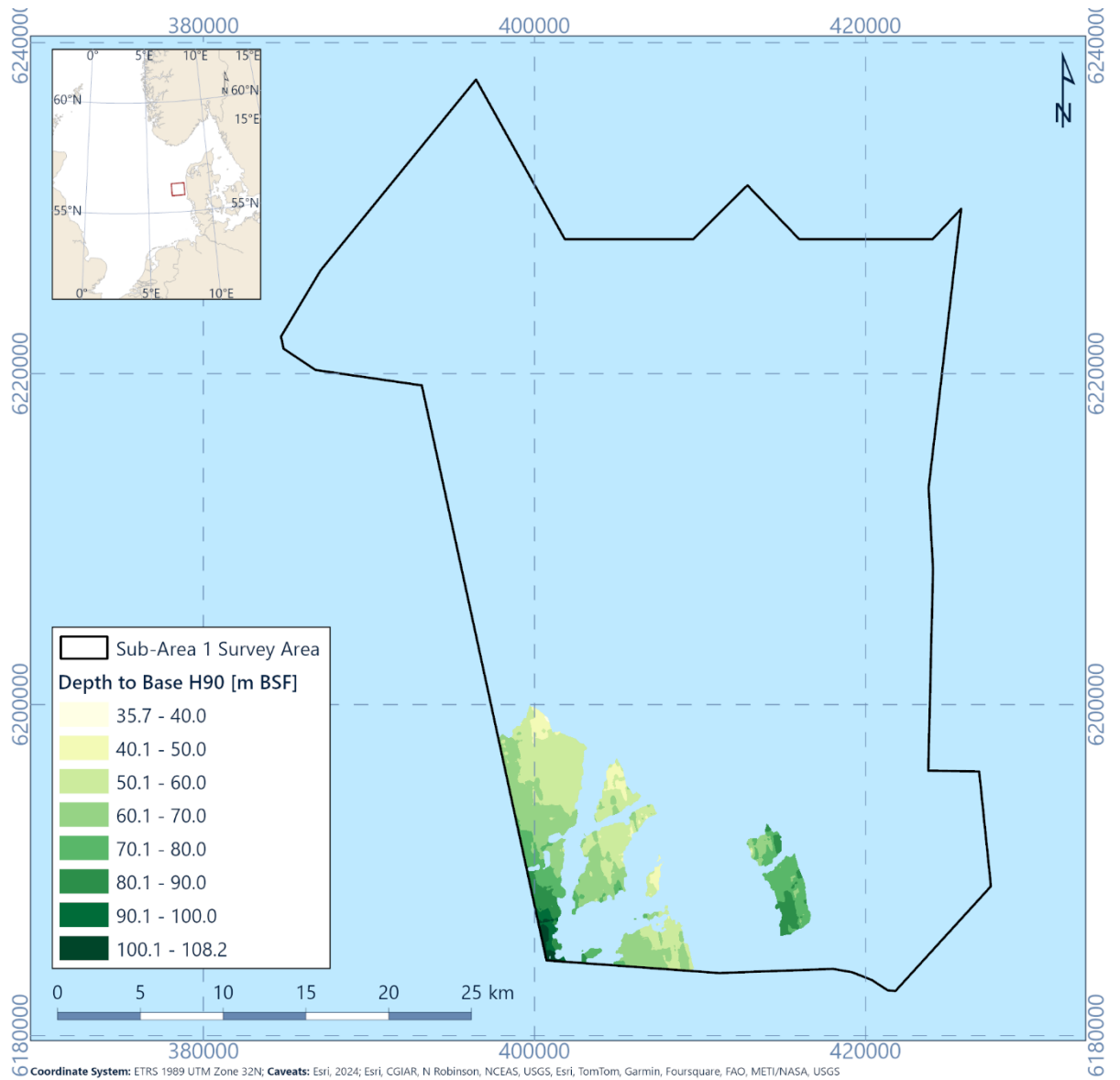
Figure 6.58: Depth to horizon H90 (Base of unit U90) relative to seabed
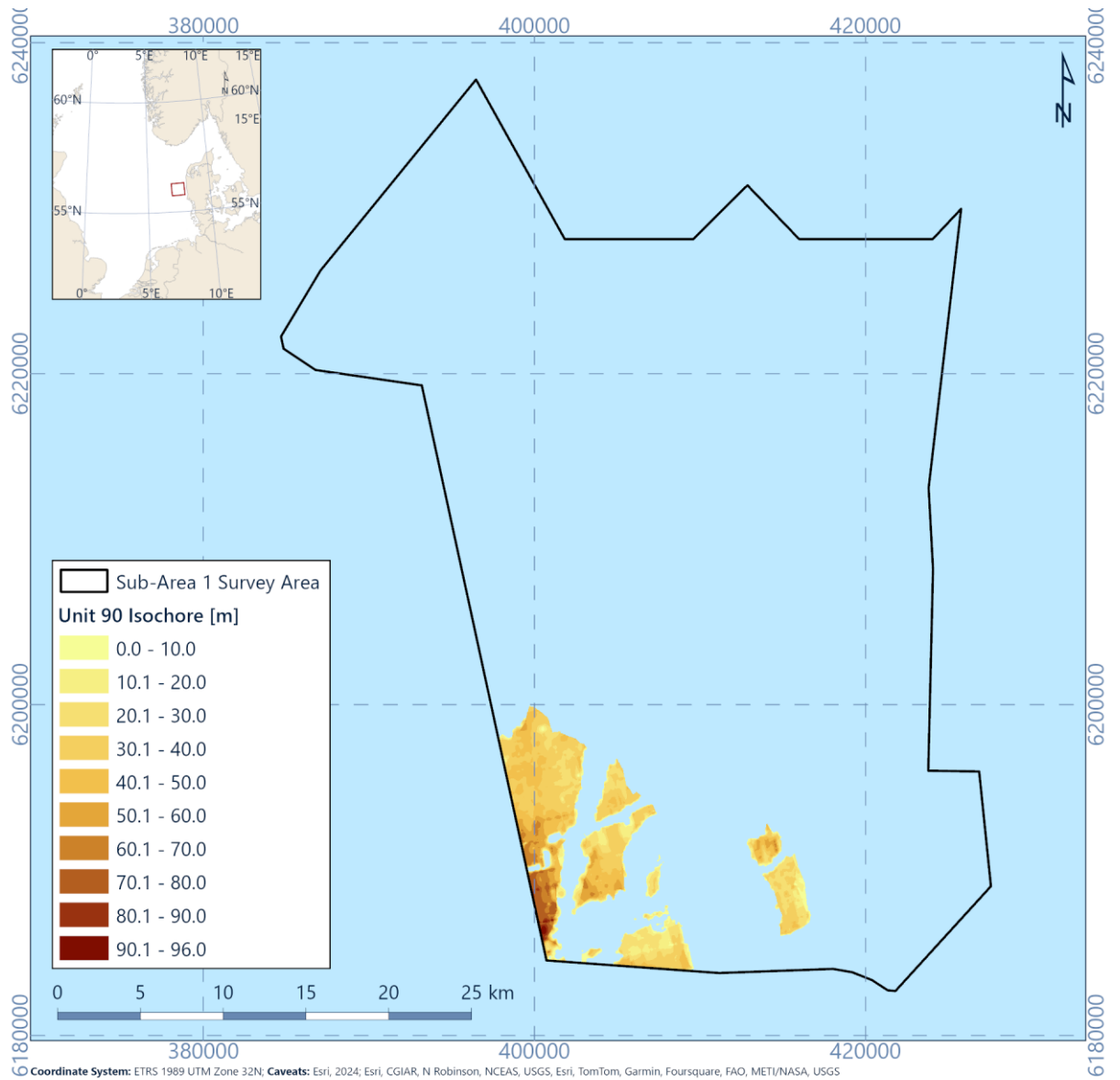
Figure 6.59: Isochore of Unit U90 (thickness in eastern areas of figure governed by base of penetration of unit)
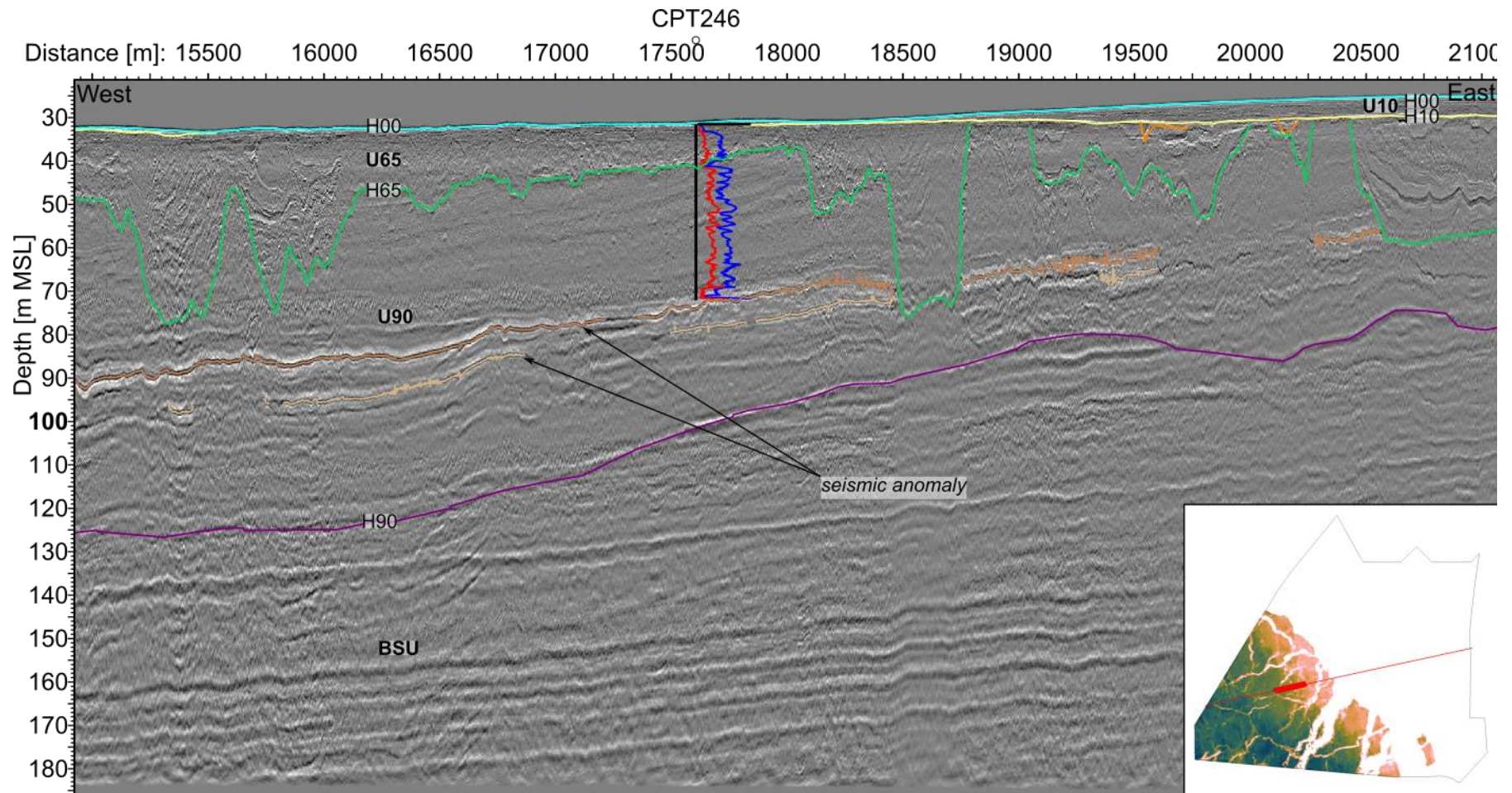
Figure 6.60: 2D UHR seismic data example of Unit U90. Line EAXC398P1, CPT246. CPT scale: Blue is q_c with a scale from 0 to 80 MPa and red is f_s with a scale of 0 to 2 MPa. Examples are from Sub-Area 2, but show good examples of seismic response and geotechncial data

6.13.2   Integration and interpretation

The geometry of the units, as well as dominant type comprising mostly sand with possible local peat beds, may indicate that Unit U90 was deposited in a meltwater (braided river in an outwash plain) depositional environment. It is interpreted that Unit U90 forms fluvial delta-top deposits of the Cenozoic delta system of the Eridanos River (Figure 3.1, Figure 3.2). This suggests a Miocene to Middle Pleistocene age. Figure 6.61 displays the integration between the thickness of U90 for the geophysics and geotechnical locations. Only limited sampling of the U90 sediments in there eastern edge are available, however based on the consistency of the sands it is not expected that these areas will have significant variability compared to the rest of the site.
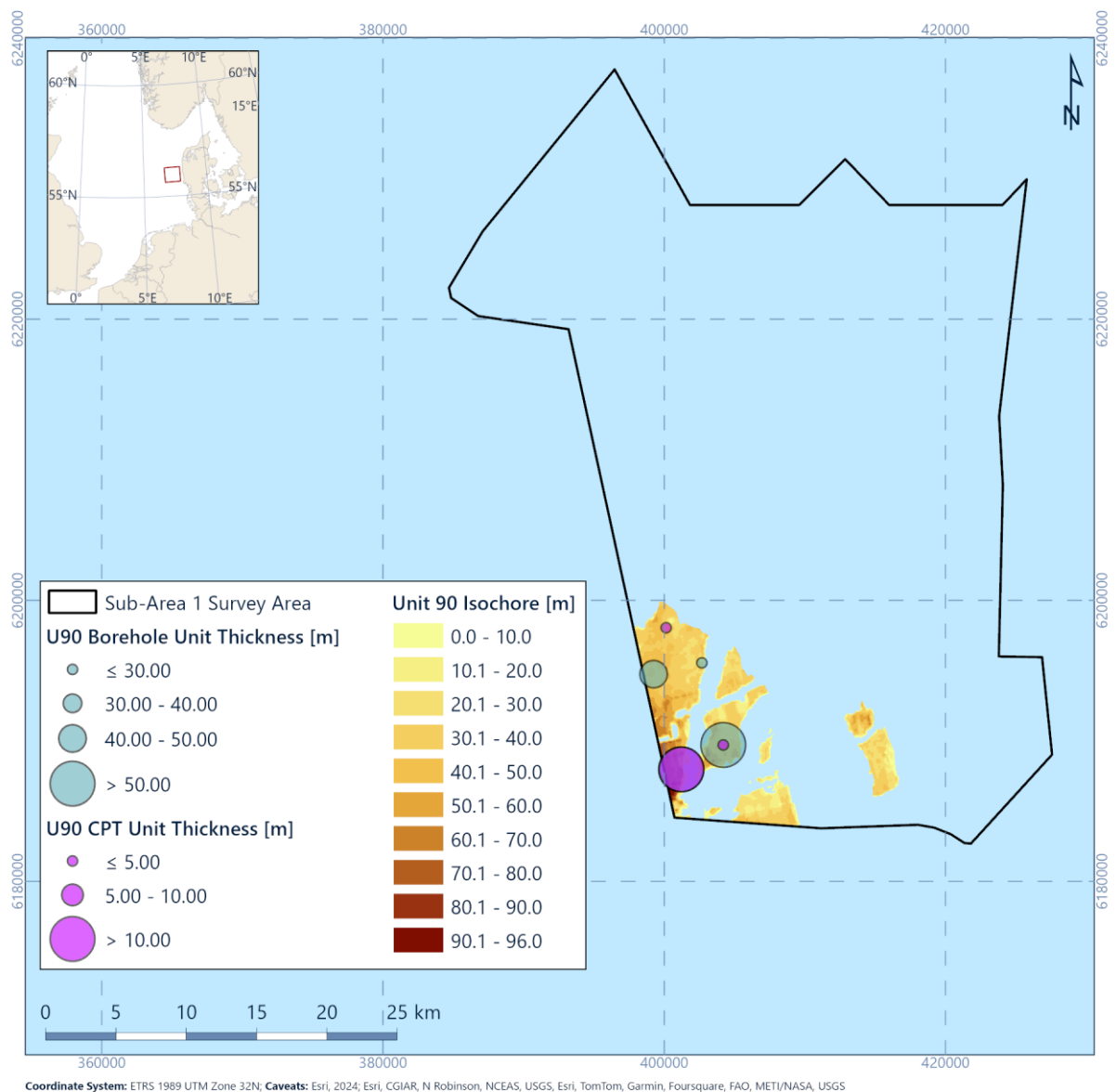
Figure 6.61: Isochore for U90 corelated with geotechnical data recoveries

6.14 Spatial Geological Model - Unit BSU (Base Seismic Unit)

6.14.1 Seismic Character

The BSU is the deepest interpreted unit within the depth of penetration of the 2D UHR seismic data. The top of the BSU is locally very close to the seafloor, namely in areas where it is thrusted upward by glaciotectonic deformation.

Internally, the unit is stratified. The parallel reflectors are horizontal to gently dipping towards the south-west (Figure 6.60, Figure 6.62). The boundary between the BSU and the overlaying Unit U90 is not marked by a clear reflector but is depicted by the change in seismic character between the two units. In the south-east of the site, a negative polarity high amplitude reflector is present in the BSU (see Section 6.15.1).

In the north, centre, and south-east of the site, the BSU is deformed by thrust faults that generally dip towards the east and north (see Section 6.15.6). In the east of the site, locally steep normal faults are present in this unit (see Section 6.15.7).

FUGRO
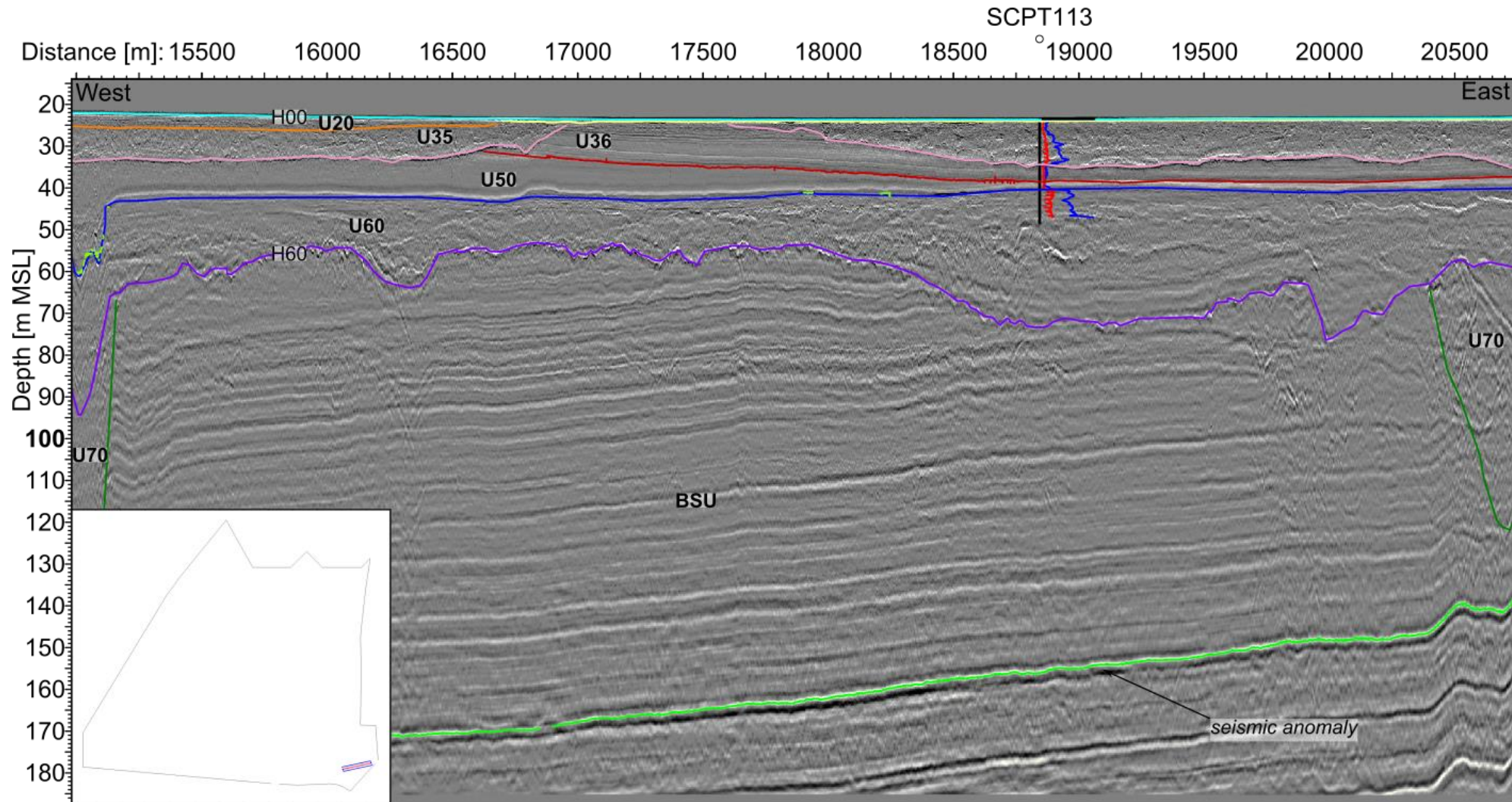
Figure 6.62: 2D UHR seismic data example of the BSU. EAAXD420P1, SCPT113. CPT scale: Blue is q_c with a scale from 0 to 80 MPa and red is f_s with a scale of 0 to 2 MPa

FUGRO

6.14.2 Integration and interpretation

Based on literature (EMODnet, 2023), the BSU is considered to be Miocene marine deposits. It is interpreted that the unit comprises coarsening upward pro-delta clay to delta-front sand deposits of the Eridanos River delta (Figure 5.2). The westward dip of the strata may be a structural dip or delta clinoforms (Overeem et al., 2001; Gibbard and Lewin, 2016). Geotechnical data shows this unit, within the depth ranges that have been sampled is not lithified, but rather is represented by high strength clay sediments. No locations reach the base of the unit, however the top of the unit shows consistency between datasets.

6.15 Geological Features and Geohazards

This section describes sub-seafloor geological features and geohazards identified in the SBP and 2D UHR seismic data in the survey area. Table 6.1 provides the overview.

Table 6.1: Overview of the geological features and geohazards

Geological feature or geohazard	Associated Units	Possible Impact
Peat and/or organic clay	U20, U30, U50, U65, U90, BSU	Peat and organic clay have a high compressibility, which may result in uneven and non-uniform support. It may also cause a chemical reaction between the soil and steel. It may also affect cable performance due to limited thermal conductivity.
Soft clays	U20	Soft clay can only give limited and potentially uneven support to structures. It may also affect cable performance due to limited thermal conductivity.
Shallow gas	U20, U50	Gassy soils may have high compressibility, low and laterally variable soil strength, and reduced bearing capacity. Migration of gas into skirted foundation may occur. There may be a risk of blowout and gas release during drilling and piling operations.
Gravel, cobbles and boulders	U30, U35, U60, U65, U70	Gravel, cobbles, and boulders may form an obstruction and result in insufficient or non-uniform support and/or penetration of foundations. They may also form an obstruction for trenching for cables.
Buried channels and tunnel valleys	U20, U35, U50, U60, U65, U70, U90	Buried channels and tunnel valleys may be associated with laterally variable soil conditions and uneven support of foundations.
Glacial deformation	U65, U90, BSU	Glacial deformation features may be associated with spatial variability in soil conditions and lower lateral resistance. Soil properties may vary laterally resulting in non-uniform support of foundations.
Faults	BSU	Due to the presence of faults, soil properties may vary laterally resulting in non-uniform support of foundations. Faults may still be active or be re-activated due to human interference. Active faults may be associated with critical stress and possible failure of structures.

FUGRO

6.15.1   Peat and/or Organic Clay

Seismic anomalies with high amplitude and negative polarity were observed in several units. They may indicate beds of peat and/or organic clay.

In Unit U20 (Figure 6.11, Figure 6.12, Figure 6.63), U30 and U50 (Figure 6.20, Figure 6.25, Figure 6.64) high negative amplitude reflectors are present with a length of up to 3 km. Locally signal attenuation is observed below. These seismic anomalies are typically at or near the base of these units and/or associated with buried channels. These high amplitude reflectors are mapped as '*2DUUHR_seismic_anomalies_U20*' and '*2DUUHR_seismic_anomalies_U30U50*' in Figure 6.63 and Figure 6.64. These anomalies are tested by CPT and BHs at several locations and have a high friction ratio as well as peat and organic-rich sediments.

In Unit U90 in the south-west of the site, continuous high amplitude, negative polarity reflectors are present with a length of up to 20 km. This high amplitude reflector is mapped as '*2DUUHR_seismic_anmolies_U90*' (Figure 6.65). These anomalies are tested by only few CPT's and BHs and may represent beds of peat and/or organic-rich clay, with some corelation between them and these deposits.

In the BSU, a continuous positive high amplitude reflector is present at a depth of 100 m to 170 m BSF and locally as shallow as 10 m BSF and a length of up to 15 km (Figure 6.62, Figure 6.66) in the south-east of the site. This high amplitude reflector is mapped as '*2DUUHR_seismic_anomalies_BSU*'. It may indicate a bed with a different soil type within the BSU such as a bed of organic clay and/or peat. Alternatively, this reflector may indicate a soil boundary from clay above the reflector to sand below the reflector. The thrust faults detach more or less at the same depth as this seismic anomaly. This observation confirms the likelihood of a change in material properties, such as at a boundary of sand and clay.
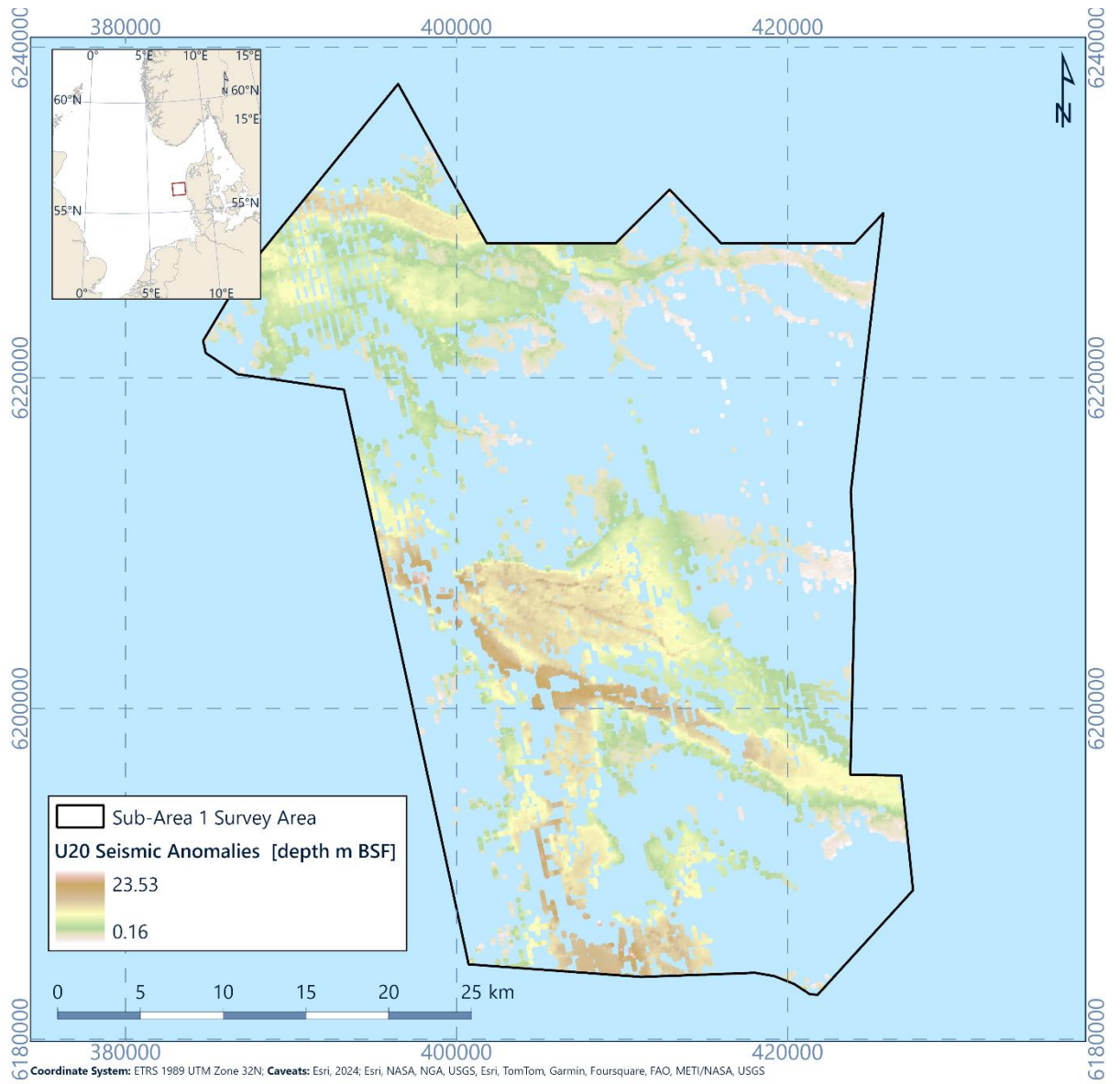
Figure 6.63: Map of seismic anomalies in Unit U20 in depth BSF
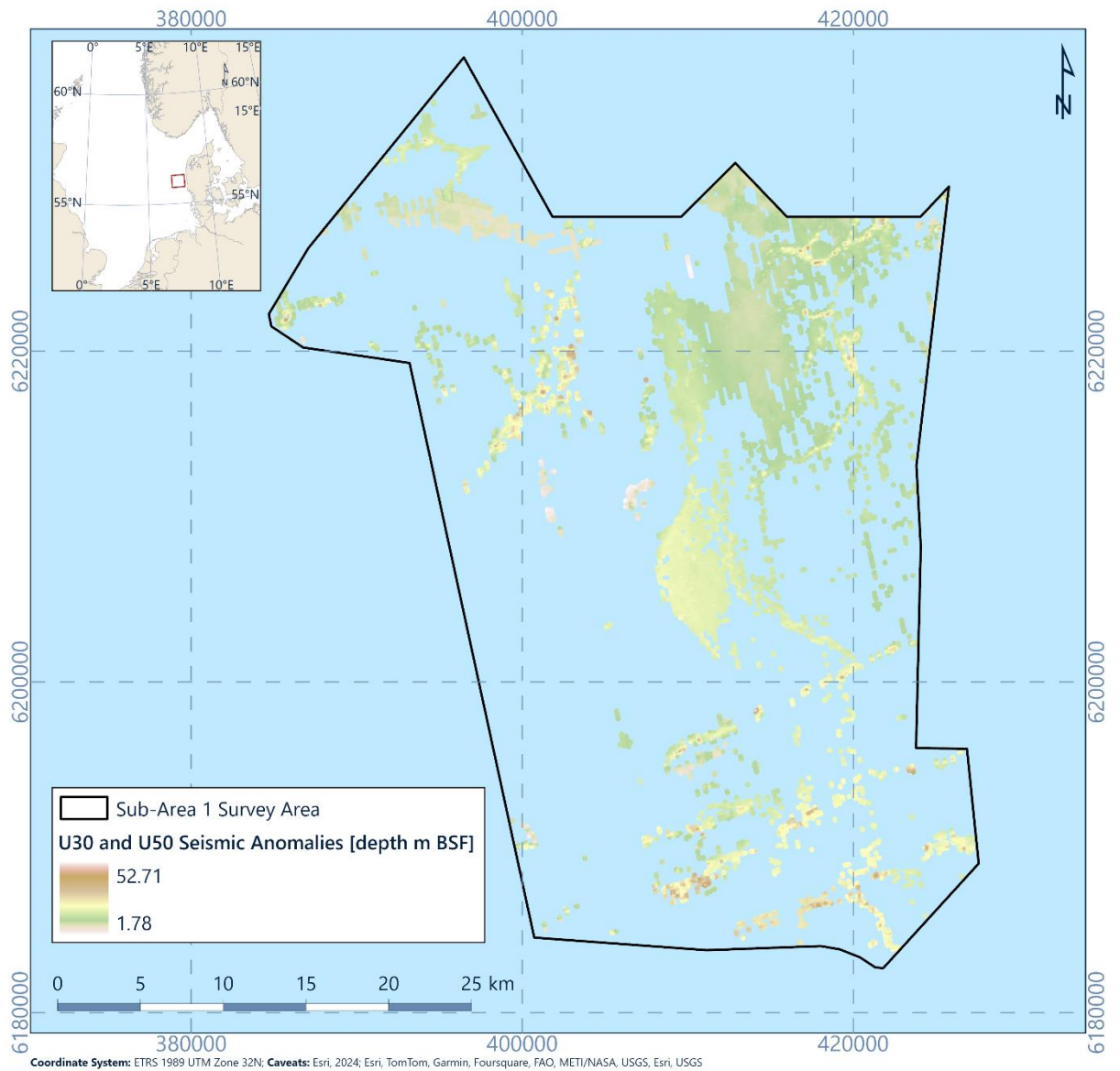
Figure 6.64: Map of seismic anomalies in Unit U30 and U50 in depth BSF
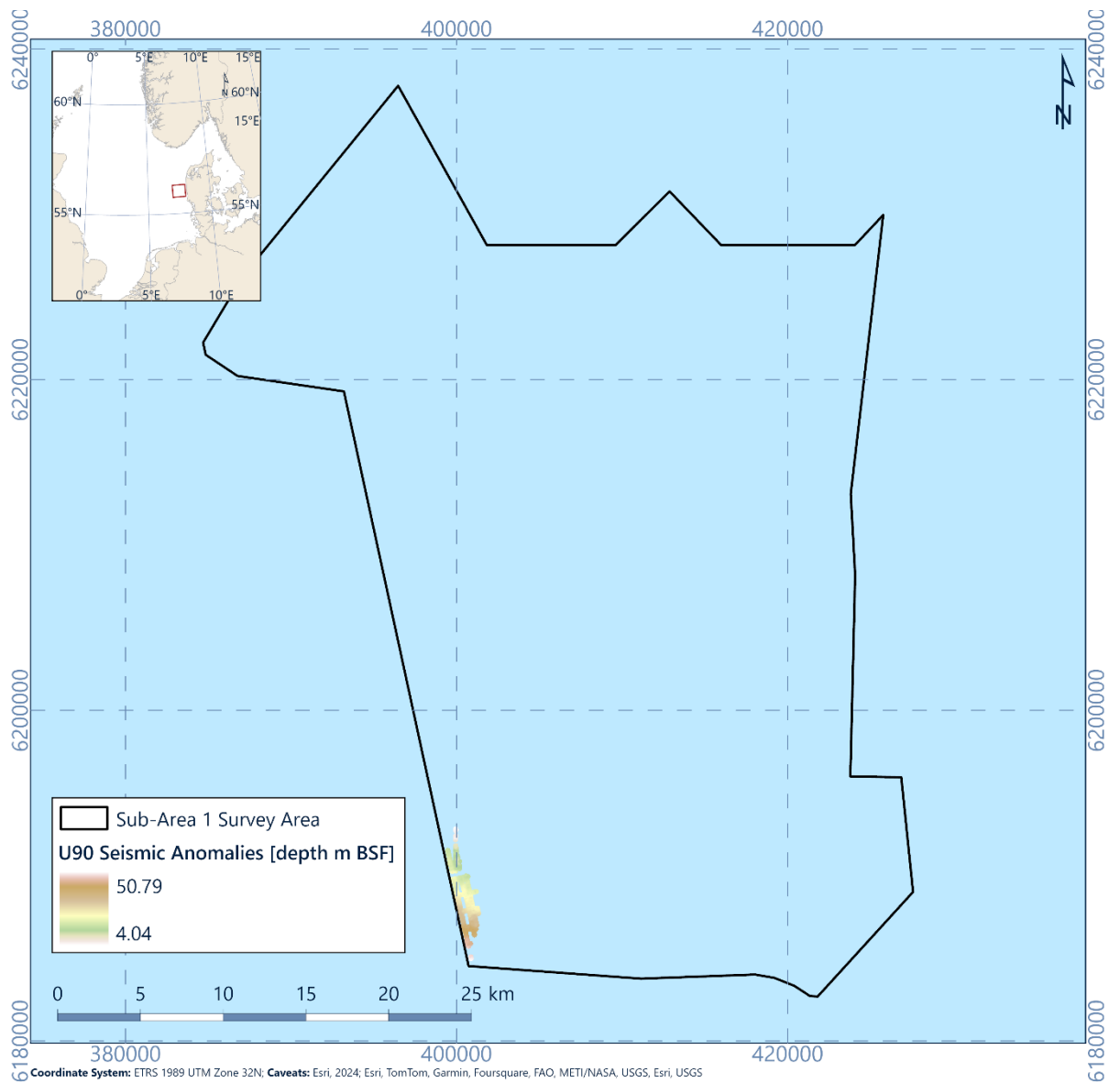
Figure 6.65: Map of seismic anomalies in Unit U90 in depth BSF
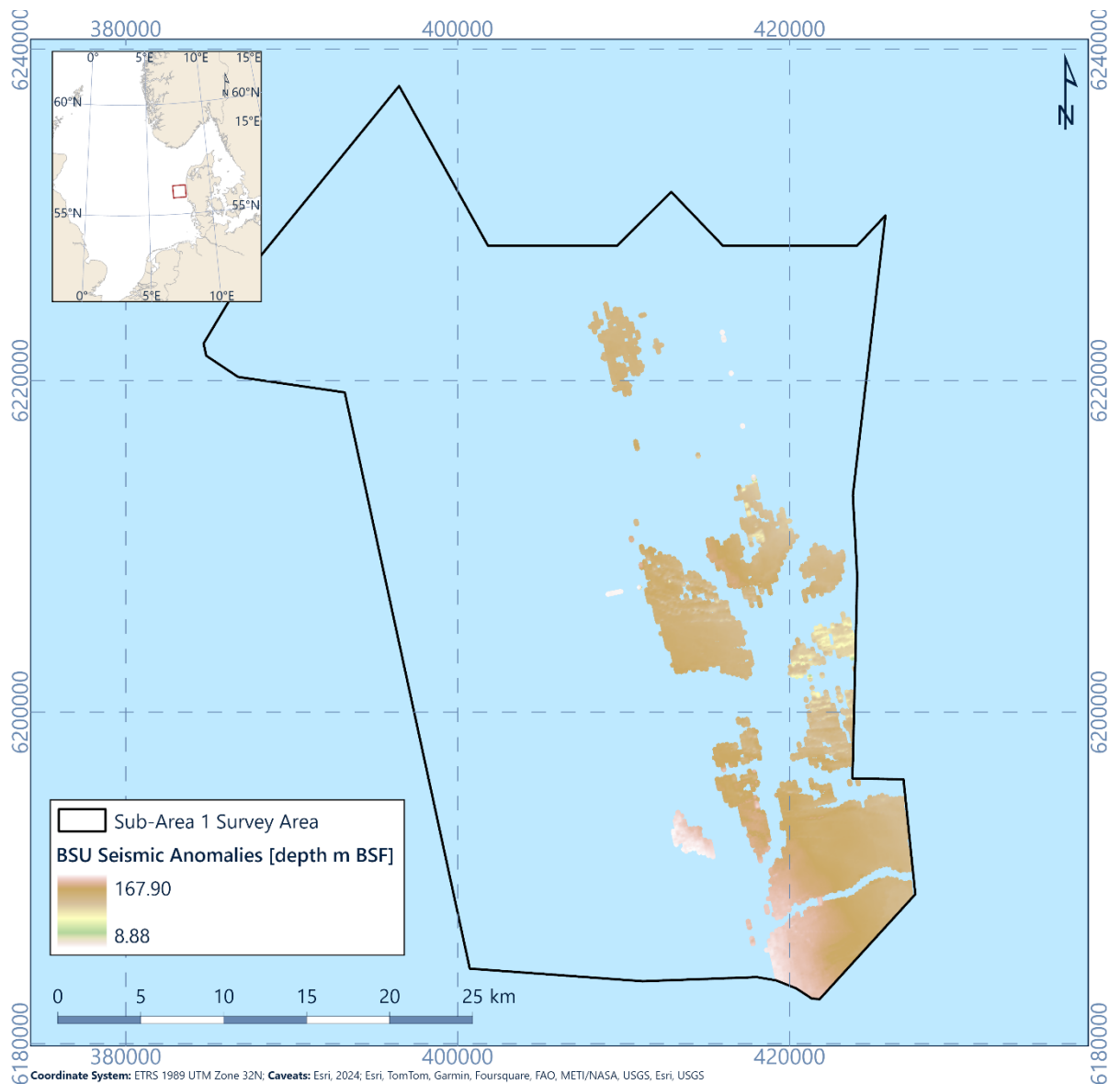
Figure 6.66: Map of seismic anomalies in the BSU in depth BSF

6.15.2 Soft Clays

Unit U20, particularly U20b contains low strength clay sediments that may represent a challenge for foundation engineering. Further details on the geotechnical characteristics of the sediments is presented in Section 7.

6.15.3 Shallow Gas

Evidence for the presence of shallow gas has been observed on the 2D UHR seismic data in the form of acoustic blanking and signal attenuation, which was often, but not always, associated with a high amplitude reflector with negative polarity. The acoustic blanking is present in Unit U20 and to a much lesser extent in Unit U50.

In Unit U20 seismic anomalies with associated acoustic blanking or signal attenuation are present at a depth of approximately 5 m and 15 m BSF (Figure 6.67Figure 6.69). The relationship of acoustic blanking with depth means that the acoustic blanking is present where Unit U20 is thick enough to develop free gas, which causes the acoustic blanking (Tóth et al., 2014). Possible correlation with organic-rich materials in U20b and the blanking area may be expected.

In Unit U50 seismic anomalies (Figure 6.68, Figure 6.70) with associated acoustic blanking and signal attenuation are only locally present, often where the base of Unit U50 is channelised. These anomalies are associated with velocity pull-downs. Velocity pull-downs, acoustic blanking and signal attenuation are indicators for the presence of gas in the soil.
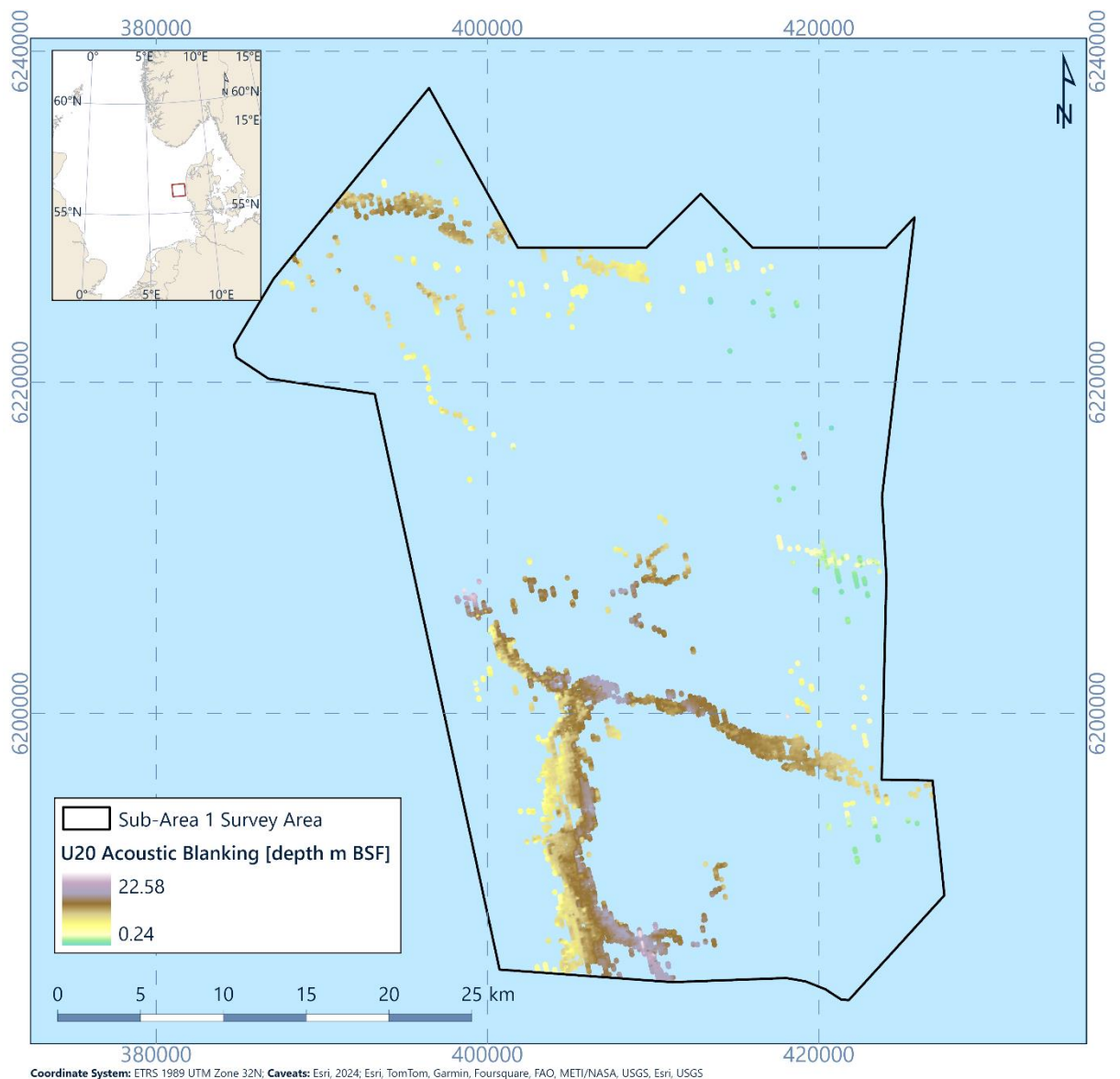
Figure 6.67: Depth to the top of acoustic blanking in Unit U20 in depth BSF
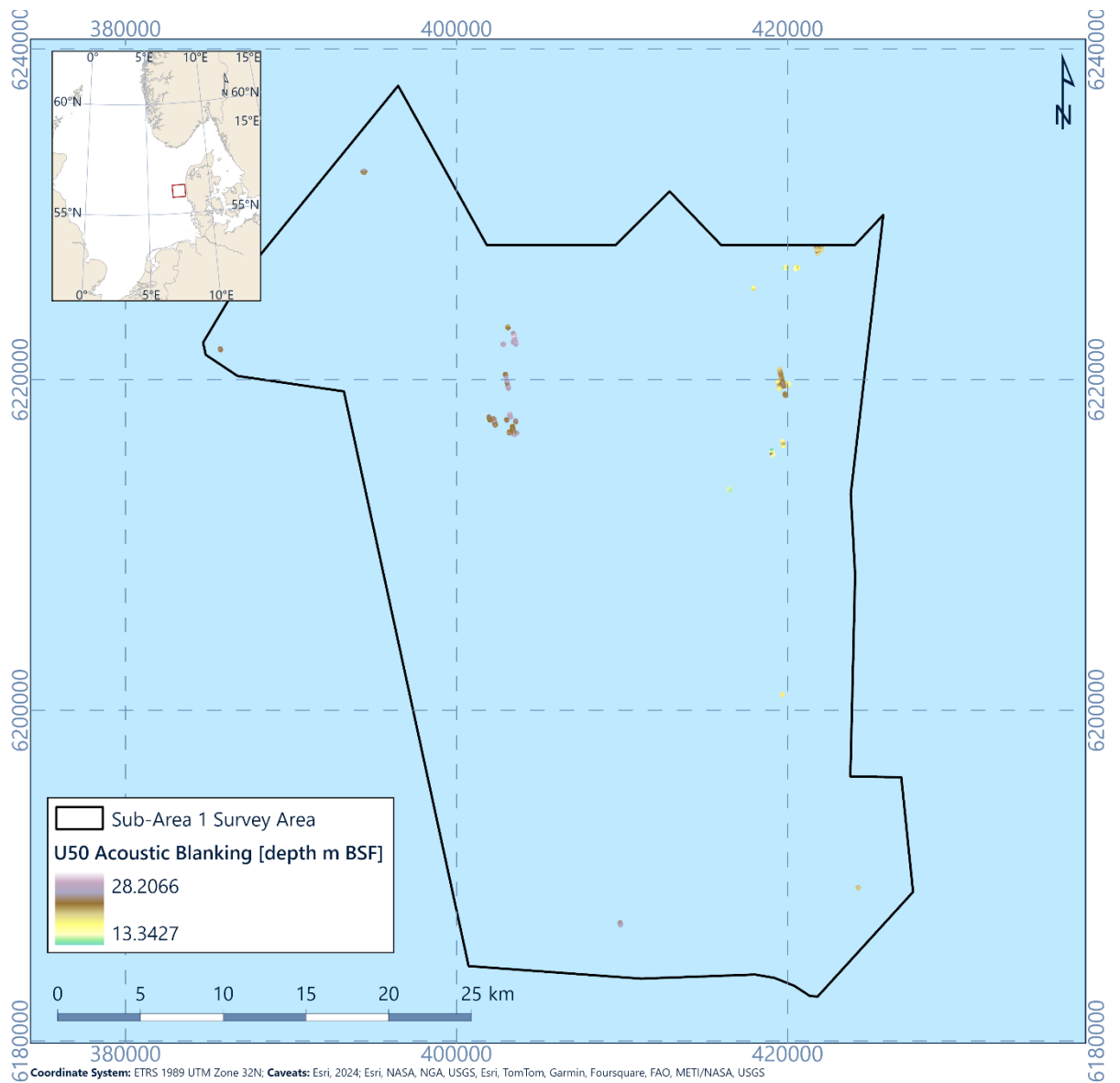
Figure 6.68: Depth to the top of acoustic blanking in Unit U50 in depth BSF
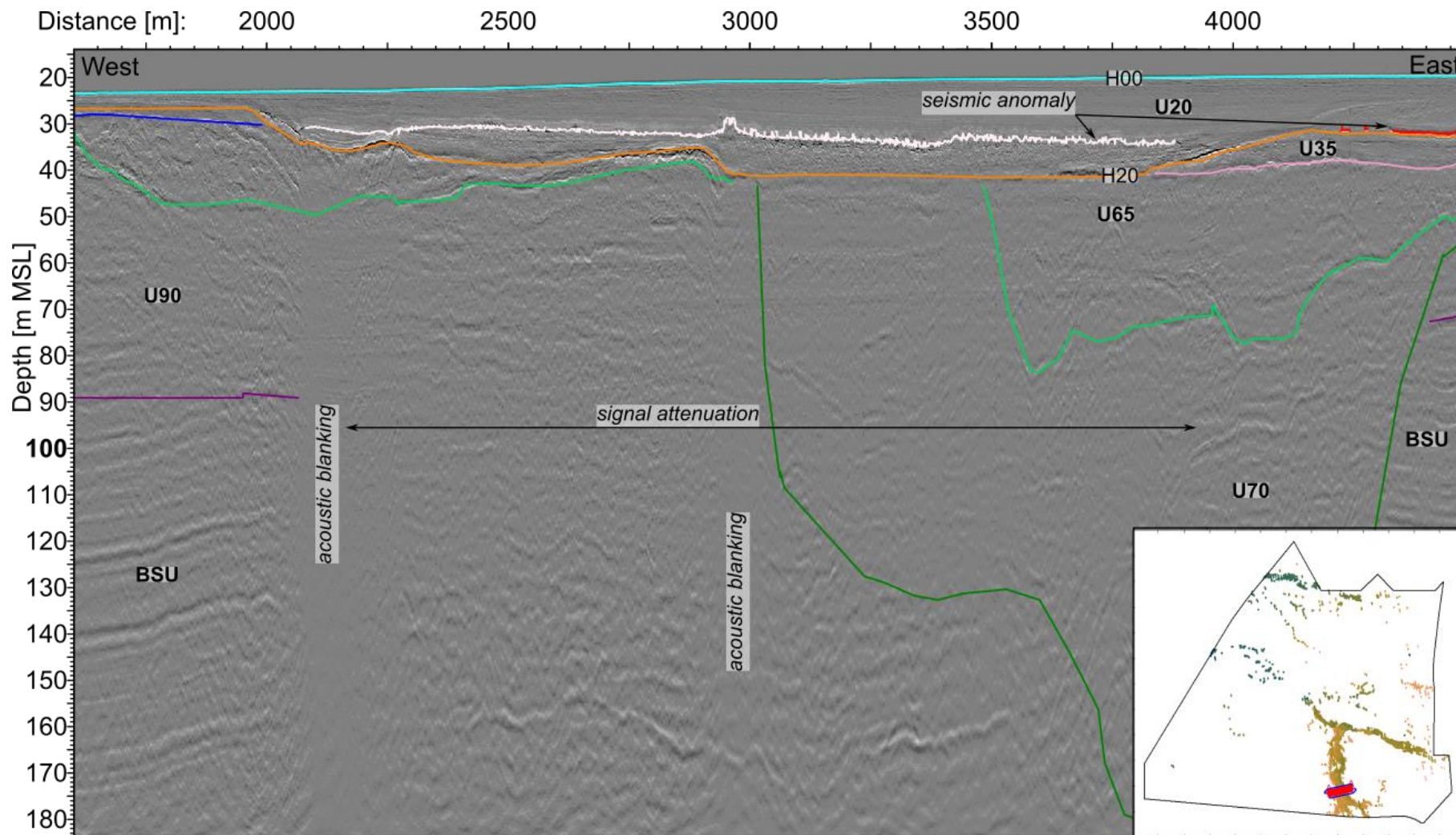
Figure 6.69: 2D UHR seismic data example of acoustic blanking and signal attenuation in Unit U20. Line EAXD415P1
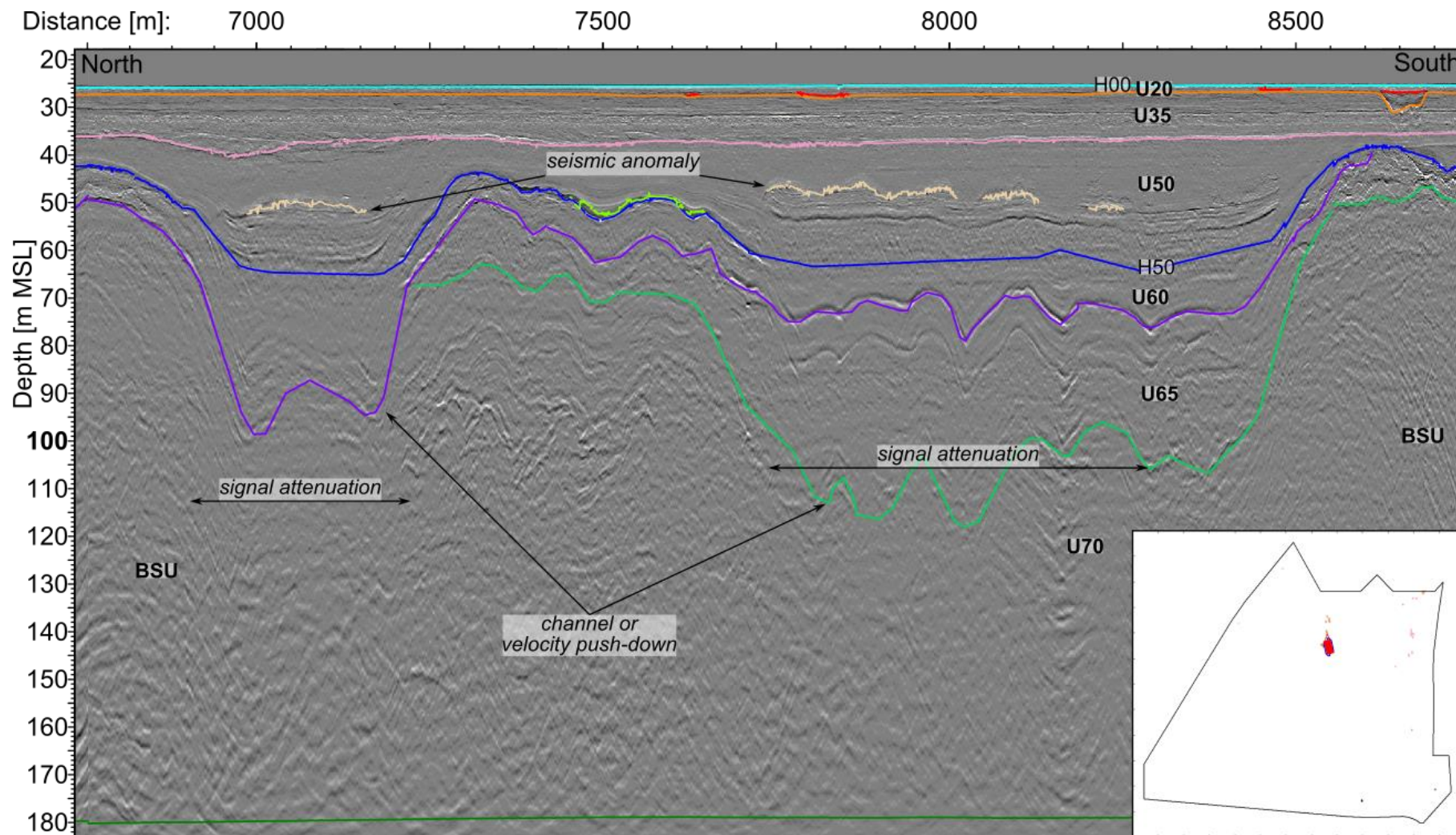
Figure 6.70: 2D UHR seismic data example of signal attenuation in Unit U50. Line EAAS267P1

6.15.4 Gravel, Cobbles, and Boulders

Unit U30, Unit U35, Unit U60, Unit U65 and Unit U90 comprise sediments interpreted to be deposited in a braided river environment. The presence of gravel and cobbles may be associated with braided rivers. In Unit U35 and Unit U60, relatively high amplitude positive internal reflectors are present which may represent gravel beds. Gravels are observed in units in BH data.

Unit U65 and U70 are interpreted to be deposited in glacial depositional environments. Glacier deposits are often poorly sorted deposits and may contain gravel, cobbles, and boulders.

A number of CPT locations refused within units due to a sudden change of cone inclination exceeds 3° over an interval of 1 m. This may indicate coarse material. For further details see Fugro, 2024b and Fugro, 2024c reports. BH data sampled gravel beds, with details of unit descriptions presented in Table 7.3.

6.15.5 Buried Channels and Tunnel Valleys

Unit U20, Unit U35, Unit U50 and Unit U60 locally form channel fills (Table 6.2). Part of these units form relatively narrow channels with a low width over depth ratio. Part of these units, especially in the east of the site, form relatively wide valleys with a high width over depth ratio.

Unit U30, Unit U35, Unit U60, Unit U65 and Unit U90 are interpreted to be (partially) deposits of braided river systems and contain internal channels and erosion surfaces.

Unit U65, Unit U69 and Unit U70 form the infill of tunnel valleys.

Table 6.2: Overview of the occurrence of buried channels and tunnel valleys

Unit	Channelised Base [Y/N]	Internal Channels and Erosion Surfaces [Y/N]
U10	N	N
U20	Y (locally)	N
U30	N	Y
U35	Y (locally)	Y
U36	N	N
U50	Y (locally)	N
U60	Y (locally)	Y
U65	Y (locally)	Y
U69	Y	N
U70	Y	Y (Similar to overlying U69 but in deeper areas)
U90	N	Y
BSU	N	N

6.15.6   Glacial Deformation

Well-defined thrust faults are widespread within the BSU in the north, centre and south-east of the site (Figure 6.71, Figure 6.72). The thrust faults in the BSU generally dip towards the east and north. The thrust faults in BSU are interpreted to be the result of ice-push (Huuse and Lykke-Andersen, 2000a; Larsen and Andersen, 2005; Winsemann *et al.,* 2020; Cartelle *et al.,* 2021). The orientation of the thrust faults indicate that the ice-push came from the north-east.

Chaotic seismic character and hints of folding and thrust faults have been observed locally within Unit U65 and Unit U70 (Figure 6.35, Figure 6.45, Figure 6.55). Unit U65 and U70 are glacial deposits which are likely to have been deformed due to glacial processes.

6.15.7   Faults

Normal faults were observed locally in Unit U70 and in the BSU (Figure 6.71, Figure 6.73). These normal faults may be of tectonic origin, collapse of the margins of tunnel valley (in the case of Unit U70), or as a result of extension upon the removal of ice sheets.

Figure 6.71: Map of the extent of glacial deformation (thrust faults) and area with normal faults in the BSU
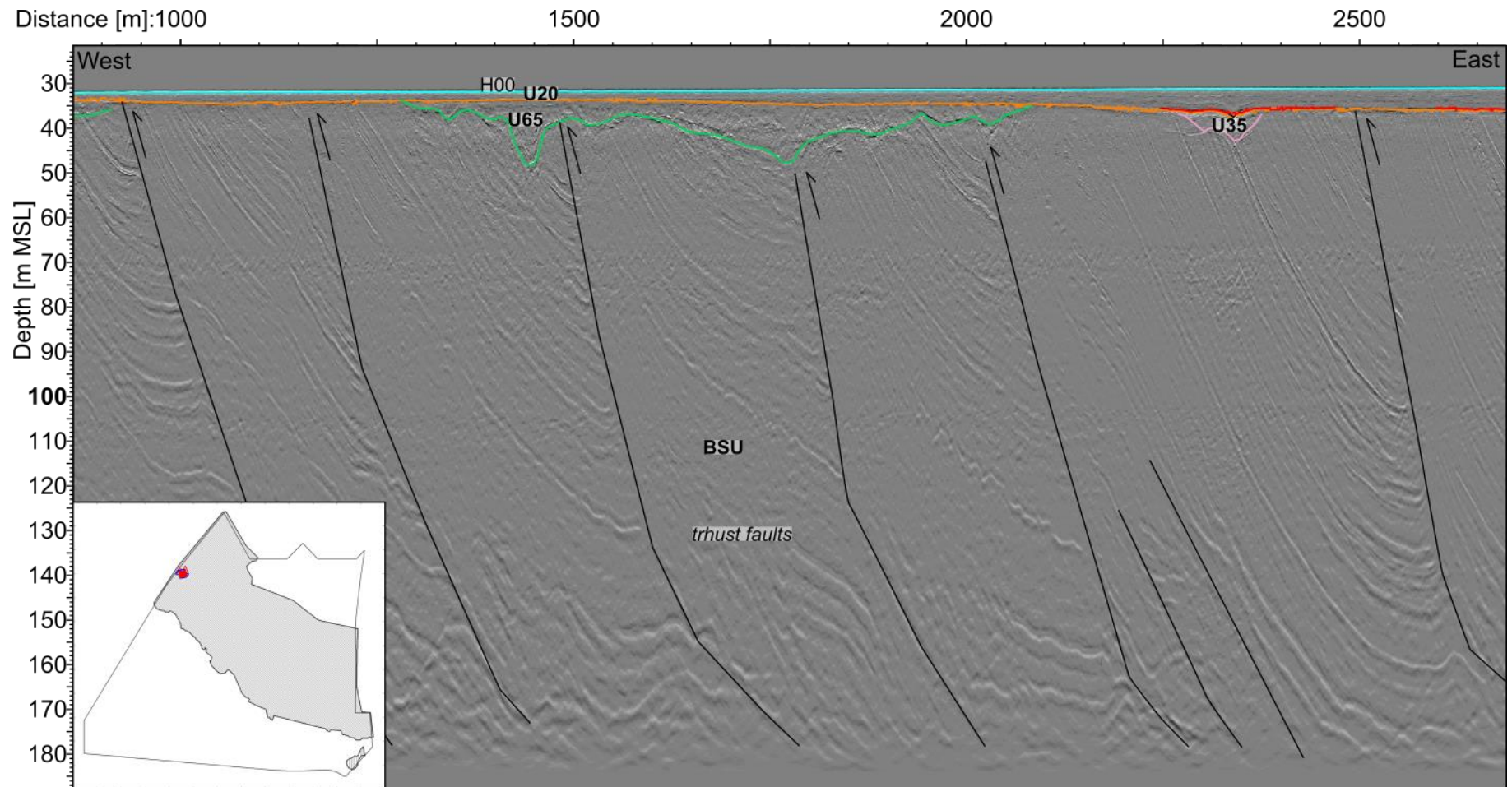
Figure 6.72: 2D UHR seismic data example of thrust faults caused by glacial deformation in the BSU. Line EAXA376P1
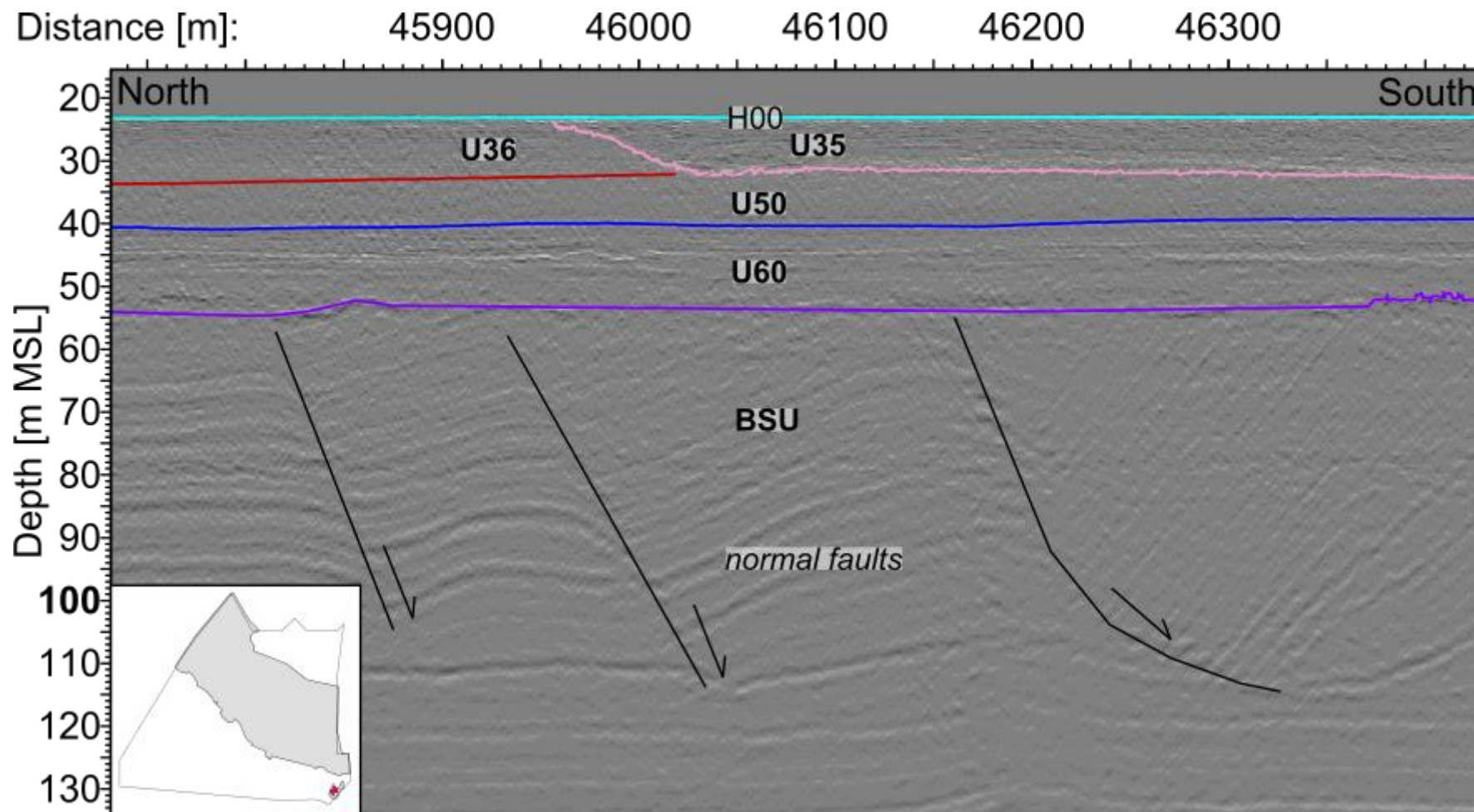
Figure 6.73: 2D UHR seismic data example of normal faults in the BSU. Line EAAZ318P1

7. Geotechnical Interpretation

7.1 Overview

Geotechnical characteristics for each of the spatial geological units has been derived from available geotechnical data. Unitisation for the geotechnical data is presented in the appendices, and is detailed in Section 6.

7.2 Geotechnical Characteristics

The following section outlines the general geotechnical characteristics of each of the units. This is supported by the unit based geotechnical characteristic values presented in Section 7.3

Based on descriptions of units from the offshore sampling campaign, Fugro have developed descriptions of each unit. These are presented in Table 7.1.

Table 7.1: Synthetic geotechnical unit descriptions

Unit	Minimum Top Depth [m BSF]*	Maximum Bottom Depth [m BSF]	Geotechnical Characteristics
U10	0.0	3.1	SAND, fine to coarse, poorly sorted to well-sorted, slightly silty to very silty, occasionally slightly gravelly, with frequent fine-grained organic matter, with few to occasionally many shell fragments, occasionally with mica crystals, light olive brown to very dark grey, non-calcareous to slightly calcareous, occasionally calcareous
U20a	0.0	5.2	SAND, fine to medium, sorted, slightly silty to very silty, occasionally clayey, occasionally slightly gravelly, with frequent fine-grained organic matter, with few to occasionally many shell fragments, olive grey to very dark grey, non-calcareous locally calcareous
U20b	0.0	5.2	SAND, fine to medium, poorly sorted to sorted, slightly clayey to clayey, slightly silty to very silty, occasionally with fine-grained organic matter, with few shell fragments, occasionally with few mica crystals, grey to dark grey, non-calcareous to slightly calcareous transitioning to CLAY, low to high plasticity, silty, slightly sandy to sandy, with few pockets of fine-grained organic matter, with few shells and shell fragments, olive grey to very dark grey, slightly calcareous transitioning to PEAT, slightly decomposed, occasionally decomposed to strongly decomposed, clayey, occasionally sandy to very sandy, dark brown to black
U30	2.0	10.85	SAND, fine, occasionally fine to medium, poorly sorted to sorted, silty, with few fine-grained organic matter, light olive brown to very dark grey, non-calcareous to slightly calcareous, with a thick to very thick bed of CLAY, low to high plasticity, silty, with pockets of fine-grained organic matter, with mica crystals, dark grey to very dark grey, calcareous
U35	0.0	9.10	SAND, fine to medium, occasionally coarse, sorted, slightly silty to silty, slightly gravelly to gravelly, with fine-grained organic matter, occasionally with mica crystals, grey to dark grey, non-calcareous to slightly calcareous, with occasional thick beds of CLAY, low to medium plasticity, slightly to very sandy, occasionally silty, grey to dark grey, slightly to highly calcareous
U36	4.0	20.2	SAND fine to medium, sorted, slightly silty to very silty, occasionally slightly gravelly, occasionally with pockets of fine-grained organic matter, occasionally with few shells and shell fragments, greenish grey to dark greenish grey, non-calcareous to slightly calcareous with occasional very thick beds of CLAY, low to medium plasticity, slightly to very silty, occasionally sandy, with pockets of fine-grained organic matter, with few shells and shell fragments, greenish grey to dark greenish grey, slightly calcareous to calcareous
U50	0.2	26.5	CLAY, low to high plasticity, slightly to very silty, sandy to very sandy, occasionally slightly gravelly, with pockets of fine-grained organic matter, with few shell fragments, dark to very dark grey, slightly calcareous to calcareous, with a basal

Unit	Minimum Top Depth [m BSF]*	Maximum Bottom Depth [m BSF]	Geotechnical Characteristics
			thick bed of SAND, fine to medium, poorly to well sorted, silty to very silty, occasionally with shell fragments, grey to dark grey, non-calcareous to calcareous
U60	9.3	60.0	SAND, fine to medium, occasionally coarse, poorly sorted to sorted, occasionally well sorted, occasionally slightly silty, occasionally slightly gravelly to gravelly, with few pockets of fine-grained organic matter, with rare wood fragments, occasionally with few shell fragments, occasionally with mica crystals, grey to dark grey, non-calcareous to slightly calcareous, with a basal medium bed to thick bed of GRAVEL, fine to coarse, unsorted to poorly sorted, occasionally sandy to very sandy, multi-coloured, non-calcareous
U65	1.55	> 70.0	thicky to very thickly interbedded CLAY, low to high plasticity, sandy to very sandy, occasionally slightly silty to silty, occasionally slightly gravelly to gravelly, with traces of fine-grained organic matter, with traces of shell fragments, occasionally with mica crystals, sark grey to very dark grey, slightly calcareous to highly calcareous and SAND, fine to medium, occasionally coarse, poorly sorted to sorted, slightly silty to silty, occasionally clayey to very clayey, occasionally with few pockets of fine-grained organic matter, with traces of wood fragments, with rare laminae of peat, occasionally with few shell fragments, grey to dark grey, non-calcareous to slightly calcareous
U69	27	> 70.0	CLAY, low to high plasticity, occasionally very high plasticity, slightly to very silty, sandy to very sandy, occasionally slightly gravelly, with few pockets of silt or sand, occasionally with few shell fragments, with few mica crystals, dark greenish grey to dark grey, calcareous
U70	0.0	> 70.0	medium to very thickly interbedded CLAY, low to high plasticity, occasionally very high plasticity, sandy to very sandy, occasionally slightly silty to silty, occasionally slightly gravelly, with few pockets of silt or sand, with few pockets of fine-grained organic matter, occasionally with mica crystals, blocky or slickensided, dark grey to very dark grey, slightly calcareous to calcareous and SAND, fine to medium, occasionally coarse, poorly sorted to sorted, slightly silty to very silty, occasionally slightly clayey to clayey, occasionally slightly gravelly to gravelly, with few laminae of fine-grained organic matter, occasionally with layers and laminae of clay, grey to dark grey, non-calcareous to slightly calcareous, occasionally with STONES, occasionally with basal thick to very thick beds of CLAY TILL to SILT TILL, low to high plasticity, occasionally very high plasticity, slightly sandy to sandy, slightly gravelly to gravelly, with few pockets of sand, dark greyish brown to very dark greyish brown, calcareous
U90	8.85	> 70.0	SAND, fine to medium, occasionally coarse, sorted, occasionally slightly silty to silty, occasionally slightly gravelly, with few laminae of fine-grained organic matter, grey to dark greyish brown, non-calcareous

Unit	Minimum Top Depth [m BSF]*	Maximum Bottom Depth [m BSF]	Geotechnical Characteristics
BSU	1.5	>70.0	medium to very thickly interbedded CLAY, medium to high plasticity, slightly silty to silty, occasionally slightly sandy, occasionally slightly gravelly, with few fine-grained organic matter, with few laminae of silt, occasionally with few shell fragments, slickensided, very dark grey to black, non-calcareous and SAND, fine, poorly sorted to well sorted, very silty, occasionally very clayey, occasionally slightly gravelly, with laminae of clay and silt, grey to very dark grey, non-calcareous to slightly calcareous
Table Notes
* Depth extracted from geotechnical data, greater depth ranges may be observed in site and within integrated geophysical datasets

In addition to the descriptions presented in Table 7.1, Fugro have also assessed the variability in sample descriptions within BH samples. Primary lithologies as outlined by Larsen et al. 1995 are presented in Table 7.2. These are based the field descriptions only of the primary lithologies and do not consider secondary descriptions. Further information on the secondary and primary constituents of the sediments please review the particle size distribution work done via dynamic image analysis (DIA) during the offshore work and reported in the investigation results report (Fugro, 2024g).

Table 7.2: Summary of primary lithologies

Unit	Primary Lithology (Larsen et al., 1995)							
	%CLAY	%CLAY TILL	%GRAVEL	%PEAT	%SAND	%SILT	%SILT TILL	%STONES
U10			<0.5		100			
U20a	2			<0.5	97			
U20b	48			6	44	2		
U30	20			3	71	6		
U35	7		<0.5		92	2		
U36	25				72	4		
U50	86			<0.5	9	5		
U60	5		1		93	<0.5		<0.5
U65	47	<0.5	<0.5	<0.5	45	7		
U69	99				1			
U70	47	2	<0.5	<0.5	44	3	4	<0.5
U90	<0.5			3	97			
BSU	83		<0.5		16	1		<0.5

Table Notes
Percentage values are from recovered sample intervals only, therefore total lithology values may vary

7.3   Geotechnical Characteristic Values

7.3.1   General

This section presents the derived geotechnical characteristic values for each of the geotechnical units predicted at the Energinet 2030 Sub-Area 1 site, providing details on the methodology and associated uncertainties. The derived values are summarised in Table 7.4 (Section 7.5).

7.3.2   Methodology

Geotechnical characteristic values are derived based on the unitised geotechnical data from the offshore site investigation (See Section 2.2.2). From these datasets Fugro have provided statistical assessment of values presented in in Table 7.3.

FUGRO

These values were derived using available offshore laboratory data, CPT and borehole data (Section 2), unitisation (Section 6) and an understanding of the regional geological setting (Section 3).

Table 7.3: Presented Characteristic Values

Symbol	Parameter	Unit	Notes
Basic Physical Properties			
γ^I	Submerged Unit Weight	kN/m^3	Submerged unit weight values were derived for each unit based on offshore geotechnical data test data. Unit weight values were from volume mass calculation, and water content test values.
WC	Water Content	%	Water content values were derived for each unit based on offshore geotechnical data test data
wP wL IP	Atterberg limits: liquid limit, plastic limit, and plasticity index	%	Atterberg limit test values derived based on offshore test data.
D_{min} D_{max}	Minimum and Maximum Dry Density	Mg/m^3	Minimum and Maximum dry density values derived based on offshore data
Cone Penetration Test Parameters			
Qc	Cone resistance	MPa	Based on downhole and seafloor CPT data collected across site
Strength Parameters			
S_u	Undrained Shear Strength (of clay)	kPa	Based on field geotechnical test data Fugro have defined Su values. Test data is derived from pocket penetrometer (PP), torvane (TV) and unconsolidated undrained (UU) testing Separate presentation of CPT derived SU values from downhole and seafloor geotechnical data. Further details on approach provided in Section 7.3.3.2
D_r	Relative Density (of sand)	%	Based on downhole and seafloor CPT data collected across site. See Section 7.3.3.3 for derivation values

For each unit minimum, maximum and average (mean) values are presented alongside the number of input values tests.

In addition to the simple statistical analysis, Fugro have reviewed datasets and provided additional statistical derivation of testing values. For statistically derived values where measured offshore laboratory data are available, Fugro adopted the statistical approach as recommended by DNV GL (2017). The recommended representative BE values were derived based on a corrected mean. The corrected mean was calculated by first establishing the average (X_{av}) and standard deviation (σ) of the dataset. Due to some variability in the dataset, outliers were considered as those values which exceeded the limits of X_{av} plus or

minus two times standard deviation (± 2σ). The recommended representative BE values were then evaluated by a recalculation of X_{av}.

In some instances, there were too few data points for a full statistical analysis to be practical. The threshold for this assessment was set at 30 tests.

Further site-specific geotechnical data acquisition and appropriate laboratory testing is required to further constrain these ranges and/or parameters. Fugro have also included further considerations for tests in Section 7.3.3.4.

The methods of derivation for each geotechnical value are discussed in Sections 7.3.3.

7.3.3   Cone Penetration Test Geotechnical Characteristic Values

The following section outlines the approach for derivation of values from the in-situ testing. For further information please see Fugro in-situ report and borehole operations reports.

7.3.3.1   Net Cone Resistance

Net cone resistance is derived from the q_c, where q_c is the cone resistance (in MPa), u_2 is the pore pressure (in kPa) and a the net area ratio of the probe.

$$q_t = q_c + (1 - a)u_2$$

<div align="right">Equation 7.1</div>

q_n is the normalised cone resistance in MPa.

$$q_n = q_t - \sigma_{v0}$$

<div align="right">Equation 7.2</div>

Where q_t is the total cone resistance and σ_{v0} is the overburden pressure.

7.3.3.2   Undrained Shear Strength

Values of undrained shear strength (s_u) for clay derived based on CPT data were calculated using Equation 3.2 from Rad & Lunne (1988).

$$s_u = 1000 \frac{q_n}{N_{kt}}$$

<div align="right">Equation 7.3</div>

N_{kt} is the correlation factor ranging between 15 and 20 for typical clays. Please note that no site-specific N_{kt} review was performed in this report. Within the derivation of geotechnical characteristic values CPT derived Su values are presented. It should be noted that these values are based on NKT values of 15 and 20, and no specific NKT values are derived for each of the units. This is recommended to be performed once laboratory test data are available.

7.3.3.3 Relative Density (Dr)

Values of relative density (Dr) for sand were derived based on available geotechnical data (CPTs). Dr was calculated from CPT data using the Jamiolkowski (2003) formula shown in Equation 7.4.

$$D_r = \frac{1}{0.0296} \ln \left(\frac{q_c}{2.494 \left\{ \frac{\sigma'_{v0} \left(\frac{1 + 2K_0}{3} \right)}{100} \right\}^{0.46}} \right)$$

<div align="right">Equation 7.4</div>

Where q_c is the cone resistance in MPa, σ'_{v0} is the effective overburden pressure and K_0 is the coefficient of earth pressure at rest (taken equal at 1). K_0 values of 0.5 and 2.0 were used in the datasets.

7.3.3.4 Statistical Values

Unlike the laboratory test data which follows the approach outlines in DNV GL (2017), values for CPT information are more variable. Therefore, only BE values derived using the approach outlined in Section 7.3.2 are presented.

7.4 Geotechnical Characteristic Values - Considerations

Current assessment of geotechnical characteristics for each unit has been performed based on the offshore dataset, which has followed the integration approach outlined in this report. It is expected that characteristic values presented will be further refined once laboratory testing is completed. Further considerations for the values are outlined in Sections 7.4.1 to 7.4.3.

7.4.1 No specific NKT review

7.4.2 Parameter Variability with Depth

For certain units some relationship between depth and parameter values may be expected. Currently characteristic values derived from the datasets do not consider variability with depth. Examples of this are the undrained shear strength values in U50, where strength appear to increase with depth. Further assessment of parameters is recommended once laboratory data is available.

7.4.3 Complex Unit Lithologies

Based on the geological processes associated with certain units, a high internal unit variability may be expected in certain units. Examples of the variability associated with lithologies in the units can be seen in Section 7.2. This can result in very high variability in values presented in Section 7.5. Unit U65 and U70 are associated with the deposition of till sediments, therefore

FUGRO

caution should be exercised when utilising values based on the units due to high local variability expected.

7.5 Characteristic Value Table

The derived geotechnical values are presented in Table 7.4 to Table 7.5. Characteristic values are presented for the sampled interval of each geotechnical unit and do not detail any anticipated change in the geotechnical conditions with depth.

Table 7.4: Derived parameters table – Classification Characteristics

Unit	Depth*	γl [kN/m3]							WC [%]						
	[m]	Number	Min	Max	Mean	LE	BE	HE	Number	Min	Max	Mean	LE	BE	HE
U10	0.05 / 2.6	220	17.2	22.3	**19.9**	18.9	19.6	20.4	94	11.3	32.3	**23.4**	18	24	30
U20a	0.1 / 9.9	946	9.7	21.9	**19.3**	18.6	19.4	20.3	404	15.8	116.7	**27.1**	21	26	32
U20b	0.1 / 18.55	452	12.1	20.7	**17.9**	16.2	18.1	20.1	170	17.1	167.9	**41.7**	19	38	58
U30	2.3 / 10.6	111	18.7	21.6	**19.9**	19.3	19.9	20.4	51	19.0	41.0	**24.6**	20	24	29
U35	0.15 / 29.6	1253	9.7	22.3	**19.9**	19.1	20.0	20.8	740	7.1	73.8	**22.7**	18	22	27
U36	4.25 / 19.70	195	17.3	20.7	**18.9**	17.8	18.8	19.9	98	19.6	38.7	**29.0**	21	29	37
U50	0.3 / 40.05	1133	14.2	24.6	**19.8**	18.7	19.8	20.8	519	8.7	80.4	**24.9**	19	25	30
U60	9.5 / 59.9	2837	17.0	35.3	**20.0**	19.3	20.0	20.7	2066	8.3	35.6	**21.7**	19	22	25
U65	1.8 / 69.9	2107	13.6	32.5	**21.0**	19.0	21.0	23.0	1089	7.9	99.6	**18.4**	9	18	27
U69	29.2 / 70.1	996	16.7	24.0	**19.4**	17.9	19.2	20.4	354	7.8	48.4	**27.9**	21	29	37
U70	8.2 / 70.75	6993	12.3	40.0	**20.4**	18.5	20.3	22.0	3518	4.5	131.3	**22.1**	14	22	30
U90	9.0 / 69.75	318	17.3	22.1	**19.8**	19.1	19.8	20.6	233	12.5	41	**22.5**	18	22	27
BSU	6.8 / 70.55	3051	12.3	25.0	**20.0**	19.1	19.9	20.7	1272	7.5	38.7	**23.8**	20	24	29

Notes:

Statistical approach to define LE BE and HE presented in Section 7.3.2

Test data is based on offshore work phase only therefore may be revised once laboratory testing is completed

No split between sediment lithology and test values has currently been performed. Caution should be exercised when using datasets

* Depth range values present the range of depths that geotechnical test data is available within. For full range of thickness please see spatial geological model

FUGRO

Table 7.5: Derived parameters table – Atterberg Limits

Unit	Depth* [m]	Atterberg Limit																			
		Liquid Limit							Plastic Limit							Plasticity Index						
		Number	Min	Max	Mean	LE	BE	HE	Number	Min	Max	Mean	LE	BE	HE	Number	Min	Max	Mean	LE	BE	HE
U10		No Tests																				
U20a		No Tests																				
U20b	3.0 / 9.15	6	34	70	50.5	Insufficient Data			6	20	50	31.3	Insufficient Data			6	14	25	19.3	Insufficient Data		
U30		No Tests																				
U35	8	1	33	33	33	Insufficient Data			1	17	17	17	Insufficient Data			1	16	16	16.0	Insufficient Data		
U36		No Tests																				
U50	4 / 18.75	38	22	51	38	26	37	48	38	6	28	19.3	15	20	24	8	7	32	17.2	8	17	26
U60	40.7	1	43	43	43	Insufficient Data			1	22	22	22	Insufficient Data			1	21	21	21.0	Insufficient Data		
U65	7.05 / 63	18	32	112	51.3	Insufficient Data			18	15	80	27.6	Insufficient Data			18	12	44	23.7	Insufficient Data		
U69	34.4 / 54.55	5	31	45	38.6	Insufficient Data			5	17	22	20.2	Insufficient Data			5	14	23	18.4	Insufficient Data		
U70	15.5 / 69.3	103	21	87	49.6	31	49	66	103	12	38	23.5	16	23	29	103	8	53	26.1	11	25	40
U90		No Tests																				
BSU	11.4 / 70.45	78	32	74	50.9	35	50	66	78	19	41	27.7	21	27	33	78	10	45	23.2	12	23	34

Notes:

Statistical approach to define LE BE and HE presented in Section 7.3.2

Test data is based on offshore work phase only therefore may be revised once laboratory testing is completed

No split between sediment lithology and test values has currently been performed. Caution should be exercised when using datasets. SU values represent clay layers within sand sediments in predominantly sand units. For split of material please see Table 7.2

* Depth range values present the range of depths that geotechnical test data is available within. For full range of thickness please see spatial geological model

FUGRO

Table 7.6: Derived parameters table – Min Max Characteristics

Unit	Depth* [m]	Min index dry density [kN/m3]							Max index dry density						
		Number	Min	Max	Mean	LE	BE	HE	Number	Min	Max	Mean	LE	BE	HE
U10	0.0 – 2.0	17	1.31	1.56	**1.44**	Insufficient Data			17	1.65	1.86	**1.75**	Insufficient Data		
U20a	0.1 – 7.0	29	1.2	1.46	**1.33**	Insufficient Data			29	1.56	1.79	**1.65**	Insufficient Data		
U20b	0.5 – 9.1	4	1.2	1.45	**1.29**	Insufficient Data			4	1.54	1.79	**1.64**	Insufficient Data		
U30	5.2 – 7.0	3	1.38	1.52	**1.45**	Insufficient Data			3	1.7	1.83	**1.77**	Insufficient Data		
U35	0.3 – 31.4	57	1.26	1.64	**1.45**	1.33	1.45	1.57	57	1.57	1.92	**1.76**	1.61	1.75	1.90
U36	11.5 – 17.6	2	1.37	1.38	**1.38**	Insufficient Data			2	1.70	1.70	**1.70**	Insufficient Data		
U50	12.3 – 18.5	2	1.43	1.53	**1.48**	Insufficient Data			2	1.72	1.84	**1.78**	Insufficient Data		
U60	11.35 – 52.5	113	1.32	1.62	**1.45**	1.36	1.44	1.53	113	1.62	1.77	**1.99**	1.68	1.77	1.86
U65	2.3 – 37.0	14	1.32	1.58	**1.45**	Insufficient Data			14	1.68	1.94	**1.81**	Insufficient Data		
U69	30.25	1		1.52		Insufficient Data			1		1.85		Insufficient Data		
U70	17.4 – 69.5	57	1.09	1.49	**1.36**	1.29	1.37	1.45	57	1.32	1.93	**1.69**	1.60	1.70	1.80
U90	10.95 – 63.5	11	1.17	1.42	**1.28**	Insufficient Data			11	1.54	1.73	**1.65**	Insufficient Data		
BSU	19.0 – 30.5	4	1.45	1.57	**1.50**	Insufficient Data			4	1.77	1.85	**1.81**	Insufficient Data		

Notes:

Statistical approach to define LE BE and HE presented in Section 7.3.2

Test data is based on offshore work phase only therefore may be revised once laboratory testing is completed

No split between sediment lithology and test values has currently been performed. Caution should be exercised when using datasets. SU values represent clay layers within sand sediments in predominantly sand units. For split of material please see Table 7.2

* Depth range values present the range of depths that geotechnical test data is available within. For full range of thickness please see spatial geological model

Table 7.7: Derived parameters table – Strength Characteristics lab test data

Unit	Depth^ [m]	Su [kPa]						
		Number	Min	Max	Mean	LE	BE	HE
U10	0.15	1	*29*	*29*	*29*	NA		
U20a	4.7 / 8.6	12	11	30	**19**	Insufficient Data		
U20b	4.7 / 17.2	90	5	195	**32**	7*	29*	50*
U30	6.35 / 10.6	7	67	200	**144**	Insufficient Data		
U35	2.6 / 16.0	29	10	258	**62**	Insufficient Data		
U36	11.6 / 12.85	6	6	22	**11**	Insufficient Data		
U50	1.5 / 21.45	418	4	358	**113**	41	109	177
U60	13.15 / 49.72	21	80	735	**393**	Insufficient Data		
U65	1.7 / 69.8	394	8	1121	**371**	*0.0~*	352	710
U69	29.2 / 70.1	412	19	613	**203**	64	187	309
U70	17.3 / 70.6	1565	32	1368	**449**	80	429	778
U90		No tests						
BSU	7.75 / 70.75	923	37	917	**412**	189*	413*	637*

Notes:
Statistical approach to define LE BE and HE presented in Section 7.3.2
Test data is based on offshore work phase only therefore may be revised once laboratory testing is completed
No split between sediment lithology and test values has currently been performed. Caution should be exercised when using datasets. SU values represent clay layers within sand sediments in predominantly sand units. For split of material please see Table 7.2
* Plot of data suggests relationship with depth, which is not currently captured in dataset. Caution should be exercised when considering values
^ Depth range values present the range of depths that geotechnical test data is available within. For full range of thickness please see spatial geological model
~ Statistical value is not considered valid. This is due to the high variability and large standard deviation in test data

FUGRO

Table 7.8: Derived parameters table – Strength Characteristics

Unit	Depth~	Cone Resistance qc [MPa]						Su from CPT Data					Dr from CPT Data				
	[m]	Number	Min	Max	Mean	LE	BE	HE	Number	Min	Max	Mean	BE	Number	Min	Max	Mean	BE
U10	0.00 / 3.6	15076	0.00	44.65	6.1	0.0	4.2	11.8	30	4.4	27.5	10.4	Insufficient data	11713	<5	>100	87.5	92
U20a*	0.00 / 19.9	38063	0.00	43.52	5.6	0.0	4.1	10.6	4947	6.0	180.7	32.3	27	31963	<5	>100	55.7	54
U20b*	0.00 / 18.71	7311	0.00	31.60	1.8	0.0	1.3	3.1	2341	0.0	95.9	18.2	31	2341	<5	95.9	18.2	14
U30	0.9 / 10.7	7115	0.58	58.95	13.4	1.4	12.6	23.8	1037	28.3	244.3	11.7	118	6078	<5	>100	83.2	87
U35	0.00 / 33.48	104177	0.00	92.34	20.8	0.9	19.0	37.1	4244	3.27	>500	198.8	165	100300	<5	>100	88.8	92
U36	3.3 / 24.5	8924	1.54	50.16	17.5	0.1	17.2	34.4	25	71.8	211.5	159.2	160	8899	<5	>100	65.1	66
U50	0.2 / 50	92223	0.28	67.43	3.6	0.0#	2.9	5.9	63419	12.8	755.5	98.9	93	28538	<5	>100	30.5	27
U60	6.1 / 55.5	147566	0.16	118.75	40.1	25.1	42.4	59.8	8561	34.2	>1000	314.2	260	135470	<5	>100	93.5	96
U65	0.4 / 56	122824	0.10	114.85	16.5^	0.0#^	14.2^	32.9^	55.44	12	>1000	285.8	245	66266	<5	>100	76.5	80
U69	33.51 / 56.48	6396	0.44	50.92	6.8	1.8	5.7	9.5	5237	24.9	908.3	214.6	207	804	14.8	88.8	47.9	47
U70	0.6 / 57.5	73973	0.18	126.10	21.6^	0.0#^	19.9^	41.5^	33767	37.5	>1000	422.5	385	35738	<5	>100	75.9	77
U90	9.2 / 56.49	17609	0.13	128.25	42.0	0.0#	40.3	83.2	4634	80.4	>1000	273.7	254	9511	<5	>100	93.4	95
BSU	3.8 / 57.5	45688	0.8	83.14	17.1	0.0#	14.5	33.6	29089	81.63	>1000	345,9	315	14705	<5	>100	85.1	88

Notes:

Statistical approach to define BE presented in Section 7.3.2

Test data is based on offshore work phase only therefore may be revised once laboratory testing is completed

Cone resistance values show build up which may affect values

No split between sediment lithology and test values has currently been performed. Caution should be exercised when using datasets. SU values represent clay layers within CPT data and DR values represent sand sediments, for split of material please see Table 7.2

* Values from locations with BH data only, which is used to split the datasets.

BE only provided for derived values due to variability of CPT data and values

^Values from both clay and sand member, results should be approached with caution and may not reflect conditions

~ Depth range values present the range of depths that geotechnical test data is available within. For full range of thickness please see spatial geological model

Statistical value is not considered valid. This is due to the high variability and large standard deviation in test data

FUGRO

8. Geotechnical Zonation

8.1 Overview

This section presents the geological provinces mapping and indicative profiles based on the extent of the mapped spatial geological model units as presented in Section 6.

8.2 Methodology

Further to the spatial geological model outlined in Section 6, a zonation was defined based on key stratigraphic variabilities within the units. These variabilities were defined in conjunction with Energinet (meeting, 2nd May 2024) and are based on horizontal and vertical variations in stratigraphies that may affect foundations within the development area.

8.3 Zonation

Soil province maps allow for better understanding of the lateral variability between soil units. A soil province map was generated for the study area to depict the spatial extent of several key factors that divide the site, based on the geometry of the spatial geological model.

The below units were incorporated into the soil province map because they are expected to result in ground conditions that may be significant for foundation design:

- Unit U20 is a Holocene channelised unit and therefore could be expected to result in areas of lower strength material that are deeper than the rest of the site;
- Glacial Units U65 and U70 represent a change in the depositional environment at the site and may be expected to be associated with an increase in soil strengths, as well as greater variability in the ground conditions. Sediments from U69 are excluded from this grouping based on the relative consistency of their nature in geotechnical data, despite being deposited in glacial periods.

Based on these two factors, soil provincing was defined for the study area. Fugro have selected their presence or absence or various depth ranges, as summarised in Table 8.1 and Table 8.2, and presented in Figure 8.1 to Figure 8.3.

Table 8.1: Unit U20 – soil thickness, spatial extent shown in Figure 8.1

Soil Condition Factor	Soil Province Naming Convention	Engineering Implication
Unit U20 absent	a	Shallow depth to intermediate strength units or high strength units
Unit U20 present, thickness between 0.1 m and 6 m	b	Shallow depth to intermediate strength units or high strength units, Unit 20 likely largely comprises sand sediments from U20a
Unit U20 present, thickness between 6 m and 10 m	c	Unit 20 likely to comprise both sand (U20a) and low to very low strength clay (U20b) sediments
Unit U20 present, thickness greater than 10 m	d	Thick areas of Unit 20 with extensive U20b low to very low strength sediments
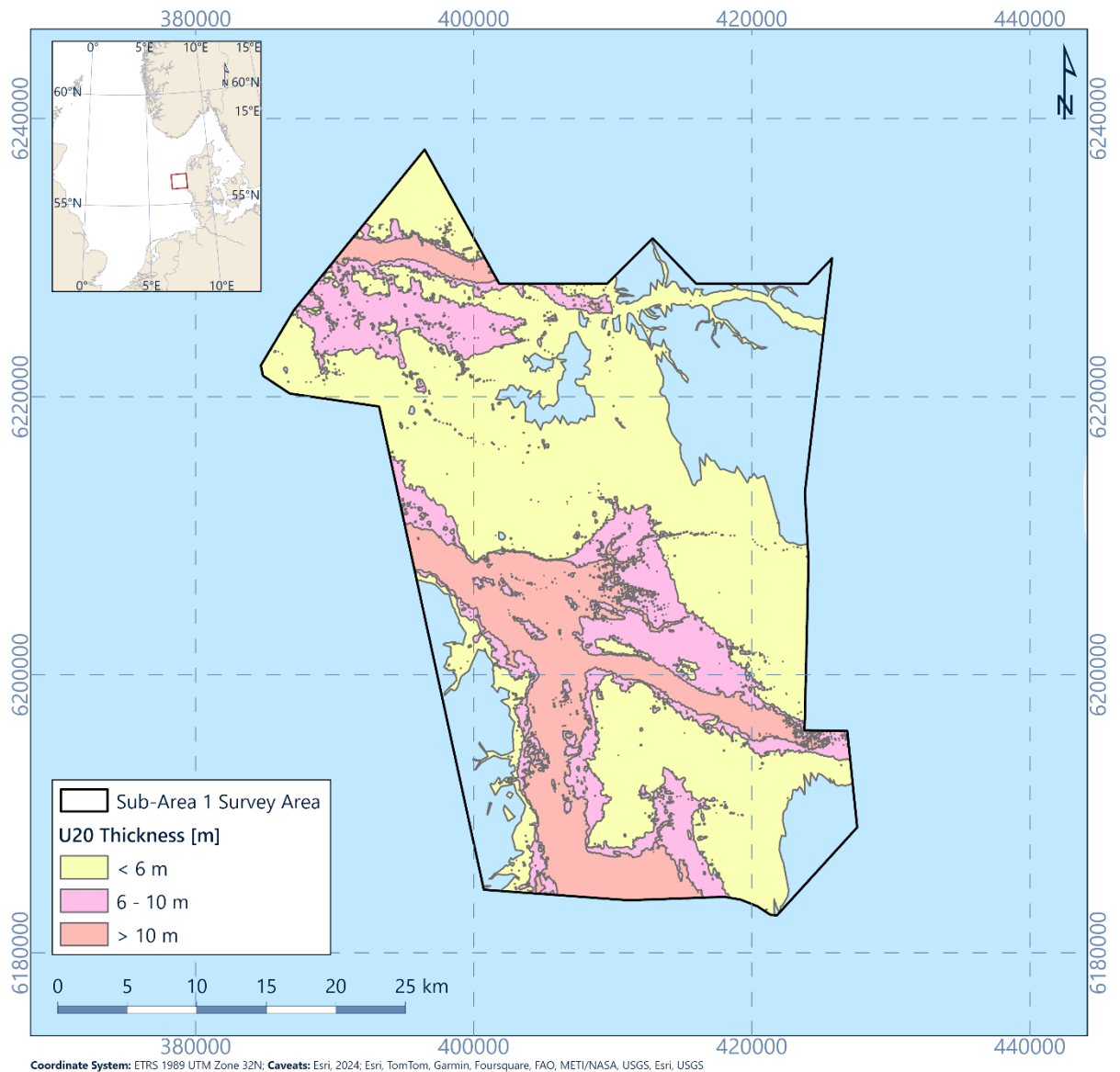
Figure 8.1: Thickness categories for Unit U20 zonation blank areas show areas of site with no U20 sediments

Depth to the base of U20 has been appraised as part of the zonation work as it is expected that the areas of thicker U20 result in the presence of lower strength units to deeper depths than the rest of the site. This may affect future foundation capacity.

The second factor is based on the depth to the top of glacial units U65 and U70. These units reflect the shallowest / youngest units associated with a period at the site history where direct glacial action is expected to affect the geotechnical properties and also result in greater variability in sediment properties. Depth intervals associated with the top of this unit were selected based on depth intervals relevant for different foundations concepts. These are where the unit was not present at any depth, when it is less than 10 m BSF (affecting most foundation types), where it is between 10 m and 40 m BSF (likely affecting deeper pile and monopile foundations) and areas where it is present >40 m BSF (likely only affecting the base

of very deep foundations). These are summarised in Table 8.2. Extents associated with these zones are presented in Figure 8.2.

Table 8.2: Unit U65/U70 – top of glacial till units across site

Soil Condition Factor	Soil Province Naming Convention	Engineering Implication
U65/U70 not present	1	Sediments comprise variable thickness of post Saalian sediments on top of either U90 or BSU sediments. Likely U90 or BSU may be encountered in depth of interest
Top of U65/U70 present <10 m BSF	2	High strength and variable units expected at less than 10 m BSF
Top of U65/U70 present between 10 m and 40 m BSF	3	High strength and variable units expected with typical depth range for foundations
Top of U65/U70 present > 40 m BSF	4	High strength and variable units may not be present within typical depth range for foundations

Figure 8.2: Depth to top of Glacial Units U65/U70 blank areas show site that has no U65/U70 sediments present

Based on these two factors, Fugro have defined a zonation map across the site. This created a total of 16 theoretical zones across the site. These are summarised in Table 8.3. It should be noted that one zone (2d) is not possible based on conflicting factors.

Table 8.3: Combined zonation naming convention

Condition Factors	U65/U70 absent	Top U65/U70 present <10 m BSF	Top U65/U70 present 10 m to 40 m BSF	Top U65/U70 present>40 m BSF
U20 Absent	1a	2a	3a	4a
U20 thickness 0.1 m to 6 m	1b	2b	3b	4b
U20 thickness 6 m to 10 m	1c	2c	3c	4c

Condition Factors	U65/U70 absent	Top U65/U70 present <10 m BSF	Top U65/U70 present 10 m to 40 m BSF	Top U65/U70 present>40 m BSF
U20 thickness >10 m	1d	-	3d	4d

The zonation across the study area is presented in Figure 8.3.

Coordinate System: ETRS 1989 UTM Zone 32N; Caveats: Esri, 2024; Esri, TomTom, Garmin, Foursquare, FAO, METI/NASA, USGS, Esri, USGS
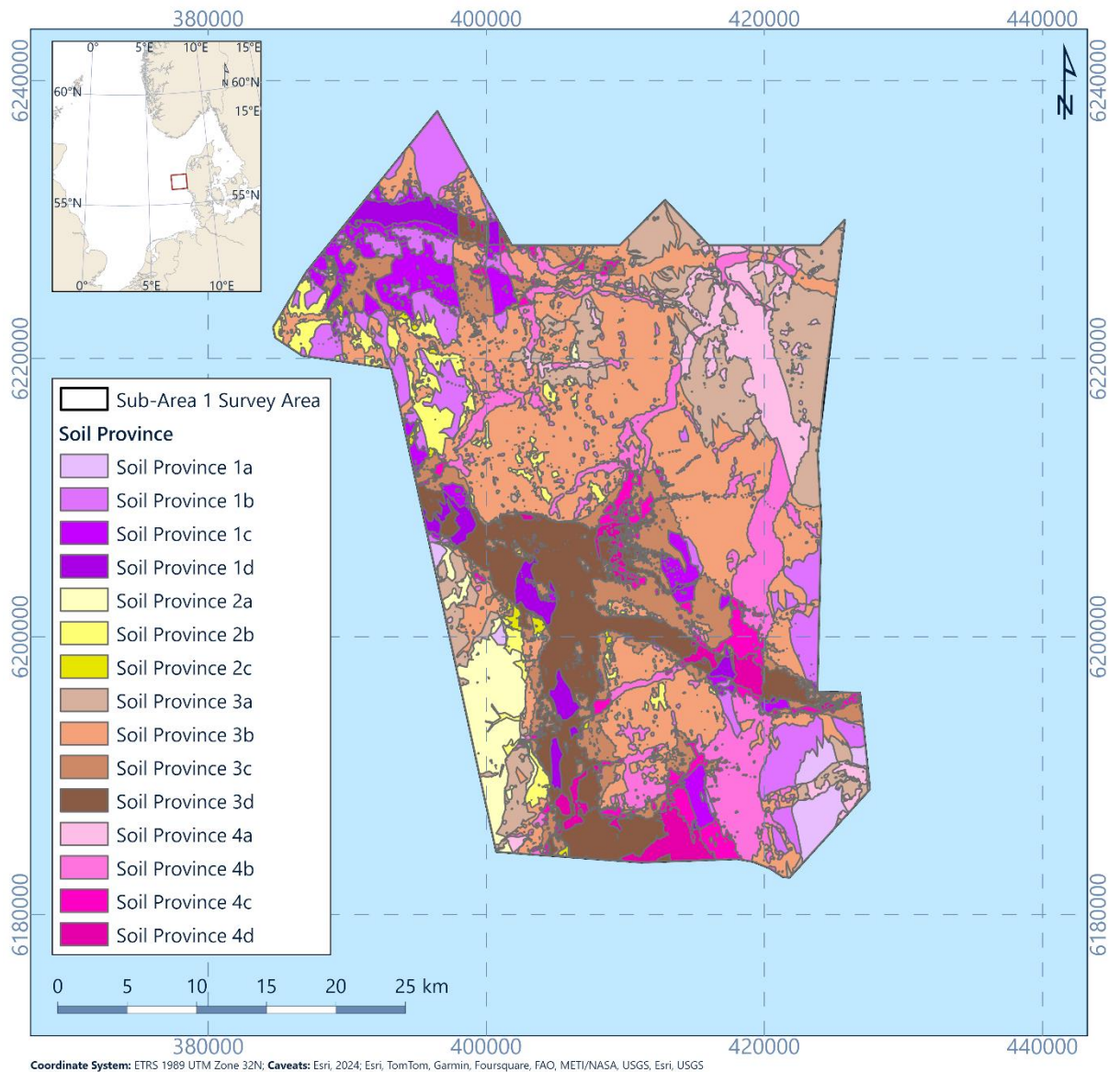
Figure 8.3: Zonation of study area

The relative percentage of the site covered by the zones is presented in Table 8.4.

Table 8.4: Coverage percentages associated with each soil zone in sub-area 1

Soil Province	Area [km²]	Coverage of Site [%]
1a	21.0	1

Soil Province	Area [km²]	Coverage of Site [%]
1b	105.8	8
1c	63.5	5
1d	36.6	3
2a	44.7	3
2b	47.0	3
2c	6.6	<1
3a	148.3	11
3b	383.6	27
3c	122.6	9
3d	138.4	10
4a	68.5	5
4b	136.3	10
4c	42.7	3
4d	32.8	2
Notes: If percentage total is > 100% this is due to rounding to the nearest whole number.		

Some minor inconsistencies were observed during the process associated with the gridding at the top of Unit U65/70. These have been adjusted in the zonation process. These were largely constrained to the areas of more limited UHRS line coverage and arose as a result of gridding between seismic lines. Further details on gridding are provided in Section 3.1.1.

8.4   Typical Soil Profiles

Fugro have defined typical soil profiles from each of the soil province areas. These are based on the spatial geological model and utilise mean depth to base of units from integrated soil horizons. These present average (mean) thickness values for unit bases within each of the soil province areas. These are presented in Sections 8.4.1 to 8.4.15. In addition, typical boreholes or CPT locations (where there is not a representative borehole), have been selected within each of the zones. These are selected to typify the conditions expected. Although these are the most representative of the province, they are variable in depth to the profiles in Figure 8.4 due to being site specific.

Figure 8.4 presents the typical soil profiles for each province using the units that cover at least 40% of the province. Soil Profile 3c is split into (i) and (ii), this is due to both U60 and U65 covering more than 40% of the area of the soil province. However, U60 and U65 are not present at the same time, therefore Fugro have presented two soil profile options to represent this.
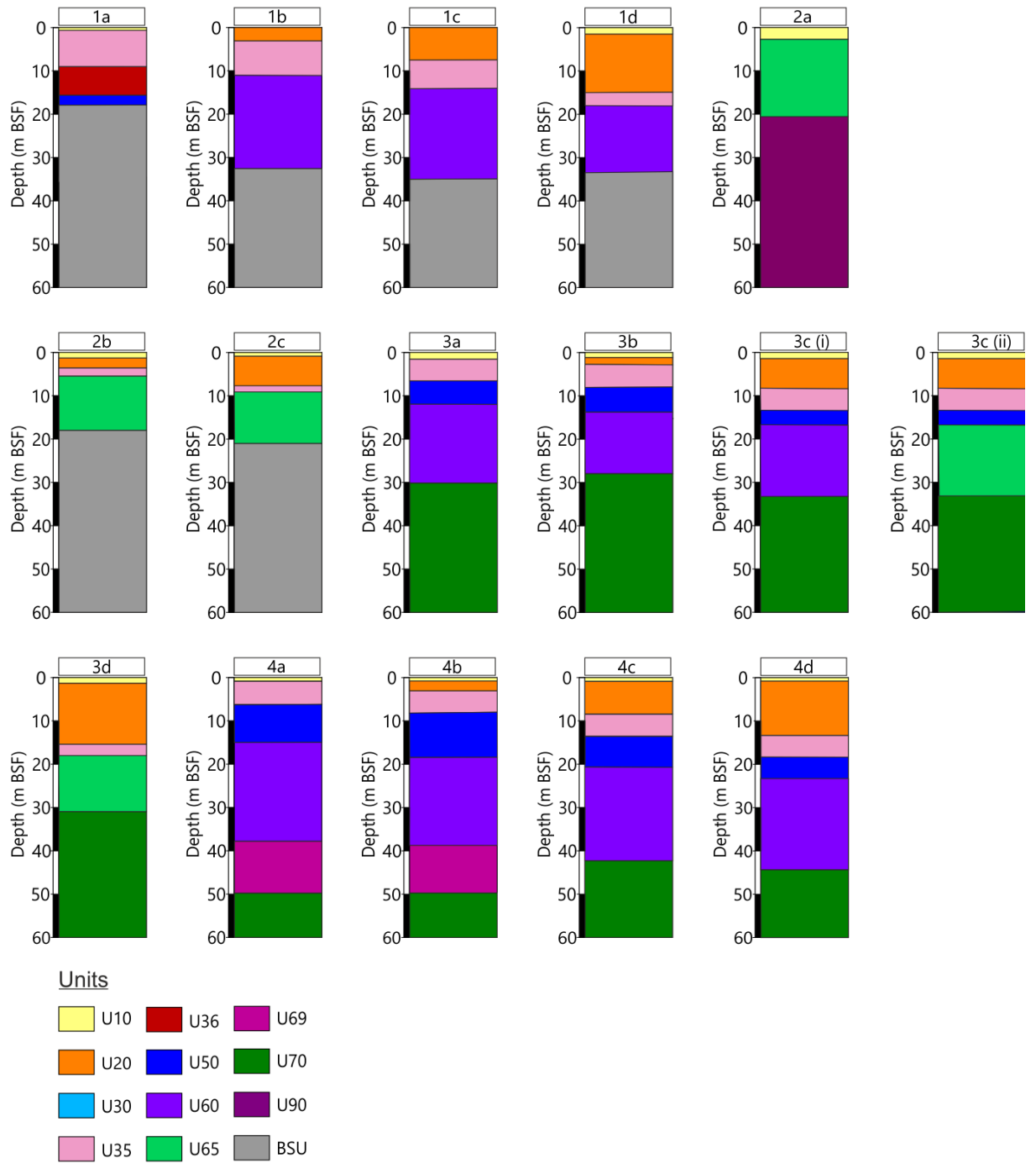
Figure 8.4: Typical soil profile where units cover > 40% of the soil province. For further detail on profile 3c see section 8.4.10

8.4.1   Soil Province 1a

Soil unit thicknesses within Soil Province 1a were derived from spatial geological model layers defined within the Soil Province 1a area. These are the mean values of the depth to base of the units and are presented in Table 8.5.

Table 8.5: Average soil unit thicknesses within Soil Province 1a

Spatial Geological Model Unit	Mean Base Unit Depth [m]	Coverage of Province [%]'
U10	0.6	91
U20	Absent	0
U30	Absent	0
U35	9.4	80
U36	15.2	70
U50	17.1	20
U60	35.8	87
U65	Absent	0
U69	Absent	0
U70	Absent	0
U90	56.2	<1
Notes:		
'- Of that soil province, the unit is present in the "coverage %" of the total province area		

Soil province 1a is defined by possibility of shallow BSU unit (absence of U20 and lack of glacial till material U65/U70) as shown on the left hand side of Figure 8.5, therefore CPT 288 is considered a type example profile from the characteristics and unit coverage in this soil province (Figure 8.5).
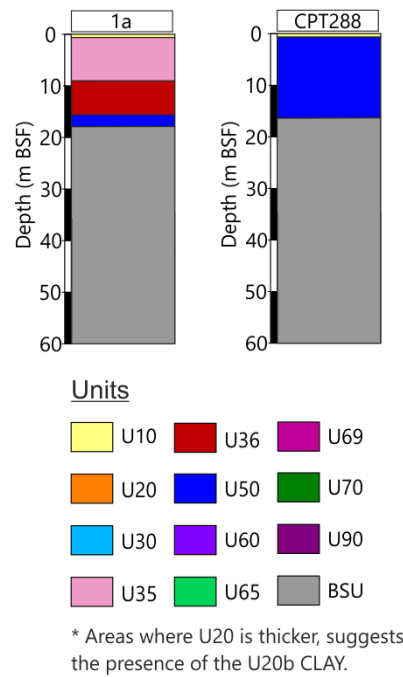
Figure 8.5: CPT288 soil profile within Soil Province 1a

8.4.2   Soil Provinces 1b

Soil unit thicknesses within Soil Province 1b were derived from spatial geological model layers defined within the Soil Province 1b area. These are the mean values of the depth to base of the units and are presented in Table 8.6.

Table 8.6: Average soil unit thicknesses within Soil Province 1b

Spatial Geological Model Unit	Mean Base Unit Depth [m]	Coverage of Province [%]'
U10	1.2	37
U20	3.6	100
U30	9.8	27
U35	10.4	91
U36	14.3	31
U50	16.5	36
U60	32.3	68
U65	Absent	0
U69	Absent	0
U70	Absent	0
U90	75.2	1
Notes '- Of that soil province, the unit is present in the "coverage %" of the total province area		

Soil province 1b is defined by the possibility of shallow BSU with a thin section of U20 in the upper profile. An example of this is CPT 166 is shown on the right hand side of Figure 8.6,

showing a thin layer of the U20 with BSU at 15 m BSF. The left hand side displays the representative soil profile.
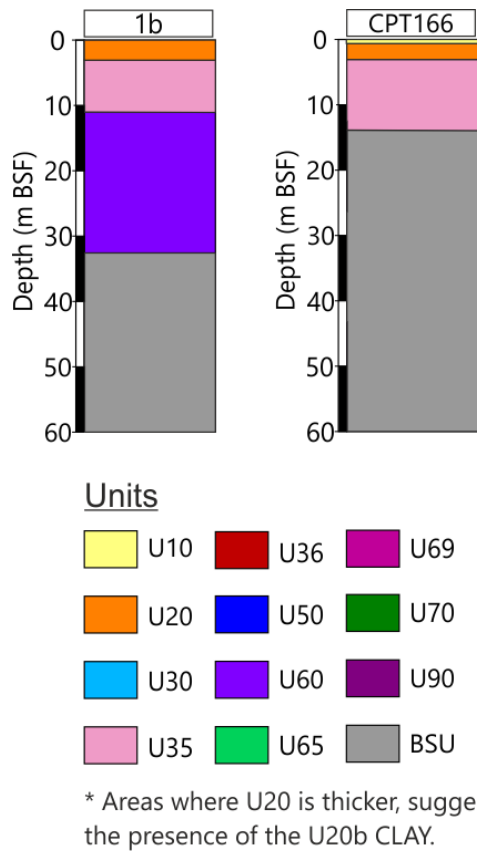
Figure 8.6: CPT166 soil profile within Soil Province 1b

8.4.3 Soil Province 1c

Soil unit thicknesses within Soil Province 1c were derived from spatial geological model layers defined within the Soil Province 1c area. These are the mean values of the depth to base of the units and are presented in Table 8.7.

Table 8.7: Average soil unit thicknesses within Soil Province 1c

Spatial Geological Model Unit	Mean Base Unit Depth [m]	Coverage of Province [%]'
U10	1.0	38
U20	8.1	100
U30	9.8	22
U35	13.8	99
U36	17.7	2
U50	18.6	35
U60	35	71
U65	Absent	0
U69	Absent	0
U70	Absent	0

Spatial Geological Model Unit	Mean Base Unit Depth [m]	Coverage of Province [%]'
U90	76.6	9
Notes '- Of that soil province, the unit is present in the "coverage %" of the total province area		

Soil province 1c is defined by thicker U20 sediments but with no glacial till units (U65/U70), Figure 8.7. A type example of this is CPT 327 showing the potential stratigraphy within this soil province (Figure 8.7). This location penetrates to 28.7 m. Below this depth BSU are expected.
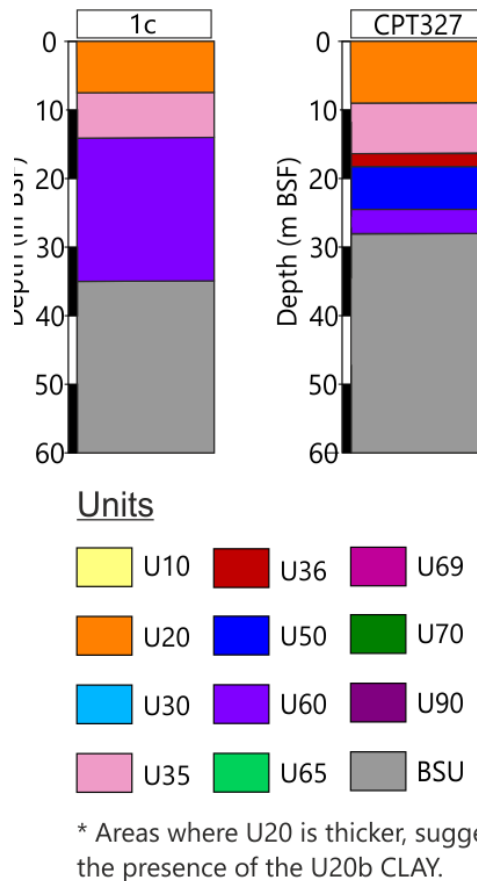
Figure 8.7: CPT327 soil profile within Soil Province 1c

8.4.4 Soil Province 1d

Soil unit thicknesses within Soil Province 1d were derived from spatial geological model layers defined within the Soil Province 1d area. These are the mean values of the depth to base of the units and are presented in Table 8.8.

Table 8.8: Average soil unit thicknesses within Soil Province 1d

Spatial Geological Model Unit	Mean Base Unit Depth [m]	Coverage of Province [%]'
U10	1.1	64
U20	14.7	100
U30	13.5*	1

Spatial Geological Model Unit	Mean Base Unit Depth [m]	Coverage of Province [%]'
U35	18.1	85
U36	19.3	1
U50	19.0*	13
U60	33.2	45
U65	Absent	0
U69	Absent	0
U70	Absent	0
U90	56.3	14
Notes: * Value less than younger units due to average values used and low coverage of soil unit area '- Of that soil province, the unit is present in the "coverage %" of the total province area		

Soil province 1d is defined by thick (>10 m) U20, and typically thick U20b sediments with no till material, represented on the left of Figure 8.8. Due to the thick U20 sediments, penetrations are frequently limited by buckling issues in CPT data collection, however Location CPT 258 is a good example location of the unit coverage within Soil Province 1d (Figure 8.8).
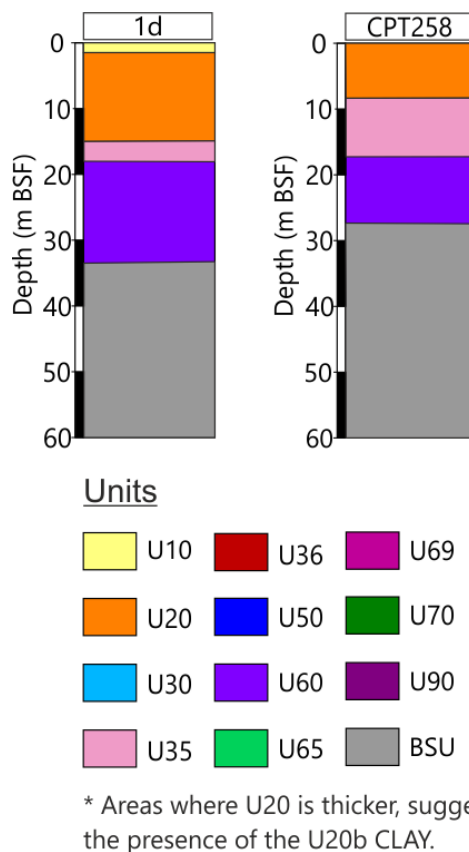
Figure 8.8: CPT258 soil profile within Soil Province 1d

8.4.5   Soil Province 2a

Soil unit thicknesses within Soil Province 2a were derived from spatial geological model layers defined within the Soil Province 2a area. These are the mean values of the depth to base of the units and are presented in Table 8.9.

Table 8.9: Average soil unit thicknesses within Soil Province 2a

Spatial Geological Model Unit	Mean Base Unit Depth [m]	Coverage of Province [%]'
U10	2.8	98
U20	Absent	0
U30	3.2	<1
U35	4.4	4
U36	Absent	0
U50	6.5	3
U60	Absent	0
U65	20.9	97
U69	Absent	0
U70	90.6	9
U90	63.9	82
Notes		
'- Of that soil province, the unit is present in the "coverage %" of the total province area		

The soil province 2a is defined by shallow glacial till material of U65/U70. Location BH089 shows a good example of the type of sediments typical of this unit outlined by the percentage coverage within Soil Province 2a, as presented in Figure 8.9.
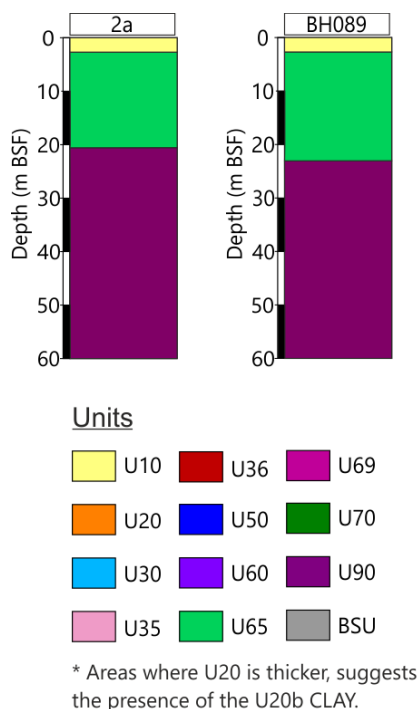
Figure 8.9: BH089 soil profile within Soil Province 2a

8.4.6 Soil Province 2b

Soil unit thicknesses within Soil Province 2b were derived from spatial geological model layers defined within the Soil Province 2b area. These are the mean values of the depth to base of the units and are presented in Table 8.10.

Table 8.10: Average soil unit thicknesses within Soil Province 2b

Spatial Geological Model Unit	Mean Base Unit Depth [m]	Coverage of Province [%]'
U10	1.2	73
U20	3.5	100
U30	4.9	7
U35	7.4	45
U36	Absent	0
U50	8.1	14
U60	Absent	0
U65	18.8	91
U69	Absent	0
U70	>100	21
U90	61.6	10
Notes		
'- Of that soil province, the unit is present in the "coverage %" of the total province area		

Soil Province 2b is defined by thin U20 sediments and shallow till material. Figure 8.10 shows the representative soil profile on the left and CPT 273 as an example of this soil profile on

right ; showing a range of sediments that are in the soil province based on their percentage coverage, with the presence of U70 that predominately is less common.

Units

* Areas where U20 is thicker, suggests the presence of the U20b CLAY.
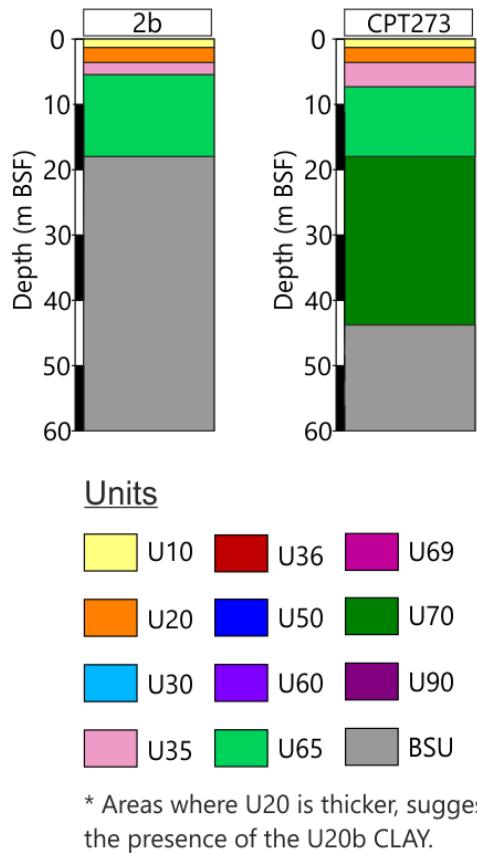
Figure 8.10: CPT273 soil profile within Soil Province 2b

8.4.7 Soil Province 2c

Soil unit thicknesses within Soil Province 2c were derived from spatial geological model layers defined within the Soil Province 2c area. These are the mean values of the depth to base of the units and are presented in Table 8.11.

Table 8.11: Average soil unit thicknesses within Soil Province 2c

Spatial Geological Model Unit	Mean Base Unit Depth [m]	Coverage of Province [%]'
U10	0.7	59
U20	7.7	100
U30	8.0	2
U35	9.1	45
U36	Absent	0
U50	9.4*	14
U60	Absent	0
U65	21.2	88
U69	Absent	0

Spatial Geological Model Unit	Mean Base Unit Depth [m]	Coverage of Province [%]'
U70	>100	18
U90	63.1	11
Notes: * Value more than older units due to average values used and low coverage of soil unit area ^ Values rounded to 10 m in zonation '- Of that soil province, the unit is present in the "coverage %" of the total province area		

BH040 is a good representative borehole within Soil Province 2c, on the right hand side ofFigure 8.11, due to the small area covered and the contrasting conditions associated with its definition (thick U20 and shallow glacial materials). BH040 displays all the units that have a higher percentage coverage of the province. The left hand soil stick in Figure 8.11 shows the representative soil profile for this province.
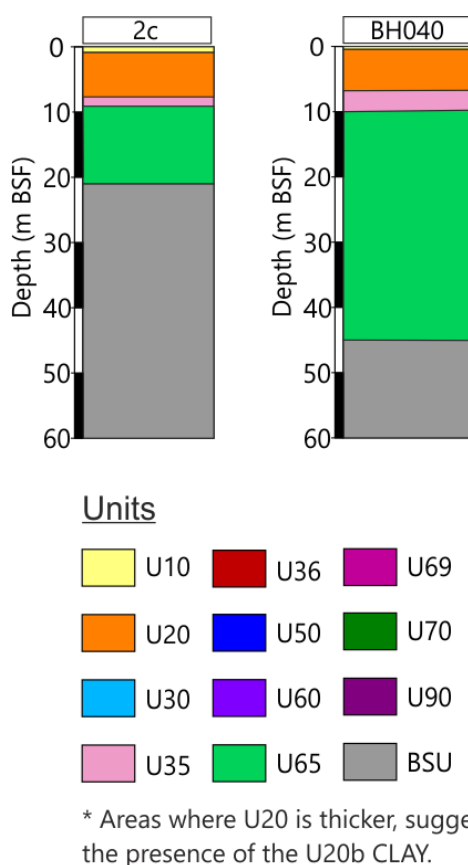
Figure 8.11: BH040 soil profile within Soil Province 2c

8.4.8 Soil Province 3a

Soil unit thicknesses within Soil Province 3a were derived from spatial geological model layers defined within the Soil Province 3a area. These are the mean values of the depth to base of the units and are presented in Table 8.12.

Table 8.12: Average soil unit thicknesses within Soil Province 3a

Spatial Geological Model Unit	Mean Base Unit Depth [m]	Coverage of Province [%]'
U10	1.0	60
U20	Absent	0
U30	4.1	3
U35	6.4	82
U36	16.7	5
U50	12.1	75
U60	30.1	78
U65	32.6	31
U69	35.5	1
U70	>100	96
U90	72.6	2
Notes		
'- Of that soil province, the unit is present in the "coverage %" of the total province area		

Soil province 3a is defined by an absence of Unit U20 with till material present beneath an intermediate depth of Quaternary sediments, which typically means thicker U50 sediments. An example of this is BH008 (Figure 8.12); although this borehole typically has a thinner U50 than would normally be expected from the representative soil profile on the left of Figure 8.12.

* Areas where U20 is thicker, suggests the presence of the U20b CLAY.
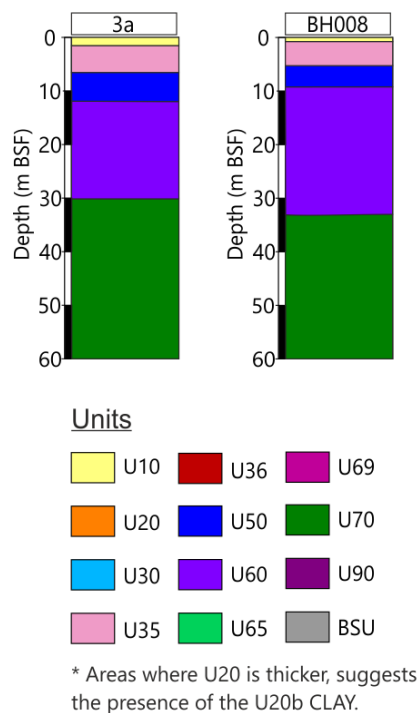
Figure 8.12: BH008 soil profile within Soil Province 3a

8.4.9   Soil Province 3b

Soil unit thicknesses within Soil Province 3b were derived from spatial geological model layers defined within the Soil Province 3b area. These are the mean values of the depth to base of the units and are presented in Table 8.13.

Table 8.13: Average soil unit thicknesses within Soil Province 3b

Spatial Geological Model Unit	Mean Base Unit Depth [m]	Coverage of Province [%]'
U10	1.1	54
U20	3.2	100
U30	7.9	7
U35	8.1	78
U36	13.0	6
U50	13.8	62
U60	30.3	52
U65	28.0	52
U69	36.1	<1
U70	>100	92
U90	70	<1
Notes		
'- Of that soil province, the unit is present in the "coverage %" of the total province area		

Soil province 3b is defined by thin U20 sediments, typically from U20a, with an intermediate package of quaternary sediments before till material. An stratigraphic type example of this is BH018 on the right of Figure 8.13, with the left showing the typical soil profile.
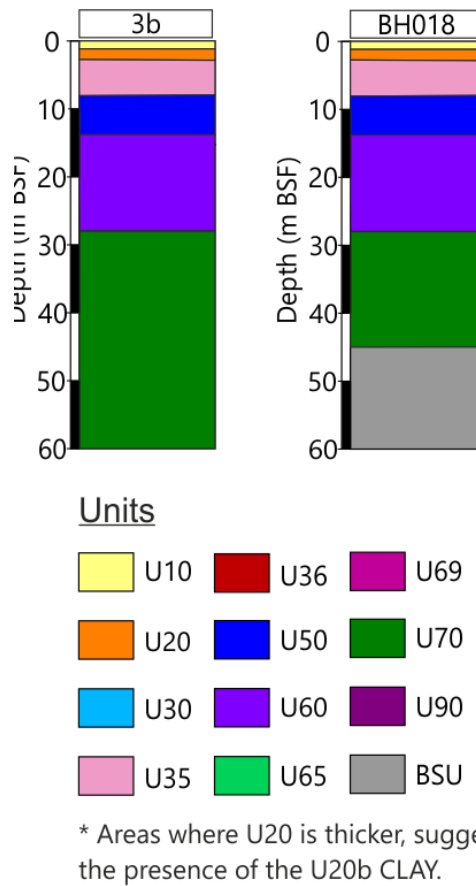
Figure 8.13: BH018 soil profile within Soil Province 3b

8.4.10   Soil Province 3c

Soil unit thicknesses within Soil Province 3c were derived from spatial geological model layers defined within the Soil Province 3c area. These are the mean values of the depth to base of the units and are presented in Table 8.14.

Table 8.14: Average soil unit thicknesses within Soil Province 3c

Spatial Geological Model Unit	Mean Base Unit Depth [m]	Coverage of Province [%]'
U10	1.1	54
U20	8.6	100
U30	10.1	4
U35	13.1	87
U36	19.4*	3
U50	17.3	46
U60	32.6	51
U65	30.9	43
U69	38.3	<1
U70	>100	82

Spatial Geological Model Unit	Mean Base Unit Depth [m]	Coverage of Province [%]'
U90	66.0	4
Notes: * Value more than older units due to average values used and low coverage of soil unit area '- Of that soil province, the unit is present in the "coverage %" of the total province area		

Soil province 3c is defined by thick U20 sediments, the thickness indicating U20b clays might be present and the presence of U65. Figure 8.14 shows the two potential soil profiles in 3c (i) and (ii) due to the equal percentage coverage of U60 and U65 within the unit on the left and on the right a typical example of this Location BH011; however this example has a thinner U20 sediment than typically expected.
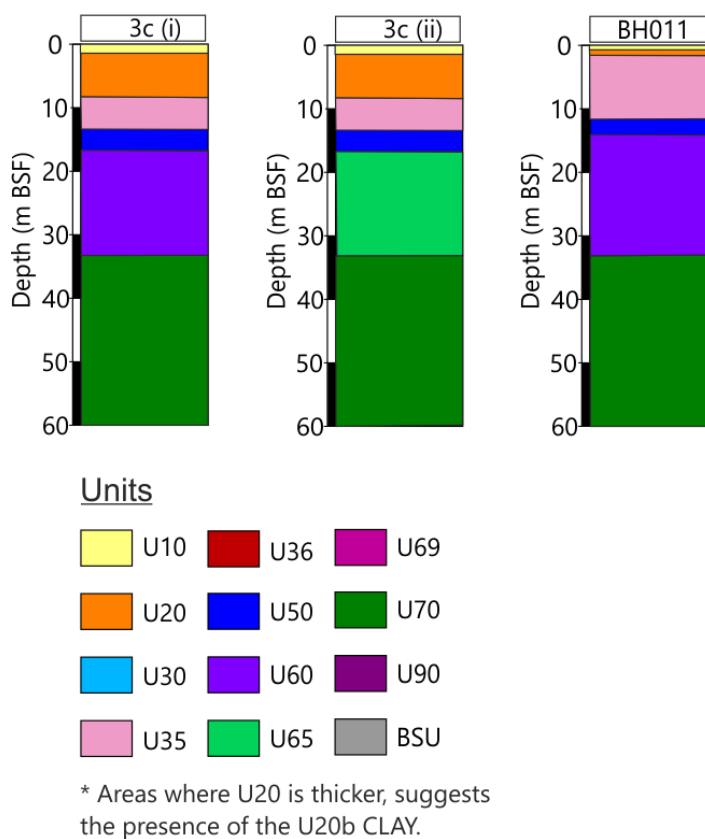
Figure 8.14: BH011 soil profile within Soil Province 3c

8.4.11 Soil Province 3d

Soil unit thicknesses within Soil Province 3d were derived from spatial geological model layers defined within the Soil Province 3d area. These are the mean values of the depth to base of the units and are presented in Table 8.15.

Table 8.15: Average soil unit thicknesses within Soil Province 3d

Spatial Geological Model Unit	Mean Base Unit Depth [m]	Coverage of Province [%]'
U10	1.1	88

Spatial Geological Model Unit	Mean Base Unit Depth [m]	Coverage of Province [%]'
U20	14.4	100
U30	13.5	2
U35	18.3	77
U36	21.8*	5
U50	19.3	9
U60	33.8	16
U65	31.9	40
U69	37.0	<1
U70	>100	81
U90	58.3	12
Notes: * Value more than older units due to average values used and low coverage of soil unit area '- Of that soil province, the unit is present in the "coverage %" of the total province area		

Soil province 3d is characterised by a thick U20, indicating the presence of U20b clays. This soil province is defined by the absence of U60 and a thicker U65 unit with U70 within 50 m BSF, shown in the representative soil profile in Figure 8.15. A closest type example of this soil province is presented in Location CPT330 (Figure 8.15).
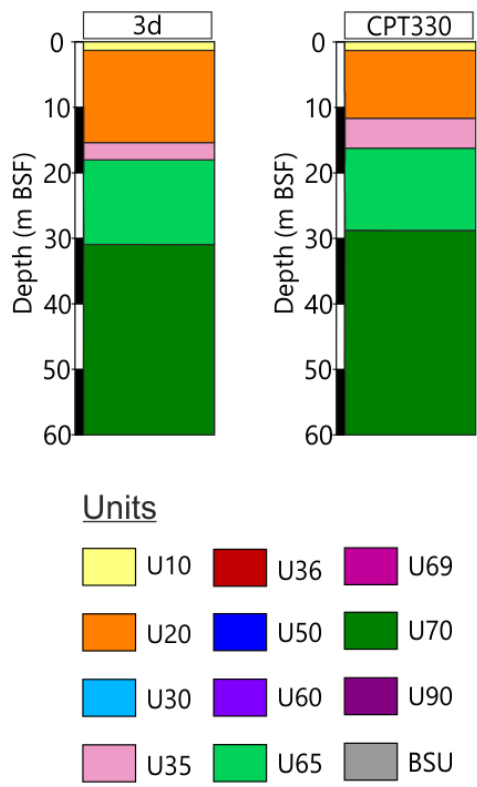
Figure 8.15: CPT330 soil profile within Soil Province 3d

8.4.12 Soil Province 4a

Soil unit thicknesses within Soil Province 4a were derived from spatial geological model layers defined within the Soil Province 4a area. These are the mean values of the depth to base of the units and are presented in Table 8.16.

Table 8.16: Average soil unit thicknesses within Soil Province 4a

Spatial Geological Model Unit	Mean Base Unit Depth [m]	Coverage of Province [%]'
U10	0.9	41
U20	Absent	0
U30	3.9	1
U35	6.7	97
U36	16.9	7
U50	14.7	91
U60	37.9	96
U65	66.7	36
U69	83.1	53
U70	>100	95
U90	80.9	<1
Notes		
'- Of that soil province, the unit is present in the "coverage %" of the total province area		

Soil province 4a is defined by the absence of U20, the presence of U50 and a thick U65 above U65 or U70 within 50 m BSF. A good example of this unit based on percentage coverage of the units is Location BH009 (Figure 8.16); however this particular location does exclude U65 and U70 and include the presence of U65 that typically sits atop of U70. This is shown on the left side of Figure 8.16.
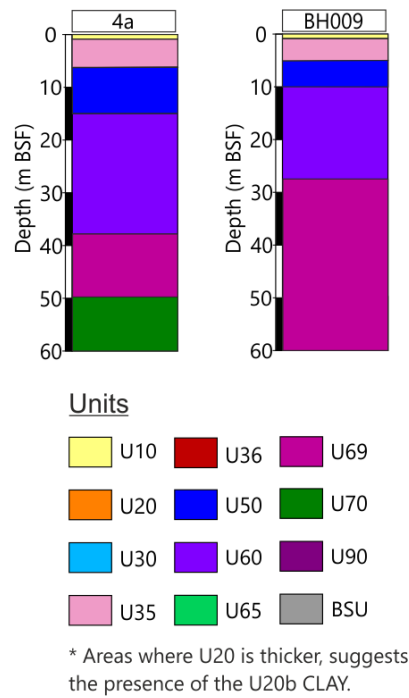
Figure 8.16: BH009 soil profile within Soil Province 4a

8.4.13 Soil Province 4b

Soil unit thicknesses within Soil Province 4b were derived from spatial geological model layers defined within the Soil Province 4b area. These are the mean values of the depth to base of the units and are presented in Table 8.17.

Table 8.17: Average soil unit thicknesses within Soil Province 4b

Spatial Geological Model Unit	Mean Base Unit Depth [m]	Coverage of Province [%]'
U10	1	56
U20	3.8	100
U30	7.3	6
U35	8.6	82
U36	10.2	16
U50	18.1	76
U60	38.9	77
U65	63.9	43
U69	79.9	28
U70	>100	98
U90	78.2	1
Notes '- Of that soil province, the unit is present in the "coverage %" of the total province area		

Soil province 4b is defined by the presence of a thin layer of U20, indicating U20a sands. It is also defined by the presence of a thick layer of U60 above U69 or U70. A typical borehole

FUGRO

within this soil province is Location BH036 (Figure 8.17), with the representative profile shown on the left.
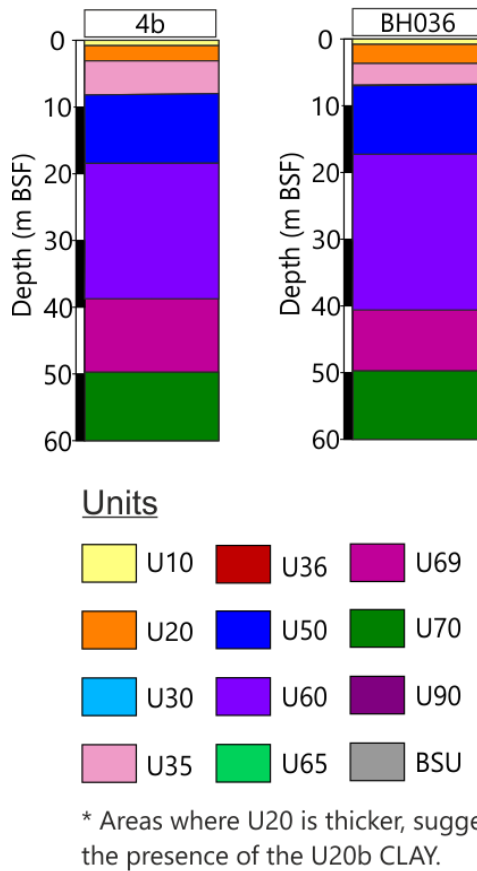
Figure 8.17: BH036 soil profile within Soil Province 4b

8.4.14   Soil Province 4c

Soil unit thicknesses within Soil Province 4c were derived from spatial geological model layers defined within the Soil Province 4c area. These are the mean values of the depth to base of the units and are presented in Table 8.18.

Table 8.18: Average soil unit thicknesses within Soil Province 4c

Spatial Geological Model Unit	Mean Base Unit Depth [m]	Coverage of Province [%]'
U10	1.0	56
U20	8.4	100
U30	8.3	3
U35	12.3	94
U36	17.0	9
U50	20.5	79
U60	42.7	84
U65	73.0	38
U69	98.7	14

Spatial Geological Model Unit	Mean Base Unit Depth [m]	Coverage of Province [%]'
U70	>100	96
U90	77.5	2
Notes: * Value less than younger units due to average values used and low coverage of soil unit area '- Of that soil province, the unit is present in the "coverage %" of the total province area		

Soil province 4c is very similar to province 4b, however it has a thicker U20, indicating the presence of both U20a and U2b likely in channelised areas. Location CPT321 is the only CPT to appear into this soil province, and only penetrates to 23 m with a good representation of this province. Figure 8.18 displays the representative soil profile for this soil province.
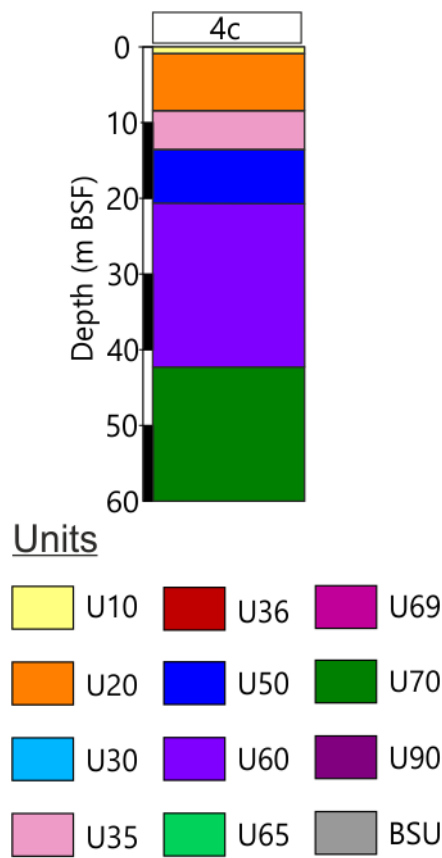
Figure 8.18: Representative soil profile for Zone 4c

8.4.15   Soil province 4d

Soil unit thicknesses within Soil Province 4d were derived from spatial geological model layers defined within the Soil Province 4d area. These are the mean values of the depth to base of the units and are presented in Table 8.19.

Table 8.19: Average soil unit thicknesses within Soil Province 4d

Spatial Geological Model Unit	Mean Base Unit Depth [m]	Coverage of Province [%]'
U10	0.9	73
U20	13.6	100
U30	13.3*	<1
U35	17	85
U36	19	6
U50	22.5	58
U60	44.5	70
U65	77.4	43
U69	79.2	13
U70	>100	98
U90	69.9	1
Notes		
'- Of that soil province, the unit is present in the "coverage %" of the total province area		

Soil province 4d is comparable to both provinces 4b and 4c, however this province has a thicker U20 unit denoting the potential presence of U20b CLAY. This soil province also has a thicker U60 overlying U70 at approximately 50 m BSF. No CPTs penetrate this soil province. Figure 8.19 displays the representative soil profile for this soil province.
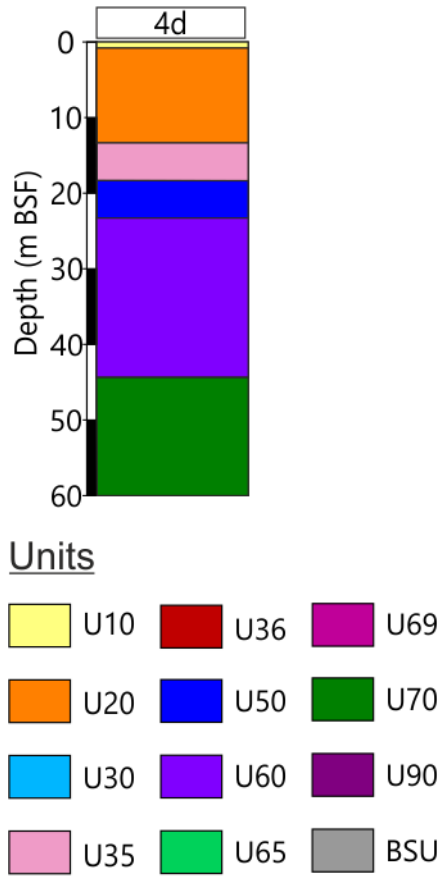
Figure 8.19: Representative soil profile for Zone 4d

9.   Drawings and Digital Deliverables

9.1   Drawings

A series of charts are provided to be reviewed alongside this report. These are summarised in Table 9.1.

Table 9.1: Summary of chart deliverables

Data Type	Chart No.	Chart Name	Description
Map Chart	1	Geotechnical Locations	Locations of geotechnical and seismic data
	2	Top BSU BSF	Depth to top of BSU below seafloor
	3	Base U10 MSL	Depth to base of U10 below sea level
	4	Base U10 BSF	Depth to base of U10 below seafloor
	5	Isochore U10	Thickness of U10
	6	Base U20 MSL	Depth to base of U20 below sea level
	7	Base U20 BSF	Depth to base of U20 below seafloor
	8	Top U20 BSF	Depth to top of U20 below seafloor
	9	Isochore U20	Thickness of U20
	10	Base U30 MSL	Depth to base of U30 below sea level
	11	Base U30 BSF	Depth to base of U30 below seafloor
	12	Top U30 BSF	Depth to top of U30 below seafloor
	13	Isochore U30	Thickness of U30
	14	Base U35 MSL	Depth to base of U35 below sea level
	15	Base U35 BSF	Depth to base of U35 below seafloor
	16	Top U35 BSF	Depth to top of U35 below seafloor
	17	Isochore U35	Thickness of U35
	18	Base U36 MSL	Depth to base of U36 below sea level
	19	Base U36 BSF	Depth to base of U36 below seafloor
	20	Top U36 BSF	Depth to top of U36 below seafloor
	21	Isochore U36	Thickness of U36
	22	Base U50 MSL	Depth to base of U50 below sea level
	23	Base U50 BSF	Depth to base of U50 below seafloor
	24	Top U50 BSF	Depth to top of U50 below seafloor
	25	Isochore U50	Thickness of U50
	26	Base U60 MSL	Depth to base of U60 below sea level
	27	Base U60 BSF	Depth to base of U60 below seafloor
	28	Top U60 BSF	Depth to top of U60 below seafloor
	29	Isochore U60	Thickness of U60
	30	Base U65 MSL	Depth to base of U65 below sea level
	31	Base U65 BSF	Depth to base of U65 below seafloor

Data Type	Chart No.	Chart Name	Description
	32	Top U65 BSF	Depth to top of U65 below seafloor
	33	Isochore U65	Thickness of U65
	34	Base U69 MSL	Depth to base of U69 below sea level
	35	Base U69 BSF	Depth to base of U69 below seafloor
	36	Top U69 BSF	Depth to top of U69 below seafloor
	37	Isochore U69	Thickness of U69
	38	Base U70 MSL	Depth to base of U70 below sea level
	39	Base U70 BSF	Depth to base of U70 below seafloor
	40	Top U70 BSF	Depth to top of U70 below seafloor
	41	Isochore U70	Thickness of U70
	42	Base U90 MSL	Depth to base of U90 below sea level
	43	Base U90 BSF	Depth to base of U90 below seafloor
	44	Top U90 BSF	Depth to top of U90 below seafloor
	45	Isochore U90	Thickness of U90
	46	Shallow Gas	Mapped areas of shallow gas
	47	Soil Provinces	Soil province mapping
Profile Chart	48	Seismic Profile EAAG218P1	Cross section of geology
	49	Seismic Profile EAAS263P1	
	50	Seismic Profile EAAY310P1	
	51	Seismic Profile EAXA381P1	
	52	Seismic Profile EAXB390P1	
	53	Seismic Profile EAXC399P1	
	54	Seismic Profile EAXD408P1	
	55	Seismic Profile EAXD420P1	
Integration Chart	56 - 136	BH Integration Sheets	Comparison on integration at each BH location

9.2 Digital Deliverables

The final deliverables were structured as per Table 9.2.

FUGRO

Table 9.2: Summary of digital deliverables

Data Type	Type	Description	Resolution	Format
Grids	Grids (Base)	MSL	5 m	ASCII XYZ + Geotiff
	Grids (Top +Base)	BSF	5 m	ASCII XYZ + Geotiff
	Grids	Isochore	5 m	ASCII XYZ + Geotiff
Kingdom Workspace	Kingdom project	SBP + 2D UHRS		Time (both) + depth (both)
GIS Deliverable	Shallow Gas			GeoTIF/ ASCII XYZ
	Geotechnical Zonation			Shapefile/GeoTIF
	Geotechnical Points			Shapefile

FUGRO

10. References

Arfai, J., Franke, D., Lutz, R., Reinhardt, L, Kley, J. & Gaedicke, C. (2018). Rapid Quaternary subsidence in the northwestern German North Sea. *Scientific Reports 8*, 11524. https://doi.org/10.1038/s41598-018-29638-6

Batchelor, C., Margold, M., Krapp, M., Murton, D., Dalton, A., Gibbard, P., Stokes, C., Murton, J. & Manica, A. (2019). The configuration of Northern Hemisphere ice sheets through the Quaternary. *Nature Communications 10*, 3713. https://doi.org/10.1038/s41467-019-11601-2

Cartelle, V., Barlow, N.L.M., Hodgson, D.M., Busschers, F.S., Cohen, K.M., Meijninger, B.M.L., and van Kesteren, W.P. (2021). Sedimentary architecture and landforms of the late Saalian (MIS 6) ice sheet margin offshore of the Netherlands. *Earth Surface Dynamics, 9*, 1399-1421. https://doi.org/10.5194/esurf-9-1399-2021

Cohen, K., Gibbard, P. & Weerts, H.J.T. (2014). North Sea palaeogeographical reconstructions for the last 1 Ma. *Geologie en Mijnbouw. 93.* 7-29. https://doi.org/10.1017/njg.2014.12

Cohen, K., Cartelle, V., Barnett, R., Busschers, F. & Barlow, N. (2022). Last Interglacial sea-level data points from Northwest Europe. *Earth System Science Data, 14.* https://doi.org/10.5194/essd-14-2895-2022

COWI. (2021). *Thor Offshore Wind Farm – Integrated Geological Model* (Document No. A205839 004, issue 2, dated 1 March 2021 to Energinet Eltransmission A/S). COWI A/S.

DNV.GL. 2017. Recommended practice. Statistical representation of soil data (Document No. DNVGL-RP-C207)

European Marine Observation and Data Network [EMODnet]. (2023, 15 June). *Sea-floor Geology.* https://emodnet.ec.europa.eu/geonetwork/srv/eng/catalog.search#/metadata/429ef6798d56 18780f9e66ff2ba8e237c852f8d6

Friborg, R. (1996). The landscape below the Tinglev outwash plain: a reconstruction. *Dansk Geologisk Forening 43*(1), 34-40. https://doi.org/10.37570/bgsd-1996-43-04

Fugro (2023a). *Operations Report – MV Arctic.* Report n° F217715-OPS-001/02

Fugro (2023b). *Operations Report – Fugro Pioneer.* Report n° F217715-OPS-002/02

Fugro (2023c). *Baseline Survey Results Report.* Report n° F217715-REP-001/02

Fugro (2024) *Report no 2, 2D UHRS Survey Geomodel Integrated with CPT Data, Full Site.* Report n° F217715-REP-002/03

Fugro (2024b). *Investigation Results, Geotechnics. Seafloor ad In Situ Test Locations, Subarea 1.* Report n° F217703/01 03 Subarea 1 results report

Fugro (2024c). *Investigation Results, Geotechnics. Seafloor ad In Situ Test Locations, Subarea 2.* Report n° F217703/02 03 Subarea 1 results report

Fugro (2024d). *Preliminary Geotechnical Investigations for Danish Offshore Wind Farm 2030 Lot 2 | Danish Sector, North Sea – Records of Operations – Excalibur.* Report n° F217703-04/02

Fugro (2024e). *Preliminary Geotechnical Investigations for Danish Offshore Wind Farm 2030 Lot 2 | Danish Sector, North Sea – Records of Operations – Gargarno.* Report n° F217703-03/02

Fugro (2024f). *Preliminary Geotechnical Investigations for Danish Offshore Wind Farm 2030 Lot 2 | Danish Sector, North Sea – Records of Operations – Voyager.* Report n° F217703-02/02

Fugro (2024g). *Danish Offshore Wind 2030 – North Sea 1 – Subarea , Investigation Results, Geotechnical Borehole Locations.* Report n° F217703/04-03

Gibbard, P.L. & Lewin, J. (2016). Filling the North Sea Basin: Cenozoic sediment sources and river styles. *Geologica Belgica, 19*(3-4), 201-217. http://dx.doi.org/10.20341/gb.2015.017

Gibbard, P.L. & Cohen, K.M. (2015). Quaternary evolution of the North Sea and the English Channel. *Proceedings of the Open University Geological Society 2*, 63-74. http://ougs.org/branch_matters/index.php?branchcode=ouc

Gibson, S.M., Bateman, M.D., Murton, J.B., Barrows, T.T., Fifield, L.K., & Gibbard, P.L. (2022). Timing and dynamics of Late Wolstonian Substage 'Moreton Stadial' (MIS 6) glaciation in the English West Midlands, UK. *Royal Society Open Science*, 9. https://doi.org/10.1098/rsos.220312

Harrison, S., Smith, D. E. & Glasser, N. F. (2018). Late Quaternary meltwater pulses and sea level change. (2018). *Journal of Quaternary Science 34(1)*, 1-15. https://doi.org/10.1002/jqs.3070

Houmark-Nielsen, M. (2011). Pleistocene Glaciations in Denmark: A Closer Look at Chronology, Ice Dynamics and Landforms. In Ehlers, J., Gibbard, P.L., & Hughues, P.D. (Eds.), *Quaternary Glaciations – Extent and Chronology* (pp. 47-58). Elsevier, Amsterdam and Oxford. https://doi.org/10.1016/B978-0-444-53447-7.00005-2

Høyer A.-S., Jørgensen, F., Piotrowski, J.A. & Jakobsen, P.R. (2013). Deeply rooted glaciotectonism in western Denmark: geological composition, structural characteristics and the origin of Varde hill-island. *Journal of Quaternary Science, 28*(7), 683-696. https://doi.org/10.1002/jqs.2667

Hughes, A., Gyllencreutz, R., Lohne. Ø., Mangerud, J. & Svendsen, J. (2015). The last Eurasian ice sheets – a chronological database and time-slice reconstruction, DATED-1. *Boreas(45),* 1–45. https://doi.org/10.1111/bor.12142

Hughes, P., Gibbard, P.L., Ehlers, J. (2020). The "missing glaciations" of the Middle Pleistocene. Quaternary Research, *96*, 161-183. https://doi.org/10.1017/qua.2019.76

Huuse, M., and Lykke-Andersen, H. (2000a). Large-scale glaciotectonic thrust structures in the eastern Danish North Sea. In Maltman, A.J., Hubbard, B., and Hambrey, M.J. (Eds.), *Deformation of Glacial Material* (pp. 293-305). Geological Society, London, Special Publications, 176.

Huuse, M., and Lykke-Andersen, H. (2000b). Overdeepened Quaternary valleys in the eastern Danish North Sea: morphology and origin. *Quaternary Science Reviews, 19*, 1233-1253. https://doi.org/10.1016/S0277-3791(99)00103-1

Jensen, J.B., Gravesen, P., and Lomholt, S. (2008). Geology of outer Horns Rev, Danish North Sea. *Geological Survey of Denmark and Greenland Bulletin, 15*, 41-44. https://doi.org/10.34194/geusb.v15.5040

Kirkham, J.D., Hogan, K.A., Larter, R.D., Self, E., Games, K., Huuse, M., Stewart, M.A., Ottesen, D., Arnold, N.S., and Dowdeswell, J.A. (2021). Tunnel valley infill and genesis revealed by high-resolution 3-D seismic data. *Geology, 49*(12), 1516-1520. https://doi.org/10.1130/G49048.1E

Knox, R.W.O.B., Bosch, J.H.A., Rasmussen, E.S., Heilmann-Clausen, C., Hiss, M., De Lugt, I.R., Kasińksi, J., King, C., Köthe, A., Słodkowska, B., Standke, G., & Vandenberghe, N. (2010). Cenozoic. In: Doornenbal, J.C., and Stevenson, A.G. (Eds.), *Petroleum Geological Atlas of the Southern Permian Basin Area* (pp. 211-223). EAGE Publications.

Konradi, P.,Larsen, B. & Sørensen, A. (2005). Marine Eemian in the Danish eastern North Sea. Quaternary International 133–134(1), 21-31. https://doi.org/10.1016/j.quaint.2004.10.003

Lang, J., Lauer, T. & Winsemann, J. (2018). New age constraints for the Saalian glaciation in northern central Europe: Implications for the extent of ice sheets and related proglacial lake systems. *Quaternary Science Reviews, 180.*,240-259. https://doi.org/10.1016/j.quascirev.2017.11.029

Lang, J., Ahlo, P., Kasvi, E., Goseberg, N. & Winsemann, J. (2019). Impact of Middle Pleistocene (Saalian) glacial lake-outburst floods on the meltwater-drainage pathways in northern central Europe: Insights from 2D numerical flood simulation. *Quaternary Science Reviews. 209*. 82-99. https://doi.org/10.1016/j.quascirev.2019.02.018

Larsen, G., Frederiksen, J., Villumsen, A., Fredericia, J., Gravesen, P., Foged, N., Knudsen, B., & Baumann, J. (1995). *A guide to engineering geological soil description*. Revision 1, Dansk Geoteknisk Forening, Aalborg Universitets trykkeri.

Larsen, B., & Andersen, L.T. (2005). Late Quaternary stratigraphy and morphogenesis in the Danish eastern North Sea and its relation to onshore geology. *Netherlands Journal of Geosciences, 84(2)*, 113-128. https://doi.org/10.1017/S0016774600023003

Möller, P., Alexandreson, H., Anjar, J. & Björck, Svante. (2020). MIS 3 sediment stratigraphy in southern Sweden sheds new light on the complex glacial history and dynamics across southern Scandinavia. *Boreas*, 389-416, https://doi.org/10.1111/bor.12433

FUGRO

Nielsen, T., Mathiesen, A., & Bryde-Auken, M. (2008). Base Quaternary in the Danish parts of the North Sea and Skagerrak. *GEUS Bulletin, 15*, 37–40. https://doi.org/10.34194/geusb.v15.5038

Overeem, I., Weltje, G.J., Bishop-Kay, C., & Kroonenberg, S.B. (2001). The Late Cenozoic Eridanos delta system in the Southern North Sea Basin: a climate signal in sediment supply? *Basin Research, 13*, 293-312. https://doi.org/10.1046/j.1365-2117.2001.00151.x

Tóth, Z., Spiess, V., Mogollón, J.M. & Jensen, J.B. (2014). Estimating the free gas content in Baltic Sea sediments using compressional wave velocity from marine seismic data. *Journal of Geophysical Research: Solid Earth, 119*. 8577-8593. https://doi:10.1002/2014JB010989

Walker, J., Gaffney, V., Fitch, S.,Muru, M., Fraser, A., Bates, M. & Bates, C. (2020). A great wave: the Storegga tsunami and the end of Doggerland?. *Antiquity, 94*(378), 1409-1425. https://doi.org/10.15184/aqy.2020.49

Winsemann, J., Koopmann, H., Tanner, D.C., Lutz, R., Lang, J., Brandes, C., and Gaedicke, C. (2020). Seismic interpretation and structural restoration of the Heligoland glaciotectonic thrust-fault complex: Implications for multiple deformation during (pre-)Elsterian to Warthian ice advances into the southern North Sea Basin. *Quaternary Science Reviews, 227*. https://doi.org/10.1016/j.quascirev.2019.106068

Wohlfarth B. (2013). A review of Early Weichselian climate (MIS 5d-a) in Europe, *Technical report/Svensk kärnbränslehantering AB, 44*(50). https://archimer.ifremer.fr/doc/00499/61046/

Appendix A

Guidelines for Use of Report

FUGRO

This report (the "Report") was prepared as part of the services (the "Services") provided by Fugro for its client (the "Client") and in accordance with the terms of the relevant contract between the two parties (the Contract") and to the extent to which Fugro relied on Client or third-party information as was set out in the Contract.

Fugro's obligations and liabilities to the Client or any other party in respect of this Report are limited to the extent and for the time period set out in the Contract (or in the absence of any express provision in the Contract as implied by the law of the Contract) and Fugro provides no other representation or warranty whether express or implied, in relation to the use of this Report, for any purpose. Furthermore, Fugro has no obligation to update or revise this Report based on any future changes in conditions or information which emerge following issue of this Report unless expressly required by the provisions of the Contract.

This Report was formed and released by Fugro exclusively for the Client and any other party expressly identified in the Contract, and any use and/or reliance on the Report or the Services for purposes not expressly stated in the Contract, will be at the Client's sole risk. Any other party seeking to rely on this Report does so wholly at its own and sole risk and Fugro accepts no liability whatsoever for any such use and/or reliance.

Appendix B

CPT methodology and
classification parameters

Use of Geodata and Advice

Introduction

This document provides important information regarding the use of Fugro geodata, analyses and advice.

Site-specific acquisition of geodata can include metocean monitoring, geophysical seafloor mapping, subsurface mapping, logging of boreholes, in situ testing, laboratory testing of samples and monitoring of structures or elements of structures.

The cost of geodata acquisition, interpretation and monitoring is a small portion of the total cost of a development such as a construction project. By contrast, the costs of correcting a wrongly designed programme or mobilising alternative construction methods are often far greater than the cost of the original investigation for a site or structure.

Attention and adherence to the information presented in this document can reduce delays and cost overruns related to site-specific factors.

The focus of this document is on construction projects. This document also applies to information and advice related to asset integrity and decommissioning.

Requirements for Quality Geodata

Project quality management should follow quality principles for project management (e.g. ISO 9001:2015) and for general principles on reliability for structures (e.g. ISO 2394:2015). Project activities usually comprise part of specific phases of a construction project. The quality plan for the entire construction project should incorporate geodata input in every phase - from the feasibility planning stages to project completion. The parties involved should do the following.

- Provide complete and accurate information necessary to plan an appropriate site investigation.

- Describe the purpose(s), type(s) and construction methods of planned structures in detail.
- Provide the time, financial, personnel and other resources necessary for the planning, execution and follow-up of a site investigation programme.
- Understand the limitations and degree of accuracy inherent in geodata.
- Understand the limitations and degree of accuracy inherent in the advice based upon site investigation data.
- During all design and construction activities, be aware of the limitations of site investigation data and analyses/ advice, and use appropriate preventative measures.
- Incorporate all geodata input in the design, planning, construction and other activities involving the site and structures. Provide the entire (set of) document(s), including digital files where applicable, to parties involved in site selection, design and construction.
- Use the site investigation data and advice for only the structures, site and activities which were described to Fugro prior to and for the purpose of planning the site investigation or the programme of analysis and advice.

Authority, Time and Resources Necessary for Site Investigations

Adequate designation of authority and accountability for site-specific aspects of construction projects is necessary. This way, an appropriate investigation can be performed, and the use of the results by project design and construction professionals can be optimised.

Figure 1 illustrates the importance of the initial project phases for gathering adequate geodata for a project. The initial phases, when site investigation requirements are defined and resources are allocated, are represented by more than 50 % of the Quality Triangle (Figure 1). Decisions and actions made during these phases have a large impact of the outcome and thus the potential of the investigation to meet project requirements.
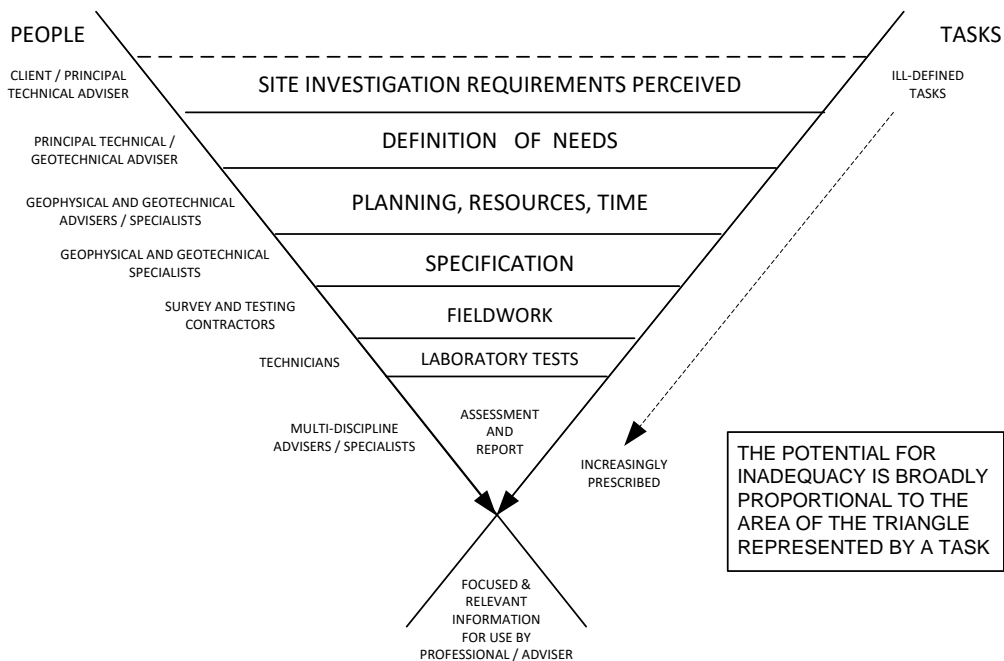
Figure 1: Quality of Site Investigation (adapted from SISG[1]).

---

[1]   Site Investigation Steering Group SISG (1993). *Site investigation in construction 2: planning, procurement and quality management*. Thomas Telford.

Data Acquisition and Monitoring Programmes

Site-specific investigations, such as geophysical and geotechnical investigations, are operations of discovery. Investigation should proceed in logical stages. Planning should allow operational adjustments deemed necessary by newly available information. This observational approach permits the development of a sound engineering strategy and reduces the risk of discovering unexpected (geo)hazards during or after construction.

Data Types and Limitations

1. Reliability of Supplied Information

Analysis and advice can involve the use of information and physical material that is publicly available or supplied by the client. Examples are geodetic data, geological maps, geophysical records, earthquake data, earlier geotechnical logs and soil samples. Fugro endeavours to identify potential anomalies but does not independently verify the accuracy or completeness of public or client-supplied information unless indicated otherwise. This information, therefore, can limit the accuracy of the geodata, analyses and advice.

2. Complexity of Ground Conditions

There are hazards associated with the ground. An adequate understanding of these hazards can help to minimize risks to a project and the site. The ground is a vital element of all structures which rest on or in the ground. Information about ground behaviour is necessary to achieve a safe and economical structure. Often less is known about the ground than for any other element of a structure.

3. Site Investigation - Spatial Coverage

Geophysical investigations typically provide information about ground conditions along survey track lines. Geotechnical investigations collect data at specific test locations. Interpretation of ground conditions away from survey track lines and test locations is a matter of extrapolation and judgement based on geological and geotechnical knowledge, as well as on experience. Nevertheless, actual conditions in untested areas may differ from predictions. For example, the interface between ground materials may be far more gradual or abrupt than indicated by the geodata. It is not realistic to expect a site investigation to reveal or anticipate every detail of ground conditions. Nevertheless, an investigation can reduce the residual risk associated with unforeseen conditions to a tolerable level. If ground problems do arise, it is important to have relevant expertise available to help reduce and mitigate safety and financial risks.

4. Role of Judgement and Opinion In Analysis and Advice

Analysis and advice that involve geodata are less exact than most other design disciplines. Extensive judgement and opinion are often required. Therefore, geodata, analyses and advice may contain definitive statements that identify where the responsibility of Fugro begins and ends. These are not exculpatory clauses designed to transfer liabilities to another party, but they are statements that can help all parties involved to recognise their individual responsibilities and take appropriate actions.

Complete Information should be Available to all Parties Involved

To prevent costly construction problems, construction contractors should have access to the best available information. They should have access to the complete original (set of) documents including digital files where applicable, to prevent or minimize any misinterpretation of site conditions and advice. To prevent errors or omissions that could lead to misinterpretation, geophysical sections, geotechnical logs and illustrations should not be redrawn or reprocessed, and users of geodata and advice should confer with the authors when applying the geodata and/or advice. A cloud-hosted, web-based geodata engagement platform can facilitate information access throughout the life cycle of an asset.

Information is Project-Specific

Fugro's investigative programmes, analyses and advice are designed and conducted specifically for the client described project and conditions. Thus the geodata, analyses and advice present information for a unique construction project. Project-specific factors for a structure include but are not limited to:

- Location;
- Size and configuration of structure;
- Type and purpose or use of structure;
- Other facilities or structures in the area.

Any factor that changes subsequent to the preparation of the geodata, analyses and advice may affect its applicability. A specialised review of the impact of changes would be necessary. Fugro is not responsible for conditions which develop after change of any factor in site investigation programming, development or structure.

For purposes or parties other than the original project or client, the geodata, analyses and advice may not be adequate and should not be used.

Changes in Site Conditions Affect the Accuracy/Suitability of the Data

Ground is complex and can be changed by natural phenomena such as earthquakes, floods, seabed scour and groundwater fluctuations. Construction operations at or near the site can also change ground conditions. The geodata, analyses and advice consider conditions at the time of investigation. Construction decisions should consider any changes in site conditions, regulatory provisions, technology or economic conditions subsequent to the investigation. Geodata, analyses and advice can become inaccurate or unreliable upon any passage of time, and a specialist should be consulted regarding the adequacy of the geodata, analyses and advice for use.

Cone Penetration Test

Introduction

The cone penetration test (CPT) involves the measurement of the resistance of ground to steady and continuous penetration of a cone penetrometer equipped with internal sensors. The measurements comprise penetration depth, cone resistance, sleeve friction and, optionally, pore pressure and inclination from vertical. These measurements permit interpretation of ground conditions.

CPT apparatus and procedures adopted by Fugro are in general accordance ISSMGE (1999), ASTM D5778-20, ISO 22476-1:2022, and ISO 19901-8:2014. General agreement also applies to Eurocode 7 (CEN, 2007).

Fugro offers CPT systems operated from (1) ground surface and seafloor (non-drilling deployment mode) and (2) downhole in a borehole (drilling deployment mode).

CPT Apparatus

General

CPT apparatus includes various parts as described below:

- Thrust machine: apparatus providing thrust to the push rods so that the recommended rate of penetration (20 mm/s) is controlled;
- Reaction equipment: reaction for the thrust machine;
- Push rod: thick-walled cylindrical tube used for advancing the penetrometer to the required test depth. Push rods may also consist of drill pipe;
- Friction-cone penetrometer (CPT): cylindrical terminal body mounted on the lower end of the push rods, including a cone, a friction sleeve and internal sensing devices for the measurement of cone resistance, sleeve friction and, optionally, inclination;
- Piezocone penetrometer (CPTU or PCPT): cylindrical terminal body mounted on the lower end of the push rods, including a cone, a friction sleeve, a filter and internal sensing devices for the measurement of cone resistance, sleeve friction, pressure and, optionally, inclination and temperature;
- Measuring system: apparatus and software, including sensors, data transmission apparatus, recording apparatus and data processing apparatus.

Deployment from Ground Surface or Seafloor

Specific additional apparatus for CPT deployment from ground surface and seafloor (non-drilling deployment) can include:

- Push rod casing: guide for the part of the push rods protruding above the soil, and for the push rod length exposed in water or soil, to prevent buckling when the required penetration pressure increases beyond the safe limit for the exposed upstanding length of push rods;
- Friction reducer to reduce soil friction acting on the push rods: (1) ring or special projections fixed on the outside of the push rods, with an outside diameter larger than the base of the cone and/or (2) injection of low-friction fluid from the push rod at a fixed distance above the cone penetrometer.

Downhole Borehole Deployment

Downhole CPT systems latch into a bottom hole assembly at the lower end of a drill pipe. System options are:

1. Operation of a downhole thrust machine by applying mud pressure in the borehole;
2. Remote control of a downhole thrust machine by hydraulic pressure transmitted through an umbilical cable connected to a surface-based pump unit, together with;
3. Application of thrust to drill rods where CPT apparatus and a short push rod are latched in the bottom hole assembly; the thrust machine is at ground surface or seafloor.

Downhole CPTs require drilling apparatus for advancing the borehole. The maximum CPT stroke is generally 1.5 m or 3 m.

Data recording can be surface-based and/or downhole.

Cone Penetrometer

Typical features of Fugro penetrometers (Figure 1) include:

- Cone base areas of 500 mm^2, 1000 mm^2 or 1500 mm^2;
- Cone and friction sleeve sensors placed in series, i.e. subtraction-type penetrometers;
- Pore pressure measurements either at the face of the cone (u_1 location) or at the cylindrical extension of the cone (u_2 location). Multiple-sensor penetrometers (u_1, u_2 and u_3 locations) are also available. The u_3 location is immediately above the friction sleeve;
- Inclinometer;
- Temperature sensor, e.g. for cone penetrometer class 0 specified in ISO 22476-1:2022;
- Storage of signals from the penetrometer in digital form for subsequent computer-based processing and presentation.

Apparatus for Additional Measurements

Add-on apparatus (and procedures) can apply to specific additional measurements, refer to section 'Additional Measurements' below.

Procedure

General

Figure 2 summarises the test procedure. The procedure includes several stages. The stage of Additional Measurements is optional.
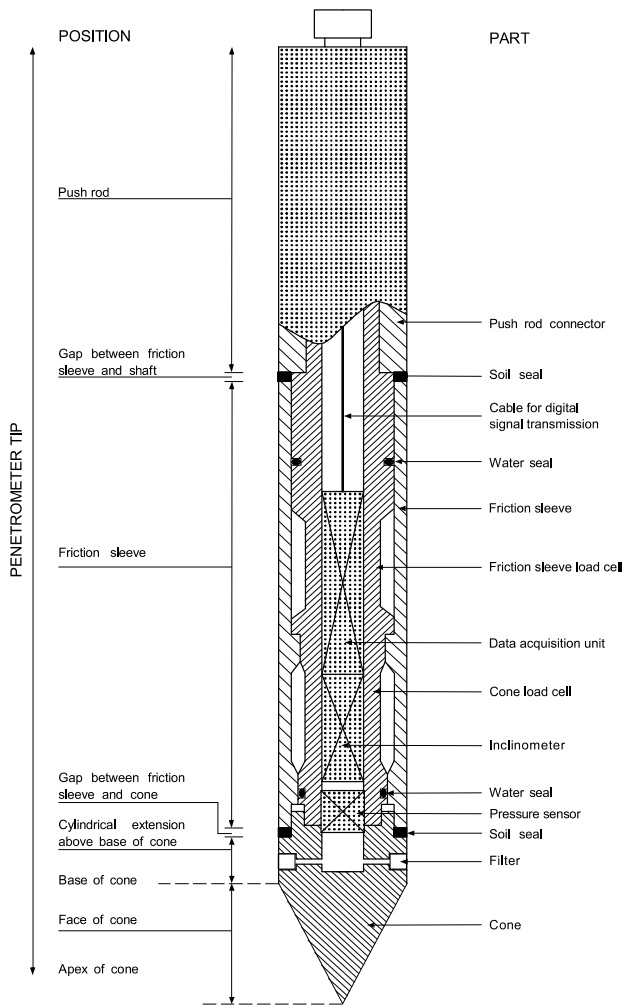
Figure 1: Piezocone penetrometer

Figure 2: Flow chart

Set-up Stage and Termination Stage

The set-up stage is at discretion of the equipment operator, particularly considering suitability of expected ground type(s), accessibility, risk of damage to equipment and safety of persons.

Set-up requires a reasonably flat, accessible, ground surface with a slope of 5° or less. Most onshore thrust machines have levelling facilities allowing a vertical start of penetration. Seabed frames used for offshore CPT activities have no levelling facilities, i.e. start of penetration may not be vertical.

For over-water (marine/ offshore activities), additional accessibility considerations include:

- Minimum water depth for the selected pontoon, jack-up or vessel and the selected test equipment;
- Maximum water depth for the selected pontoon, jack-up or vessel;
- Maximum depth below water (sea) level of selected test equipment;
- Metocean conditions, particularly wind, waves, currents.

The set-up stage typically includes selection of equipment and procedures according to a required type of cone penetrometer, application class, cone penetrometer class, test category and data processing/ submission.
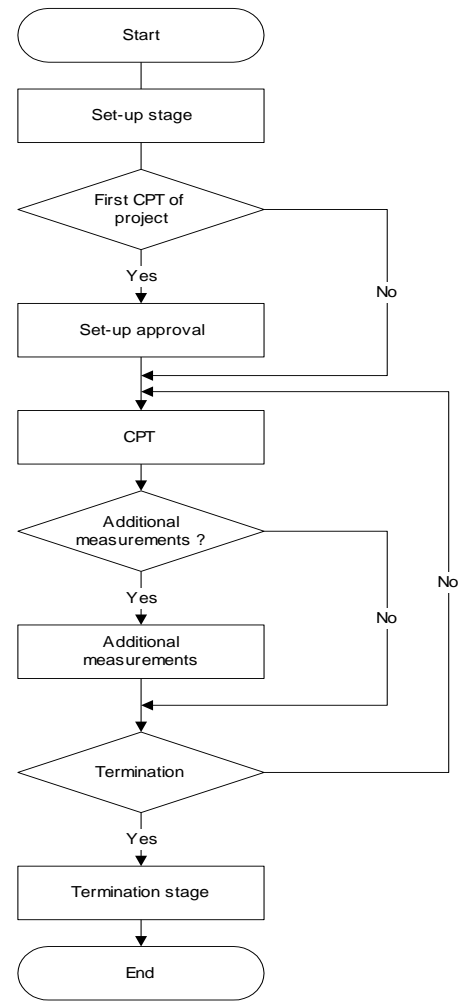
The set-up stage or the termination stage includes the location survey, i.e. the determination of the coordinates and the ground surface elevation (or the water depth).

The set-up stage and the termination stage for a downhole CPT include lowering of the CPT apparatus into the borehole and lifting respectively. Most projects require multiple downhole tests in a single borehole.

For piezocone testing, the set-up stage also includes the following steps:

- Office-based or site-based: de-airing of the filter in glycerine by application of 24-hour vacuum and storage in a glycerine-filled container;
- On-site: glycerine filling of hollow space in the cone penetrometer and subsequent mounting of the filter;
- On-site: application of a flexible membrane around the filter to prevent loss of saturating fluid prior to the start of a test.

Land-based tests may include specific measures to help retention of filter saturation during penetration of partially saturated zones. Relaxation of requirements typically applies to offshore tests where water pressures will force entrapped air into solution.

Criteria for test termination are as follows, unless specifically agreed otherwise:

- As instructed by client;
- Reaching target penetration;
- Reaching maximum capacity of the thrust machine, reaction equipment, push rods and/or measuring sensors;

- Sudden increase in penetrometer inclination;
- Risk of damage to apparatus or safety of persons, at discretion of equipment operator or as determined by software algorithms;

whichever occurs first and as applicable. Note that ASTM and ISO standards provide no specific requirements for maximum penetrometer inclination from vertical. A value of 15° is commonly considered.

Application Classes – ISO 19901-8:2014

Table 1 summarises application classes specified in ISO 19901-8:2014 for offshore and nearshore CPTs. The allowable minimum accuracy of a measured parameter is the larger value of the two quoted. A percentage value applies to the measured value and not to the measuring range.

Table 1: Application classes (ISO 19901-8:2014)

Application Class	Parameter	Allowable Minimum Accuracy
1	Cone resistance	35 kPa or 5 %
	Sleeve friction	5 kPa or 10 %
	Pore pressure	25 kPa or 5 %
2	Cone resistance	100 kPa or 5 %
	Sleeve friction	15 kPa or 15 %
	Pore pressure	50 kPa or 5 %
3	Cone Resistance	200 kPa or 5 %
	Sleeve friction	25 kPa or 15 %
	Pore pressure	100 kPa or 5 %

The concept of application classes considers intended soil conditions for selection of an application class. For example, Application Class 1 of ISO 19901-8:2014 can be selected for 'very soft to soft soil deposits', which is approximately equivalent to $q_c < 0.5$ to $q_c < 1$ MPa. In other words, Application Class 1 should not apply to 'mixed bedded soil profiles with weak to strong layers'.

The accuracy values apply to seafloor as reference. They are uncoupled from uncertainty of spatial position below ground surface or seafloor.

Historically, the concept of application classes was based on an international reference test procedure (ISSMGE, 1999), which specifies 'performance' criteria for cone penetration test measurements. The test results should meet the requirements of one of the application classes.

The following comments apply:

- Accuracy is the 'closeness of a measurement to the true value of the quantity being measured'. It is the accuracy as a whole that is ultimately important not the individual parts. Precision is the 'closeness of each set of measurements to each other'. The resolution of a measuring system is the 'minimum size of the change in the value of a quantity that it can detect'. It will influence the accuracy and precision of a measurement.
- Application Class 3 typically represents industry practice. They are approximately equivalent to the more implicit requirements of ASTM International. Class 3 applies, unless specifically agreed otherwise.

Differences in interpretation about compliance with the ISO box values for accuracy became apparent after publication of a predecessor of ISO 22476-1:2022 and, subsequently, publication of ISO 19901-8:2014. Unfortunately, the interpretational challenges emerged from contractual disputes, unnecessary re-work and CPT results assigned higher confidence than actual (e.g. Peuchen and Parasie, 2019).

The zero drift of a measured parameter can be compared with the allowable minimum accuracy according to the selected application class, per test. This comparison considers the maximum range of values of q_c, f_s and, where applicable, u_1 or u_2 for calculation of the percentage box values (Table 1: Application classes (ISO 19901-8:2014)). Zero drift of a measured parameter is an approximate performance indicator for the measuring system (Peuchen and Terwindt, 2014). Zero drift is the absolute difference of the zero readings, reference readings or zero reference reading of a measuring system between the start and completion of the cone penetration test. The reference readings can be taken at (1) atmospheric pressure at ground surface or above water level or (2) under hydrostatic water pressure close to seafloor.

Cone Penetrometer Classes and Test Categories – ISO 19901-8:2023

ISO 19901-8:2023 includes cone penetrometer classes and test categories that are similar to those of ISO 22476-1:2022. Fugro's implementation of ISO 19901-8:2023 is in progress (*for future update of this document*).

Cone Penetrometer Classes and Test Categories – ISO 22476-1:2022

The applicability of ISO 22476-1:2022 is onshore and nearshore. The standard allows selection of cone penetrometer classes and test categories, i.e. method-based criteria. Compliance with a particular cone penetrometer class and test category then provides some indication for uncertainty of CPT results.

Cone penetrometer classes rely on results of detailed laboratory calibration and verification of cone penetrometers. The results determine compliance of a cone penetrometer with one of four cone penetrometer classes (Table 2). A cone penetrometer can conform to more than one cone penetrometer class, for the case of multiple intervals for calibration.

Input criteria for the cone penetrometer classes include:

- Minimum measurands per cone penetrometer class (Table 2);
- Laboratory cone resistance and sleeve friction: (1) selected uncertainty components for axial force, (2) resolution and output stability, (3) verification values of ambient temperature stability, transient temperature stability and bending influence;
- Laboratory pore pressure: (1) selected uncertainty components for water (or gas) pressure, (2) resolution and output stability, (3) verification values of ambient temperature stability, transient temperature stability and bending influence;
- Inclination: expanded measurement uncertainty for inclination values determined in a calibration laboratory.

Table 2: Required measurands per cone penetrometer class (ISO 22476-1:2022)

Cone Penetrometer Class	q_c	f_s	u_2	T
0	√	√	√	√
1	√	√	√	
2	√	√		
3	√	√		
Notes				
q_c = cone resistance		u_2 = pore pressure (and/or u_1)		
f_s = sleeve friction		T = temperature		

FUGRO

Test categories consider requirements for (1) cone penetrometer class and (2) reference readings and output stability of a cone penetrometer recorded just before the cone penetrometer penetrates the ground and just after the cone penetrometer leaves the ground (Table 3). The requirements for pore pressure u_2 (or u_1) apply according to cone penetrometer class (Table 2).

Table 3: Requirements for test categories (ISO 22476-1:2022)

Test Category	Reference Readings [kPa]	Output Stability [kPa]	Cone Penetrometer Class
A	$\Delta q_{c;0} \leq 15$	$2\hat{u}_{qc} \leq 1$	0
	$\Delta f_{s;0} \leq 5$	$2\hat{u}_{fs} \leq 0.5$	
	$\Delta u_{2;0} \leq 3$	$2\hat{u}_{u2} \leq 0.5$	
B	$\Delta q_{c;0} \leq 35$	$2\hat{u}_{qc} \leq 5$	0 or 1
	$\Delta f_{s;0} \leq 5$	$2\hat{u}_{fs} \leq 1.5$	
	$\Delta u_{2;0} \leq 10$	$2\hat{u}_{u2} \leq 3$	
C	$\Delta q_{c;0} \leq 100$	$2\hat{u}_{qc} \leq 11$	0, 1, or 2
	$\Delta f_{s;0} \leq 15$	$2\hat{u}_{fs} \leq 3$	
	$\Delta u_{2;0} \leq 25$	$2\hat{u}_{u2} \leq 8$	
D	$\Delta q_{c;0} \leq 200$	$2\hat{u}_{qc} \leq 33$	0, 1, 2, or 3
	$\Delta f_{s;0} \leq 25$	$2\hat{u}_{fs} \leq 5$	
	$\Delta u_{2;0} \leq 50$	$2\hat{u}_{u2} \leq 16$	

Notes

$\Delta q_{c;0}$ = difference in reference readings for cone resistance q_c
$\Delta f_{s;0}$ = difference in reference readings for sleeve friction f_s
$\Delta u_{2;0}$ = difference in reference readings for pore pressure u_2 (or u_1)
$2\hat{u}_{qc}$ = output stability for q_c
$2\hat{u}_{fs}$ = output stability for f_s
$2\hat{u}_{u2}$ = output stability for u_2 (or u_1)

The difference in reference readings (e.g. $\Delta q_{c;0}$) of a sensor is calculated from sensor output recorded at a frequency of ≥1 Hz, as follows:

- Subtracting the mean value of reference readings of a particular sensor (e.g. sensor for q_c), for a period of one minute shortly before the penetration phase from the mean value of reference readings for a period of one minute shortly after the extraction phase, expressed as an absolute value;
- Cone penetrometer is vertical and under no load, atmospheric or selected ambient water pressure;
- Cone penetrometer is under temperature conditions close to ground temperature.

Calculation of output stability (peak-to-peak) of a sensor (e.g. $2\hat{u}_{qc}$) makes use of reference readings as described above. The calculation considers the larger value of subtracting the maximum and minimum sensor values for a period of one minute shortly before the penetration phase and for a period of one minute shortly after the extraction phase.

Results

CPT Parameters

Presentation of results from cone penetration tests typically includes:

- CPT parameters q_c, f_s and R_f versus depth below ground surface or versus elevation;
- Additional CPTU parameters u_1 or u_2 and, optionally, q_t, q_n, B_q, Q_t, Q_{tn}, F_r, I_c, I_B and CD for tests with pore pressure measurements;
- Additional CPTU parameter T, temperature;
- Inclination i for tests with inclination measurements;

- Standard graphical format and digital (tabular) ASCII or AGS formats.

Presentation of temperature T versus depth only applies to test results meeting the requirements of both cone penetrometer class 0 of Table 2 and test category A of Table 4.

Most standards specify scales for graphical presentation as follows:

- Axis for penetration depth z: 1 scale unit = 1 m;
- Axis for cone resistance q_c, corrected cone resistance q_t and net cone resistance q_n: 1 scale unit = 2 MPa or 0.5 MPa;
- Axis for sleeve friction f_s: 1 scale unit = 50 kPa;
- Axis for friction ratio R_f: 1 scale unit = 2 %;
- Axis for pore pressure u: 1 scale unit = 0.2 MPa or 0.02 MPa;
- Axis for pore pressure ratio B_q: 1 scale unit = 0.5.

Graphical presentation aims for these scale units and scale ratios, where suitable and practicable.

The reference level of a test is (1) the ground surface for onshore tests, (2) the seafloor for nearshore and offshore tests. Data processing presumes a hydrostatic pore pressure profile relative to seafloor, unless specifically indicated otherwise. The definition of CPT parameters is as follows:

z = penetration depth relative to ground surface or seafloor, corrected for inclination from vertical (i) where a test includes inclination measurements, as follows:

$$z = \int_0^l \cos i \cdot \mathrm{d}l$$

where:

z = penetration depth for the conical base of the cone penetrometer
l = recorded penetration length
i = recorded inclination from vertical

q_c = cone resistance relative to the reference level of the test.

f_s = sleeve friction relative to the reference level of the test. A calculated depth correction applies so that the presented sleeve friction corresponds with the cone depth.

f_t = corrected sleeve friction relative to the reference level of the test. Sleeve friction is corrected for pore pressures acting on the end areas of the friction sleeve

$$f_t = f_s - \frac{(u_2 * A_{sb} - u_3 * A_{st})}{A_s}$$

or simplified to:

$$f_t = f_s - u_2 \frac{(A_{sb} - A_{st})}{A_s} \qquad \text{or}$$

$$f_t = f_s - (u_2 * a_{fs})$$

where:

A_{sb} = cross sectional area in the gap between the friction sleeve and the cone
A_{st} = cross sectional area in the gap above the friction sleeve
A_s = surface area of the friction sleeve
a_{fs} = net area ratio of the friction sleeve $(A_{sb} - A_{st})/A_s$

R_f = ratio of sleeve friction to cone resistance (f_s / q_c). This calculated ratio is for the cone depth.

R_{ft} = corrected friction ratio (f_s / q_t). The ratio f_t/q_t applies if f_t is known.

u_1 = pore pressure at the face of the cone, relative to the reference level of the test.

u_2 = pore pressure at the cylindrical extension above the base of the cone or in the gap between the friction sleeve and the cone, relative to the reference level of the test.

u_3 = pore pressure immediately above the friction sleeve or in the gap above the friction sleeve, relative to the reference level of the test.

Commonly, no measurement of u_3 applies. An estimate can be obtained using $u_3 = 0.7\,(u_2 - u_0) + u_0$ according to SGI (1991). This estimate is independent of positive or negative values of $u_2 - u_0$.

u_0 = hydrostatic pore pressure at the cone, relative to the phreatic surface or the seafloor. This is a calculated value.

q_t = corrected cone resistance (also called total cone resistance). This includes corrections for hydrostatic and transient pore pressures, and cone construction. The corrected cone resistance is relative to ground surface or seafloor:

$q_t = q_c + (1\text{-}a)u_2$ or

$q_t = q_c + (1\text{-}a)[K(u_1 - u_0) + u_0]$

Historically, equations for downhole tests were:

$q_t = q_c + (1\text{-}a)u_2 + u_{0i}$ or

$q_t = q_c + (1\text{-}a)[K(u_1 + u_{0i} - u_0) + u_0] + a * u_{0i}$

where:

a = net area ratio of the cross-sectional steel area at the gap between cone and friction sleeve to the cone base area. This ratio is penetrometer-type dependent. The a-factor indicates the effect of pore pressure on unequal cross-sectional areas of the cone.

u_{0i} = hydrostatic pore pressure at the bottom of the borehole, relative to seafloor. This is a calculated value.

K = adjustment factor for the ratio of pore pressure at the cylindrical extension above the base of the cone to pore pressure on the cone face $K = (u_2 - u_0)/(u_1 - u_0)$

The term $u_2 - u_0$ refers to excess pore pressure (with respect to hydrostatic pore pressure). Common symbols for excess pore pressure are du_2 and Δu_2. Similarly, du_1 and Δu_1 can represent the term $u_1 - u_0$.

The K-factor is only of interest for processing of CPTU results with pore pressure measurement at the cone face (u_1). The factor depends on soil characteristics such as fabric, overconsolidation ratio, compressibility and crushability. The K-factor (Peuchen et al., 2010) can be estimated from:

$K = 0.91 \mathrm{e}^{-0.09 Q_t^{0.47}} \left(\frac{1}{1 + F_r(0.17 + 0.061(Q_t - 21.6)^{1/3})} - \mathrm{e}^{-2F_r} \right)$

q_n = $q_t - \sigma_{vo}$ = net cone resistance. This includes corrections for hydrostatic and transient pore pressures, in situ stress, and cone construction. The symbol for q_n may also be q_{net}.

where:

σ_{vo} = total in situ vertical stress at the cone base, relative to ground surface or seafloor. This is a calculated value.

B_q = pore pressure ratio $B_q = (u_2 - u_0)/q_n$ or

$B_q = K(u_1 - u_0)/q_n$

Q_t = q_n/σ'_{v0} = normalized cone resistance

where:

σ'_{v0} = effective in situ vertical stress at the cone base, relative to ground surface or seafloor. This is a calculated value.

Q_{tn} = normalized cone resistance with variable stress exponent n, where:

$Q_{tn} = [(q_t - \sigma_{v0})/P_a](P_a/\sigma'_{v0})^n$

$n = 0.381\,(I_c) + 0.05\,(\sigma'_{vo} / P_a) - 0.15$ and $n \le 1$
(Zhang et al., 2002)

where:

P_a = atmospheric pressure

F_r = f_t/q_n = normalized friction ratio

U_2 = normalized excess pore pressure $(u_2 - u_0)/\sigma'_{v0}$

I_B = soil behaviour type index (Robertson, 2016)

$I_B = 100(Q_{tn} + 10)/(70 + Q_{tn}F_r)$

I_c = soil behaviour type index (Robertson and Wride,1998)

$I_c = [(3.47 - \log Q_{tn})^2 + (\log F_r + 1.22)^2]^{0.5}$

I_{SBT} = soil behaviour type index (Robertson, 2010)

$I_{SBT} = [(3.47 - \log (q_c/P_a))^2 + (\log R_f + 1.22)^2]^{0.5}$

CD = contractive-dilative boundary (Robertson, 2016)

$CD = (Q_{tn} - 11)(1 + 0.06F_r)^{17}$

Presented values for u_2, q_t, q_n and B_q may be denoted by u_2^*, q_t^*, q_n^*, B_q^*, Q_t^* and F_r^* if u_2 is derived rather than measured, for example if derived by applying a K-factor.

Pore pressure u_2 at the cylindrical extension is commonly assumed equal to u_{2g} in the gap. The assumption $u_2 = u_{2g}$ is probably reasonable for deepwater CPTs and associated high values of ambient pressure that promote saturated conditions in the gap. A similar comment applies to u_3. Note that CPTU saturation procedures apply to the pore pressure measuring system only. These procedures exclude the gaps below and above the friction sleeve.

Some deployment systems allow monitoring of CPT parameters in reverse mode, i.e. upon retraction of the cone penetrometer. This optional feature presents additional information that can improve interpretation of ground behaviour, for example strength sensitivity of fine-grained soil.

Metrological Confirmation

CPT results include information on metrological confirmation. Examples covered by CPT standards include reporting of

FUGRO

application class, cone penetrometer class, test category and reference readings.

The ISO standard on metrological confirmation (ISO 10012:2003) provides the general framework for assessment of performance compliance.

Cone penetration test standards can follow a 'prescriptive' approach, whereby specific detailed measures provided a 'deemed to comply' practice. ASTM D5778-20 and ISO 22476-1:2022 provide examples of this approach.

The level of detail required by standards can be high. For example, ISO 22476-1:2022 includes detailed procedures for calibration and verification of CPT systems, with normative references to ISO/IEC 17025:2017. Fugro's calibration laboratory holds formal accreditation for cone penetrometer calibration and verification according to ISO/IEC 17025:2017.

Peuchen and Terwindt (2014, 2015) provide guidance on uncertainty estimation for cone penetration test results. The calculation model for uncertainty estimates for q_c, f_s and u considers the following uncertainty contributions, where applicable: (1) force and pressure sensors, (2) geometry of the cone penetrometer, (3) effects from ambient and transient temperature, (4) non-axial force on cone penetrometer (bending moment), (5) ambient fluid pressure in soil and (6) zero offsets for q_c, f_s and u relative to seafloor.

Temperature Stability of Cone Penetrometer

Uncertainty considerations for strongly layered soils should allow for heat flux phenomena. Heat flux gives an apparent shift in cone resistance. For example, friction in dense sand causes a cone to heat by about 1°C/MPa cone resistance. Resulting heat flux changes cone resistance by an apparent shift in the order of 100 kPa to 200 kPa for a penetrating probe going from dense sand into clay. This is a temporary change lasting about 5 minutes. Penetration interruption can serve as mitigation measure for transient temperature effects. The incorporation of one or more add-on temperature sensors in a cone penetrometer, and associated data algorithms, can reduce the effects from ambient and transient temperature fluctuations (Peuchen et al. 2020).

Pore Pressures

A CPTU pore pressure measuring system is intended for use in water-saturated uncemented fine-grained soil. Pore pressure measurements (u) are commonly assumed to represent pore water pressures. This assumption is reasonable for soils saturated under in situ stress conditions and remaining saturated during penetration of the cone penetrometer.

Pore pressure results obtained for ground conditions such as partially saturated soils, very dense sands and cemented soils may not be representative and/or repeatable. For example, stiffness differences between the steel components of the cone penetrometer and the piezocone filter can affect results for very dense sands.

Loss of saturation of the pore pressure measuring system can occur during a test (Peuchen et al. 2020). Loss of saturation usually causes a sluggish pore pressure response during penetration of ground below the zone causing desaturation of the pore pressure measuring system. Reasons for loss of saturation include:

- Penetration of partially saturated ground, for example ground containing significant amounts of gas;

- Reduction of pore pressure to below in situ pore pressure, causing gas in solution to become free gas;
- Penetration interruption for a stationary in situ test or for add-on of a push rod, that will cause:
  - Abrupt cone penetrometer deceleration and acceleration, with a possibility of upward movement of the cone penetrometer
  - Change of stress conditions around the cone penetrometer, including pore pressure and gas migration where applicable
  - Small volume change of the gaps below and above the friction sleeve of the cone penetrometer
- For u_2 filter position: proximity of gap between cone tip and friction sleeve, i.e. net area ratio $a < 1$. This gap may not be water-saturated, which in turn can lead to (1) substantial, local (undesired) pore pressure gradients and (2) loss of saturation of the u_2 filter itself;
- Measurement of negative pore pressures such that cavitation occurs; for example, this is not uncommon for a piezocone filter located at the cylindrical extension above the base of the cone (u_2 location), at the time of penetration of dense sand or overconsolidated clay layers.

Re-saturation of a pore pressure measurement system can take place upon further penetration into soil. Particularly, re-saturation may take place in saturated low-permeability soils (clays) that are normally consolidated or lightly overconsolidated and where the gap can become saturated by adequate supply of water and/or water pressure.

Measured pore pressures affected by desaturation of the pore pressure measurement system may not be representative of soil behaviour. Consequently, derived parameter values that use pore pressure may also not be representative.

Shallow Penetration

Shallow penetration will affect CPT measurements. Values of q_c, f_s and u for initial penetration of a cone penetrometer below ground surface, seafloor or bottom of a borehole will differ from a fully embedded cone penetrometer. As a general guide, initial penetration effects can be expected for a distance of about 8 times the diameter of the cone penetrometer for q_c, u_1 and u_2, and for a distance of about 15 times the diameter of the cone penetrometer for f_s. Initial penetration effects can be deeper for downhole borehole deployment. This is because of (1) complex ground stress conditions immediately below the required borehole and (2) borehole-induced ground disturbance that cannot be avoided.

Use of reaction equipment will affect stress conditions for shallow penetration. Particularly, offshore conditions may include extremely soft ground at seafloor. Soil disturbance, pore pressure build-up and consolidation of near-surface soft soil may take place.

Penetration Rate

CPT standards typically provide limits of ± 5 mm/s for a nominal penetration rate of 20 mm/s. Considerations include:

- A typical thrust machine provides a push speed with an uncertainty within ± 5 mm/s under favourable conditions. Under adverse conditions, penetration rates may be outside these limits, for example with strongly varying thrust and towards the thrust limit of a thrust machine;
- The penetration rate is not necessarily equal to the push speed because of inevitable vertical movements of the thrust machine and length variation and bending of the push-rod string.

Penetration Interruption

A penetration interruption may be unavoidable, for example to add a push rod or to perform a pore pressure dissipation test. This will affect test results.

Consolidation of low-permeability soil around a cone tip is of particular interest. A stationary cone penetrometer can apply local stresses that approach failure conditions, i.e. about 9 times the undrained shear strength or about 2 times the in situ mean effective stress. Pore pressure re-distribution and dissipation occur, resulting in a local increase in undrained shear strength and hence cone (bearing) resistance. A doubling of cone resistance may not be unreasonable for 100 % consolidation. Supplementary considerations include:

- Small downward movement of a penetrometer (order of millimetres) during a test can contribute to maintaining local stresses approaching failure conditions;
- Soil consolidation around a cone penetrometer may lead to soil/penetrometer adhesion that is sufficient to give an increase in 'cone' diameter. Resumption of penetration will lead to loss of adhered soil, usually within an equivalent distance of a few times the cone diameter;
- A low B_q value may imply partially drained penetration conditions. It is likely that any steady-state penetration conditions will not apply instantaneously upon resumption of penetration;
- Measuring sensors in a probe generate heat, but this is probably not significant for any stationary measurement. Fugro's strain-gauge load sensors are compensated for ambient temperature fluctuations.

Depth Measurement for Offshore Conditions

Table 4 presents depth accuracy classes according to ISO 19901-8:2014. The type of uncertainty is undefined (e.g. combined standard uncertainty or expanded measurement uncertainty with a coverage factor $k = 2$).

Peuchen and Wemmenhove (2020) present a probabilistic approach to depth uncertainty assessment for in situ testing data points, with reference to these accuracy classes.

Offshore definition of the seafloor (ground surface) is difficult for extremely soft ground at seafloor (ISO 19901-8:2014). Penetration of the reaction equipment into a near-fluid zone of the seabed may take place unnoticed. Such settlement affects the start of penetration depth z. Also, settlement may continue at the time of testing.

Downhole CPT systems rely on depth control applicable to borehole drilling. Depth control according to Z2 of Table 4 is typically feasible for drilling systems deployed from a fixed platform, for example a jack-up. This value excludes uncertainty associated with determination of seafloor level. Drilling control from floating equipment, for example a geotechnical survey vessel, may be subject to the additional influence of waves and tides. Z2 is typically feasible for favourable conditions. Z3 or Z4 may apply for adverse conditions.

Table 4: Depth accuracy classes (ISO 19901-8:2014)

Depth Accuracy Class	Maximum Data Point Depth Uncertainty [m]
Z1	0.1
Z2	0.5
Z3	1.0
Z4	2.0
Z5	> 2.0

Zero-Correction for Offshore Conditions

Water pressures generate significant values of cone resistance and pore pressure. The standardised practice is to correct these reference readings to zero at seafloor. CPT systems for non-drilling mode and for seafloor drilling mode allow zero-correction to hydrostatic conditions prior to the start of a test, typically with a zero-correction uncertainty approaching the resolution of the CPT system. Downhole borehole CPT systems latch into the lower end of a drill pipe. The pressure conditions in the drill pipe may not be in full equilibrium with the surrounding ground water pressure and zero-correction will be subject to increased uncertainty, i.e. uncertainty for pore pressure in the order of 100 kPa for deepwater tests (Peuchen, 2000). This uncertainty depends on factors such as the free-flow and viscosity of drill fluid between the drill bit and the seafloor. The uncertainty typically decreases with decreasing depth of the drill bit below sea level and below seafloor. Uncertainty for the zero-correction of cone resistance is approximately equivalent, but by a factor representing the net area ratio effect.

Deepwater Tests

A deepwater environment presents some favourable conditions for cone penetration tests, notably temperature. Ambient temperature conditions are practically constant and the measuring system has ample time to adjust to these temperatures. In addition, transient heat flow phenomena in a cone penetrometer are usually not applicable. This is because a cone penetrometer accumulates negligible (frictional) heat when penetrating the generally prevalent soils of very soft consistency.

Deepwater (piezocone) pore pressure measurements are essentially similar to shallow-water measurements, with the exception of an increased measuring range for pore pressure leading to some reduction in sensor accuracy. Saturation of a pore pressure measuring system is excellent for a deepwater environment, as the high pressures will force any gas bubbles into solution.

Currently available evidence indicates that a high-quality subtraction-type cone penetrometer is adequate for very soft soil characterisation to a water depth of 3000 metres and probably beyond.

Additional Measurements

Friction-cone and piezocone penetrometers allow specific additional measurements, such as friction set-up tests, pore pressure dissipation tests and measurements of ground water pressure. These additional measurements require a penetration interruption or may be feasible at the end of a test. It is also common to add other in situ test devices to a cone penetrometer. Table 5 presents the more common types.

Table 5: Probes for additional in situ tests

Type of Probe	Properties	Units
Electrical Conductivity Penetrometer (ECPT)	Electrical conductivity, K	S/m
Temperature Cone Penetrometer (TCPT)	Temperature T, thermal conductivity k, volumetric heat capacity C	K, W/(m·K), MJ/m^{3}K
Seismic Cone Penetrometer (SCPT)	S-wave velocity v_s	m/s
Cone Pressuremeter (CPMT)	Stress-strain-time response σ, ε, t	MPa, -, s
Natural Gamma Penetrometer (GCPT)	Natural gamma ray γ	CPS
Cone Magnetometer (CMMT)	Magnetic flux density B, magnetic field horizontal angle θ, vertical angle ϕ	µT, °, °
Hydraulic Profiling Tool (HPT)	Permeability k	m/s
Notes		
S = Siemens	J = Joule	
m = metre	s = second	
K = Kelvin (or °C)	Pa = Pascal	
W = Watt	CPS = counts per second	
	T = Tesla	

References

ASTM. (2020). Standard test method for electronic friction cone and piezocone penetration testing of soils (ASTM D5778-20). ASTM International. DOI: 10.1520/D5778-20.

CEN. (2010). *Eurocode 7 - geotechnical design – Part 2: Ground investigation and testing* (EN 1997-2:2007+ AC:2010). European Committee for Standardization. https://standards.cencenelec.eu/dyn/www/f?p=CEN:110:0::::FSP_PROJECT,FSP_ORG_ID:34660,6231&cs=106BCF2003C57E77F5AE21C7C352536A8.

ISO. (2003). *Measurement management systems - requirements for measurement processes and measuring equipment* (ISO 10012:2003). International Organization for Standardization. https://www.iso.org/standard/26033.html.

ISO. (2017). *General requirements for the competence of testing and calibration laboratories* (ISO/IEC 17025:2017). International Organization for Standardization. https://www.iso.org/standard/66912.html.

ISO. (2014). *Petroleum and natural gas industries – specific requirements for offshore structures – part 8: marine soil investigations* (ISO 19901-8:2014). International Organization for Standardization. https://www.iso.org/standard/61145.html.

ISO. (2023). *Oil and gas industries including lower carbon energy – offshore structures – part 8: marine soil investigations* (ISO 19901-8:2023). International Organization for Standardization. https://www.iso.org/standard/83302.html.

ISO. (2022). *Geotechnical investigation and testing – Field testing – Part 1: Electrical cone and piezocone penetration test* (ISO 22476-1:2022). International Organization for Standardization. https://www.iso.org/standard/75661.html.

ISSMGE. (1999). International reference test procedure for the cone penetration test (CPT) and the cone penetration test with pore pressure (CPTU). Report of the ISSMGE Technical Committee 16 on ground property characterisation from in situ testing. In F.B.J. Barends, J. Lindenberg, H.J. Luger, L. de Quelerij & A. Verruijt (Eds.). *Geotechnical engineering for transportation infrastructure: Theory and practice, planning and design, construction and maintenance: Proceedings of the 12th European conference on soil mechanics and geotechnical engineering* (Vol. 3, pp. 2195–2222). Balkema.

Peuchen, J. (2000). Deepwater cone penetration tests. In *32nd Annual Offshore Technology Conference, 2000: OTC Paper 12094* https://doi.org/10.4043/12094-MS

Peuchen, J., VandenBerghe, J.F. & Coulais, C. (2010), Estimation of u$_1$/u$_2$ conversion factor for piezocone. In *CPT'10: 2nd International symposium on cone penetration testing, Huntington Beach, California: conference proceedings*.

Peuchen, J. & Terwindt, J. (2014). Introduction to CPT accuracy. In *3rd International symposium on cone penetration testing CPT14: May 12-14 (2014) - Las Vegas, Nevada*.

Peuchen, J. & Terwindt, J. (2015). Measurement uncertainty of offshore cone penetration tests. In V. Meyer (ed.) *Frontiers in offshore geotechnics III: proceedings of the third international symposium on frontiers in offshore geotechnics (ISFOG 2015), Oslo, Norway, 10-12 June 2015.* (pp. 1209-1214) CRC Press..

Peuchen, J. & Parasie, N. (2019). Challenges for CPT accuracy classes. *Proceedings of the XVII ECSMGE-2019: geotechnical engineering foundation of the future.* IGS publishing https://www.ecsmge-2019.com/uploads/2/1/7/9/21790806/0049-ecsmge-2019_peuchen.pdf.

Peuchen, J. & Wemmenhove, R. (2020). Depth accuracy of data points in marine soil investigation. In Z. Westgate (ed.). 4*th International Symposium on Frontiers in Offshore Geotechnics (ISFOG 2020): proceedings* (pp. 1036-1045). Deep Foundations Institute.

Peuchen, J., Santos, R., Yetginer, A.G., Eckart, W.S., Carrington, T.M. & Lunne, T. (2020). CPT data showing anomalies – assessment and potential postprocessing. In Z. Westgate (ed.). *4th International Symposium on Frontiers in Offshore Geotechnics (ISFOG 2020): proceedings* (pp. 1026-1035). Deep Foundations Institute.

Robertson, P.K. & Wride (Fear), C.E. (1998). Evaluating cyclic liquefaction potential using the cone penetration test. *Canadian Geotechnical Journal*, *35*(3), 442-459. https://doi.org/10.1139/t98-017.

Robertson, P.K. (2010). Soil behaviour type from the CPT: an update. In *2nd International symposium on cone penetration testing, Huntington Beach, CA, Vol. 2.* (pp. 575-583*)*.

Robertson, P.K. (2016). Cone penetration test (CPT)-based soil behaviour type (SBT) classification system — an update. *Canadian Geotechnical Journal*, *53*(12) 1910-1927 https://doi.org/10.1139/cgj-2016-0044

SGI. (1991). *Piezocone tests in clay.* Swedish Geotechnical Institute Report No 42.

Zhang, G., Robertson, P.K. & Brachman, R.W.I. (2002). Estimating liquefaction induced ground settlements from CPT for level ground. *Canadian Geotechnical Journal*, *39*(5) 1168-1180. https://doi.org/10.1139/t02-047.

Geotechnical Parameter Values

Scope

This document presents a summary of interpretation methods for derived values of geotechnical parameters. The definition of derived value is according to CEN (2009), CEN (2010), and ISO (2021a): 'value of a geotechnical parameter obtained from test results by theory, correlation or empiricism'.

Figure 1 illustrates geotechnical parameter values in the context of structure design or structure (re)assessment (e.g. ISO, 2015), where GP refers to geotechnical parameter values, GM refers to ground model, and SC to wider site characterisation.
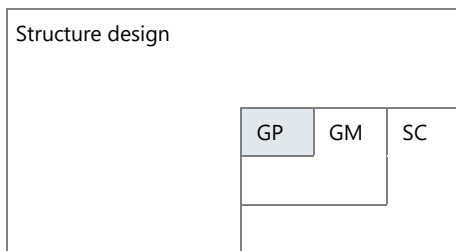
Figure 1: General context for geotechnical parameter values

The focus of this document is on:

- Mechanical properties of in situ soil, notably soil behaviour type and stress-strain-time dependent properties;
- Common data sources, i.e. ground intrusive technologies, particularly in situ testing, borehole geophysical logging, and laboratory testing;
- Methods that can provide parameter values by a transformation model and/or by empiricism, such as interpretation methods for cone penetration test (CPT) results.

This focus implies limited coverage of mechanical properties derived from (1) methods dedicated to obtaining derived values for a specific parameter, such as deriving undrained shear strength from an unconsolidated undrained triaxial compression test and (2) non-intrusive technologies (requiring no in-ground deployment of equipment), e.g. seismic reflection and seismic refraction.

Some of the presented methods suit computer-based interpretation of data records, machine learning and artificial intelligence.

The project-specific selection of methods and level of data integration depends on the agreed project requirements.

Procedure

Figure 2 outlines the procedure for development of geotechnical parameter values. Comments are given in 'Parameter Interpretation', below.
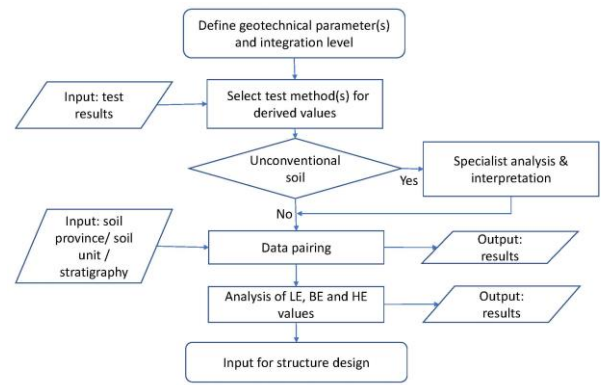
Figure 2: General procedure

Parameter Interpretation

Input for Structure Design

Derived values typically provide input for selection of characteristic values (e.g. CEN, 2009) and representative values (e.g. ISO, 2019) for geotechnical calculation models.

Conventional models are typically based on plasticity theory for ultimate limit states, and on elasticity theory and consolidation theory for serviceability limit states. Features of these geotechnical models are:

- Analysis of either drained (sand model) behaviour or undrained (clay model) behaviour for plasticity models;
- Analysis for the ultimate limit state differs from that for the serviceability limit state.

Many interpretation methods apply a transformation model to 'conventional' sands (drained soil behaviour) and clays (undrained soil behaviour). Drained or undrained behaviour (strain rate dependence) for the geotechnical analysis at hand may or may not coincide with respectively drained or undrained behaviour for a particular test method.

Integrated Geosciences

Project-specific integration levels for parameter interpretation can range from (1) a basic scope covering geodata processing and presentation of relevant, site-specific data and comments on any apparent data anomalies to (2) integrated use of multidisciplinary (e.g. geotechnical and geophysical) data that include representative ground profiles of derived values of geotechnical parameters.

This document excludes details of advanced methods for integrated use of multidisciplinary data.

Applicability of Methods

Parameter interpretation typically considers applicability of methods for data acquisition and for data analysis. If a method is applied outside of the intended applicability, then parameter values can be obtained that are uncertain, incorrect and/or anomalous. In practice, the following approaches are taken for parameter values outside of intended applicability:

- Present the parameter values and apply appropriate judgement when using the results;
- Remove data by intervention (manually or by algorithms), such as by data clipping;
- Provide (approximate) corrections to parameter values, e.g. by post-processing.

Examples are given below.

A particular method may not be appropriate for silts, sand/clay/gravel mixtures, varved or layered soils, gassy soils, underconsolidated soils, peats, carbonate soils, cemented soils, and residual soils. These unconventional soils can require specialist analysis and interpretation. ISO (2021a) includes a list of unconventional soils and potential difficulties.

Most methods for data acquisition and parameter interpretation consider applicability in terms of lower and upper limits of stress, strain and temperature. Such limits are typically given or implied for a particular test method. Parameter values outside of these ranges can be subject to high uncertainty.

Results of a cone penetration test depend on a standardised penetration rate. Inevitably, the penetration rate will (shortly) differ from the standardised penetration rate at the start of a test and at the end of a test or planned interruption of penetration. In some cases, data are clipped to remove sections with a non-standard penetration rate.

A transformation model can include assumptions about soil (un)disturbance and ambient stress conditions. This can mean that laboratory test results for a soil sample taken immediately below ground surface or immediately below the bottom of the borehole may be outside of the applicability of a transformation model. Similarly, a short section of cone penetration data immediately below ground surface or immediately below the bottom of the borehole can cause a situation of no or limited applicability.

Data Pairing

Data pairing can be required for obtaining derived values for some of the geotechnical parameters. For example, correlation of CPT net cone resistance q_n and laboratory undrained shear strength s_u for clays requires:

- Derived values for q_n;
- Derived values for s_u;
- Pairing of q_n data points and laboratory s_u data points applicable to a nearby, but not the same, location in space;
- A correlation equation such as $N_{kt} = q_n/s_u$, where N_{kt} is a cone factor.

Considerations for data pairing typically include:

- Data checks, data detrending and data enhancement by integrated geosciences, see above;
- Applicability of methods, including undrained, partially drained or drained conditions;
- Uncertainties of the parameter values (source geodata) for data pairing;
- Representativeness of soil specimens and/or in situ test zone, e.g. bias may be introduced by selecting laboratory test specimens from the more cohesive, homogeneous parts of samples, particularly where soil conditions are not uniform;
- Geo-spatial proximity between data points selected for pairing, particularly with respect to soil homogeneity and soil correlation length;
- Decision rules and engineering judgement for screening of datasets for retention or removal of data;
- Use of specific weight factors for e.g. data assessed of higher of lower quality or importance.

Low Estimate, Best Estimate, High Estimate Values

The project requirements can include assessment of *low estimate* (LE), *best estimate* (BE) and *high estimate* (HE) values for derived values.

Analysis of derived values for LE, BE and HE values can be performed and enhanced by one or more of the following methods:

- Application of statistical methods,
- Data pairing, including geodata from multiple sources;
- Use of relevant prior information, including public domain information;
- Judgement and opinion.

This document excludes further details of possible methods for geotechnical analysis on this topic.

CPT-based Interpretation Methods

CPT interpretation methods are mostly based on empirical correlations with limited theoretical backing. Data integration with other, complementary investigation techniques (such as geological analysis, borehole/sample logging and laboratory testing) can improve confidence levels.

CPT-based interpretation techniques discussed below are subject to limitations such as:

- CPT measurements, including measurement uncertainty (Peuchen & Terwindt, 2014 and 2015) and effects resulting from deployment method, initial embedment of a cone penetrometer, penetration interruption and inevitable loss of saturation of a pore pressure measuring system;
- CPT interpretation techniques can be indirect, i.e. requiring estimates of various other parameters. This is consistent with an integrated geotechnical investigation approach. Inevitably, this approach also includes some redundancy of data;
- Empirical correlations can rely on data pairing, for example pairing of CPT net cone resistance at a point in space with laboratory undrained shear strength applicable to another, nearby spatial position. Data pairing uncertainty can be limited by applying judgement;
- Empirical correlations can use reference parameters such as the undrained shear strength determined from a laboratory single-stage isotropically consolidated undrained triaxial compression test on an undisturbed specimen obtained by means of push sampling techniques (e.g. Van der Wal et al., 2010). The reference parameter may not be appropriate for the selected geotechnical model, and adjustment may be necessary. Also, adjustment for test conditions may be necessary, for example in situ temperature versus laboratory temperature;
- The cone penetration test offers limited direct information on serviceability limit states (deformation), as the penetration process imposes large strains in the surrounding soil. In comparison to ultimate limit states, better complementary data will usually be required;
- The interpretations typically apply to conditions as encountered at the time of the geotechnical investigation. Geological, environmental, and construction/operational factors may alter as-found conditions.

Laboratory Test Methods

Laboratory test standards often specify procedures for obtaining derived values, particularly where it is possible to obtain a derived value by means of a conversion model or theory. Such derived values are thus part of the laboratory test report. An example is the unconsolidated undrained triaxial compression test. Normalised load and displacement data are the basic measured values. The measured values and the use of theory allow the calculation of a derived value of undrained shear

strength by consideration of principal stress conditions and a theoretical deformation model.

A project-specific scope design for laboratory test results can be of a confirmatory nature. An example would be a limited scope that targets confirmation of CPT-based methods rather than detailed site-specific integration and correlation of data.

Non-intrusive Technologies

Results of non-intrusive technologies can serve as important input data for deriving geotechnical parameter values for semi-continuous profiles along a geophysical survey line (2D) and for voxel (3D) models (e.g. ISO, 2021b; Nauroy et al., 1998; Carpentier et al., 2021). Key features of this approach typically include (1) general input from an initial ground model, (2) a training data set of non-intrusive data (e.g. seismic reflection data) and ground-truthing data (e.g. CPTs), (3) machine learning and (4) correlation of geotechnical parameter values for spatial positions with non-intrusive data points.

The training phase typically includes validation of derived geotechnical parameter values (e.g. CPT cone resistance or shear modulus at small strain) at control locations. The validation results at the control locations allow comparison of accuracy of the derived values at non-intrusive data points with derived values of the ground truthing data.

CPT Penetration Behaviour

Soil behaviour during cone penetration testing shows large displacements in the immediate vicinity of the penetrometer, and small elastic displacements further away from the penetrometer. Density/structure, stiffness and in situ stress conditions significantly affect the measured parameters.

The measured cone resistance (q_c) includes hydrostatic water pressures as well as induced pore pressures resulting from stresses and strains related to the penetration process. The induced pore pressures are usually negligible for clean sand because the ratio of effective stress to pore pressure is high. This ratio can be low for penetration into normally consolidated and slightly overconsolidated clays. Knowledge of pore pressures around the penetrometer can thus be important. CPT parameters that take account of pore pressure effects include corrected cone resistance (q_t), net cone resistance (q_n) and pore pressure ratio (B_q). These parameters can be calculated if piezocone penetration test (PCPT or CPTU) data are available. The influence of pore pressures on sleeve friction f_s is relatively small. It is common to ignore this influence. Calculation of friction ratio R_f (defined as f_s/q_c) includes no allowance for pore pressure effects.

The penetration rate with respect to soil permeability determines whether soil behaviour is primarily undrained, drained, or partially drained. Partial drainage may also be denoted as partial consolidation. In general, soil behaviour during cone penetration testing is:

- Drained in clean sand, i.e. no measurable pore pressures because of (1) soil displacements and (2) soil volume change depending on dilative/contractive soil behaviour;
- Undrained in clay, i.e. no significant soil volume change immediately around the cone penetrometer and pore pressure change depending on dilative/contractive soil behaviour;
- Partially drained in soils with intermediate permeability, such as sandy silt, i.e. potential for (1) some soil volume change depending on dilative/contractive soil behaviour and (2) potential for pore pressure change depending on dilative/contractive soil behaviour.

Results of a pore pressure dissipation test can provide indications for partial drainage conditions. Particularly, partial drainage conditions should be considered when t_{50} is less than about 100 s (DeJong & Randolph, 2012). The term t_{50} represents the time for 50 % dissipation of excess pore pressure at the u_2 location of a cone penetrometer.

CPT parameters can be influenced by the presence of thin (< 0.2 m thick) layers in a ground profile. Boulanger and DeJong (2018) proposed a method that provides estimates of corrected q_c and f_s values based on an inverse filtering procedure that accounts for thin layer and transitional effects during cone penetration.

The following sections mostly consider interpretation of drained soil behaviour (sand) and undrained soil behaviour (clay).

CPT-based Soil Behaviour Type Identification

Figures 3, 4 and 5 show soil behaviour type identification according to procedures given by Robertson (2009), representing an update of Robertson (1990) and Robertson (1991) respectively by exchange of Q_t with Q_{tn}. The procedures consider a normalised soil behaviour classification that provides general guidance on likely soil type (silty sand for example) and a preliminary indication of parameters such as angle of internal friction φ', overconsolidation ratio (OCR) and clay sensitivity (S_t). Classification is in general possible for $1 \leq Q_{tn} \leq 1000$, $0.1 \leq F_r \leq 10$ and $-0.5 \leq B_q \leq 1.4$, with exceptions for classification using a Q_{tn}-B_q chart for the areas where no classification is presented.

Classification charts use following soil behaviour type zones:

1. Sensitive, fine grained
2. Organic soils – peats
3. Clays – clay to silty clay
4. Silt mixtures – clayey silt to silty clay
5. Sand mixtures – silty sand to sandy silt
6. Sands – clean sand to silty sand
7. Gravelly sand to sand
8. Very stiff sand to clayey sand*
9. Very stiff, fine grained*

(*) Heavily overconsolidated or cemented
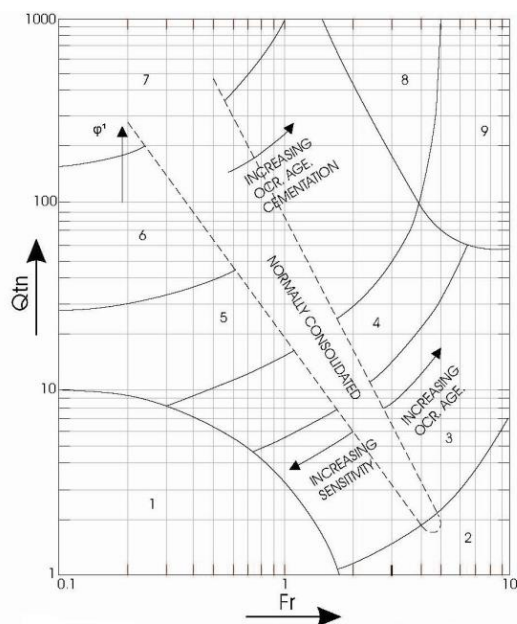
Figure 3: Classification chart Robertson (1990) with exchange of Q_t with Q_{tn}
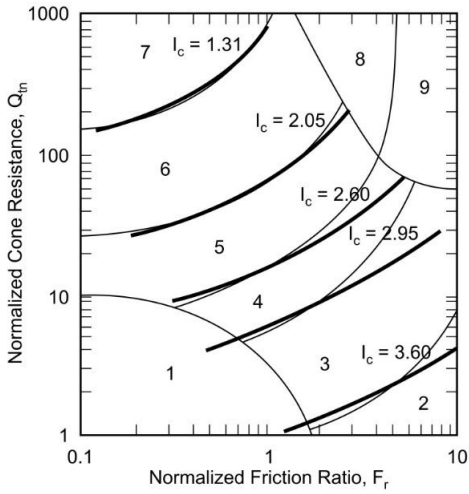
Figure 4: Soil behaviour type index I_c superimposed on Robertson (2009) classification chart
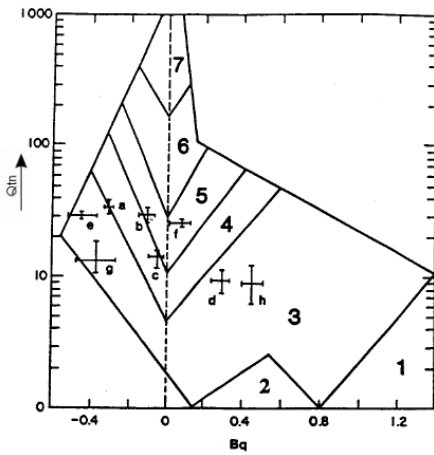
Figure 5: Classification chart Robertson (1991) with exchange of Q_t with Q_{tn}

The procedures require piezocone test data:

$$Q_{tn} = [(q_t - \sigma_{v0})/P_a](P_a/\sigma'_{v0})^n \qquad Q_t = \frac{q_t - \sigma_{vo}}{\sigma'_{vo}}$$

$$F_r \text{ or } nR_f = \frac{f_s}{q_t - \sigma_{vo}} 100\% \qquad B_q = \frac{u - u_0}{q_t - \sigma_{vo}}$$

where:

B_q	= pore pressure ratio
F_r	= normalised friction ratio
Q_{tn}	= normalised cone resistance with variable stress exponent
Q_t	= normalised cone resistance
q_t	= corrected cone resistance
σ_{vo}	= total in situ vertical stress
σ'_{vo}	= effective in situ vertical stress
P_a	= atmospheric pressure
n	= stress exponent
f_s	= measured sleeve friction
u	= measured pore pressure
u_0	= theoretical hydrostatic pore pressure.

The stress exponent n is according to Zhang et al. (2002):

$$n = 0.381 \, (I_c) + 0.05 \, (\sigma'_{vo}/P_a) - 0.15$$

where $n \leq 1$.

Robertson and Wride (1998) defined soil behaviour type index I_c as follows:

$$I_c = [(3.47 - \log Q_{tn})^2 + (\log F_r + 1.22)^2]^{0.5}$$

Soils with $I_c < 2.05$ are generally cohesionless, coarse grained, where cone penetration is generally drained and soils with $I_c > 2.60$ are generally cohesive, fine grained, where cone penetration is generally undrained (Robertson & Wride, 1998). Cone penetration in soils with $2.05 < I_c < 2.60$ is often partially drained.

Figure 6 presents a classification chart for friction cone data according to Robertson (2010). This procedure requires no pore pressure input. A non-normalised soil behaviour type index, I_{SBT} applies:

$$I_{SBT} = [(3.47 - \log (q_c/P_a))^2 + (\log R_f + 1.22)^2]^{0.5}$$

I_{SBT} is similar to I_c. Values for I_{SBT} and I_c are typically comparable for effective in situ vertical stress between 50 kPa and 150 kPa.
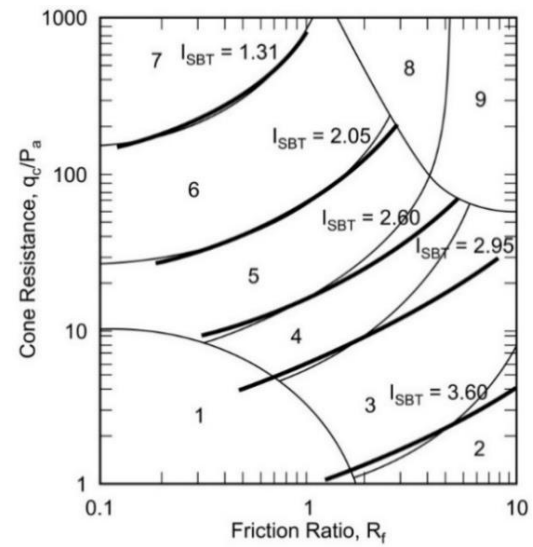
Figure 6: Robertson (2010) classification chart including I_{SBT}

Figure 7 presents a classification chart focusing on contractive and dilative soil behaviour, according to Robertson (2016a). The equations for the contractive-dilative boundary (CD) and soil behaviour type index (I_B) are as follows:

$$CD = (Q_{tn} - 11)(1 + 0.06F_r)^{17} \text{ and}$$

$$I_B = 100(Q_{tn} + 10)/(70 + Q_{tn}F_r)$$

Suggested values of CD are $CD = 60$ (low value) and $CD = 70$ (high value). Suggested values for I_B are $I_B = 32$, representing a low value for sand-like soil behaviour types and $I_B = 22$ representing a high value for clay-like soil behaviour types. The region between $I_B = 32$ and $I_B = 22$ represents soils typically showing transitional or intermediate soil behaviour types.
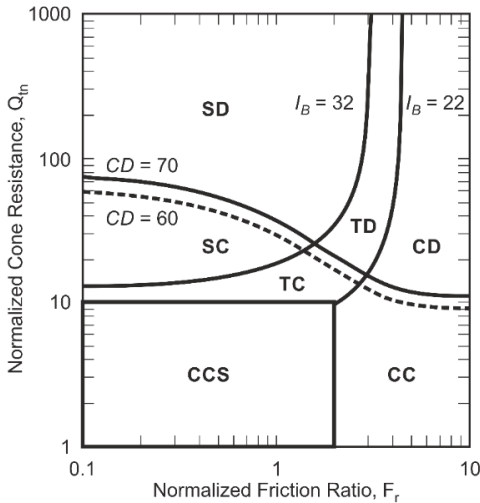
Figure 7: Classification chart according to Robertson (2016a)

CCS Clay-like – Contractive - Sensitive
CC Clay-like – Contractive
CD Clay-like – Dilative
TC Transitional – Contractive
TD Transitional – Dilative
SC Sand-like – Contractive
SD Sand-like – Dilative

Sand Model – CPT-based Methods

Unit Weight – Sand

Unit weight of uncemented (silica) sand, silt and clay soils may be derived according to Mayne et al. (2010):

$$\gamma = 1.95\gamma_w \left(\frac{\sigma'_{vo}}{P_a}\right)^{0.06} \left(\frac{f_t}{P_a}\right)^{0.06}$$

where total unit weight γ and unit weight of water γ_w are in kN/m³ and effective in situ vertical stress σ'_{vo} is in kPa. The symbol f_t refers to sleeve friction corrected for pore pressures acting on the end areas of the friction sleeve, with units in kPa. Atmospheric pressure P_a is in kPa.

Unit weight may also be derived according to Lengkeek et al. (2018):

$$\gamma = \gamma_{ref} - \beta \cdot (\log(q_{t,ref}/q_t))/ (\log (R_{f,ref}/R_f))$$

where γ_{ref} is a reference unit weight at which q_t is constant regardless of friction ratio R_f, β is a factor for unit weight contouring, $q_{t,ref}$ is a reference for total cone resistance q_t at which γ is constant regardless of R_f, and $R_{f,ref}$ is a reference friction ratio. The default values are: $\gamma_{ref} = 19$ kN/m³, $\beta = 4.12$, $q_{t,ref} = 5$ MPa, and $R_{f,ref} = 30$ %. The correlation allows development of project-specific estimation of unit weight.

Shear Wave Velocity – Sand

If no in situ measurements of shear wave velocities (v_s) are available, then empirical correlation with CPT parameters may be considered. Hegazy and Mayne (2006) published a statistical correlation derived from 73 sites worldwide representing a range of soil types including sands, clays, soil mixtures and mine tailings (Figure 8). The correlation considers a normalized cone resistance (q_{c1N_hm}) and a soil behaviour type index (I_{c_hm}) as follows:

$$v_s = 0.0831q_{c1N\_hm}(\sigma'_{vo}/P_a)^{0.25}e^{(1.786I_{c\_hm})}$$

(Hegazy & Mayne, 2006)

where shear wave velocity v_s is in m/s and q_{c1N_hm} and I_{c_hm} are dimensionless. Calculations for q_{c1N_hm} and I_{c_hm} require iteration and consider cone resistance q_c or corrected cone resistance q_t, sleeve friction f_s, total in situ vertical stress σ_{vo}, effective in situ vertical stress σ'_{vo} and atmospheric pressure P_a.
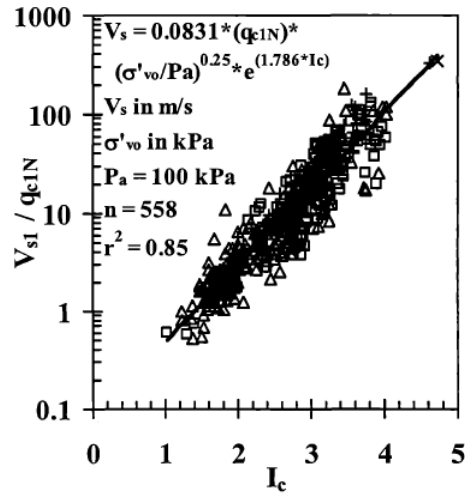
Figure 8: $v_s - q_c$ correlation according to Hegazy & Mayne (2006)

Robertson and Cabal (2015) present a v_s correlation incorporating net cone resistance q_n (= $q_t - \sigma_{vo}$) and soil behaviour type index (I_c) as defined by Robertson and Wride (1998):

$$v_s = [\alpha_{vs}(q_t - \sigma_{vo})/P_a]^{0.5} \text{ where } \alpha_{vs} = 10^{(0.55 I_c + 1.68)}$$

(Robertson & Cabal, 2015)

where shear wave velocity v_s is in m/s and corrected cone resistance q_t, total in situ vertical stress σ_{vo} and atmospheric pressure P_a are in kPa. The method can be applied to a wide range of soil behaviour types, notably uncemented Holocene to Pleistocene age soils. Older deposits could have a higher shear wave velocity. Exceptions are Zones 1, 8 and 9 of Robertson (1990 and 2009).

Baldi et al. (1989) derived a correlation between shear wave velocity v_s and cone resistance q_c for uncemented silica sands. This correlation is based on data from CPT, cross-hole, and Seismic cone penetration tests (SCPTs) performed in quaternary deposits of the predominantly silica Po River sand and Gioia Tauro sand with gravel.

$$v_s = 277q_c^{0.13}\sigma'_{vo}^{0.27}$$

(Baldi et al., 1989)

where shear wave velocity v_s is in m/s and cone resistance q_c and effective in situ vertical stress σ'_{vo} are in MPa.

Shear wave velocity may be normalised according to Robertson and Cabal (2015):

$$v_{s1} = v_s \cdot (P_a/\sigma'_{vo})^{0.25}$$

(Robertson & Cabal, 2015)

In Situ Stress Conditions – Sand

A knowledge of in situ stress conditions is required for estimation of parameters such as relative density D_r and angle of internal friction of a sand deposit φ'. The effective in situ vertical stress σ'_{vo} can be calculated with a reasonable degree of accuracy but the effective in situ horizontal stress $\sigma'_{ho} = K_0 \cdot \sigma'_{vo}$ is generally a more approximate. Usually, it is necessary to consider a range of conditions for K_0 (coefficient of earth pressure at rest). The range can consider overconsolidation as inferred from a geological assessment, preconsolidation

pressures of intermediate clay layers and/or theoretical limits of K_0.

Geological factors concerning overconsolidation include ice loading, soil loading and groundwater fluctuations (influence from desiccation). Possible subdivisions for these factors are mechanical, suction, cyclic and ageing consolidation.

The following approach can be applied for direct estimation of K_0 based on Agaiby and Mayne (2019):

$$K_0 = 0.45\sqrt{(OCR)}$$

using: $OCR = \frac{\sigma'_p}{\sigma'_{vo}}$ $\sigma'_p = 0.33 \cdot q_n^{m'}$ $m' = 1 - \frac{0.28}{1+\left(\frac{I_c}{2.64}\right)^{25}}$

where OCR is overconsolidation ratio, σ'_p is effective preconsolidation stress, σ'_{vo} is effective in situ vertical stress, q_n is net cone resistance in kPa and I_c is soil behaviour type index. Typical values for m' are 0.72, 0.8 and 0.85 for clean sands, silty sands, and silts respectively.

The $K_0 - OCR$ relationship represents a schematisation of $K_0 = (1 - sin\varphi') \cdot OCR^{sin\varphi'}$ proposed by Mayne and Kulhawy (1982). Mayne and Kulhawy (1982) investigated mechanical overconsolidation of reconstituted laboratory specimens for over 170 different soils. For many soil types (e.g. Mayne, 2020), it can be shown that the $K_0 = 0.45\sqrt{(OCR)}$ equation provides similar statistics to the Mayne and Kulhawy correlation using φ' (effective angle of internal friction):

$$K_0 = (1 - sin\varphi') \cdot OCR^{sin\varphi'}$$

Figure 9 presents an approximate CPT-based correlation for K_0 according to Robertson (2016b). K_0 limits are typically set to 0.5 and 2. Linear interpolation is applied for the region between $K_0 = 0.5$ and $K_0 = 2$.
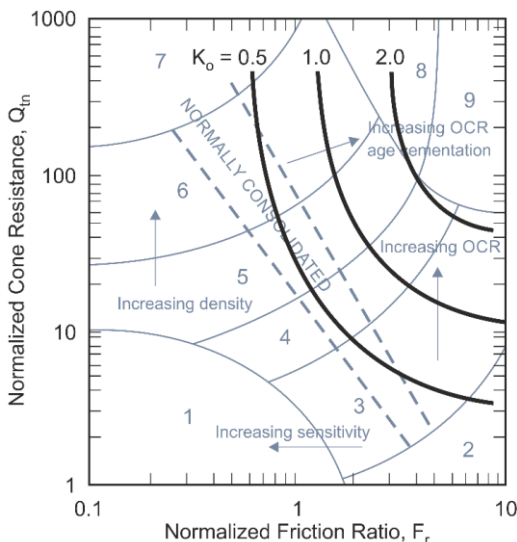
Figure 9: K₀ correlation according to Robertson (2016b)

No laboratory study can fully capture in situ behaviour. Particularly, K_0 may be underestimated if effects such as ageing and cyclic loading are relevant.

In general, in situ K_0 values are limited to the range $K_0 = 0.5$ to $K_0 = 1.5$. For many situations, K_0 values are believed to be relatively low at greater depths (say $K_0 < 1$ for depths exceeding 50 m). Jamiolkowski et al. (2003) recommend using a limiting value $K_0 = 1$ in practice, for limit states where low values of soil resistance and soil stiffness are critical.

Relative Density – Sand

The relative density concept applies to sands with a percentage fines of less than about 15 %.

Relative density is defined as $D_r = (e_{max} - e)/(e_{max} - e_{min})$, where e_{max} is maximum index void ratio, e represents in situ void ratio and e_{min} is minimum index void ratio. Maximum and minimum index void ratios are defined by laboratory testing. Relative density can exceed 100 %, because in situ void ratio can be lower than laboratory values for minimum index void ratio.

Determination of laboratory minimum and maximum index void ratios forms the basis for the relative density concept (loose, dense sand, etc.). No internationally agreed procedure is available.

CPT-based correlations are commonly used for estimation of in situ relative density. These correlations rely on database results of CPTs carried out in sand samples reconstituted in laboratory calibration chamber tests. Use of such correlations implies dependence on, for example:

- soil type of database versus soil type in situ;
- reference laboratory test method for determination of index void ratios, particularly sensitivity to minimum index void ratio;
- range of stress levels and K_0 values for calibration testing;
- results applicable to reconstituted sand samples, sample preparation method and soil stress history simplifications.

Calibration chamber test results apply to a limited range of stress conditions, typically:

50 kPa	<	σ'_{vo}	<	400 kPa
0.4	<	K_0	<	1.5

Sample preparation for laboratory chamber tests is usually by means of dry pluviation. Soil stress history application is by mechanical overconsolidation.

Jamiolkowski et al. (2003) proposed the following relationship between q_c and D_r for normally and overconsolidated silica (dry) sands:

$$D_{r(dry)} = \frac{1}{2.96} \ln \left[\frac{\frac{q_c}{P_a}}{24.94 \left(\frac{\sigma'_{vo} \left(\frac{1 + 2K_o}{3} \right)}{P_a} \right)^{0.46}} \right]$$

and for saturated sands:

$$D_{r(sat)} = \left(\frac{-1.87 + 2.32 \ln \frac{q_c}{(P_a * \sigma'_{vo})^{0.5}}}{100} + 1 \right) \frac{D_r(dry)}{100}$$

where relative density D_r is a fraction. The correlation for saturated sands results in relative densities that can be up to about 10 % higher compared to the correlation for dry sands.

It is understood that Jamiolkowski et al. (2003) used results from one of the ASTM vibratory table methods for determination of minimum index void ratio. It is not clear which specific ASTM method was used, i.e. a vibratory table method requiring oven-dried soil or wet soil.

Kulhawy and Mayne (1990) proposed:

$$D_r^2 = Q_{tn*}/Q_f \qquad \text{where: } Q_{tn*} = \left(\frac{q_t}{P_a} \right) / \left(\frac{\sigma'_{vo}}{P_a} \right)^{0.5}$$

and q_t is corrected cone resistance, P_a is atmospheric pressure, σ'_{v0} is effective in situ vertical stress. Kulhawy and Mayne (1990) suggested using $Q_f = 280$ for highly compressible normally consolidated sands and $Q_f = 450$ for highly compressible overconsolidated sands (overconsolidation ratio of > 8) based on their dataset. Robertson and Cabal (2015) suggested $Q_f = 350$ for clean, uncemented, medium compressible quartz sands of about 1 000 years old. Values for Q_f can be closer to 300 for fine sands and closer to 400 for coarse sands. Furthermore, Q_f increases with age and increases significantly when age exceeds 10 000 years.

Krogh et al. (2021) consider an empirical correction for D_r estimates as obtained according to Jamiolkowski et al. (2003). The correction is for the upper few metres below ground surface ($\sigma'_{v0} < 50$ kPa). The equations are as follows:

$$D_{r(sat)} = \left(\frac{-1.87 + 2.32 \ln \frac{q_c}{(P_{a*} \, \sigma'_{v0})^{0.5}}}{100} + 1 \right) \frac{D_{r(dry)}}{100}$$

where $D_{r(dry)}$ is given by

$$D_{r(dry)} = \frac{1}{2.96} \ln \left[\frac{\frac{q_c}{P_a}}{24.94 \left(\frac{\sigma'_{v0} \left(\frac{1+2K_0}{3} \right)}{P_a} \right)^{0.46}} \right]$$

and where q_c is cone resistance, P_a is atmospheric pressure, σ'_{v0} is effective in situ vertical stress and K_0 is coefficient of earth pressure at rest.

Effective Angle of Internal Friction – Sand

The effective shear strength parameter φ' is not a true constant. It depends on factors such as density, stress level, shearing mode and mineralogy. There is evidence that overconsolidation ratio, method of deposition and in situ stress anisotropy is less important.

Correlation of angle of internal friction φ' to cone resistance q_c may be done at various levels of sophistication. Simple procedures rely on a conservative assessment of soil behaviour classification. A more sophisticated empirical correlation consists of:

a. Estimation of in situ stress conditions σ'_{vo} and σ'_{ho}
b. Estimation of relative density D_r
c. Empirical correlation of angle of internal friction φ' with D_r, σ'_{vo} and σ'_{ho}.

Estimation of stress conditions and relative density has been discussed above.

The empirical procedure proposed by Bolton (1986 and 1987) is used for estimation of φ'. This correlation applies to clean sands and considers peak secant angle of internal friction in Isotropically Consolidated Drained triaxial compression (CID) of reconstituted sand. This procedure requires estimation of the dilatancy index and the critical state angle of internal friction.

Kulhawy and Mayne (1990) determined an equation based upon 20 data sets obtained from calibration chamber tests. This equation is almost identical to the empirical formula determined earlier by Trofimenkov (1974) which was based on mechanical cone data. Mayne (2007) validated the use of total cone resistance q_t instead of cone resistance q_c used in the equation from Kulhawy and Mayne (1990).

$$\varphi' = 17.6 + 11.0 \log \left(\left(\frac{q_t}{P_a} \right) \Big/ \left(\frac{\sigma'_{vo}}{P_a} \right)^{0.5} \right) \qquad \text{(Mayne, 2007)}$$

Undrained Shear Strength – Sand

Kaltekis and Peuchen (2022) presented the following site-specific correlation between net cone resistance q_n and undrained shear strength s_u of sand and transitional soil (Figure 10):

$$\frac{s_u}{\sigma'_{v0}} = \begin{cases} 0.0096 \cdot \frac{q_n}{\sigma'_{v0}} - 0.4823 & , \text{for } \frac{q_n}{\sigma'_{v0}} \geq 124 \\ 0.703 & , \text{for } \frac{q_n}{\sigma'_{v0}} < 124 \end{cases}$$

where s_u, q_n and effective in situ vertical stress σ'_{v0} are in kPa.

The definition of s_u considers:

- Consolidated undrained triaxial test (ISO, 2018) as reference;
- Reconstituted specimens prepared by moist reconstitution and intact specimens;
- $(\sigma'_1/\sigma'_3)_{max}$ as failure criterion for undrained shear strength, where σ'_1 and σ'_3 are the effective principal stresses.

The applicability of this correlation to soils other than those of the source data (Southern North Sea) is unknown.
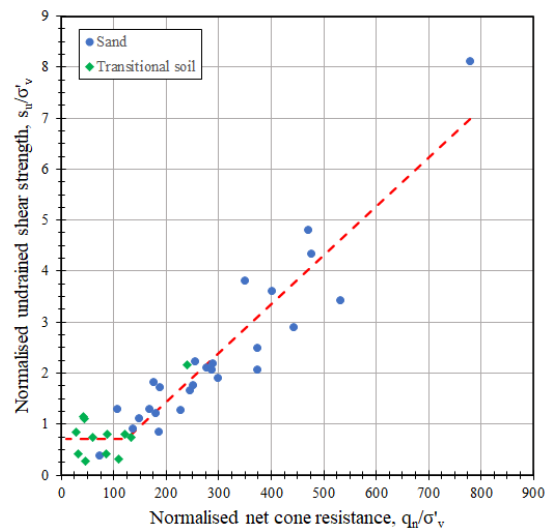
Figure 10: $s_u - q_n$ correlation according to Kaltekis and Peuchen (2022)

Constrained Modulus – Sand

Kulhawy and Mayne (1990) derived two formulas for the determination of the constrained modulus for both normally consolidated and overconsolidated sands by indicating that the modulus is a function of relative density. The determination of relative density can be done with, for example, the methods indicated above.

$$M = q_c * 10^{1.09 - 0.0075 D_r}$$
(normally consolidated sands, Kulhawy & Mayne, 1990)

$$M = q_c * 10^{1.78 - 0.0122 D_r}$$
(overconsolidated sands, Kulhawy & Mayne, 1990)

where D_r is in %, and q_c and M in kPa respectively.

Young's Modulus – Sand

A common guideline is an empirical correlation given by Baldi et al. (1989). The correlation is for silica-based sand and considers cone resistance q_c, in situ stress conditions and secant Young's modulus for drained stress change E'. The ratio of E'/q_c typically ranges from about 3 to 5 for recently deposited normally consolidated sands up to about $E'/q_c = 6$ to $E'/q_c = 25$ for overconsolidated sands. The correlation has been inferred from laboratory conditions; including CPTs in a calibration chamber

and conventional triaxial compression tests on reconstituted sand samples. It takes account of the degree of deformation and overconsolidation. In this regard, it is noted that secant deformation moduli are strongly dependent on strain level: the elastic modulus increases with decreasing strain to an upper limit at about 10^{-4} % strain.

Shear Modulus at Small Strain – Sand

For estimation of initial (small strain) or dynamic shear moduli, ratios of G_{max}/q_c of between about 4 and 20 can be considered, in accordance with Baldi et al. (1989). The basis for this correlation is similar to that of secant Young's modulus, except that laboratory resonant column tests serve as reference instead of triaxial compression tests. Results of limited in situ seismic cross-hole and downhole tests provide an approximate check of this correlation.

Interpretation of small strain shear modulus can also be estimated from a correlation proposed by Rix and Stokoe (1991) in which data from calibration test measurements is compared to the correlation obtained between G_{max} and q_c by Baldi et al. (1989).

$$G_{max} = 1634(q_c)^{0.25}(\sigma'_{vo})^{0.375}$$

<div align="right">(Rix & Stokoe, 1991)</div>

where G_{max}, q_c and σ'_{vo} are in kPa.

Clay Model – CPT-based Methods

Unit Weight – Clay

Empirical correlation between unit weight of clay and CPT parameters is as described in 'Unit Weight – Sand' above.

Shear Wave Velocity – Clay

Hegazy and Mayne (2006) and Roberson and Cabal (2015) present empirical correlations between shear wave velocity and CPT parameters for a wide range of soils including clays, as described in 'Shear Wave Velocity v_s – Sand' above. The Hegazy and Mayne correlation is sensitive to use of q_c or q_t. It should be used with caution for soils showing undrained or partially drained CPT response.

Mayne and Rix (1995) derived a correlation between shear wave velocity v_s and cone resistance q_c for intact and fissured clays. A database from Mayne and Rix (1993) was used including 31 different clay sites.

$$v_s = 1.75q_c^{0.627}$$

<div align="right">(Mayne & Rix, 1995)</div>

where shear wave velocity v_s is in m/s and cone resistance q_c is in kPa.

In Situ Stress Conditions – Clay

Similar to sand, a knowledge of in situ stress conditions is generally necessary for estimation of other parameters such as consistency (soft, stiff, etc.) of a clay deposit and compressibility. The effective in situ vertical stress σ'_{vo} can be calculated with a reasonable degree of accuracy but the effective in situ horizontal stress $\sigma'_{ho} = K_0 \cdot \sigma'_{vo}$ is generally more approximate.

The following approach can be applied for K_0 based on Agaiby and Mayne (2019):

$$K_0 = 0.45\sqrt{(OCR)}$$

using: $\quad OCR = \frac{\sigma'_p}{\sigma'_{v0}} \qquad \sigma'_p = 0.33 \cdot q_n^{m'} \qquad m' = 1 - \frac{0.28}{1+\left(\frac{I_c}{2.64}\right)^{25}}$

where OCR is overconsolidation ratio, σ'_p is effective preconsolidation stress, σ'_{v0} is effective in situ vertical stress, q_n is

net cone resistance in kPa and I_c is soil behaviour type index. Typical values for m' are 0.9, 1.0, and 1.1 for sensitive clays and organic clays, intact clays, and fissured clays respectively.

For normally consolidated clays and silts, K_{0nc} may be correlated with angle of internal friction, in accordance with Jaky (1944), or more simply, in accordance with Mayne and Kulhawy (1982). For many soil types (e.g. Mayne, 2020), it can be shown that the $K_0 = 0.45\sqrt{(OCR)}$ equation provides similar statistics to the Mayne and Kulhawy correlation using φ' (effective angle of internal friction):

$$K_0 = (1 - sin\varphi') \cdot OCR^{sin\varphi'}$$

The plasticity index together with OCR may also be used for preliminary estimates of K_{0oc} as indicated by Brooker and Ireland (1965).

No laboratory study can fully capture in situ behaviour. Particularly, K_0 may be underestimated if effects such as ageing and cyclic loading effects are relevant.

Overconsolidation Ratio – Clay

Overconsolidation ratio is defined as $OCR = \sigma'_p/\sigma'_{vo}$ where σ'_p is the effective preconsolidation stress considered to correspond with the maximum vertical effective stress to which the soil has been subjected in the past, and σ'_{vo} is the current effective in situ vertical stress. The effective preconsolidation stress approximates a stress level where relatively small strains are separated from relatively large strains occurring on the virgin compression stress range. The reference OCR is usually based on laboratory oedometer tests carried out on undisturbed samples. It may thus be influenced by factors such as sample disturbance, strain rate effects and interpretation procedure.

The following approach can be applied (Agaiby and Mayne, 2019):

$$OCR = \frac{\sigma'_p}{\sigma'_{v0}} \qquad \sigma'_p = 0.33 \cdot q_n^{m'} \qquad m' = 1 - \frac{0.28}{1+\left(\frac{I_c}{2.65}\right)^{25}}$$

where OCR is overconsolidation ratio, σ'_p is effective preconsolidation stress, σ'_{v0} is effective in situ vertical stress, q_n is net cone resistance in kPa and I_c is soil behaviour type index. Typical values for m' are 0.9, 1.0, and 1.1 for sensitive clays and organic clays, intact clays, and fissured clays respectively.

Chen and Mayne (1996) presented the following correlation for 205 clay sites around the world:

$$OCR = 0.317 \cdot Q_t$$

Overconsolidation ratio may also be inferred indirectly from a geological assessment and from undrained strength ratios. Geological factors concerning overconsolidation have been discussed under 'in situ stress conditions - sand'. An empirical procedure for estimation of OCR based on undrained strength ratio s_u/σ'_{vo} is given by Wroth (1984). The procedure uses the strength rebound parameter Λ. Guidance for selection of Λ and normally consolidated undrained strength ratio is given by Mayne (1988). Historically, much use has also been made of the Skempton (1957) relationship between normally consolidated undrained strength ratio and plasticity index I_P. This equation is useful for preliminary estimates, considering that I_P probably relates to φ' in some complex manner.

Undrained Shear Strength – Clay

No single undrained shear strength exists. The in situ undrained shear strength s_u depends on factors such as mode of failure, stress history, anisotropy, strain rate and temperature.

Various theoretical and empirical procedures are available to correlate q_c with s_u. Theoretical approaches use bearing capacity, cavity expansion or steady penetration solutions, all of which require several simplifying assumptions. Empirical approaches are more common in engineering practice because of difficulties in realistic soil modelling. An empirical correlation for soft to stiff, intact, and relatively homogeneous clays is given by Battaglio et al. (1986) as follows:

$$s_u = (q_c - \sigma_{vo})/N_c$$

where s_u, σ_{vo} and q_c are in kPa. N_c is an empirical factor that typically ranges between 10 and 25. The higher N_c factors typically apply to clays with a relatively low plasticity index and/or apply to heavily overconsolidated clays. Lower N_c factors are generally appropriate for normally consolidated and slightly overconsolidated clays. The reference undrained shear strength is that determined from in situ vane test results. The term σ_{vo} (total in situ vertical stress) becomes insignificant for stiff clays at shallow depth so that the equation reduces to $s_u = q_c/N_c$.

If piezocone test data are available, then improved correlations are feasible because of the pore pressure information. Empirical correlations of piezocone test results with laboratory undrained shear strengths are commonly used, as considered by Rad & Lunne (1988), expressed as follows:

$$s_u = q_n/N_{kt}$$

N_{kt} ranges typically between 8 and 30 with the higher N_{kt} factors applying to heavily overconsolidated clays.

Mayne and Peuchen (2022) account for N_{kt} variation according to B_q:

$$N_{kt} = 10.5 - 4.6 \cdot ln(B_q + 0.1)$$

where $B_q > -0.1$. The equation is based on 497 paired CPT and laboratory test results from 70 clay sites, particularly anisotropically consolidated triaxial compressive strength. Factoring of N_{kt} can be applied by multiplying the calculated N_{kt} factor by, for example, 0.85 and 1.2.

Mayne et al. (2015) recommend a mean $N_{kt} = 12$ with a standard deviation of 2.8 for correlation with laboratory anisotropically consolidated triaxial compressive strength. The recommendations are based on a study of 51 onshore and offshore clays and apply to normally consolidated to slightly overconsolidated clays with q_n values of typically less than 8 MPa. Slightly higher N_{kt} values can be expected for average laboratory undrained shear strength, defined as the average of laboratory triaxial compression, simple shear and triaxial extension.

Clay Sensitivity

The sensitivity of a clay (S_t) is the ratio of undisturbed undrained shear strength to remoulded undrained shear strength. Sensitivity may be assessed from the CPT friction ratio R_f, in accordance with Schmertmann (1978):

$$S_t = N_s/R_f$$

where N_s is a correlation factor typically ranging between 5 and 10. The correlation is expected to be inaccurate for sensitive clays where uncertainty in very low values for sleeve friction may dominate results.

The reference S_t value is often taken to be that determined from undisturbed and remoulded laboratory unconsolidated undrained triaxial tests. This reference S_t value may differ from that determined from other tests, for example laboratory miniature vane tests. This is partly related to the definition of

sensitivity. For vane tests, several measurements of undrained shear strength are possible:

- Intact (I) = undisturbed undrained shear strength as measured on an intact/undisturbed specimen;
- Intact-Residual (I-R) = measured post peak during initial shearing of the intact specimen;
- Intact-Vane Remoulded (I-VR) = measured after multiple-quick rotations of the vane after completion of the intact test;
- Hand Remoulded (HR) = steady state (post-peak if exists) resistance of hand remoulded test specimen;
- Hand Remoulded – Vane Remoulded (HR-VR) = steady state resistance of hand remoulded specimen measured after applying multiple-quick vane rotations.

Skempton and Northey (1952) present a correlation of sensitivity and laboratory liquidity index I_L. This correlation may allow a check on CPT-based interpretation of sensitivity.

Effective Shear Strength Parameters – Clay

Measurement of pore water pressures during penetration testing has led to development of interpretation procedures for estimation of effective stress parameters of cohesive soils. Background information may be found in Sandven (1990). Currently available procedures are evaluated to be 'experimental' and are yet not commonly adopted.

In general, CPT interpretation of effective shear strength parameters for clay and silt relies on soil behaviour-type classification.

It is noted that significant silt and sand fractions in a clay deposit will increase φ', while a significant clay fraction in silt will decrease φ'.

Masood and Mitchell (1993) provide an equation for the determination of φ' by combining sleeve friction with the Rankine earth-pressure theory. The equation is based on the following assumptions:

- Unit adhesion between soil and sleeve is negligible;
- Friction angle between soil and sleeve = $\varphi'/3$;
- Lateral earth pressure coefficient during penetration is equal to the Rankine coefficient of lateral earth pressure under passive conditions.

$$\frac{f_s}{\sigma'_{vo}} = \tan^2\left(45° + \frac{\varphi'}{2}\right)\tan\left(\frac{\varphi'}{3}\right)$$

(Masood & Mitchell, 1993)

Mayne (2001) proposed an approximation of the Masood and Mitchell equation, as follows:

$$\varphi' = 30.8\left[\log\left(\frac{f_s}{\sigma'_{vo}}\right) + 1.26\right]$$ (Mayne, 2001)

Mayne (2001) also proposed the following approximation of friction angle φ' based on pore pressure ratio B_q and the cone resistance number N_m (Senneset, Sandven and Janbu, 1989):

$$\varphi' = 29.5B_q^{0.121}(0.256 + 0.336B_q + \log N_m)$$

(Mayne, 2001)

where

$$N_m = \frac{q_t - \sigma_{vo}}{\sigma'_{vo} + a}$$

where the cone resistance number N_m is dimensionless, total cone resistance q_t, total in situ vertical stress σ_{vo} and effective in situ vertical stress σ'_{vo} are in kPa.

Senneset et al. (1989) use the attraction value a as a function of soil type. In general, the attraction value ranges from 5 to > 50

fugro

for both sands and clays and may be estimated directly from CPT results. The correlation is valid if the angle of plastification β is zero. In general, a plastification angle of zero applies to medium sands and silts, sensitive clays and highly compressible clays.

Constrained Modulus – Clay

Mitchell and Gardner (1976) present an approximate correlation of cone resistance with constrained modulus M (or coefficient of volume compressibility m_v, where $M = 1/m_v$). Typical ratios of M/q_c range between 1 and 8 for silts and clays. Refinements include q_c ranges and soil type (silt, clay, low plasticity, high plasticity, etc.). The correlation relies on the results of conventional laboratory oedometer tests carried out on undisturbed clay and silt samples.

Kulhawy and Mayne (1990) correlated constrained modulus M with net cone resistance data. This relationship is based on data from 12 (clay) test sites, with constrained moduli up to 60 MPa. The published standard deviation is 6.7 MPa.

$$M = 8.25 \; q_n \qquad \text{(Kulhawy \& Mayne, 1990)}$$

Young's Modulus – Clay

Young's modulus E_u can be derived as follows:

- Estimation of undrained shear strength s_u from CPT data, as outlined above;
- Estimation of secant Young's moduli for undrained stress change in general accordance with correlations based on s_u, as presented by Ladd et al. (1977).

Laboratory undrained triaxial tests carried out on undisturbed clay specimen form the basis for the E_u versus s_u correlations. Typical E_u/s_u ratios at a shear stress ratio of 0.3 range between about 300 and 900 for normally consolidated clays and $E_u/s_u = 100$ to $E_u/s_u = 300$ for heavily overconsolidated clay. Higher E_u/s_u ratios would apply to lower shear stress ratios, and vice versa.

Shear Modulus at Small Strain – Clay

Mayne and Rix (1993) determined a relationship between G_{max} and q_c by studying 481 data sets from 31 sites all over the world. G_{max} ranged between about 0.7 MPa and 800 MPa.

$$G_{max} = 2.78 \; q_c{}^{1.335} \qquad \text{(Mayne \& Rix, 1993)}$$

where G_{max} and q_c are in kPa.

References

Agaiby, S.S. & Mayne, P.W. (2019). CPT evaluation of yield stress in soils. *Journal of Geotechnical & Geoenvironmental Engineering* 145(12).

Baldi, G., Bellotti, R., Ghionna, V.N., Jamiolkowski, M., & Lo Presti, D.C.F. (1989). Modulus of sands from CPTs and DMTs. In *Proceedings of the 12th international conference on soil mechanics and foundation engineering, Rio de Janeiro, 13–18 August 1989* (pp. 165–170). Balkema.

Battaglio, M., Bruzzi, D., Jamiolkowski, M., & Lancellotta, R. (1986). Interpretation of CPTs and CPTUs, part 1: Undrained penetration of saturated clays. In *Field instrumentation and in-situ measurements: Proceedings of the fourth international geotechnical seminar, 25–27 November 1986, Mandarin Hotel, Singapore* (pp. 129–143). Nanyang Technological Institute.

Bolton, M.D. (1986). The strength and dilatancy of sands. *Géotechnique, 36*(1), 65–78. http://www-civ.eng.cam.ac.uk/geotech_new/people/bolton/mdb_pub/14_Geotechnique_No36_Is1_65_78.pdf

Bolton, M.D. (1987). Author's reply to discussion of the strength and dilatancy of sands. *Géotechnique*, 37(2) 225-226 https://doi.org/10.1680/geot.1987.37.2.219

Boulanger, R.W. & DeJong, J.T. (2018). Inverse filtering procedure to correct cone penetration data for thin-layer and transition effects. In M.A. Hicks, F. Pisanò & J. Peuchen. (eds.) *Cone Penetration Testing 2018: Proceedings of the 4th International Symposium on Cone Penetration Testing (CPT18): Delft, The Netherlands, 21-22 June 2018* (pp. 25-44). CRC Press

Brooker, E.W. & Ireland, H.O., 1965. Earth pressures at rest related to stress history. *Canadian Geotechnical Journal, 2*(1), 1–15. https://doi.org/10.1139/t65-001

CEN. (2009). *Eurocode 7: geotechnical design - Part 1: General rules (with corrigendum)* (EN 1997-1:2004). European Committee for Standardization. https://standards.cencenelec.eu/dyn/www/f?p=CEN:110:0:::FSP_PROJECT:12442&cs=147466E4C0BF2C1A6AB4E291281FD3E53

CEN. (2010). *Eurocode 7 - geotechnical design – Part 2: Ground investigation and testing* (EN 1997-2:2007+ AC:2010). European Committee for Standardization. https://standards.cencenelec.eu/dyn/www/f?p=CEN:110:0:::FSP_PROJECT,FSP_ORG_ID:34660,6231&cs=106BCF2003C57E77F5AE21C7C352536A8.

Chen, B.SY., & Mayne, P.W. (1996). Statistical relationships between piezocone measurements and stress history of clays. *Canadian Geotechnical Journal, 33*(3), 488–498. doi.org/10.1139/t96-070

DeJong, J.T. & Randolph, M.F. (2012). Influence of partial consolidation during cone penetration on estimated soil behavior type and pore pressure dissipation measurements. *Journal of Geotechnical and Geoenvironmental Engineering*, 138(7) 777-788.

Hegazy, Y.A., & Mayne P.W. (2006, June). *A global statistical correlation between shear wave velocity and cone penetration data* [conference presentation]. GeoShanghai International Conference, Shanghai, China. ASCE. https://doi.org/10.1061/40861(193)31

ISO. (2018). *Geotechnical investigation and testing – laboratory testing of soil - Part 9: Consolidated triaxial compression tests on water saturated soils* (ISO 17892-9:2018). International Organization for Standardization. https://www.iso.org/standard/70954.html

ISO. (2015). *General principles on reliability for structures* (ISO 2394:2015). International Organization for Standardization.https://www.iso.org/standard/58036.html

ISO. (2019). *Petroleum and natural gas industries – general requirements for offshore structures* (ISO 19900-2019). International Organization for Standardization. https://www.iso.org/standard/69761.html

ISO. (2021a). *Petroleum and natural gas industries – specific requirements for offshore structures – part 8: marine soil investigations* (ISO/DIS 19901-8:2021). International Organization for Standardization. https://www.iso.org/standard/83302.html

ISO. (2021b). *Petroleum and natural gas industries – specific requirements for offshore structures – part 8: marine geophysical investigations* (ISO 19901-10:2021). International Organization for Standardization. https://www.iso.org/standard/77017.html

Jaky, J. (1944). The coefficient of earth pressure at rest. *Magyar Mérnök és Epitész Egylet Közlönye,* 78(22) 355-358. (in Hungarian).

Jamiolkowski, M., Lo Presti, D.C.F., & Manassero, M. (2003). Evaluation of relative density and shear strength of sands from CPT and DMT. In J.T. Germaine, T.C. Sheahan & R.V. Whitman (Eds.), *Soil behavior and soft ground construction* (pp. 201–238). American Society for Civil Engineers. https://doi.org/10.1061/9780784406595

Kaltekis, K. & Peuchen, J. (2022). A CPT-based method for estimation of undrained shear strength of sands and transitional soils. In G. Gottardi & L. Tonni (eds.). *Cone Penetration Testing 2022: proceedings of the 5th International Symposium on Cone Penetration Testing (CPT'22), 8-10 June 2022, Bologna, Italy* (pp. 486-490). CRC Press. DOI: 10.1201/9781003308829-68

Krogh, L., Quinteros, S., Engin, H. K. & Lunne, T. (2022). Revisiting interpretation of relative density from shallow depth CPTs in sand. *Canadian Geotechnical Journal,* 59(6), 808-826. https://doi.org/10.1139/cgj-2021-0200

Kulhawy, F.H., & Mayne, P.W. (1990). *Manual on estimating soil properties for foundation design.* (Report EL-6800). Electric Power Research Institute.

Ladd, C.C., Foott, R., Ishihara, K., Schlosser, F. & Poulos, H.G. (1977). Stress-deformation and strength characteristics. In *Proceedings of the ninth international conference on soil mechanics and foundation engineering, 1977, Tokyo* (volume 2) (pp. 421-494). Japanese Society of Soil Mechanics and Foundation Engineering

Lengkeek, H.J., De Greef, J. & Joosten, S. (2018). CPT based unit weight estimation extended to soft organic soils and peat. In M.A. Hicks, F. Pisanò & J. Peuchen (eds.) *Cone Penetration Testing 2018: Proceedings of the 4th International Symposium on Cone Penetration Testing (CPT18): Delft, The Netherlands, 21-22 June 2018* (pp. 389-394). CRC Press

Masood, T. & Mitchell, J.K. (1993). Estimation of in situ lateral stresses in soils by cone-penetration test. *Journal of Geotechnical Engineering,* 119(10) 1624-1639: doi.org/10.1061/(ASCE)0733-9410(1993)119:10(1624)

Mayne, P.W. (1988). Determining OCR in clays from laboratory strength. *Journal of Geotechnical Engineering,* 114(1) 76-92

Mayne, P.W. (2001). *Geotechnical site characterization using cone, piezocone, SCPTu, and VST.* Georgia Institute of Technology.

Mayne, P.W. (2020). The 26th Széchy Lecture: Use of in-situ geotechnical tests for foundation systems. *Proceedings of the Széchy Károly Emlékkonferencia*, published by the Hungarian Geotechnical Society, Budapest: 12-73

Mayne, P.W. (2007). In-situ test calibrations for evaluating soil parameters. In T.S. Tan, K.K. Phoon, D.W. Hight & S. Leroueil (eds.) Characterisation and *Engineering Properties of Natural Soils* (Volume 3) (pp. 1601-1652). Taylor & Francis.

Mayne, P.W., & Kulhawy, F.H. (1982). K_0-OCR relationships in soil. *Journal of the Geotechnical Engineering Division*, 108(6), 851–872.

Mayne, P.W. & Rix, G.J. (1993). G_{max}-qc relationships for clays. *Geotechnical Testing Journal,* 16(1) 54-60 https://doi.org/10.1520/GTJ10267J

Mayne, P.W., & Rix, G.J. (1995). Correlations between shear wave velocity and cone tip resistance in natural clays. *Soils and Foundations*, 35(2), 107–110. https://doi.org/10.3208/sandf1972.35.2_107

Mayne, P.W., Peuchen, J. & Bouwmeester, D. (2010). Soil unit weight estimation from CPTs. In *CPT'10: 2nd International symposium on cone penetration testing, Huntington Beach, California: conference proceedings*.

Mayne, P.W., Peuchen, J. & Baltoukas, D.B. (2015). Piezocone evaluation of undrained strength in soft to firm offshore clays. In V. Meyer (ed.) *Frontiers in Offshore Geotechnics III: proceedings of the Third International Symposium on Frontiers in Offshore Geotechnics (ISFOG 2015), Oslo, Norway, 10-12 June 2015.* (pp. 1091-1096) CRC Press.

Mayne, P.W. & Peuchen, J. (2022). Undrained shear strength of clays from piezocone tests: a database approach. In G. Gottardi & L. Tonni (eds.). *Cone Penetration Testing 2022: proceedings of the 5th International Symposium on Cone Penetration Testing (CPT'22), 8-10 June 2022, Bologna, Italy* (pp. 546-551). CRC Press. DOI: 10.1201/9781003308829-78

Mitchell, J.K. & Gardner, W.S. (1976). In situ measurement of volume change characteristics. In *Proceedings of the conference on in situ measurement of soil properties, June 1-4, 1975, Raleigh, North Carolina: Specialty Conference of the Geotechnical Engineering Division, ASCE, II* (pp. 279-345). American Society of Civil Engineers.

Nauroy, J.-F., Dubois, J.-C., Colliat, J.-L., Kervadec, J.P. & Meunier, J. (1998). The Geosis method for integrating VHR seismic and geotechnical data in offshore site investigations. In D.A. Ardus et al. (eds.). *Offshore site investigation and foundation behaviour: 'new frontiers': proceedings of an international conference held in London, UK, 22/23/24 September 1998* (pp. 175-198). Society for Underwater Technology.

Peuchen, J. & Terwindt, J. (2014). Introduction to CPT accuracy. In *3rd International symposium on cone penetration testing CPT14: May 12-14* (2014) - Las Vegas, Nevada.

Peuchen, J. & Terwindt, J. (2015). Measurement uncertainty of offshore cone penetration tests. In V. Meyer (ed.) *Frontiers in offshore geotechnics III: proceedings of the third international symposium on frontiers in offshore geotechnics (ISFOG 2015), Oslo, Norway, 10-12 June 2015.* (pp. 1209-1214) CRC Press.

Rad, N.S. & Lunne, T. (1988). Direct correlations between piezocone test results and undrained shear strength of clay. In J. De Ruiter (Ed.). *Penetration testing 1988 : proceedings of the first International Symposium on Penetration Testing, ISOPT-1, Orlando, 20-24 March 1988* (Vol. 2, pp. 911-917). Balkema.

Rix, G.J. & Stokoe II, K.H. (1991). Correlation of initial tangent modulus and cone penetration resistance. In A.B. Huang (Ed.). *Calibration chamber testing: proceedings of the first international symposium on calibration chamber testing, ISOCCT1, Potsdam, New York, 28-29 June 1991* (pp. 351–362). Elsevier.

Robertson, P.K. (1990). Soil classification using the cone penetration test. *Canadian Geotechnical Journal,* 27(1), 151–158. https://doi.org/10.1139/t90-014

Robertson, P.K. (1991). Soil classification using the cone penetration test: Reply. *Canadian Geotechnical Journal,* 28(1), 176–178. https://doi.org/10.1139/t91-024

Robertson, P.K. (2009). Performance based earthquake design using the CPT. In T. Kokusho, Y. Tsukamoto, & M. Yoshimine (Eds.), Performance-based design in earthquake geotechnical engineering: From case history to practice (pp. 3–20). CRC Press.

Robertson, P.K. (2010). Soil behaviour type from the CPT: an update. In *2nd International symposium on cone penetration testing, Huntington Beach, CA,* Vol. 2. (pp. 575-583)

fugro

Robertson, P.K. (2016a). Cone penetration test (CPT)-based soil behaviour type (SBT) classification system — an update. *Canadian Geotechnical Journal, 53*(12) 1910-1927 https://doi.org/10.1139/cgj-2016-0044

Robertson, P.K. (2016b). Estimating K0 in sandy soils using the CPT. In B.M. Lehane, H.E. Acosta-Martinez & R.B. Kelly (eds.) *Geotechnical and geophysical site characterization 5: proceedings of the fifth international conference on geotechnical and geophysical site characterization (ISSMGE TC-102 - ISC'5), Gold Coast, Queensland, Australia, 5-9 September 2016* (pp. 515-518). Australian Geomechanics Society

Robertson, P.K. & Cabal, K.L. (2015) *Guide to cone penetration testing for geotechnical engineering*. (6th ed.) Gregg Drilling & Testing.

Robertson, P.K. & Wride (Fear), C.E. (1998). Evaluating cyclic liquefaction potential using the cone penetration test. *Canadian Geotechnical Journal*, *35*(3), 442-459. https://doi.org/10.1139/t98-017

Robertson, P.K., Woeller, D.J. & Finn, W.D.L. (1992). Seismic cone penetration test for evaluating liquefaction potential under cyclic loading. *Canadian Geotechnical Journal, 29*(4) 686-695 https://doi.org/10.1139/t92-075

Sandven, R. (1990). *Strength and deformation properties of fine grained soils obtained from piezocone tests* [Thesis]. Norwegian Institute of Technology, Department of Civil Engineering

Schmertmann, J.H. (1978). *Guidelines for cone penetration test: Performance and design* (Report no. FHWA-TS-78-209). Federal Highway Administration, US Department of Transportation.

Senneset, K., Sandven, R., & Janbu, N. (1989). The evaluation of soil parameters from piezocone tests. *Transportation Research Record*, *1235*, 24–37. http://onlinepubs.trb.org/Onlinepubs/trr/1989/1235/1235-003.pdf

Skempton, A.W. (1957). Discussion on Airport Paper No. 35: The planning and design of the new Hong Kong Airport. *Proceedings of the Institution of Civil Engineers, 7*(2) 306.

Skempton, A.W., & Northey, R.D. (1952). The sensitivity of clays. *Géotechnique*, *3*(1), 30–53. https://doi.org/10.1680/geot.1952.3.1.30

Trofimenkov, J.G. (1974). Penetration testing in USSR: state-of-the-art report. in *Proceedings of the European symposium on penetration testing ESOPT, Stockholm, June 5-7, 1974, 1* (pp. 147-154). National Swedish Building Research.

Van der Wal, T., Goedemoed, S. & Peuchen, J. (2010). Bias reduction on CPT-based correlations. In *CPT'10: 2nd international symposium on cone penetration testing, Huntington Beach, CA: conference proceedings*.

Wroth, C.P. (1984). The interpretation of in situ soil tests. *Géotechnique*, *34*(4), 449–489. https://doi.org/10.1680/geot.1984.34.4.449 https://www.icevirtuallibrary.com/doi/pdf/10.1680/geot.1984.34.4.449

Zhang, G., Robertson, P.K. & Brachman, R.W.I. (2002). Estimating liquefaction induced ground settlements from CPT for level ground. *Canadian Geotechnical Journal*, *39*(5) 1168-1180. https://doi.org/10.1139/t02-047

fugro